NASA / USRA 1987
SENIOR DESIGN PROJECT

AEROASSISTED MANNED TRANSFER VEHICLE (TAXI)

For Advanced Mars Transportation

LANGLEY
LIBRARY
HAMPTON VIRGINIA

Department of Aerospace & Ocean Engineering
Virginia Polytechnic Institute & State University
Blacksburg, Virginia.

AEROASSISTED MANNED TRANSFER VEHICLE (TAXI)

For Advanced Mars Transportation

Department of Aerospace & Ocean Engineering
Virginia Polytechnic Institute & State University
Blacksburg, Virginia.

Abstract

This report presents a conceptual design study of an aeroassisted orbital transfer vehicle, nicknamed TAXI, for ferrying personnel and cargo (a) between low Earth orbit and a spacecraft circling around the sun in permanent orbits intersecting gravitational fields of Earth and Mars and (b) between the cycling spacecraft and a Mars orbiting station, co-orbiting with Phobos. Throughout the design process, considerations of crew safety and mission flexibility (in terms of ability to provide a wide range of ΔV) were generally given higher priority than any other considerations. Three versions of the TAXI have been considered. They use the same overall configuration based on a low L/D aerobrake having the geometry of a raked-off elliptical cone with ellipsoidal nose and a toroidal skirt. The propulsion system consists of three gimbaled LOX/LH2 engines firing away from the aerobrake. The versions differ mainly in the size of aeroshields and propellant tanks. TAXI A version resulted from an initial effort to design a single transfer vehicle able to meet all possible ΔV requirements during a 15-year period (2025-2040) of Mars missions operations. TAXI B represents a transfer vehicle designed to function with the cycling spacecraft moving in a simplified, "nominal" trajectory, proposed by the University of Michigan design team, which designed the cycling spacecraft. In real-world, actual Mars missions, the TAXI B would be able to meet the requirements of all the missions, for which the relative approach velocity near Mars is less than 9.3 km/sec. Finally, TAXI C is a revised version of the TAXI A and defines a transfer vehicle capable to serve in those missions which have the relative velocity near Mars larger than 9.3 km/sec. All versions are designed to carry a crew of 9 (or possibly 11 with some modifications) and a cargo of 10,000 lbm. Trip duration varies from about 1 day for transfer from LEO to the cycling ship to nearly 5 days for transfer from the cycling ship to the Phobos orbit.

Acknowledgements

CONTENTS

1. Introduction

1.1 Project Team/Organization

Instructor: Dr. A. K. Jakubowski

Teaching Assistant: Samir Deshpande

Management: Steven R. Hawk
             Clifford S. Barney

Orbital Mechanics:	James R. Mack Paul F. Farnsworth Robert D. Sincoskie David C. Slack
Propulsion:	Benjamin R. Smith Lance H. Carter Joseph Gelardi Luke T. Helbling Fei T. Kwok Garrett W. Roy
Aerobraking:	Matthew M. Pesce Ernest W. Buford Richard S. Butler C. Randolph Hyde Peter S. King David H. Wright
Vehicle Structures and Crew Support Systems:	Leonard Bowen Annette Ballangee Kathleen Fallon Miklos Klempa Mark D. Knight Chris S. Martin Mark C. Render Lee Ann Snyder Michele M. Trumpore
SNC, Communications and Power Systems:	J. Richard Gardiner Vineet Mehta Edward A. Robertson Christopher J. Tan

1.2 Background

1.2.1 Project Background

In 1985 the U.S. Congress and President Ronald Reagan appointed a special <u>National Commission on Space</u> to formulate recommendations for a long term agenda in space exploration. In 1986 the Commission published its report, "Pioneering the Space Frontier". Among the goals mentioned prominently was the exploration of Mars, the establishment of a long term base at Mars and an advanced system of transportation to Mars.

Each year the Senior class of Aerospace and Ocean Engineering at Virginia Polytechnic Institute and State University engages in a number of year-long aerospace system design projects. For the Class of 1987, one of the major projects was the development of a conceptual design for a manned transportation system (and/or vehicle) to and from the planet Mars. This goal closely paralleled concepts covered in the Commission's report. Specifically, concentration on the design of an Aeroassisted Manned Transfer Vehicle (AMTV) for use in an advanced, Cycling Ship based, Mars transportation system, was decided upon.

1.2.2 Definition of Concept

The concept for an established Mars transportation system focused upon here is based on the idea of utilizing a multi-vehicle system with extended lifetime reusability, reduced duplication of effort and reduced energy and trip requirements. By placing large, space-station sized Cycling Spacecraft in permanent orbits about the sun that intersect the orbits of Earth and Mars at regular intervals, trip times to and from Mars can be reduced to only a few months. These Cycling Spacecraft would not accelerate or decelerate substantially at either planet. The gravitational fields of Earth and Mars would be used, in conjunction with occasional propulsive firings, to produce orbit change maneuvers. Since the Cycling Spacecraft would not stop at either planet, smaller AMTV's would be used to bring crews from Low Earth Orbit (LEO; 270 n.mi) to the Cycling Spacecraft as it passes by Earth and also to take those crews to a Space Station orbiting Mars as the Cycling Spacecraft passes Mars. Such Transfer Vehicles would also be used on the Earthbound leg of the journey in a similar fashion. This method of ferrying crews around has led to the nickname of "TAXI" for the Aeroassisted Manned Transfer Vehicle. In the scenario just described, the Space Station in LEO and a Mars Orbiting Station (MOS) placed in the orbit of Phobos (or, else, the Phobos itself) are to be used as staging points (space ports) for the Mars missions.

The Cycling Spacecraft became the design responsibility of the University of Michigan. The design team at Virginia Tech took responsibility for designing the TAXI vehicle. Some coordination of these two design programs was required to make the vehicles compatible on major points such as docking facilities, fuel transfer systems and other connection systems.

2

1.3 Primary Design Criteria

In establishing a proper design for a spacecraft such as the TAXI investigated here, several major design criteria should be kept in mind throughout the design process. Among these considerations were 1) crew safety, 2) technical soundness, 3) reusability and 4) mission flexibility.

The feature of safety is paramount for a space vehicle carrying human beings. This criterion is often referred to as a design being "man-rated". This means that a vehicle's design must place the safety of its crew above all other design considerations. One common application of this criterion would be the use of a larger safety factor in design calculations than would be customary.

Secondly, such a design effort should attempt to achieve technical feasibility and practicality in its work. A design must be functional in the role intended for it. It should stand up to considerable technical scrutiny as to the correctness and workable nature of the solutions presented. For this purpose a concentration on the utilization of current technology, with reasonably justified extrapolations to the timeframe of the project, is made to ensure soundness.

Other primary criteria include modularity and flexibility of the design in meeting potential mission variations, reusability of the vehicle and its maintainability (extended lifetime).

1.4 General Mission Scenario

1.4.1 Basic Mission Assumptions

As explained in 1.2.2, the Mars transportation system will consist of two major components. Since a long period of time is spent in transit between Earth and Mars, the cycling ship should be able to comfortably accommodate humans for long periods of time. This craft would be built primarily for human safety and comfort, having systems on board that smaller space vehicles would not have. The size of this cycling spacecraft makes it an unrealistic craft for utilization near large gravity pools such as Earth and Mars. For this reason a small transfer craft, or TAXI, was conceived. The TAXI's only purpose is to transfer crew and small cargos from LEO and Mars Orbiting Station (MOS) to the Cycling Spacecraft as well as from the Cycling Spacecraft to LEO and MOS.

The TAXI will have to be designed with a large aeroshield capable of withstanding heating that will occur during its pass through the atmosphere. Since the TAXI will be travelling at hyperbolic velocity as it nears the gravity pool, it will need to aerodynamically decelerate to circular velocity to establish a low planetary orbit. This represents a savings in energy in that no extra fuel has to be brought along for deceleration, although it introduces other technical and safety concerns.

On leaving LEO, the TAXI will carry enough fuel to perform the Cycling Ship-to-MOS transfer and on leaving the Mars, the TAXI will have to carry fuel required for the transfer from the Cycling Ship to LEO. This is required because the Cycling Ship currently designed at the University of Michigan will carry only a small amount of excess fuel which may be accessed in case of an emergency. It was assumed that the TAXI would be refueled at Mars, conceivably from a fuel production facility located at the Martian moon Phobos. As will be discussed in chapter 3, the fuel that a spacecraft must carry to achieve a certain velocity change increases exponentially as a function of the total delta-V. Remote fuel production would eliminate the need to carry return-trip fuel and greatly simplifies the design as well as reduces the size of the craft. Although such fuel production facilities are currently unfeasible, they are expected to become technologically plausible in the next few decades prior to the 2025-2035 time frame. For the purpose of our project, it has been assumed that the Earth-Mars transportation system based on a Cyclic Ship/TAXI concept will be established around 2025 or shortly thereafter.

Other assumptions that have been made are that construction of the TAXI as well as the cycling spacecraft will be feasible, both technologically and economically. This involves assuming that a heavy-lift launch vehicle will be available for transport of materials and people from the Earth's surface and that a space station will be in place in LEO at which construction and launching will take place. It is assumed that advanced robotic missions to Mars will have taken place prior to the missions' commencement and that all components of the mission, cycling spacecraft, Mars Orbiting Station, fuel production facilities, will already be in place. Further assumptions have been made that there will be a series of communications satelites in Martian orbit and that possibly fuel could be produced at the Earth's moon for use by the TAXI and other space vehicles.

1.4.2 Vehicle Technological Requirements

At the present rate of advancement in science, it is not unreasonable to expect significant strides in space-related fields. Since the space industry is closely tied to the willingness of governments to spend money on space-borne activities, such advancement will also be determined by political and social factors.

The critical portion of our design, which assumes significant improvement over 1987 technology, is the aerobrake. The outer skin of the aerobrake will undergo significant heat transfer during deceleration in the atmosphere and as of this date, no 100% effective material exists. Scientific advancement in materials engineering will be necessary in the design of major components such as the structure of the aerobrake, crew module, engine support frame and fuel tank insulation. Many of these components are to be fabricated from composite materials that, although in existence, are still in a stage of development and are unwieldly, costly and of questionable performance.

Propulsion systems will have to see some advances resulting in lighter liquid hydrogen-liquid oxygen engines capable of ISP's greater than 470 seconds and having extended throttling capabilities.

Significant developments will also have to occur in the technologies of power supply, guidance/navigation and communications systems in terms of weight, performance and cost.

Since the construction of most of the major components will take place in low Earth-orbit during the time frame 2020-2030, new space construction techniques will have to be developed and perfected. Since many construction operations common on Earth will be impossible in space, the components will have to be as pre-fabricated as possible before launch to the construction area.

## 1.5 Vehicle Configuration/Design Evolution

A discussion of the selected configuration design for the TAXI is now in order. Explanation concerning the design of individual systems will follow in subsequent chapters.

Since it was assumed that our spacecraft would decelerate around planetary bodies by aerobraking through their atmospheres, the first major portion of the design configuration involved selecting the proper aerobraking shape. On the basis of the available literature it was decided that for our TAXI the optimum shape was an ellipsoidally blunt raked-off elliptic cone with a toroidal skirt. Viewing the aerobrake along the lateral axis it appears to have a circular cross-section, although its depth is greater at one end than the other.

The layout of the vehicle was established after considering several preliminary configurations, a few of them are sketched in Fig. 1.5.1. Various requirements and considerations such as propellant tank size and number, main engine number, crew module shape and dimensions, stability during propulsion and aerobraking maneuvers, modularity and ease of assembly in LEO had to be examined and balanced. The maximum propellant tank size is limited by the space available for transportation to LEO in a potential future launch vehicle (assumed to be 25 ft dia. x 90 ft). Three main engines are included in the design. If one engine fails, the remaining two can be used to safely complete the trip.

A major question concerned integration of the propulsion system with two other main components, the aerobrake and the crew module. Engine firing through the aerobrake (Fig. 1.5.1a), favored in many published studies of the Orbital Transfer Vehicle (OTV) concepts, requires a door in the aerobrake. This adds complexity and introduces a risk of possible leaks which would have fatal consequences for a manned mission. Since we considered the crew safety to be of paramount importance, the arrangement with firing through the aerobrake was rejected for this first-generation of the TAXI vehicle. Side-firing arrangement (Fig. 1.5.1b) requires extendable nozzle design to prevent both the impingement of the engine exhaust on the aerobrake (during thrusting) and the impingement of the hot wake flow on the nozzle (during aerobraking). Also, this arrangement may call for somewhat greater engine gimbaling capability. After extensive deliberations, a configuration with firing away from the aerobrake was chosen. To prevent engine exhaust impingement upon the crew and payload modules, the engines will be mounted on a supporting structure which raises the nozzle exits above these modules. For connecting the TAXI to the

(a) Engine firing through aerobrake

Air lock / docking mechanism

Crew cabin and payload storage

Fuel tanks

Engines

Aerobraking shield

(b) Side-firing engine
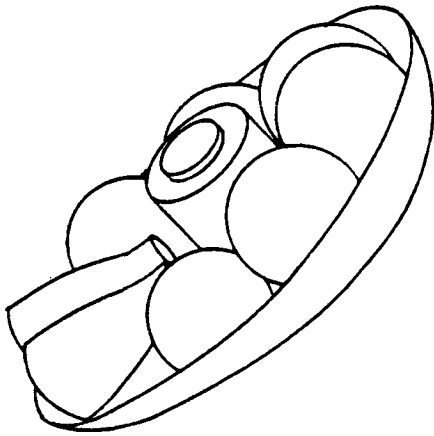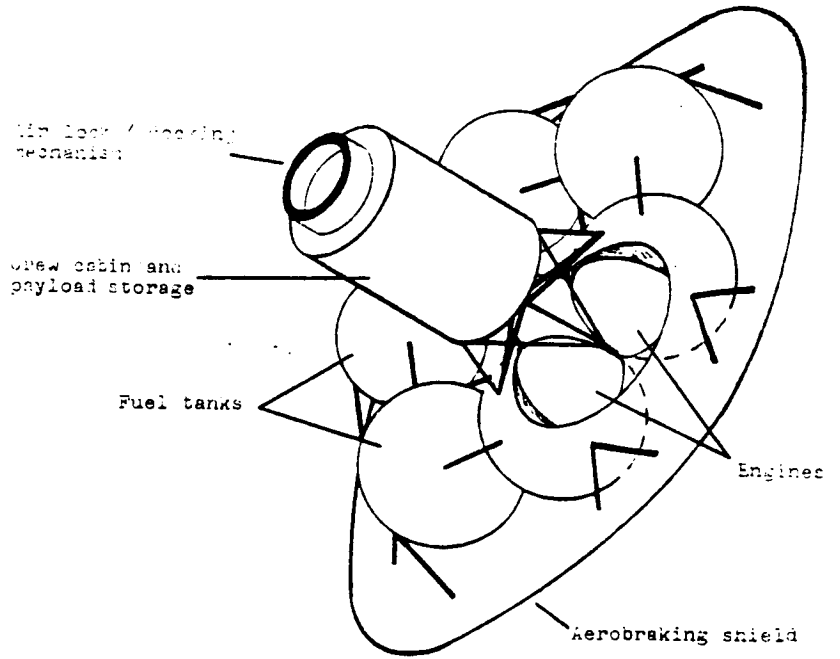
(c) Engine firing away from aerobrake

Engines

Crew cabin with air lock and docking mechanism

Fuel tanks

Aerobraking shield
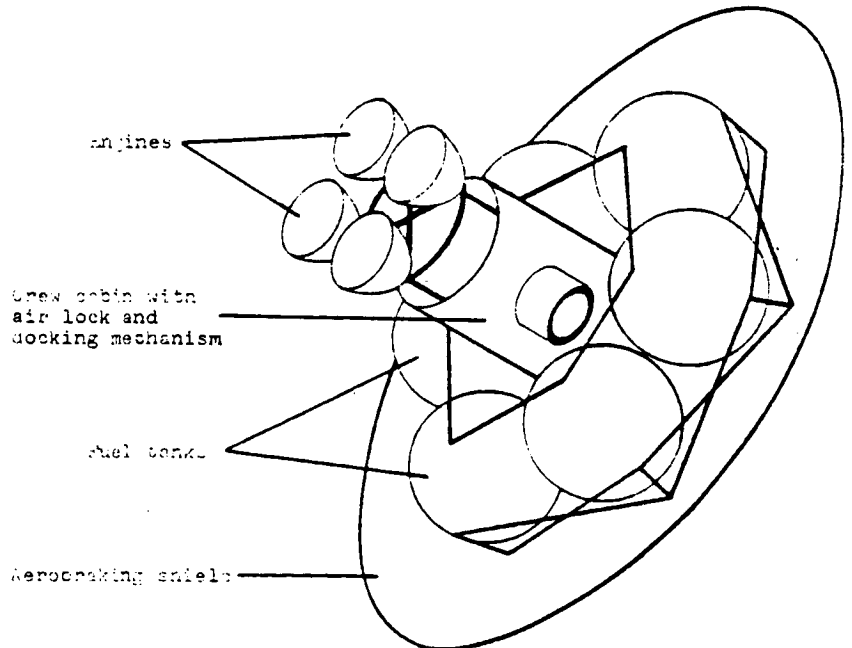
Fig. 1.5.1 Aeroassisted Transfer Vehicle Configurations

6

Cycling Ship or to the orbiting Space Stations, the tubular docking ports on the Cycling Ship and the Space Stations will have to be of sufficient length.

The overall configuration of the TAXI is shown in Figs. 1.5.2 and 1.5.3. For added safety, a somewhat oversized aerobrake was selected for preliminary design. The aerobrake is held together by eight truss frames arranged in a four-by-four pattern and intersecting one another to resemble an egg carton. The aerobrake truss system is the foundation upon which all vehicle components are attached. The three main engines are arranged in a triangular cluster placed near the center of the aerobrake.

The crew module is attached to the aerobrake supporting trusses next to the engine cluster on the side where two of the engines are parallel to the aerobrake cross-beam. The space on the opposite side of the engine cluster (next to the third engine) is reserved for the payload.

The six fuel tanks are placed in two lines of three tanks on either side of the engine supporting structure. Each line consists of an oxygen tank between two hydrogen tanks. Each oxygen tank is submerged into the aerobrake about one-fourth of its radius more than the hydrogen tanks, which are only submerged halfway. Each fuel tank has a pod which holds the tank in place and allows it to be attached securely to the aerobrake truss system. Stability of the vehicle during thrusting/aerobraking maneuvers will be maintained by gimbaling the engines or by shifting fuel.

Establishing the major parameters of the TAXI depended to a large extent upon the value of the required total ΔV for the transfers: Earth to Cycling Ship/Cycling Ship to Mars and Mars to Cycling Ship/Cycling Ship to Earth. Our initial calculations of the TAXI transfer trajectories indicated a maximum required ΔV-value of 9.5 km/s for the return trip from Mars to Earth (which is always greater than the ΔV-value for an outgoing trip from Earth to Mars). This value was used to determine the propellant mass and to size the propellant tanks, and then, to proceed with sizing and structural design of aerobrake. The TAXI design which resulted from these initial calculations is designated as the TAXI version A (initial mass 760.4 klbm; aeroshield diameter = 120 ft). The aerobrake structure and truss frame structures were designed for this version.

In the meantime, the design team at the University of Michigan carried out calculations of the Cycling Ship trajectory and adapted a nominal trajectory as a base for the Cycling Ship design.[*] Our calculations of

_____

[*] The nominal trajectory assumes that the Earth and Mars are in co-planar, circular orbits about the sun. The relative velocities of the Cycling Ship near the Earth and Mars are 6 and 9.3 km/s, respectively.

the TAXI transfer orbits were then adjusted correspondingly and after several iterations yielded a significantly lower value of the required ΔV. A value of 7.27 km/s has been selected for the revised version of the TAXI (TAXI B); this value should provide some flexibility for aeroassisted maneuvering near Earth and a sufficiently wide launch window, particularly if we realize that: (a) further refinement of the trajectories and a possible use of multiple burns will undoubtedly result in additional reductions of the required ΔV, (b) in all actual, real-world Mars missions for which TAXI B would be used (i.e., those with relative velocity at Mars being less than 9.3 km/sec), ΔV of 7.27 km/sec provides an adequate to quite large extra ΔV for unplanned maneuvers and needs, particularly during aeroassisted transfers. The propellant requirements, tank sizes, propulsive maneuvers, engine parameters and the aerobrake size were determined for the new value of ΔV. The overall configuration of the vehicle and the modules unaffected by the aerobrake size were kept unchanged. In particular, the composition of the Thermal Protection System (TPS) of the aeroshield was taken to be essentially the same and its thickness, already sized rather conservatively, was increased only slightly (by 8%); this can be justified by the fact that for a given L/D value, the insulation requirement is not strongly dependent on the ballistic coefficient if the latter is greater than about 5 lbm/ft^2. In our case, the ballistic coefficient increased by less than 50% for the new version of the TAXI (from 6.26 to 9.15 lbm/ft^2). Also, the electrical power requirements were assumed to be essentially the same. As there was not enough time left for a detailed design of the aerobrake and its supporting structure for the TAXI B, evaluation of these components was carried out mostly by scaling down the aerobrake of the TAXI A. The parameters, sizes and masses of the propulsion system, tankage and RCS have been reexamined and evaluated according to the max ΔV of 7.27 km/s. The TAXI B (initial mass when leaving Mars = 350.8 klbm; aerobrake diameter = 80 ft) represents our conceptual design of a transfer vehicle, compatible with the Cycling Ship designed at the University of Michigan, which can be used for most of the Mars missions during a 15-year cycle period.

The real-world trajectories will differ from the nominal trajectory (assumed by the University of Michigan team) and for two or three rotations of the Cycling Ship around the sun, the relative velocity of the Cycling Ship will exceed the nominal trajectory value of 9.3 km/s. Considerations of the real-world trajectories led again to a required total ΔV-value of about 9.5 km/s[*] and thus, essentially, back to the TAXI version A. Upon reexamination of this version it was concluded

---

[*] required ΔV = minimum ΔV for the nominal trajectory (6.8 km/s) + difference between the expected velocity (11.7 km/s) and the nominal relative velocity (9.3 km/s) + margin for a sufficiently wide launch window and safeguard against malfunctions (0.3 km/s).

that the aeroshield (and, possibly, RCS system) had been overdesigned
and could be reduced without imperilling the safety of the crew and
integrity of the vehicle. At the same time, the weights of some of the
subsystems (propellant feed system; engine gimbal system) may have been
underestimated. The reexamination resulted in the version C of the
TAXI, having an initial mass (on leaving Mars) of 682.6 klbm and the
aeroshield diameter of 100 ft. The version C is proposed for crew and
cargo transfers during approximately 5-year period of high relative
velocity of the Cycling Ship near Mars.

The main design parameters of the TAXI versions A, B, and C are listed
in Table 1.5.1. All versions are designed to carry crew of 9 (max 11)
and a cargo of 10,000 lbm. Transfer duration is typically 1-5 days (max
7 days). The TAXI versions B and C (Figs. 1.5.4a, b) differ primarily
in the aeroshield size, supporting structure, fuel tankage, engine size
and RCS. Crew module, power units, GNC and communications modules are
essentially the same. Obviously, various modifications and other
configurations should be investigated. For instance, a TAXI using one
size of the aerobrake for all possible transfers may be considered.
Such a TAXI may use the aeroshield of the version C, and be fitted with
different tanks and/or engines depending on the required ΔV of the
mission. Another possibility is to use the version C with its full size
tanks for both the higher and lower ΔV missions. When used in lower ΔV
missions, the TAXI, while serving as the crew and cargo (10,000 lbm or
more) transfer vehicle, can additionally supply the Cycling Ship with a
substantial if not a full amount of fuel needed for the Cycling Ship's
propulsive maneuvers.

As the crew safety was considered to be of paramount importance, it
would be very desirable to provide the TAXI with a capability of
returning to LEO or MOS in the event of an unforseen accident or failure
which would make it impossible for the TAXI to join the Cycling Ship.
At Mars (where a safe return requires a higher ΔV), ability of returning
to the orbiting station exists until the moment of the last burn, i.e.,
for the first 2-3 days of the transfer trip. To provide ability of
returning after the last burn, the TAXI would have to nearly double its
fuel capacity which effectively rules out such solution.

Table 1.5.1 Main Design Parameters of the TAXI Transfer Vehicles

Vehicle Desig- nation	Aero- shield dia- meter ft	Dry Mass (without LOX/LH2 propellant) lbm	LOX/LH2 Propellant Mass (max) lbm	ΔV Range km/s Prop	ΔV Range km/s Aero	#	Main Engines (LH2/LOX) Thrust lbf	Main Engines (LH2/LOX) Throttling Range % Design thrust
TAXI A	120	83,365	677,000	4.9-9.5	1.8-5.5	3	315,000	40-120
TAXI B	80	65,120	285,702	4.9-7.27	1.8-5.5	3	220,000	40-100
TAXI C	100	77,600	605,000	4.9-9.5	1.8-5.5	3	315,000	40-110

References:

Paine et al, "Pioneering the Space Frontier: The Report of the National
Commision on Space", Bantam Books, New York, 1986

REAR AND SIDE VIEW OF   TAXI
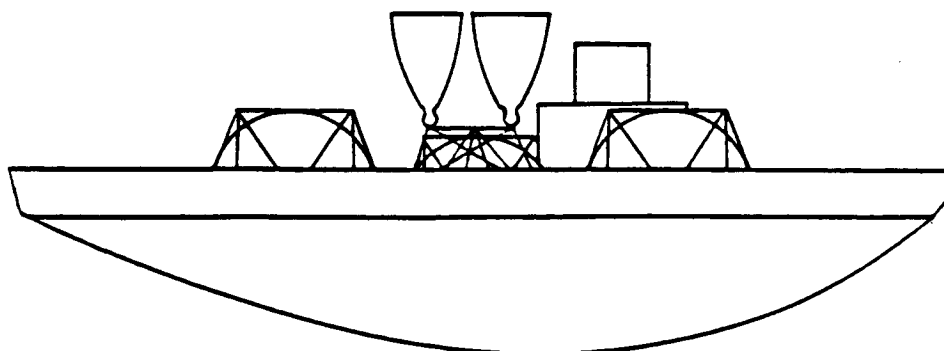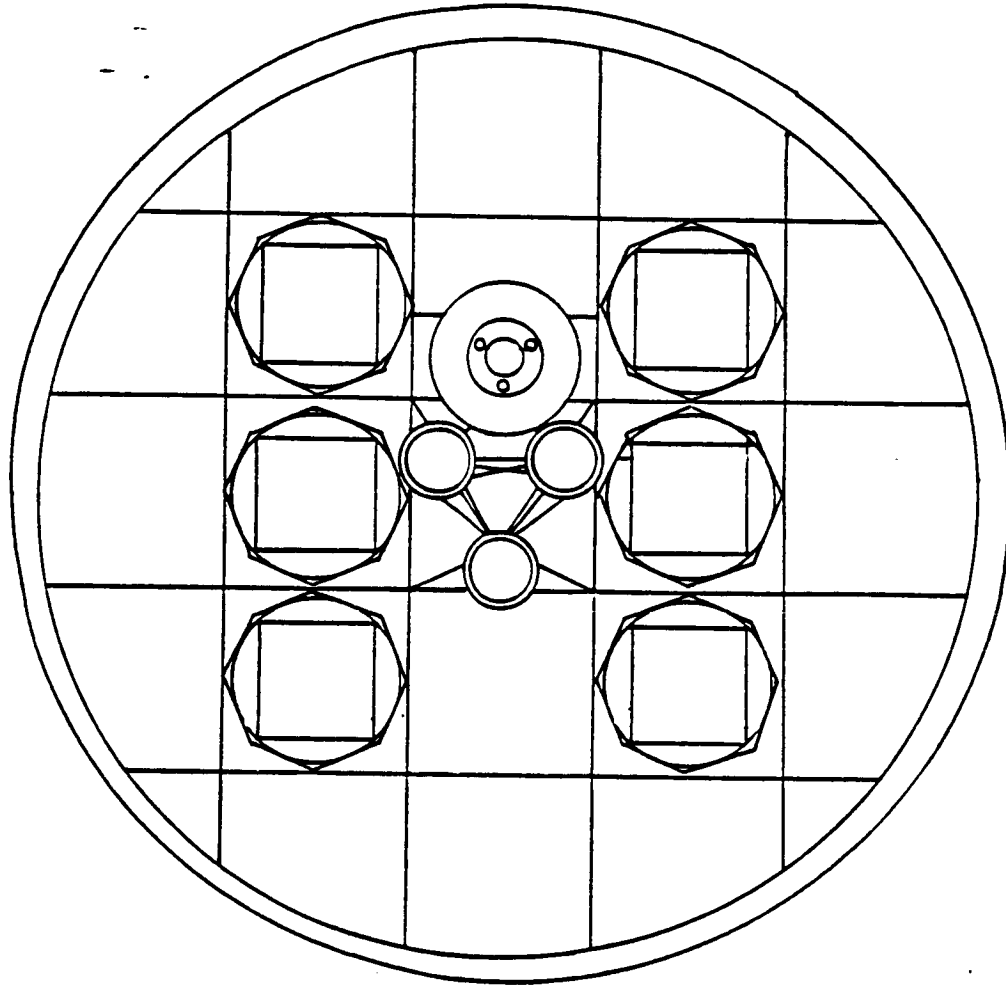
FIGURE 1.5.2

ISOMETRIC VIEW OF TAXI
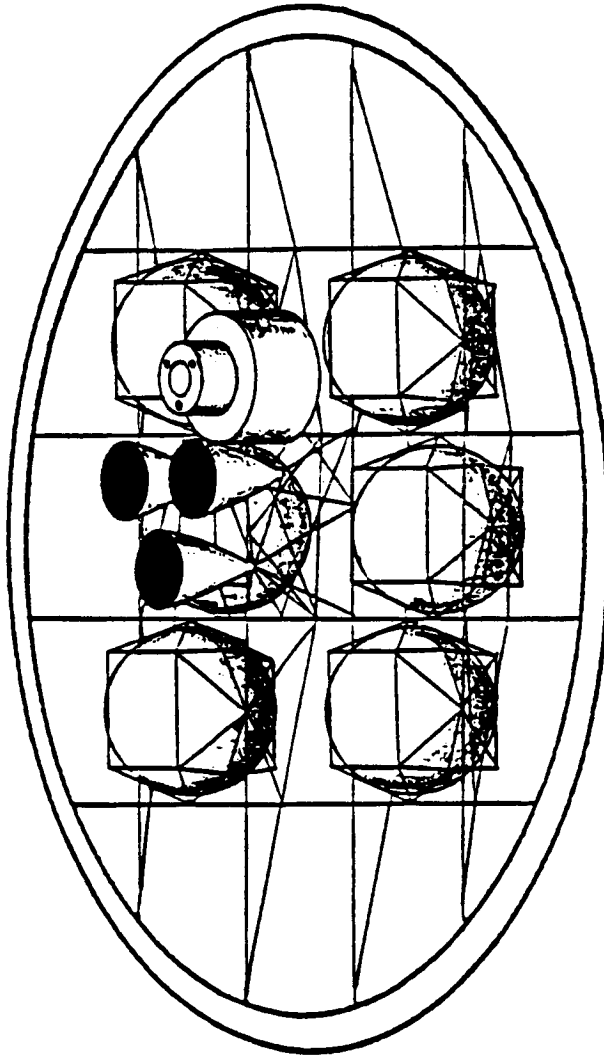
FIGURE 1.5.3

2. Trajectory Analysis

2.1 General Requirements and Criteria

According to our scenario for a series of missions to Mars, a transfer vehicle (TAXI) is needed to bridge the gap between the Cycling Spacecraft and planetary orbit. To improve the performance/propellant requirement characteristics of the TAXI, aerobraking capability is to be built into the craft in addition to rocket propulsion to maneuver the TAXI. Therefore, the trajectory to a planet from the Cycling Spacecraft and back to the Earth will make full use of aerobraking. More importantly, the trajectory must strike a balance between keeping travel time short and keeping the propellant needed to a minimum. The necessity to keep the required amount of propellant, and thus the TAXI mass, to a minimum was considered somewhat more important than keeping flight time to a minimum. These last two requirements call for a compromise which became a major consideration of the trajectory design.

2.2 Cycling Spacecraft Orbit

The Cycling Spacecraft and its trajectory around the sun were the subject of a design project at the University of Michigan (U. of M., 1987). The physical characteristics needed to plan for the approach trajectories to the planet appear in Table 2.2.1. Notice that at Mars the relative velocity is much greater than at the Earth. This places greater demands on the propellant at Mars than at Earth. The sphere of influence (SOI) is defined as a given distance from a planet beyond which its gravitational effects may be considered negligible. The TAXI trajectories and ΔV requirements presented in this chapter have been designed to match the nominal trajectory established at the University of Michigan. These trajectories and ΔV's have been used in defining the TAXI version B.

Table 2.2.1

Important Properties of the Cycling Spacecraft's Trajectory at the Planetary Spheres of Influence

	EARTH	MARS
Closest Approach to Surface	1000 km	16300 km
Velocity at the Sphere of Influence	5.98 km/sec	9.04 km/sec

The Cycling Spacecraft trajectory is an ellipse intersecting the orbits of both Earth and Mars which features a relatively short trip from Earth to Mars and a long trip back. This trajectory requires a course change about half way into its circuit so that the Cycling Spacecraft can meet the Earth at the end of each circuit. This trajectory was designed with the simplifying assumptions of circular co-planar orbits for Earth and Mars. The resultant requirements on the propulsion system of the Cycling Spacecraft are fairly accurate despite these assumptions.

2.3 Orbital Transfer Background

2.3.1 Assumptions

For the purpose of designing the following trajectories, certain assumptions were made: (1) the burn of a rocket engine was assumed to impart an instantaneous change in velocity, or delta V, on the TAXI and (2) the aerobraking was considered as an impulse 180 degrees from the velocity vector of the TAXI. Though the positions predicted with these assumptions will not be totally accurate, the propulsive requirements would be fairly accurate. A more thorough analysis using more sophisticated methods will be needed to lay out the physical appearance of the trajectories with a fair degree of accuracy. However, these methods do exist and will not pose a problem in the future.

2.3.2 Design Approach

The general classes of maneuvers needed to carry the TAXI between the Cycling Spacecraft and the destination orbit around the planet were the separation and rendezvous maneuvers with the Cycling Spacecraft, changing the plane of the TAXI orbit, and circularization into the destination orbit. These maneuvers can then be examined independently of a specific trajectory. The complete trajectories were then put together using the points at which the TAXI aerobraked or used engine thrust as points of connection. For the points in between the connection points the trajectories were known from Kepler's equations as presented in a standard text (Bate, Mueller and White, 1971).

The first class is the velocity change for both leaving and rendezvousing with the Cycling Spacecraft. This impulse can be found from considering only the difference in periapsis distance of both craft and the time the TAXI spends in the coast period between the Cycling Spacecraft and the planet (Friedlander, 1986). In leaving the Cycling Spacecraft, the TAXI makes a burn which puts it on an intercept course with a planet's atmosphere. This burn is a function of both the difference in periapsis distance (delta B) of the two trajectories and time spent coasting between separation and the TAXI's first aerobrake. Given that the TAXI can only aerobrake in a narrow band of altitudes above a planet's surface, the delta B of the Cycling Spacecraft and TAXI courses can be estimated for each planet. Therefore the impulse needed to separate from the Cycling Spacecraft is primarily a function of the time before the encounter with the atmosphere and thus can be plotted for each planet. The plot for Earth appears in Figure 2.3.1 and Mars in Fig. 2.3.2. For departure the important coast period is between the last boost and Cycling Spacecraft intercept. A feature of both of these plots is that the greater the distance and thus the coast time between

DELTA V AS A FUNCTION OF COAST PERIOD AT EARTH
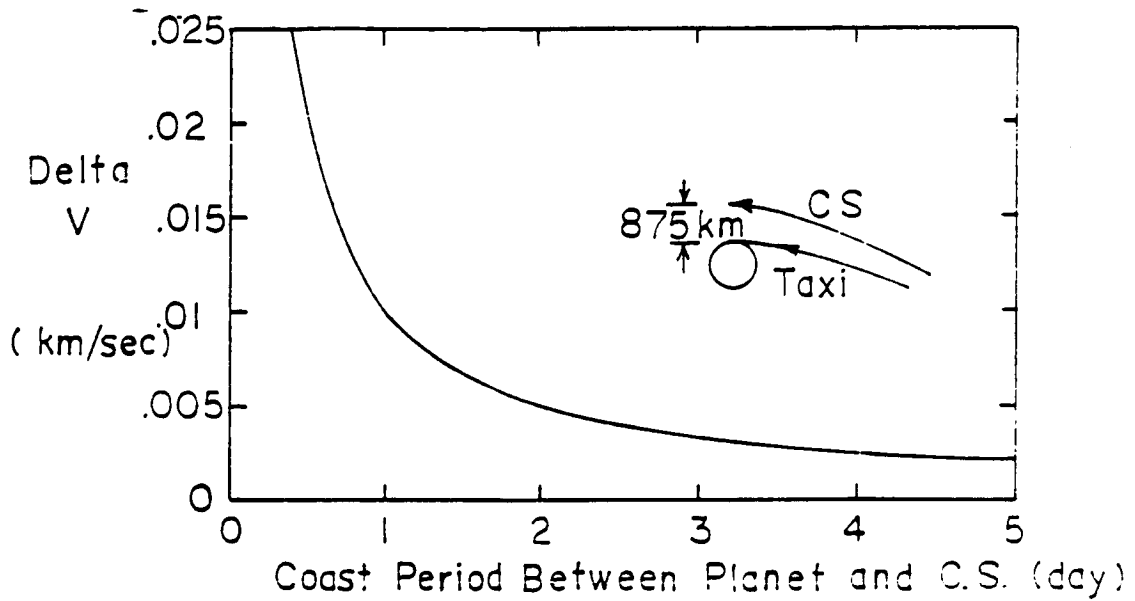
FIGURE 2.3.1

DELTA V AS A FUNCTION OF COAST PERIOD AT MARS

FIGURE 2.3.2

14
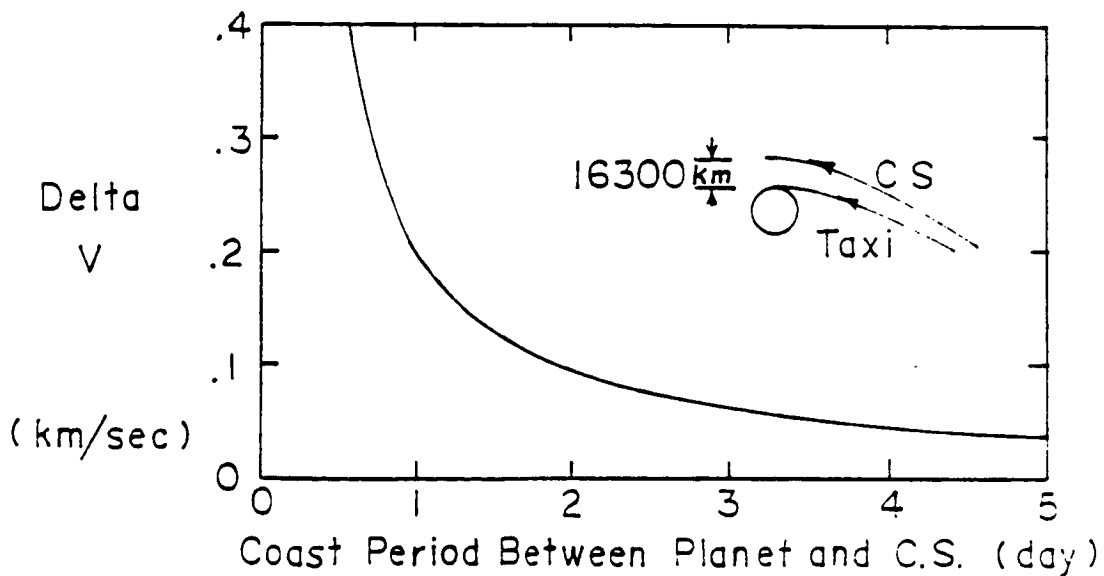
planet and the Cycling Spacecraft, the lower the impulse needed to effect the proper separation of trajectories. Another feature of the plots is that the change in the delta V requirements for a reasonable range of departure times is modest.

Another feature needed in the TAXI trajectories is changing the plane of its orbit so that it coincides with the plane of the target orbit around the planet. The Cycling Spacecraft passes by the planets in the plane of the ecliptic, yet the final destination orbits of the TAXI are inclined to the ecliptic a significant amount. The ecliptic is the plane in which the Earth orbits the sun. For the TAXI to end up in the orbit of Phobos at Mars it must incline its orbit 24 degrees. To get in the plane of the space station orbit at Earth the TAXI must change its inclination by a minimum of 6 degrees or a maximum of 53 degrees. The disparity between the numbers for Earth is caused by uncertainty concerning the orientation of the orbit of the Earth Space Station. For the purposes of design a plane change of 53 degrees was used. This plane change can most efficiently be done at the furthest point (apoapsis) of an elliptical orbit (Bate, 1971). Thus, the impulse to change orbit inclination is solely a function of the minimum and maximum points of that orbit. Figure 2.3.3 presents these results for Mars. The plane change impulse falls off exponentially with increasing apoapsis distance. The value for the minimum distance was kept constant since the plane change takes place after aerobraking or leaving Phobos orbit. The results for Earth using the minimum and maximum plane change needed differ only by a constant, which is the mass of the Earth. This is illustrated in the results for Earth which appear in Fig. 2.3.4.

2.4 TAXI Transfer Trajectories

The details of the trajectories decided upon as most useful for the TAXI mission fill the remainder of the report. The principle information needed from these orbits is the duration of flight, propellant needed, indicated in the form of a required delta V, and the deceleration needed from the aeroshield.

In addition to computing trajectories for the TAXI which are considered the best for the missions, an investigation was made to find out what off design trajectories would look like over a delta V range used by the TAXI. These results appear in various figures which show the delta V required for a given time of flight and trajectory geometry.

2.4.1 LEO to the Cycling Spacecraft

The drawing of the trajectory appears in Fig. 2.4.1. From low Earth orbit the TAXI will perform a delta-V burn which will place it in a highly elliptical orbit. At the orbit's apoapsis the TAXI will perform a burn which will change its orbit plane and enlarge the orbit so that at periapsis the TAXI is tangent with the orbit of the Cycling spacecraft. This last maneuver has the effect of drastically reducing travel time and also keeping the propellant required to a minimum. The plane change would take place at the end of a highly elliptical orbit so as to keep the plane change impulse as low as possible.

PLANE CHANGE DELTA V AT
APOAPSIS VERSUS DISTANCE

R_{min} = 3437 km   Plane Change = 24°

Delta V

(km/sec)

Apoapsis Distance
(Martian Radii)
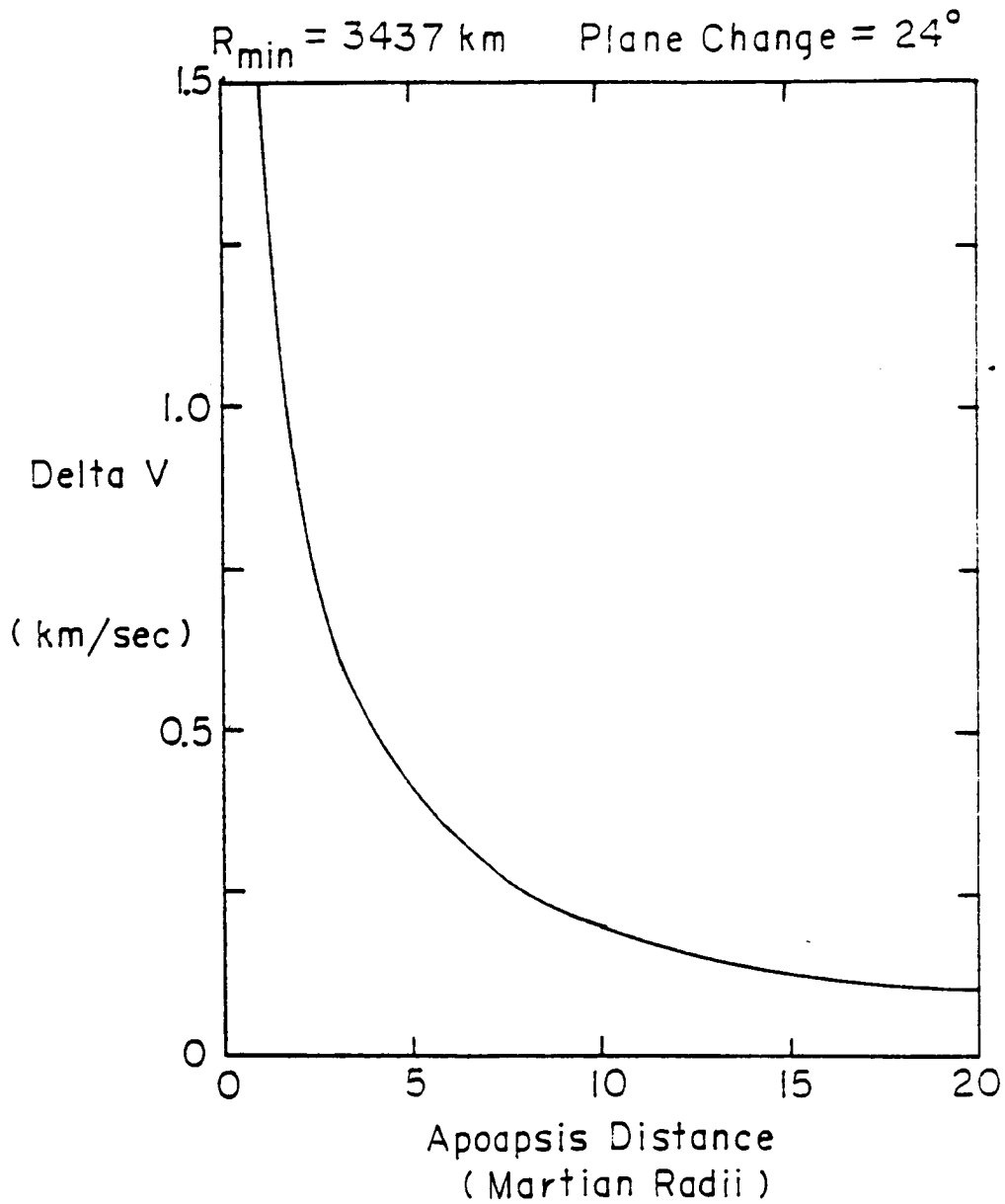
FIGURE   2.3.3

PLANE CHANGE DELTA V AT
APOAPSIS VERSUS DISTANCE

R_{min} = 6778 km

Delta V (km/sec)

Plane Change = 53°
Plane Change = 6°

Apoapsis Distance
(Earth Radii)
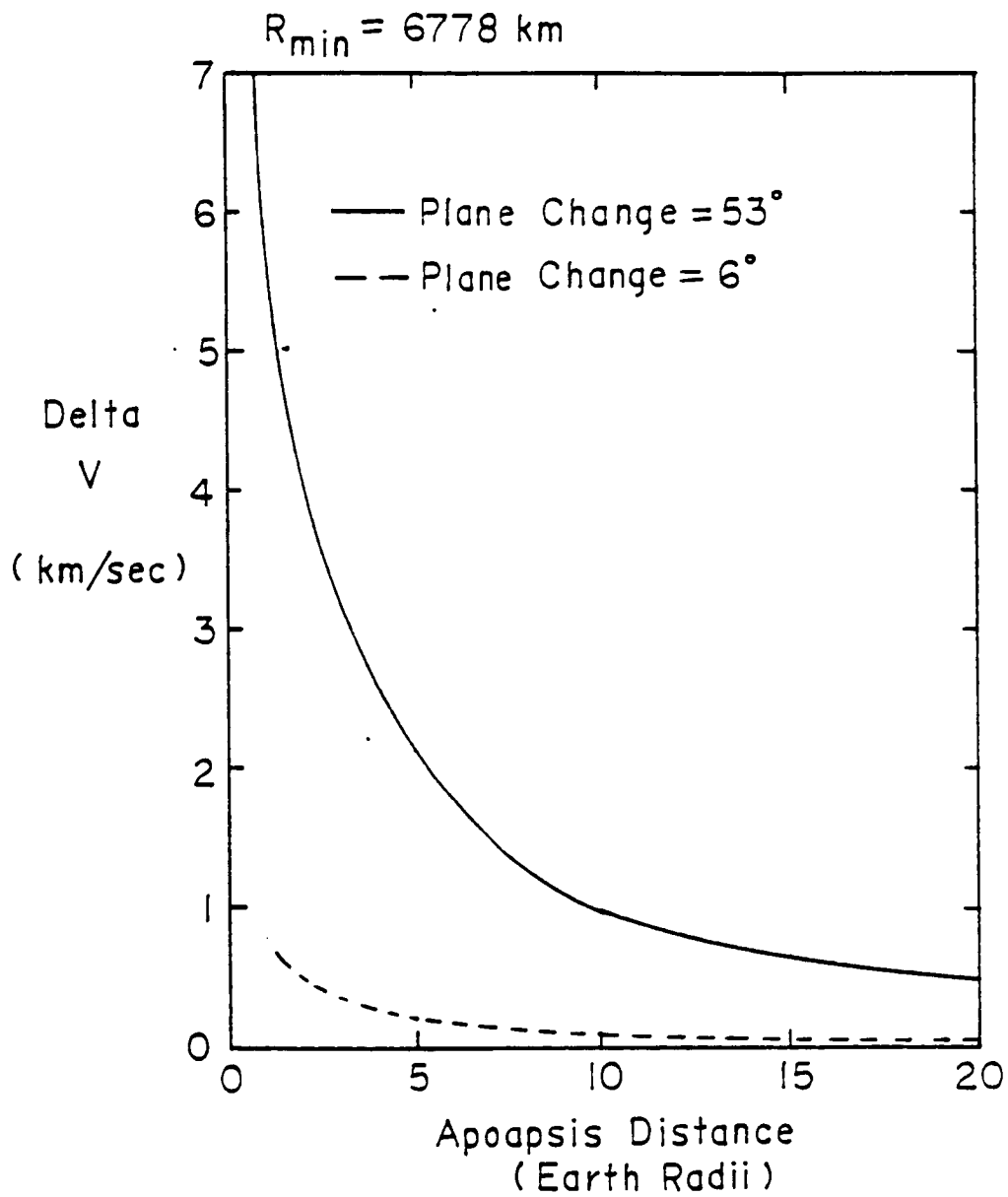
FIGURE 2.3.4

EARTH DEPARTURE TRAJECTORY SCHEMATIC

Low Earth Orbit Plane

Ecliptic Plane

Taxi

Earth Radii

LEO

Taxi

Taxi

Cycling Spacecraft

Rendezvous
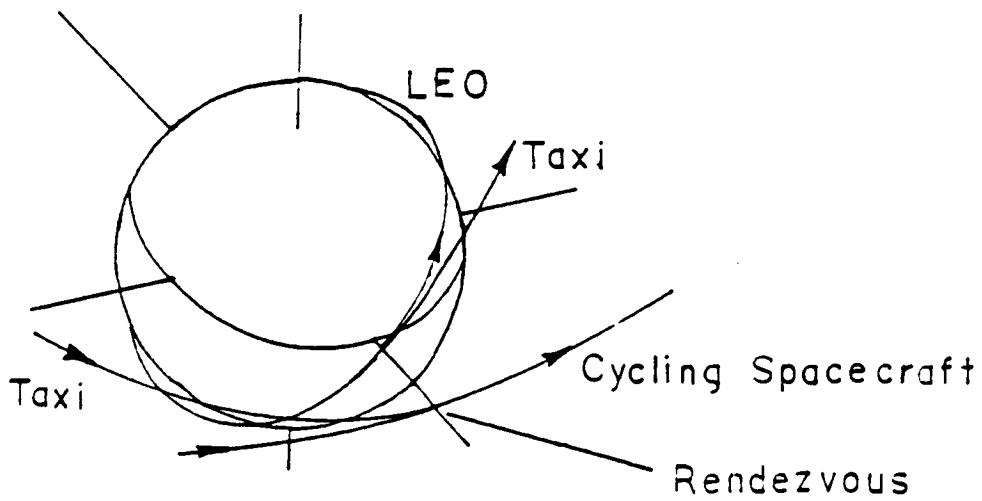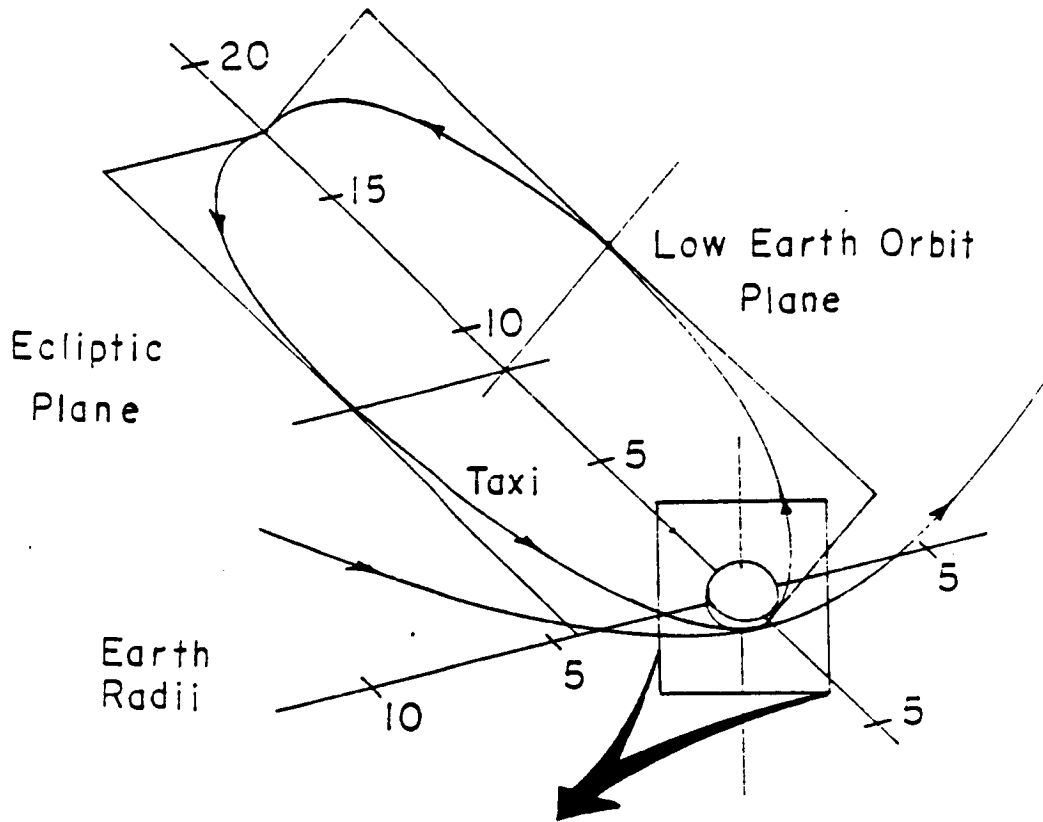
FIGURE 2.4.1

The cases were computed assuming a worst case plane change of 53 degrees, which represents the space station being completely out of phase with the TAXI. This phase relation is determined by the tilt of both the Earth and the plane of the Earth orbiting space station. The Earth is tilted 23 degrees to the ecliptic and the typical Space Shuttle orbit is tilted 28.3 degrees with the equator of the Earth. The tilts of these orbits could be against each other, so that the inclination of the station is only 6 degrees, or the tilts could be in the same direction, producing a space station inclination of 53 degrees. The resulting propulsive requirements for plane change vary widely. To be safe a plane change of 53 degrees was used for fuel requirement analysis.

The expected physical characteristics for a departure from low Earth orbit appear in Table 2.4.1. It provides a trip time of about 1.5 days and uses a delta V of 4.94 km/sec. An additional trajectory is given in Table 2.4.2 which shows the characteristics of a departure trajectory using a 10 percent increase in delta V over Table 2.4.1. The size of the trajectory is smaller and thus so is the trip time. The new time of flight is 14 hours. This means that if the TAXI is fueled for the greater of the two delta V capabilities it has a launch window of one day from the optimum time of launch to reach the Cycling Spacecraft.

A complete analysis of the Earth departure trajectory appears in Fig. 2.4.2. The variations in this trajectory are limited since the only variable that can change is the size of the plane change orbit. The savings in delta V drop off exponentially with increasing apoapsis radius of the plane change orbit. The trajectory in Table 2.4.1 represents the longest time of flight possible that still shows a noticeable savings in fuel. By increasing the delta V a fairly large launch window can be provided.

TABLE 2.4.1

Maneuver Schedule and Delta V Chart for the TAXI Mission From L E O to the Cycling Spacecraft

Comments	Delta V (km/sec)	Range (km)	Time (hour)	Orbit Angle to Ecliptic (deg)
Leaving LEO	2.853	6778	0.0	53.0
Plane Change	0.587	108430	19.1	0.0
Orbit Change to Meet Cycling Spacraft	0.0267	108430	19.1	0.0
Earth Exit Burn at Cycling Spacecraft	1.470	7378	38.4	0.0

Total Propulsive Delta V = 4.936 km/sec

TABLE 2.4.2

<u>Maneuver Schedule and Delta V Chart for the TAXI
Mission From L.E.O. to the Cycling Spacecraft</u>

<u>Comments</u>	<u>Delta V</u> (km/sec)	<u>Range</u> (km)	<u>Time</u> (hour)	<u>Orbit Angle to Ecliptic</u> (deg)
Leaving L.E.O.	2.556	6778	0.0	53.0
Plane Change	1.141	54213	7.36	0.0
Orbit Change to Meet Cycling Spacecraft	0.0489	54213	7.36	0.0
Earth Exit Burn at Cycling Spacecraft	1.766	7378	14.8	0.0

Total Propulsive Delta V = 5.512 km/sec

EARTH DEPARTURE DELTA V VERSUS ORBIT GEOMETRY

L.E.O. Radius 6778 km
Rendezvous Radius 7378 km

FIGURE 2.4.2

21
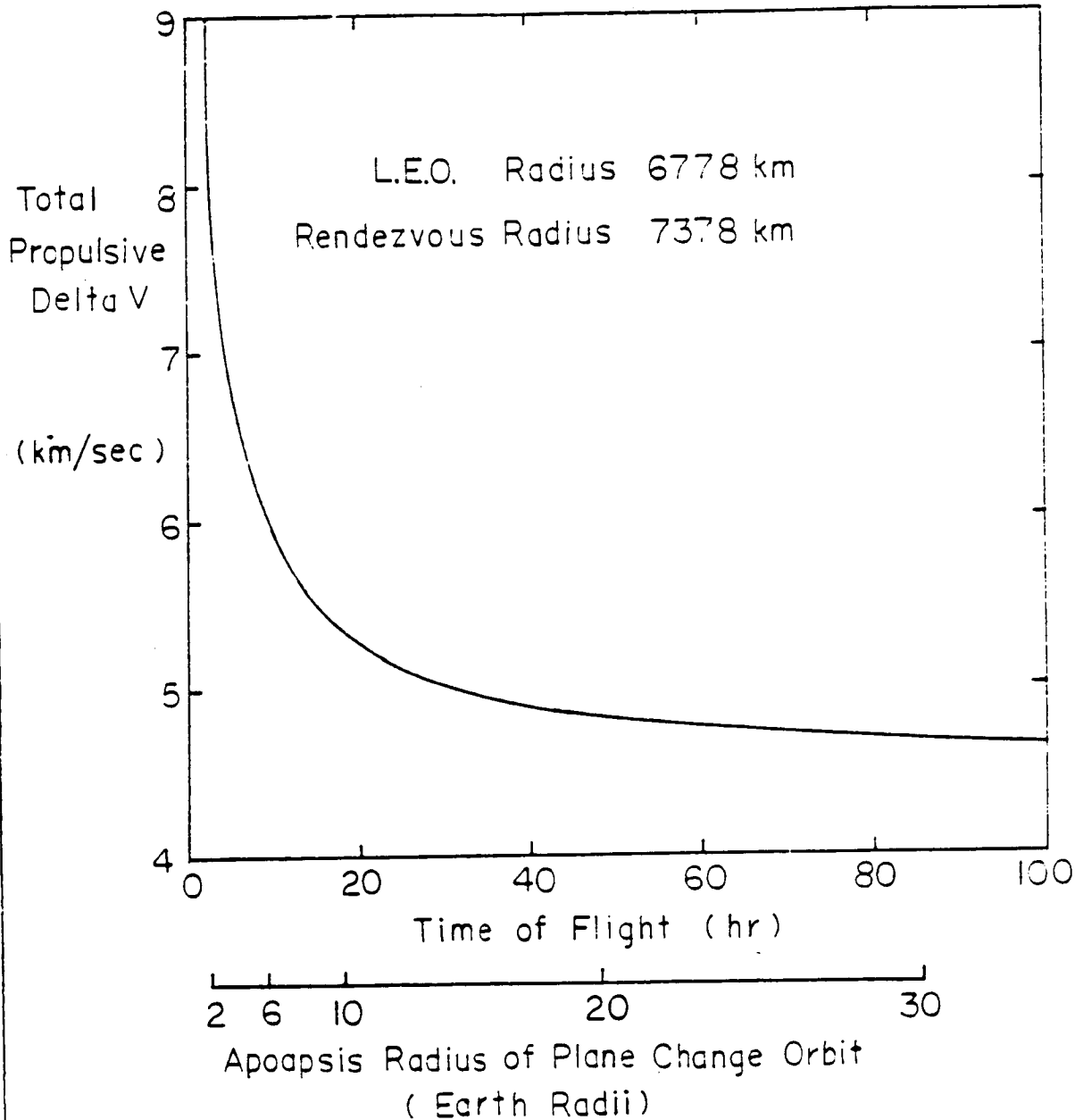
2.4.2 Cycling Spacecraft to Mars Transfer

The drawing of this trajectory appears in Fig. 2.4.3. The trajectory
calls for the first pass through the Mars atmosphere to decelerate the
TAXI enough to place it in a highly elliptical orbit. At the apoapsis
of this orbit the TAXI fires its engines to change the plane of its
orbit to that of Phobos. The second pass through the atmosphere
decelerates the TAXI enough so that the new elliptical orbit is tangent
at its furthest point to the orbit of Phobos. There, the TAXI will fire
again to circularize its orbit. The TAXI will then be in a position to
carry out intercept and rendezvous. Once at Phobos the TAXI can dock
with the fuel production facilities there and refuel.

The physical characteristics of several variations on the trajectory
appear in Tables 2.4.3 and 2.4.4. Table 2.4.3 represents the expected
characteristics of the arrival trajectory at Mars. Time of flight of
the TAXI to Phobos orbit is about 4.5 days and the delta V for the trip
is 0.77 km/sec. Table 2.4.4 illustrates the difference which an
additional 10% in delta V capability makes in the size of the trajectory
and the time of flight. The trip time falls by 37 hours, which would
mean that, in this state, the TAXI has a launch window to separate from
the Cycling Spacecraft of about 1.5 days.

A complete analysis of the Mars arrival trajectory appears in Fig.
2.4.4, which details the delta V to be used for a given orbit size and
coast period from the Cycling Spacecraft. The launch window for this
trajectory is almost totally determined by the coast period between
separation and the first aerobraking pass through the Martian
atmosphere. Thus if the TAXI is late that time must be made up in the
coast period. Though by increasing the size of the plane change orbit
the delta V penalty to be paid for the initial delay can be reduced.
The trajectory choice in Table 2.4.4 can be justified by the wide launch
window possible with a small increase in delta V used.

22

TABLE 2.4.3

Maneuver Schedule and Delta V Chart for the TAXI Mission from the Cycling Spacecraft to Mars

Comments	Delta V (km/sec)	Range (km)	Time (hour)	Orbit Angle to Ecliptic (deg)
Delta V Leaving the Cycling Spacecraft	0.0942		0.0	0.0
First Aerobraking Pass Entry V =10.33 km/sec	(5.457)	3437	48.0	0.0
Plane Change Delta V	0.102	67940	76.4	24.0
Second Aerobraking Pass Entry V=4.87 km/sec	(0.60)	3437	104.9	24.0
Circularizing Delta V	0.571	9380	107.0	24.0

Total Propulsive Delta V = 0.768 km/sec

( ) Refers to an Aerobraking Maneuver

Table 2.4.4

Maneuver Schedule and Delta V Chart for the TAXI Mission from the Cycling Spacecraft to Mars

Comments	Delta V (km/sec)	Range (km)	Time (hour)	Orbit Angle to Ecliptic (deg)
Delta V Leaving the Cycling Spacecraft	0.151		0.0	0:0
First Aerobraking Pass Entry V=10.33 km/sec	(5.496)	3437	30.0	0.0
Plane Change Delta V	0.136	50955	48.9	24.0
Second Aerobraking Pass	(0.562)	3437	67.8	24.0
Circularizing Delta V	0.571	9380	70.0	24.0

Total Propulsive Delta V = 0.857

( ) Refers to an Aerobraking Maneuver

MARS ARRIVAL TRAJECTORY SCHEMATIC

Ecliptic Plane

16

12

Phobos Orbit Plane

8

4

4

Martian Radii

8

4

Taxi

4

Cycling Spacecraft
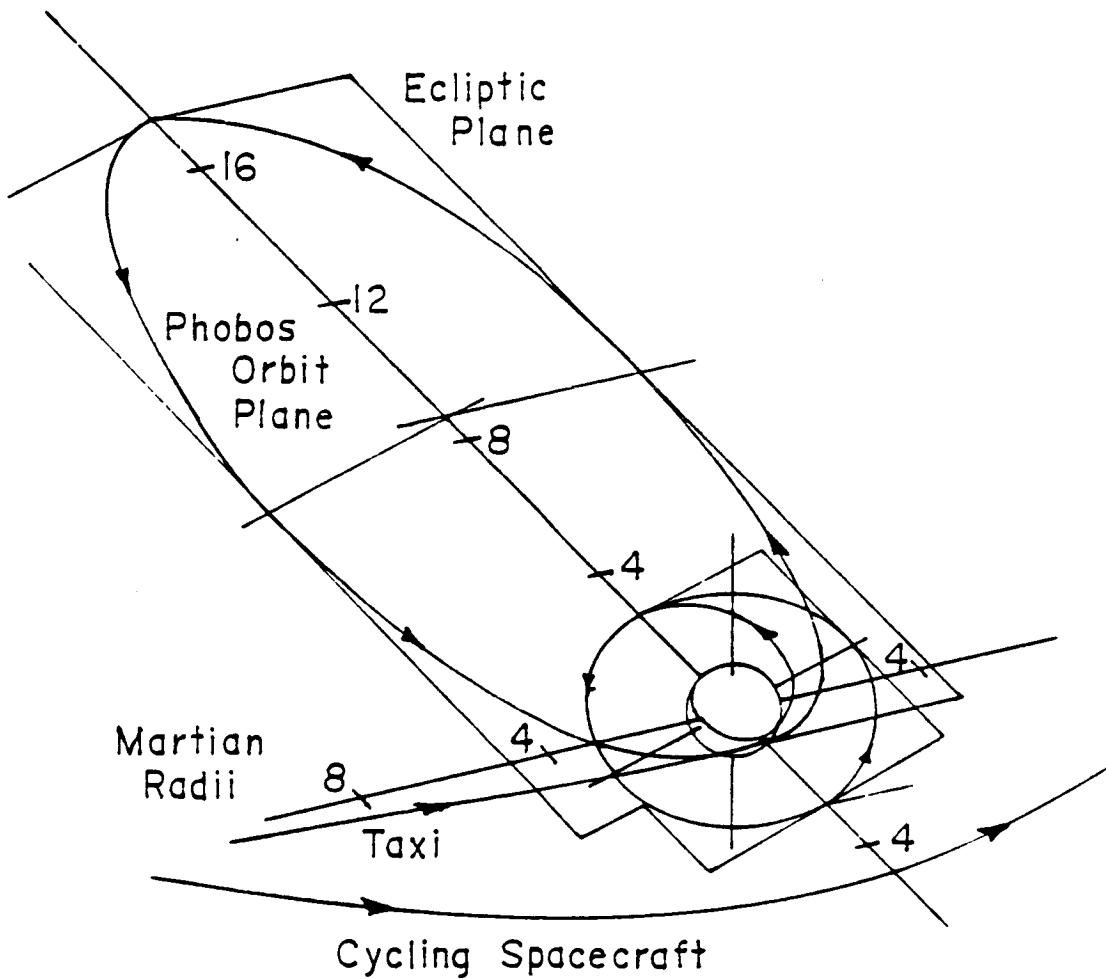
FIGURE 2.4.3

MARS ARRIVAL DELTA V VERSUS
TIME OF FLIGHT
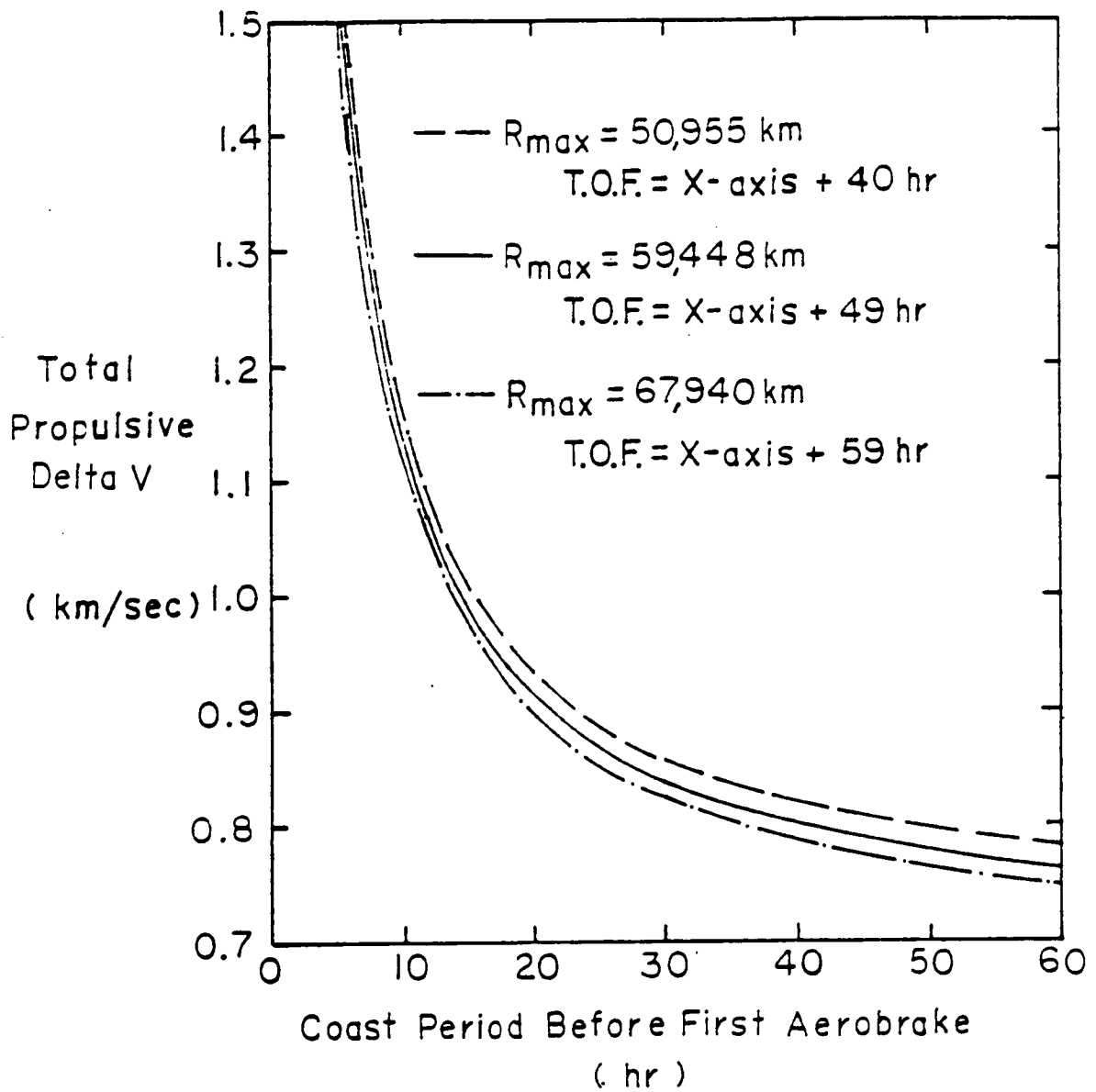
FIGURE 2.4.4

2.4.3 Mars to Cycling Spacecraft

Figure 2.4.5 presents the general trajectory for departure from Mars. The TAXI would leave from Phobos and go into a highly elliptical orbit. At the apoapsis of this orbit the TAXI will fire its engines to change the orbit plane from that of Phobos's orbit to that of the ecliptic. A delta V maneuver will also take place minutes later to change the orbit so that the TAXI can make a non-aerobraking close approach to Mars to build up speed by and reduce the delta V needed to escape from the Mars system (Edelbaum, 1967). The delta V to leave the Mars system will be performed at Martian close approach. After a period of coasting the trajectory of the TAXI will cross the trajectory of the Cycling Spacecraft. At this point of intersection the TAXI will make a small propulsive burn to match orbits with the Cycling Spacecraft. The TAXI will then maneuver to dock and transfer its crew to the quarters of the Cycling Spacecraft.

Table 2.4.5 presents the expected characteristics of a departure trajectory from Mars. The time of flight is about four days and the total delta V is 6.62 km/sec. The TAXI is expected to carry an additional ten percent delta V of fuel to provide a cushion against malfunctions. Table 2.4.6 shows a trajectory which makes use of this additional fuel. The new trip time is only 29 hours for a total delta V of 7.2 km/sec. The TAXI would thus have a launch window of about three days (compare transfer time in Tables 2.4.5 and 2.4.6).

The results of a more detailed analysis of the Mars departure trajectory appear in Fig. 2.4.6. The total delta V as a function of orbit size and coast period to the Cycling Spacecraft is given. It shows that as the time of flight increases the delta V to reach the Cycling Spacecraft decreases but the savings become smaller as the time of flight gets larger.

Table 2.4.5

Maneuver Schedule and Delta V Chart for the TAXI
Mission from Mars to the Cycling Spacecraft

Comment	Delta V (km/sec)	Range (km)	Time (hour)	Orbit Angle to Ecliptic (deg)
Leaving Phobos Orbit	0.673	9380	0.0	24.0
Plane Change	0.185	59450	26.9	0.0
Orbit Change to Effect Close Mars Approach	0.159	59450	26.9	0.0
Mars Exit Burn	5.510	3547	50.4	0.0
Rendezvous Burn	0.0936		98.4	0.0

Total Propulsive Delta V = 6.620 km/sec

Table 2.4.6

Maneuver Schedule and Delta V Chart for the TAXI
Mission from Mars to the Cycling Spacecraft

Comment	Delta V (km/sec)	Range (km)	Time (hour)	Orbit Angle to Ecliptic (deg)
Leaving Phobos Orbit	0.448	9380	0.0	24.0
Plane Change	0.397	25478	9.68	0.0
Orbit Change to Effect Close Mars Approach	0.311	25478	9.68	0.0
Mars Exit Burn	5.680	3547	17.0	0.0
Rendezvous Burn	0.374		29.0	0.0

Total   Propulsive   Delta   V   =   7.21   km/sec

MARS DEPARTURE TRAJECTORY SCHEMATIC

Phobos Orbit
Plane

16

12

8

Rendezvous

Ecliptic
Plane

Phobos
Orbit

4

Taxi

Martian
Radii

8

4

4

Cycling Spacecraft
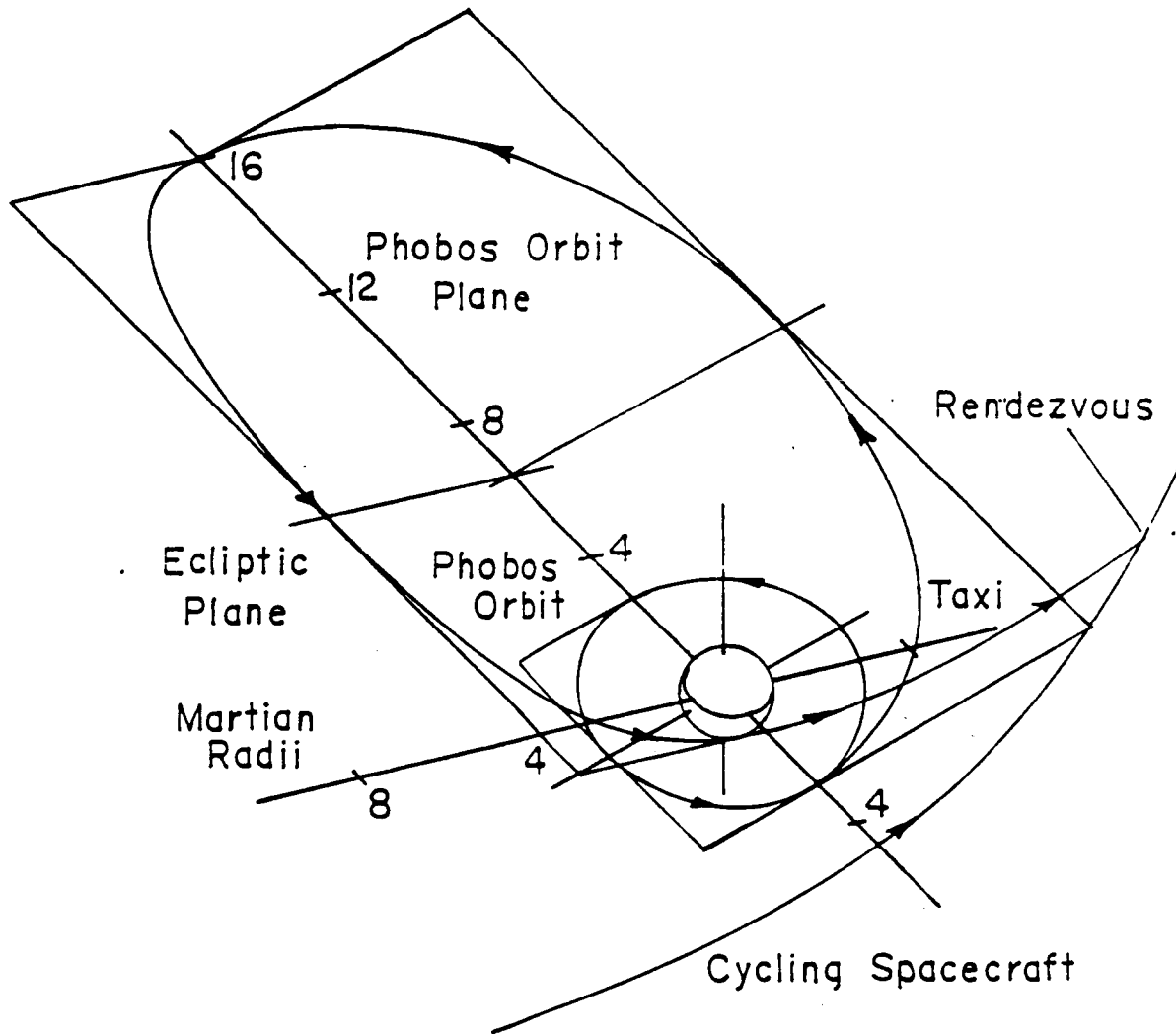
FIGURE 2.4.5

MARS DEPARTURE DELTA V VERSUS ORBIT GEOMETRY
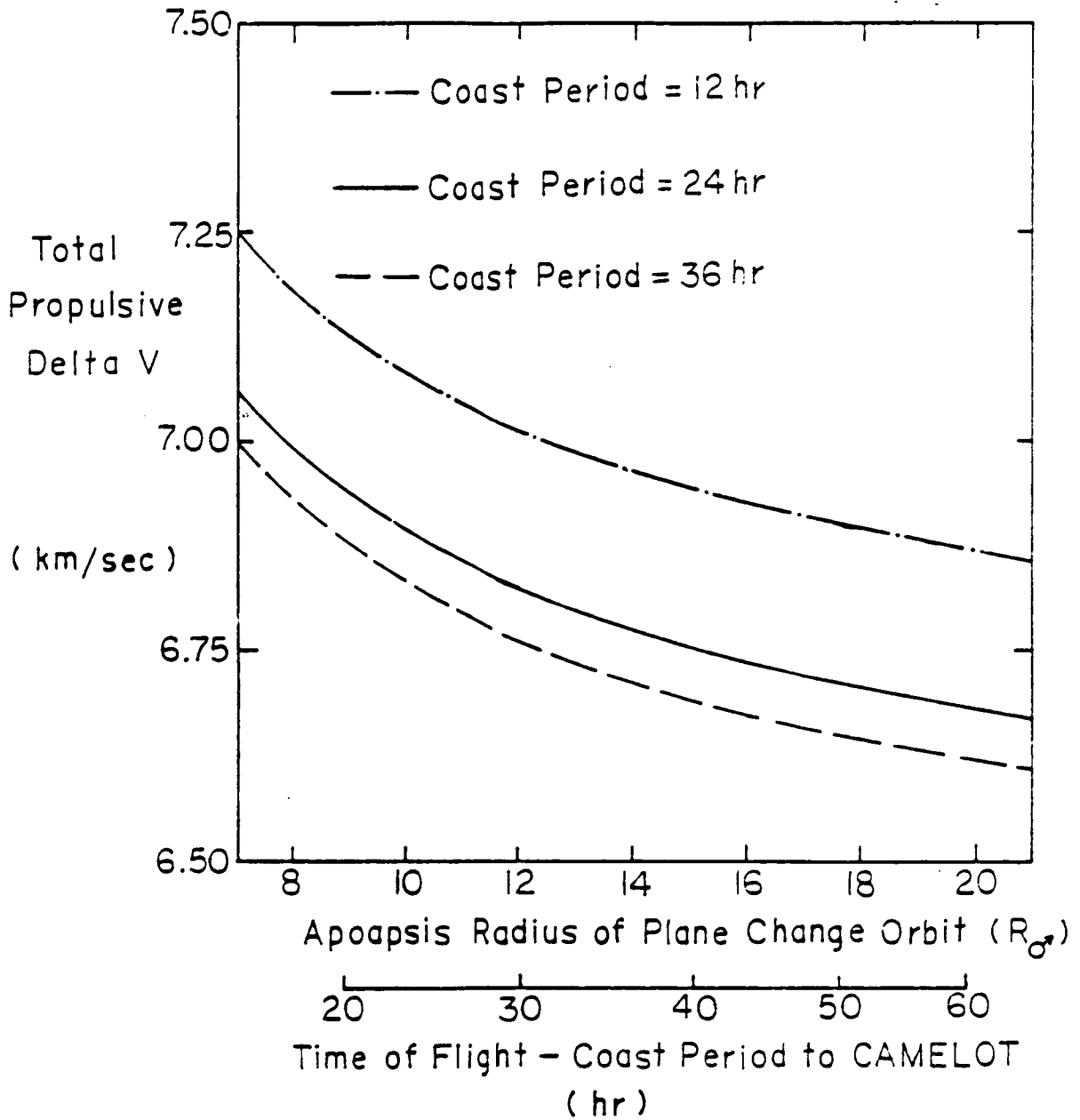
FIGURE 2.4.6

2.4.4 Cycling Spacecraft to Low Earth Orbit

The arrival at Earth would constitute one complete cycle of the TAXI. The trajectory drawing appears in Fig. 2.4.7. The trajectory is of the same type as that of the arrival trajectory for the TAXI at Mars. The TAXI first aerobrakes to become captured in the Earth's gravity. The orbit becomes highly elliptical and at the furthest point of the ellipse the TAXI changes plane. The second aerobrake puts the TAXI on a Hohmann transfer to low Earth orbit. At the right altitude the TAXI circularizes its orbit and prepares for rendezvous.

The physical characteristics of the optimal trajectory appear in Table 2.4.7. Another trajectory, which appears in Table 2.4.8 shows that by increasing the delta V capability of the TAXI by about 30 percent, a 60 percent reduction in the time of flight can be achieved. A more detailed analysis of the possible range of delta V and trip times appear in Fig. 2.4.8. This figure shows that it is more economical, in terms of delta V, to reduce the coast period rather than to reduce the plane change orbit's apoapsis to make up for any delay from the time of optimum departure from the Cycling Spacecraft. One could tailor a mission to the amount of available propellant by using this figure.

Table 2.4.7
Maneuver Schedule and Delta V Chart for the TAXI
Mission from the Cycling Spacecraft to Earth

Comments	Delta V (km/sec)	Range (km)	Time (hour)	Orbit Angle to Ecliptic (deg)
Delta V Leaving the Cycling Spacecraft	0.0052		0.0	0.0
First Aerobraking Pass Entry V=12.6 km/sec	(1.817)	6478	48.0	0.0
Plane Change Delta V	0.559	111615	67.8	53.0
Second Aerobrake Pass Entry V=10.8 km/sec	(2.85)	6478	87.7	53.0
Circularizing Delta V	0.0873	6778	88.4	53.0

Total Propulsive Delta V = 0.651 km/sec

( ) Refers to an Aerobraking Maneuver

Table 2.4.8
Maneuver Schedule and Delta V Chart for the TAXI
Mission from the Cycling Spacecraft to Earth

Comments	Delta V (km/sec)	Range (km)	Time (hour)	Orbit Angle to Ecliptic (deg)
Delta V Leaving the Cycling Spacecraft	0.021		0.0	0.0
First Aerobraking Pass Entry V=12.6 km/sec	(1.93)	6478	12.0	0.0
Plane Change Delta V	0.774	79725	24.4	53.0
Second Aerobrake Pass Entry V=10.8 km/sec	(2.74)	6478	36.7	53.0
Circularizing Delta V	0.0873	6778	37.5	53.0

Total Propulsive Delta V = 0.882 km/sec

( ) Refers to an Aerobraking Maneuver

References

Bate, Mueller and White, "Fundamentals of Astrodynamics", Dover Publications Inc.,New York, N.Y., 1971

Edelbaum, T., N., How Many Impulses; Astronautics and Aeronautics, Nov 1967

Friedlander, A. L.,Niehoff, J. C.,Byrnes, D. V.,Longuski, J. M., Circulating Transportation Orbits Between Earth and Mars, AIAA 86-2009

Hoffman, S. J., A Comparison of Aerobraking and Aerocapture Vehicles for Interplanetary Missions, AIAA paper 84-2057

University of Michigan Aerospace Design Class, Final Report on CAMELOT, Chapter 2, et al

Walberg, G.,D, 'A Survey of Aeroassisted Orbit Transfer', Journal of Spacecraft and Rockets, Vol 22, No 1, Jan-Feb 1985

EARTH ARRIVAL TRAJECTORY
SCHEMATIC
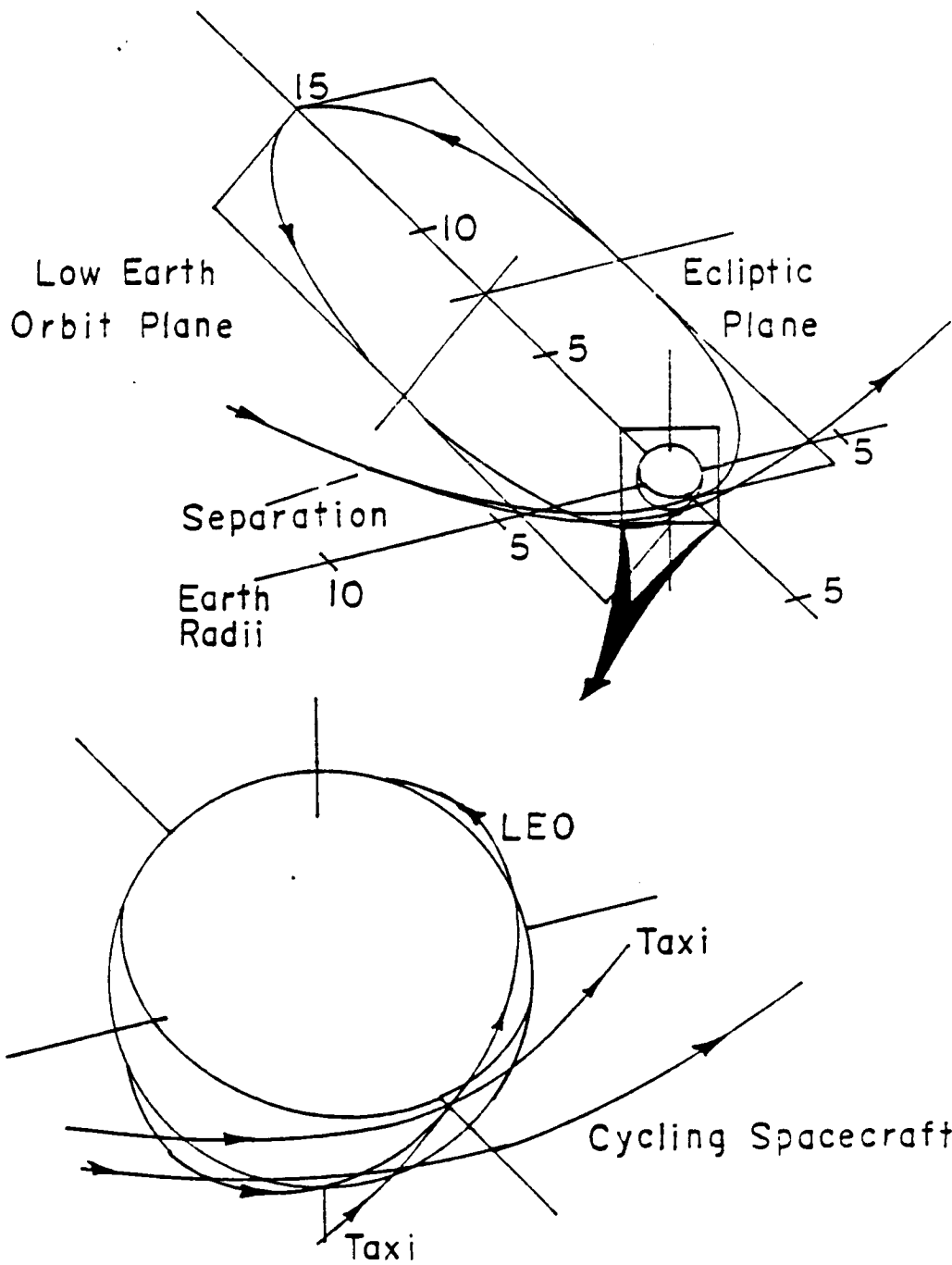
FIGURE 2.4.7

EARTH ARRIVAL DELTA V VERSUS TIME OF FLIGHT
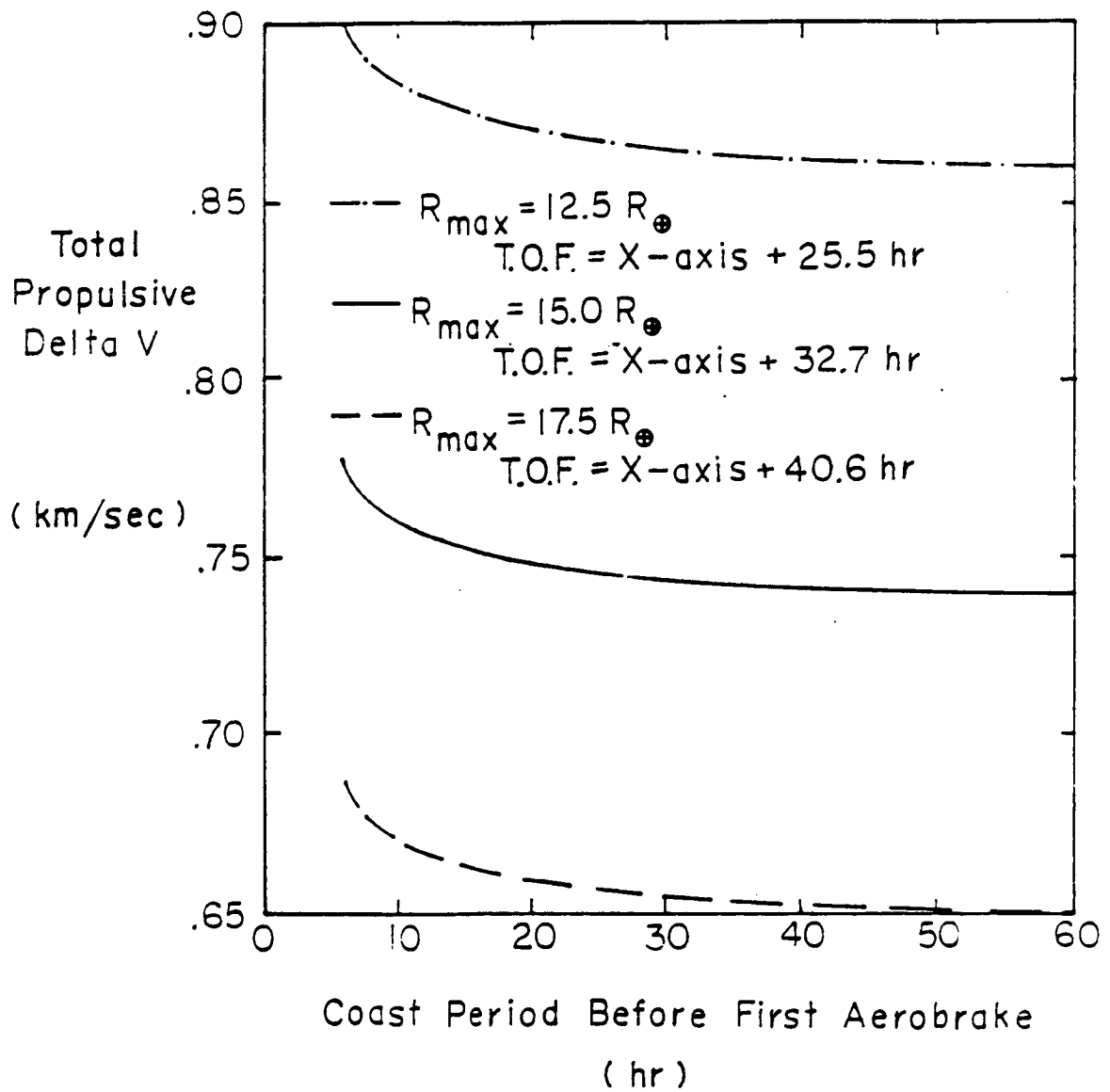
FIGURE 2.4.8

3. Propulsion

3.1 Propulsion System Design Criteria

The TAXI vehicle will have to match the orbit of the Cycling Ship (CS) traveling at very high velocities. Since the transfer time must not exceed one week and for the most part is kept to a few days, the TAXI vehicle needs to have a high acceleration, 1-5 g's, and a high thrust to weight ratio. A significant acceleration is also needed to reduce gravity induced velocity losses because the propulsive maneuvers are all within gravity fields. The velocity increments needed range from several feet per second to 18076 ft/s (5.51 km/s) depending on the burn. In order to cover all required delta V's, the propulsion system must be both versatile and reusable. The reusability must extend over a fifteen year period and be capable of carrying out five or six missions. Any maintenance required during the system's lifetime will be made easier by a modular design where feasible.

In order to achieve the best performance possible, the engine system must have a high specific impulse in order to have reasonable payload ratios. High thrust is also a premium consideration because of the time constraints and the velocity requirements. Altogether, safety, versatility (meeting a range of delta V's), reusability, modularity and reliability dictate the design of the propulsion system.

The assumption of having fuel production at Mars is critical to the design of the propulsion system. The feasibility of producing hydrogen and oxygen at both Mars surface and Phobos has been documented. Figure 3.1.1 shows the payload ratio penalties for the nonrefueling case versus the refueling at Mars scenario. Because the TAXI is to be used for multiple missions, the amount of fuel required at Earth becomes prohibitive if refueling facilities are not available at Mars. Both cost and size of the TAXI can be minimized with refueling capabilities.

3.2 Propulsion System Alternatives

Three types of propulsion systems are considered for the TAXI vehicle: electric, nuclear, and chemical. Exotic systems such as anti-matter propulsion and mass drivers are discounted immediately because of inadequate technology available within the next 20 to 30 years. After examining each system, a liquid chemical rocket is found to best meet the design criteria.

Electrical Rockets

Electrical rockets, although producing very high specific impulses (Isp's), have very low thrust-to-weight ratios and are limited to very low accelerations. Thus, electrical rockets are good for continuously accelerating over long periods of time in order to reach a necessary velocity increment. For the TAXI's required mission times, electrical rockets could not provide the acceleration necessary to achieve the needed velocity increment in the short time span.

Payload ratio vs Delta V (Isp=485 sec)

Refueling vs Nonrefueling Cases

Payload Ratio

Delta V (ft/sec)
(Thousands)

△ Refueling At Mars

◇ Nonrefueling Case
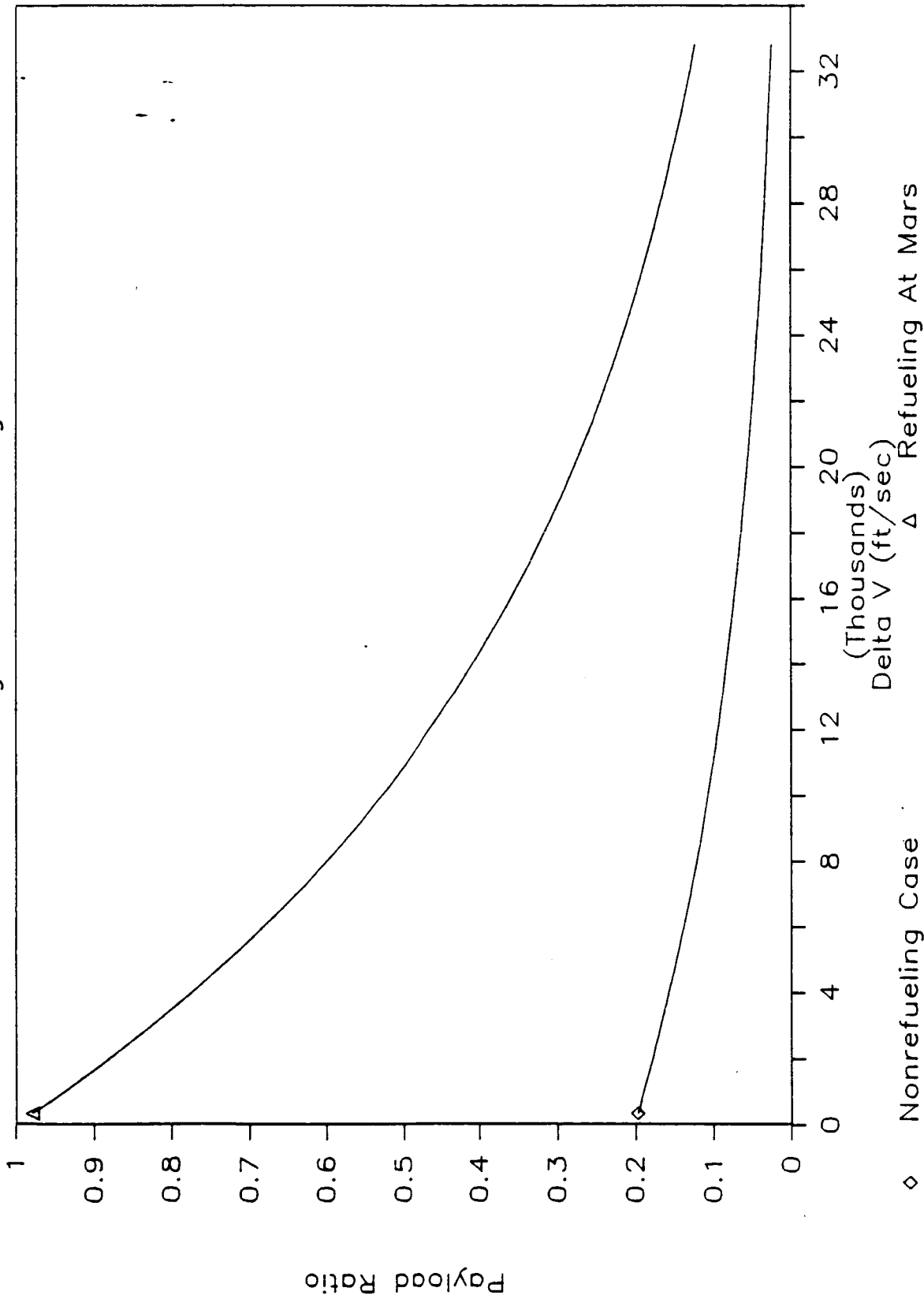
FIGURE 3.1.1

Nuclear Rockets

Nuclear propulsion systems can be broken up into four general types: solid core rockets, liquid core rockets, gaseous core rockets, and fusion rockets. In light of probable technological developments in the next 20 to 30 years, only a solid core nuclear rocket is considered for the TAXI.

Solid core nuclear rockets provide specific impulses on the order of twice that of chemical rockets and therefore can provide better payload ratios. The thrust to weight ratios of nuclear rockets are comparable to that of the chemical systems so that the mission requirements could be met by either of the systems. Although the nuclear rocket may produce better performance than the chemical rocket, at the same time nuclear rockets have some fairly troublesome disadvantages. The principle drawback of a solid-core nuclear rocket is the impact of neutron and gamma-ray radiation on the vehicle and its payload. There are four different ways radiation can compromise the feasibility of a nuclear rocket:

1. Engine components in or near the reactor can overheat from absorbed radiation energy.
2. Neutron and gamma-ray integrated flux during a mission can result in prohibitive radiation damage to sensitive engine or avionics components.
3. Energy deposition in the propellant can lead to boiloff or to pump-inlet boiling, especially in the case of liquid hydrogen propellant.
4. The total radiation dosage to the payload, particularly if manned, can be unacceptable.

A further problem with nuclear rockets is the problem with politics in that there is not much public support for nuclear development. Accordingly, although a solid-core nuclear rocket looks attractive in terms of performance parameters, problems with radiation shielding coupled with a negative public reaction to nuclear reactors in space make this system unattractive for development in the near future.

Chemical Rockets

Chemical rockets provide high thrust to weight ratios but do not have the specific impulse of nuclear or electric rockets. Of the chemical systems available only liquid cryogenic propellants provide energetic enough fuels to produce an Isp which yields a respectable payload ratio.

The propellant combination which provides the highest energy content without being overly toxic, volatile or corrosive is liquid hydrogen (LH2) and liquid oxygen (LOX). Tri-propellant and hybrid systems give comparable or better Isp's, but the gain in Isp in these cases does not justify adding complexity nor additional cost to the propulsive system. For bi-propellant combinations, hydrogen-flourine and hydrogen diflouride combinations give the best Isp's. However, flourine is extremely caustic and corrosive as well as very expensive. Oxygen, though it does not give the highest Isp, compensates in terms of safety and expense. Thus, in short, the best propellant which combines

performance with safety and practicality considerations is LH2-LOX. LH2-LOX systems will be technologically developed close to perfection by the year 2020. Accordingly, the LH2-LOX TAXI propulsion system will be close to fail_safe for the operational times proposed.

3.3 Primary Engine System Selection and Design

General performance analysis and engine system selection presented here center on the TAXI version B designed for transfer trajectories matching the nominal Cycling Ship trajectory (University of Michigan, 1987). Also given are engine data and parameters determined for the propulsion of the TAXI version A. The subsequent sections dealing with combustion chamber and nozzle design pertain to the TAXI version A.

3.3.1 General Performance Analysis

The engine system used on the TAXI vehicle will be designed for a broad range of conditions. The propellant tanks are designed for conditions of maximum trip duration and maximum velocity. These conditions occur on the return trip from Mars back to Earth, which requires a total velocity increment of 23,851 ft/sec (7.27 km/sec). The weight of the ship, including fuel, for this trip is 350,822 lbm. In order to meet the time/velocity requirements of the transfer, the total engine thrust should be in the range of 600,000 to 700,000 lbf. To acquire this thrust a system of three engines each producing 220,000 lbf design thrust has been chosen. It seems reasonable to expect that within one to two decades, throttling capabilities will be 40% to 120%. The minimum throttle needed for our TAXI will be around 40% of the design thrust. Thus the least amount of thrust that the engine system can deliver is the case of one engine at 40%. This minimum value is important in analysis of small velocity increments at times when the TAXI vehicle is nearing completion of the mission and the weight is at a minimum. Due to structural and human limitations the engine system will be constrained to producing no more than a 5 g acceleration. The constraint on burn time due to turbopump charging and chamber pressure build up also requires that the thrust be at a minimum in some phases of the mission.

Thrust Chamber and Propellant Thermochemistry

A preliminary analysis of the thrust chamber and nozzle design is found in sections 3.3.2 and 3.3.3. The important design parameters from that analysis are:

Combustion Stagnation Pressure	2600.0 psia
Chamber Throat Area	42.3 in²

A thermochemical evaluation of the combustion process of LOX-LH2 propellants reveals that an Isp of 485 seconds can be achieved at the design pressure of 2600 psia. Isp is associated with equivalent exhaust velocity:

$$Ueq = 15,602 \text{ ft/sec}$$

The above Isp can be attained provided the combustion process yields a chamber temperature of 6700 R. This value of combustion temperature is slightly above current temperatures used for design of rocket chambers. It is assumed that advances in materials technology and advanced heat transfer methods will allow for this rise in chamber temperature. Section 3.3.2 discusses materials such as nickel and copper alloys with certain liners which will provide higher temperature capabilities.

Thermochemistry also yields an average value for propellant molecular weight MW = 13.5 and a specific heat ratio k = 1.2 in the combustion chamber. The thermochemical calculations are provided by NOTS thermochemistry program (Perini, 1986; appendix 10.3.1). These values can now be used to calculate the characteristic velocity C^* of the rocket engine:

$$C^* = 7801 \text{ ft/sec}$$

The mass flow rate at a design thrust level, corresponding to combustion pressure of 2600 psia, is obtained as

$$\dot{m} = 453.6 \text{ lbm/sec}$$

A preliminary analysis of the nozzle design can be found in section 3.3.3. Some of the design parameters that will be used in this section are listed below:

Throat area	$A^* = 42.3 \text{ in}^2$	
Area ratio	$A_e/A^* = 176$	
Nozzle exit area	$A_e = 51.7 \text{ ft}^2$	
Nozzle pressure ratio	$P_o/P_e = 2500$	
Exit pressure	$P_e = 0.96 \text{ psia}$	

The thrust coefficient calculated from the given chamber and nozzle data is

$$C_T = 2.0$$

and the engine design thrust is

$$T = 220,000 \text{ lbf}$$

The overall engine parameters are summarized in Table 3.3.1. Tables 3.3.2 and 3.3.3 show fuel requirements, thrust levels and burn time for each phase of trajectory maneuvers.

Table 3.3.1 Main Engine Parameters (TAXI B)

Thrust   220,000 lbf
Specific Impulse, Isp   485 sec
Propellant: Oxidizer   LOX
           Fuel   LH2
           Mixture ratio   6

           Mass flow rate, $\dot{m}$ 453.6 lbm/sec
Combustion Pressure, P_o 2600 psia

Combustion Temperature, T_o 6700 R

Characteristic Velocity, C^* 7801 ft/sec
Thrust Coefficient, C_T 2

Throat Area, A^* 42.3 in²
Exit Area, A_e 51.7 ft²

Nozzle Length (from throat), L   10.65 ft
Operational Characteristics: Throttleable 40%-100%
                                               Reusable
                                               Gimbal Angle ± 11°

Table 3.3.2 Fuel Requirements, Thrust Levels and Burn Times (TAXI B)
LEO to Cycling Ship/Cycling Ship to MOS

Total ΔV required	19,753	ft/sec
Vehicle total initial mass	271,980	lbm
LOX/LH2 propellant mass	206,860	lbm
Vehicle mass without LOX/LH2	65,120	lbm

Phase	ΔV ft/sec	LH2/LOX Propellant Required lbm	Post Burn Mass lbm	# Engine/ Throttle	Total Thrust lbf	Burn Time sec
Leaving LEO	9360.2	122,701	149,278	3/100%	660,000	90.2
Plane change	1925.9	17,334	131,944	2/80%	352,000	23.9
Orbit change	88.6	ΔV achieved by using orbital correction engines				
Earth exit burn	4822.8	35,083	96,861	3/100%	660,000	25.8
Leaving CS	1236.4*	7,379	89,482	1/90%	198,000	18.1
Plane change	446.1*	2,522	86,960	1/40%	88,000	13.9
Circular-ization	1873.4	9,839	77,121	1/100%	220,000	21.7

*These values reflect a 4-fold (leaving CS) and 1 1/3-fold (plane change) increases of the calculated near-minimum values, to provide additional flexibility and safety factor for aeroassisted maneuvers in the Mars atmosphere.

Table 3.3.3 Fuel Requirements, Thrust Levels and Burn Times (TAXI B)
MOS to Cycling Ship/Cycling Ship to LEO

Total ΔV required   23,857 ft/sec
Vehicle total initial mass   350,820 lbm
LOX/LH2 propellant mass   285,700 lbm
Vehicle mass without LOX/LH2   65,120 lbm

Phase	ΔV ft/sec	LOX/LH2 Propellant Required lbm	Post Burn Mass lbm	# Engines/ Throttle	Total Thrust lbf	Burn Time sec
Leaving Phobos orbit	2209.3	46,319	304,503	3/100%	660,000	34
Plane change	606.9	11,617	292,886	1/100% or 2/50%	220,000	25.6
Approach correction	521.6	9,629	283,257	1/100% or 2/50%	220,000	21.2
Exit burn	18,076.2	194,331	88,926	3/100%	660,000	111.3 ⎫
				3/100% → 3/67%*	660,000 → 445,000	37.8 ⎬ 149.1
Rendez-vous burn	307.1	1,733	87,193	1/40%	88,000	9.6
Leaving CS	17.1	ΔV achieved by using orbital correction engines				
Plane change	1832.6	9,663	77,530	1/100% or 2/50%	220,000	21.3
Circular-ization	286.4	1,410	76,120	1/40%	88,000	7.8

*The thrust must be gradually throttled from 100% to 67% to hold acceleration below a 5 g value.

The specifications of the main engines selected for the TAXI A are given in Table 3.3.4.

Table 3.3.4 Main Engine Specifications (TAXI A)

Thrust	315,000 lbf
Specific Impulse, Isp	485 sec
Propellant: Oxidizer	LOX
Fuel	LH2
Mixture ratio	6
Mass flow rate, $\dot{m}$	649.5 lbm/sec
Combustion Pressure, P_o	2600 psia
Combustion Temperature, T_o	6700 R
Characteristic Velocity, C^*	7801 ft/sec
Thrust Coefficient, C_T	2
Throat Area, A^*	60.6 in²
Exit Area, A_e	74.04 ft²
Nozzle Length (from throat), L	
Operational Characteristics:	Throttleable 40%-120%
	Reusable
	Gimbal Angle ± 11°

The specifications of the main engines for the TAXI C are the same as for the TAXI A except the throttling range which will be 40%-110% for TAXI C.

3.3.2 Combustion Chamber Design

Chamber Geometry

The two main design considerations for the geometry of a combustion chamber are volume and shape. The chamber volume must be large enough to insure adequate mixing, evaporation, and complete combustion of the propellants. At the same time, the volume must not be so large as to cause excessive cooling requirements, weight, and space.

The shape must also promote adequate mixing and combustion, minimize surface to volume ratio, and be easy to fabricate. The three shapes considered for this design are spherical, near spherical, and cylindrical. Although the spherical and near spherical shapes have smaller cooling requirements and are lighter for a given volume, the cylindrical shape is chosen because it is easier to fabricate and offers better performance (Huzel, 1971). Figure 3.3.3 shows the possible configurations of the combustion chamber.

The minimum chamber volume needed for complete combustion is directly dependant upon the stay time (t_s) of the propellants:

$$V_c/A^* = \dot{m}vt_s/A^* = L^*$$

where:

A^* = nozzle throat area

L^* = characteristic length

v = propellant mixture specific volume

V_c = chamber volume

$\dot{m}$ = propellant mass flow rate

The characteristic length can be estimated by Spalding's theory or can be found experimentally. Experimental data indicates that an appropriate value of L^* for this propellant combination, mixture ratio and combustion temperature is 30 inches (Quentmeyer, 1986). With L^* established and the nozzle throat area known, the chamber volume and stay time is calculated (see Table 3.3.5).

To determine actual combustion chamber dimensions, the contraction ratio (ratio of chamber cross sectional area to throat area) has to be found. Through optimization studies (Huzel, 1971) the contraction ratio suited for this design is 2.5.

The complete dimensions, along with the parameters used to calculate them, are summarized in Table 3.3.5 and are shown on Figure 3.3.4.

Table 3.3.5 Combustion Chamber Parameters (TAXI A and C)

Propellants:	LOX/LH2
Mixture Ratio:	6/1 (by mass)
Combustion Temperature:	6700 °R
Combustion Pressure:	2600 psi
Weight Flow Rate:	650 lbm/sec
Characteristic Length:	30 in.
Contraction Ratio:	2.5
Chamber Volume:	1.0938 ft³
Stay Time:	.04 sec
Cylinder Diameter:	13.77 in.
Cylinder Length:	.97 ft.
Contraction Angle:	30°
Inside Surface Area:	4.74 ft²

Some of the above parameters are found from thermochemical calculations (Appendix 11.3.1).

CHAMBER SHAPES
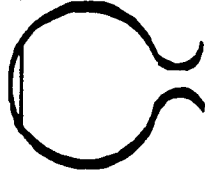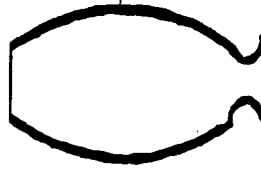
Spherical   Near Spherical   Cylindrical

FIGURE 3.3.3

COMBUSTION CHAMBER GEOMETRY

Volume = 1.035 cu. ft.

1.15 ft

Nozzle Throat

0.97 ft

Contraction Ratio = 2.5
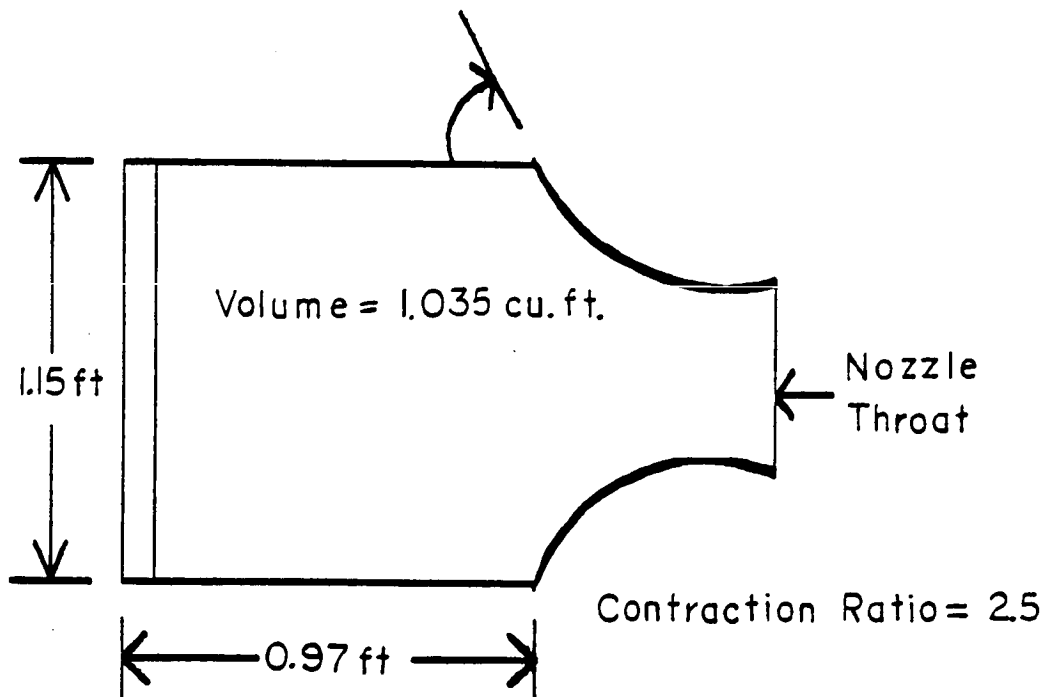
FIGURE 3.3.4

Injector Design

A good injector system is essential for optimum chamber performance and combustion stability. One of the critical-design parameters of an injector system is its impingement pattern. For this design the triplet impingement pattern has been chosen. Since two streams of one propellant impinge symmetrically on the other, the change of the vector angle due to the mixture ratio is eliminated. Huzel indicates that from existing systems this arrangement provides good mixing and excellent performance characteristics.

Another critical design parameter of an injector is its pressure drop, dP. A low pressure drop means a lighter turbo pump system, but a high pressure drop is needed for combustion stability. A rule of thumb for preliminary design calculations is that the orifice pressure drop be 15 to 20 percent of the chamber pressure. A 15% dP is chosen since the combustion pressure is high.

The next step is to determine the total orifice area, oxygen and hydrogen orifice sizes, number of orifices, and injection velocity. The basis equation relating these parameters is:

$$dP_i = \rho/(2g)(V_i/C_d)^2 = 1/(2g\rho)(\dot{m}/C_d A)^2$$

where:

A = total orifice area (of particular propellant)
C_d = dimensionless discharge coefficient
g = gravitational constant
ρ = propellant density
V_i = injection velocity

The discharge coefficient, Cd, is a function of injector orifice configuration. A short tube with conical entrance is chosen because it gives favorable injection stream characteristics (see Fig. 3.3.5).

Experimental data (Sutton, 1956) shows that the discharge coefficient for this type of configuration is approximately 0.8. Using the above equation and estimated pressure drop, the total orifice area and injection velocity is calculated for each propellant. To calculate orifice size and number, the following relation is used:

$$A/N = D^2/4$$

where:

D = orifice diameter
N = number of orifices

First the LO_2 orifices are considered assuming an orifice diameter of

about .12 in. to match discharge coefficient data. The resulting calculation for the number of oxygen orifices is rounded up to the

nearest even integer. Since there are 2 hydrogen orifices for every oxygen orifice, the number of H_2 orifices is known, and the hydrogen orifice diameter is calculated. Table 3.3.6 summarizes injection design parameters along with related data.

Table 3.3.6 Injector Design Parameters

L. Hydrogen Density:	4.395 lbm/ft³
L. Oxygen Density:	70.637 lbm/ft³
Hydrogen Weight Flow:	92.8 lbm/sec
Oxygen Weight Flow:	556.7 lbm/sec
Injector Type:	Triplet Impinging
Injector Configuration:	Conical Tube
Discharge Coefficient:	0.8
Pressure Drop:	56160 lb/ft²
Total H_2 Orifice Area:	4.244 in²
Total O_2 Orifice Area:	6.310 in²
Number of H_2 Orifices:	1120.
Number of O_2 Orifices:	560.
H_2 Orifice Diameter:	.0695 in.
O_2 Orifice Diameter:	.1198 in.
H_2 Injection Velocity:	727.8 ft/sec
O_2 Injection Velocity:	180.4 ft/sec

INJECTOR ORIFICE CONFIGURATION

$C_d = 0.8$
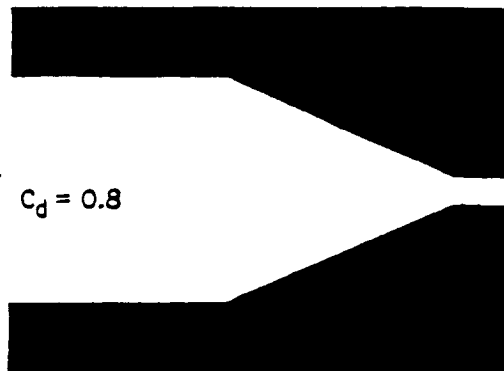
Short Tube With Conical Entrance

FIGURE 3.3.5

Combustion Chamber Materials

A good combustion chamber material has a high strength, light weight, and high thermal conductivity. The material(s) must also have a long design life. Existing state of the art systems (such as the SSME) use a nickel alloy shell with a copper alloy (NARLOY-Z) liner. To accommodate the high combustion temperatures and pressures and still reduce weight from existing systems, the TAXI vehicle will use a nickel alloy shell and a copper-tungsten composite liner coated with a zirconium oxide ceramic (see Fig. 3.3.6). The copper composite consists of tungsten wires (10% by volume) imbedded in a copper matrix. Laboratory data (NASA, TM-87280) shows that the Cu/W composite will have a rupture strength 80% higher than NARLOY-Z with only a 5% reduction in thermal conductivity. This will improve design life and reduce weight.

The zirconium oxide coating will also improve design life by providing a thermal barrier. Tests in a chamber using LO2/LH2 (Quentmeyer, 1986) show the hot-gas-side wall temperature and the theoretical maximum strain were reduced by 80 and 92 percent, respectively. The idea of using a ceramic coating is not new, but difficulties with applying the coating without it peeling or flaking off have kept this design concept from being implemented. Advances in this area for the projected time frame should take care of this problem.


CHAMBER CROSSECTION & MATERIALS

Cu/W Composite

Zirconium Oxide

Nickel Alloy
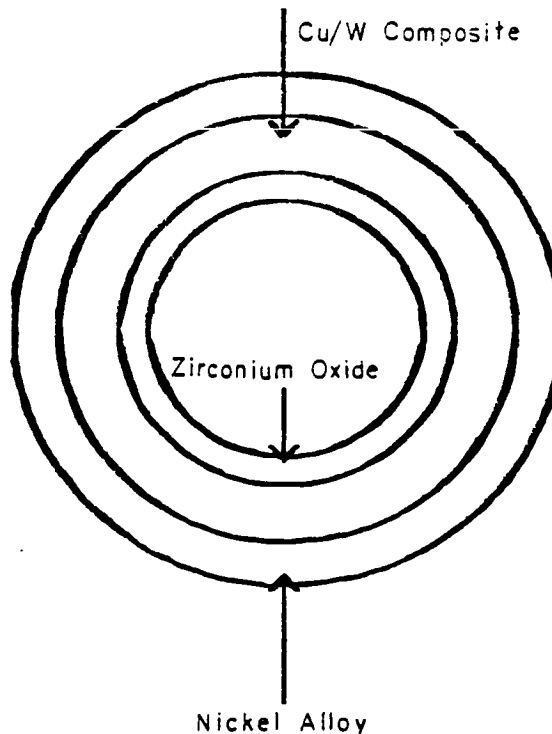
FIGURE 3.3.6

3.3.3 Nozzle Characteristics

When determining the nozzle characteristics, certain parameters are given and from these the rest are derived. To get these results a set of Perfect Bell Nozzle optimization curves is used (Blount, 1983).

These curves are generated by a program written by United Technologies, Pratt and Whitney Aircraft Group for NASA. The report presents data for untruncated nozzle expansion area ratios from 10 to 6100 for a specific heat ratio of 1.2. The specific heat ratio varies along the length of the nozzle as our thermochemistry calculations have shown but 1.2 is well within the calculated range. Since this is only a preliminary design study, the numbers generated by using this program can be considered good estimates. The program is based on the method of characteristics for an axisymmetric nozzle flow. A corner expansion is chosen because it results in a shorter nozzle than one with a radius downstream of the throat.

The given parameters include the throat diameter, which was calculated from the maximum thrust, thrust coefficient, and combustion chamber pressure. The other parameter, which actually depends on the throat diameter is the exit area ratio. For best performance the nozzle should be expanded as much as possible, but the exit area is limited by the vehicle configuration (see configuration sketch). A maximum area ratio of 176 is determined based upon the given restrictions and the throat area of 60.6 in^2. The possibility of truncating the nozzles even more to cut down nozzle mass is examined. It is determined that shortening the nozzle and decreasing the area ratio will result in a loss of thrust. Although this loss seems small (between 2.7% for A_e/A^* of 50 and 0.5% for A_e/A^* of 110) it results in an increased fuel mass (see Table 3.3.7). The mass saving from the nozzle is easily consumed by the added fuel mass. Therefore, the nozzle should be expanded as much as possible in order to use the fuel most efficiently.

Table 3.3.7 Extra Fuel for Truncated Nozzles

A_e/A^*	Isp	Thrust lbf	Loss %	Fuel lbm
150	483	314200	0.254	2293
130	481	313330	0.530	4619
110	479	312360	0.838	6978
90	476	310840	1.321	10581

A minimum weight restriction is placed on the nozzle design. To achieve this goal the plots given in Blount, 1983) are used to produce minimum surface area nozzles. A design area ratio (A_D) is determined. With this A_D the selection process can be done somewhat in reverse.

Table 3.3.8 lists the various parameters and their given or calculated values.

Table 3.3.8 Nozzle Characteristics (TAXI A and C)

Parameter	Value
Chamber Pressure, P_o	2600 psia
Thrust Coefficient	2
Throat Area A^*	60.6 in^2
Throat Diameter D^*	8.78 in
A_e/A^*	176
Exit Area, A_e	74.065 ft^2
Exit Diameter, D_e	9.7 ft
A_D	330
L/D^*	18
Length, L	13.18 ft
A_s/A^*	650
Surface Area, A_s	273.54 H^2
P_e/P_o	3.69 x 10^{-4}
Exit Pressure, P_e	0.96 psia
Contour Angle at Exit	9.68°

Once the above parameters are known, an approximation of the contour can be created. Appendix 11.3.2 gives a parabolic equation approximating the nozzle contour and lists the nozzle radius as a function of axial distance along the nozzle.

Nozzle Construction

The nozzle/combustion chamber assembly will be fabricated as one unit. It was decided that since maximum stress occurs near the throat that there should be no seam at this location if it could be avoided. Since the assembly will be fabricated as a single piece and will not be separated at any time the ceramic lining can be applied early in the process (i.e., on Earth). The nozzle/combustion chamber will use a regenerative cooling system. This system will consist of 4 to 6 separate conduits wrapped in a helical pattern with the return flow axially along the outside.

3.3.4 Thrust Vector Control

The three main engines of the TAXI will be gimbaled from the head of the combustion chamber. The gimbal is essentially a universal joint about which the whole engine is pivoted on a bearing. Each engine will be able to swivel 11 degrees in all directions, but will rarely if ever need the full degree of motion. The 11 degree angle will allow keeping the thrusters angled through the center of mass (CM) of the TAXI for the varying locations of the CM throughout thrusting. The Guidance, Navigation and Control (GNC) section describes the CM limits for fully fueled and dry mass center of mass locations.

For needed pitch, yaw and roll moments, both variable throttling and gimbaling will be used. Most moments, however, will be taken care of by the RCS thrusters discussed in the GNC section.

3.4 Propellant Storage and Distribution Systems

3.4.1 Propellant Tank System Design

The tank system for carrying the LH2 and LOX is designed with emphasis on reliability, reusability, versatility, modularity and safety. The sizes of the tanks are determined by the use of the maximum ΔV required which occurs on leaving Mars. Additional tank volume is used for carrying extra propellant for reserve and residual, for off optimum trajectory maneuvers and for consumption in fuel cells. The tank sizes and volumes are calculated with a single program described in Appendix 11.3.3. Table 3.4.1 lists the tank sizes and volumes for the TAXI versions A, B and C.

Table 3.4.1 Propellant Tank Sizes

TAXI Version	Design Value of ΔV	Diameter (ft)		Volume (ft³)	
		LOX	LH2	LOX	LH2
A	9.5 km/sec 31,168 ft/sec	19.88	21.9	4114	5501
B	7.27 km/sec 23,851 ft/sec	14.9	16.43	1733	2322
C	9.5 km/sec 31,168 ft/sec	19.14	21.1	3671	4919

Spherical tanks are chosen for a few reasons. First, spherical tanks can handle the anticipated stresses better than a cylinder. Second, pumping with spherical tanks is simpler and more efficient. Finally, spherical tanks provide much nicer modularity for maintenance and positioning purposes. There will be four tanks of LH2 and two tanks of LOX placed between the LH2 tanks as shown in the overall configuration sketch as well as Figure 3.4.4. With these numbers of tanks, the volumes and diameters are kept to a reasonable size as shown in Table 3.4.1.

3.4.2 TAXI Vehicle Propellant Feed System

The TAXI vehicle's propulsion system consists of four spherical tanks of liquid hydrogen and two tanks of liquid oxygen feeding into three, staged-combustion cycle engines.

For oxygen and hydrogen, there are two separate main propellant feed systems as shown in Figures 3.4.1 and 3.4.2. The oxidizer has a single main feed pipe running out of each tank. These two pipes are aligned in the center of the nozzle arrangement. The two tanks are connected by a valve at midlength. On either side of this valve, two branching pipes feed the propellant to a common collector. This cross-connection scheme provides reliability and redundancy. For instance, in the contingency where a tank is not functioning or its feed line is jammed at the collector inlet, the tank can be shut down and isolated by opening the interconnection valve and allowing the oxidizer from one tank to merge with the oxidizer from the operational tank. The collector inlet valve of the failing tank can then be closed. Gas pressurization forces the propellant out of the inoperable tank. Moreover, the collector serves as a junction where all the propellant can accumulate and be directed to the three engines; the common collector system allows any engine to be fed from any tank. Also, because this vehicle only has two LOX tanks but three engines, this collection point is necessary to allocate the propellant to all three engines. At the collector, a pump is connected to drive the oxidizer into the engines and aid in pumping the oxidizer out of the tanks. This pump pressure is necessary since the oxidizer must work back against the thrust of the vehicle to reach the oxidizer prevalves located on the engine assembly. From there, the engine systems take over. There is also a separate line that runs out of the collector which feeds oxygen to the fuel cells.

LOX   TANK-TO-ENGINE SCHEMATIC

LOX

LOX

1

2

3

LOX
Collector

4

5

6

Engine

Engine

Engine

VALVES

1   Tank connection
2-3 Collector
4-6 Pre-engine
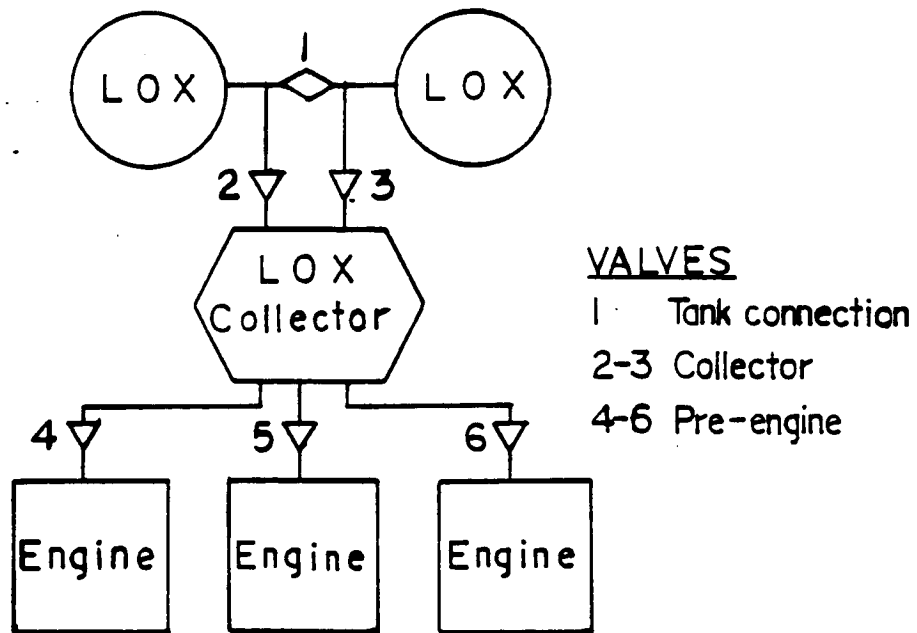
FIGURE 3.4.1

LH2 TANK-TO-ENGINE SCHEMATIC

LH2

LH2

LH2

LH2

1

2

3

4

5 6

7 8

LH2
Collector

9

10

11

Engine

Engine

Engine

VALVES

1-4 Tank connection
5-8 Collector
9-11 Pre-engine
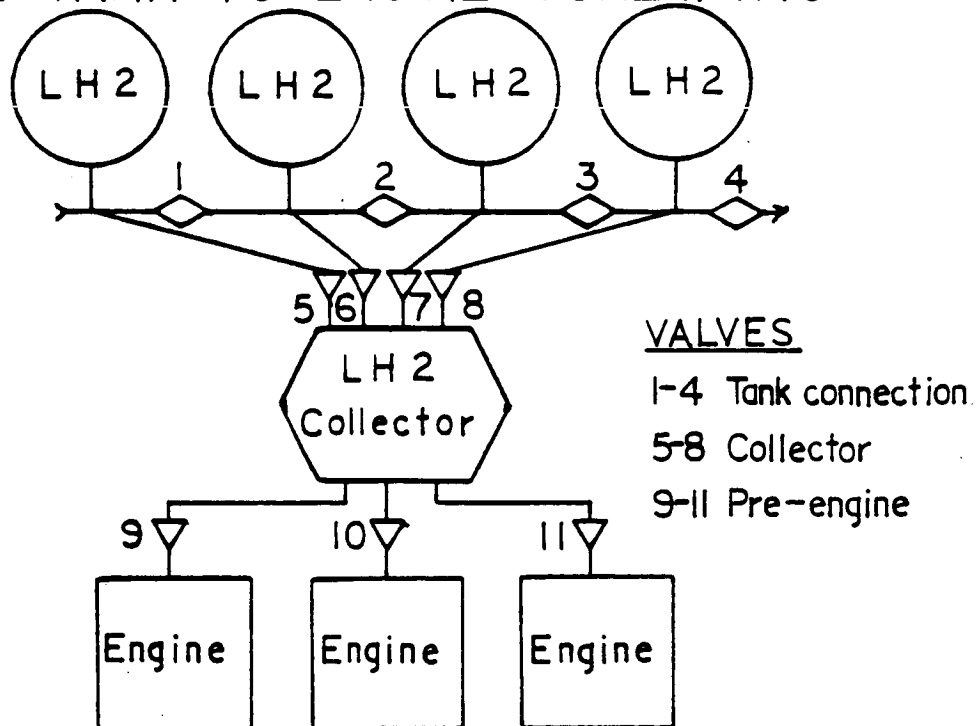
FIGURE 3.4.2

On the fuel side, there is a single flow pipe from each LH2 tank that leads to a square network of piping above the LH2 collector (Figure 3.4.3). The LH2 collector arrangement is also located in the space among the three nozzles, next to the LOX collector. As LH2 fuel is drawn from the tanks, it flows to this square and then to the collector through pipes emanating at the corners of the square. This piping is connected to the collector inlet valves to regulate the flow. One cross-connection valve is located at the center of each side of the square network to connect all pipes from all the LH2 tanks providing redundancy. The LH2 collector is also hooked up to a pump to force the fuel against the thrust of the TAXI vehicle and into the fuel prevalves. A similar turbine-pump machine used to run the pump at the oxidizer collector can be used to run the pump at the LH2 collector. Again, a siphoning line directs a fraction of the fuel supply to the fuel cells.

Figures 3.4.4 and 3.4.5 give the network positioning relative to the TAXI vehicle. The LOX tanks are connected by a straight pipeline while the LH2 tanks' lines run in an X-pattern to the collector. As can be seen by Figure 3.4.4, to have a cross-connection system, requiring that the collector-feed pipes branch off the interconnecting lines reduces the amount of material and complexity of the propellant-feed network. In this scheme, only one pipe into each tank is needed whereas if the cross-connections are separate from the collector feed lines, another similar pipe network is required. Thus, this plan is the least expensive in terms of material costs. The LOX lines are arranged slightly lower than the LH2 lines since the lines cross over and the LOX tanks are situated lower on the aerobrake shield. The lines and collectors have insulation from heat generated by the nozzles and outside radiation sources.

Each engine has a closed-system, dual-staged combustion cycle consisting of preburners and turbopumps. The dual-staged cycle is currently the most energetic system and gives best performance. Figure 3.4.6 shows the engine flow plan (NASA, 1982). The operation of this engine system is detailed in the same reference. In brief, the dual-staged combustion cycle here allows for the operation of high-pressure turbopumps by feeding fuel-rich propellants in from preburners. Low-pressure pumps are used to raise the pressure of the flow entering the high-pressure turbopumps. Regenerative cooling is employed as well. The final mixture ratio is 6:1 (oxidizer: fuel). Main chamber pressure and temperature are 2600 psia and about 6700 deg R.

For the propellant lines, some good materials are certain steel alloys such as austenitic and semiaustenitic stainless steels. These steels resist corrosion and are easily formed and welded. They also operate well at cryogenic and elevated temperature conditions. At set intervals, these lines are connected by sections which move slightly to allow for motion, temperature effects, misalignment, and engine gimbaling. Universal joints with bellows that connect rigid sections serve this purpose. Bellows are crinkled outside liners which allow a flexible joint to move in a limited fashion. Some frequently used bellow materials include aluminum alloys and inconel. Also, near the engines, flexible tubing and bellows are used to feed the propellants into the engine to permit gimbaling. Parts for the pumps, turbines, and casings are constructed of aluminum and steel alloys. In the future,

LH2 SQUARE NETWORK
SYSTEM

LH2 Flow
From Tank

Tank
Connection
Valve

Collector

Collector Inlet
Valve
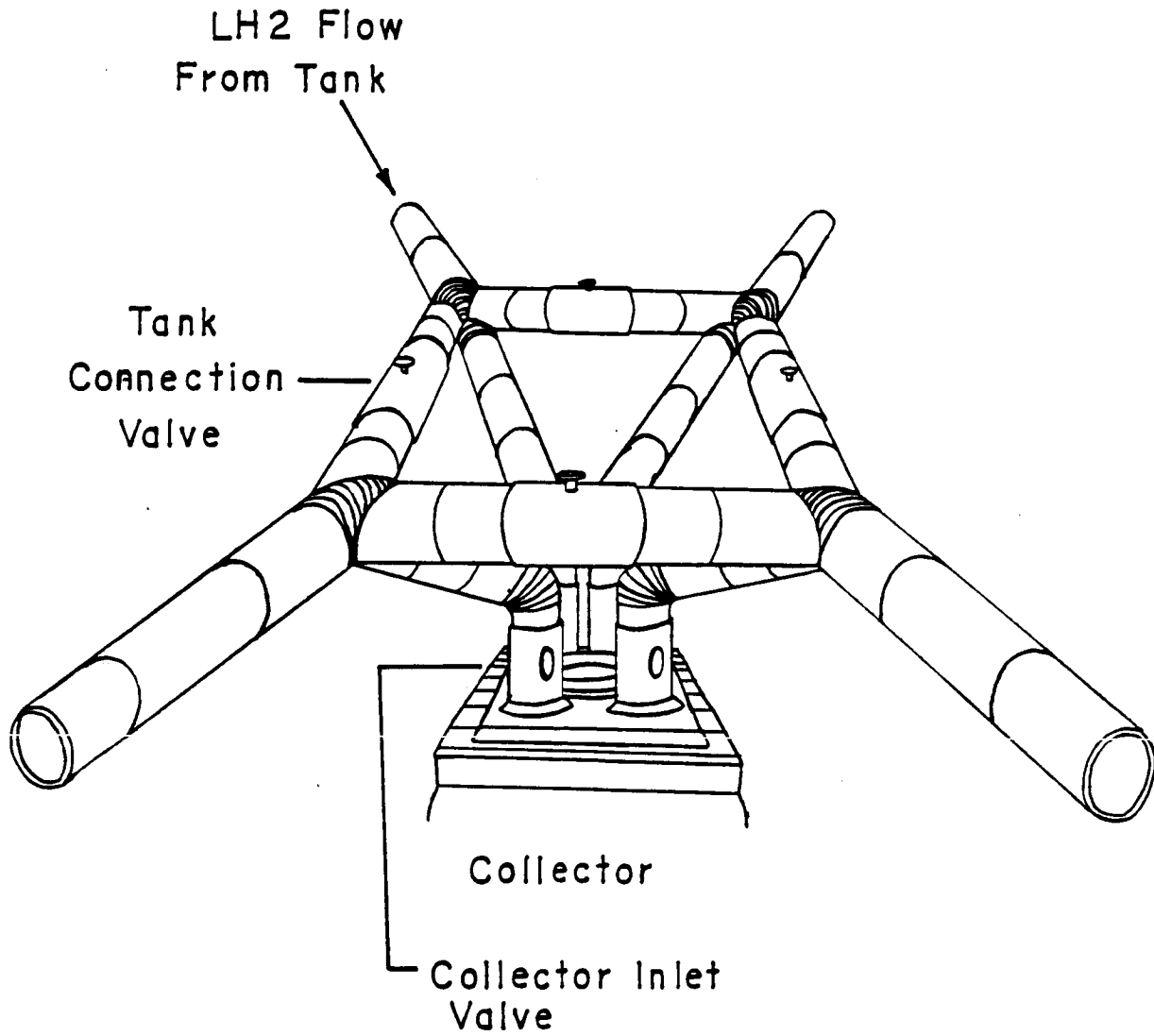
FIGURE 3.4.3

MAIN PROPELLANT FEED
SYSTEM
(TOP VIEW)
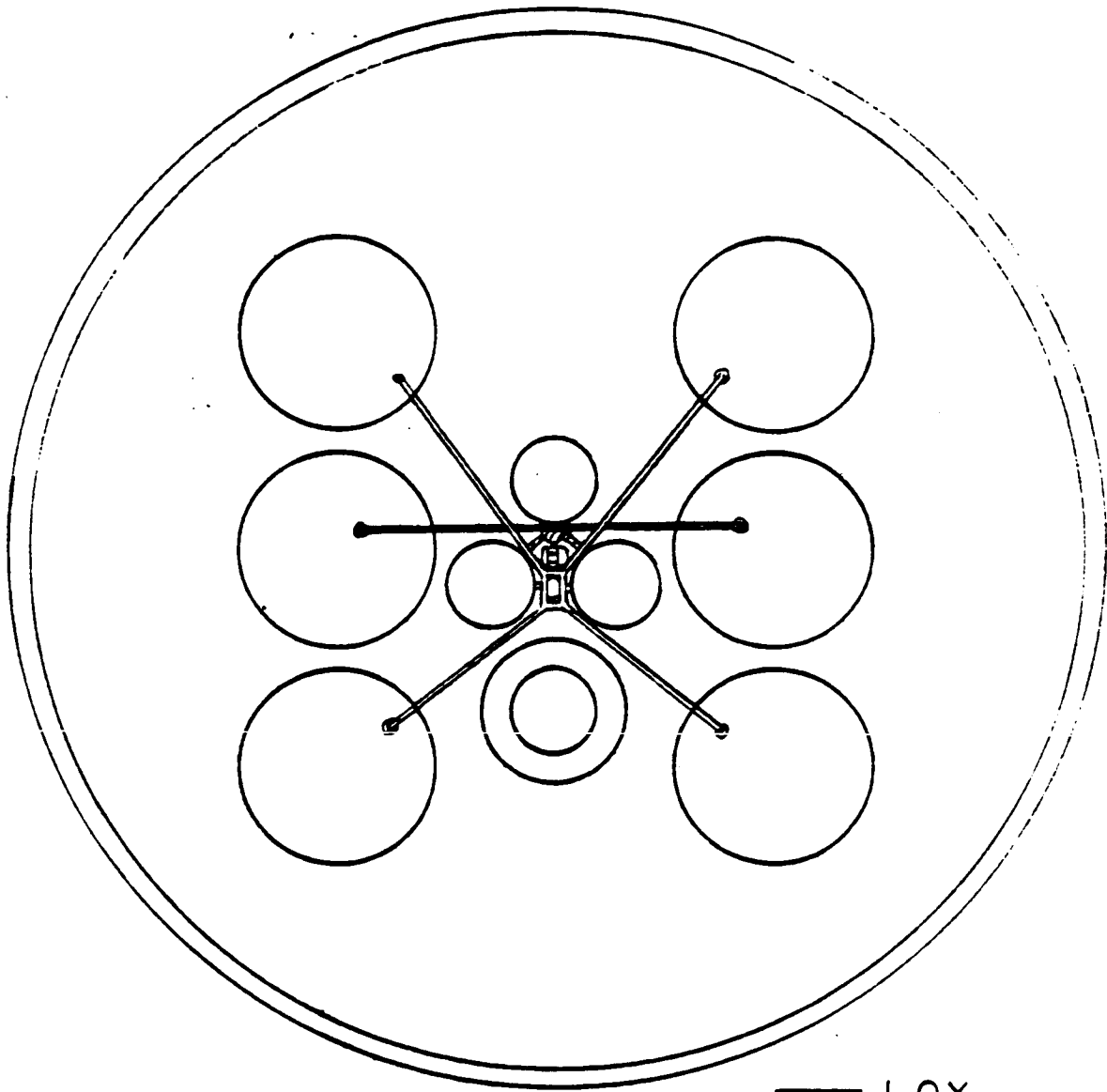

////// LOX
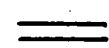
==== LH2

FIGURE 3.4.4

MAIN PROPELLANT FEED
SYSTEM
(SIDE VIEW)
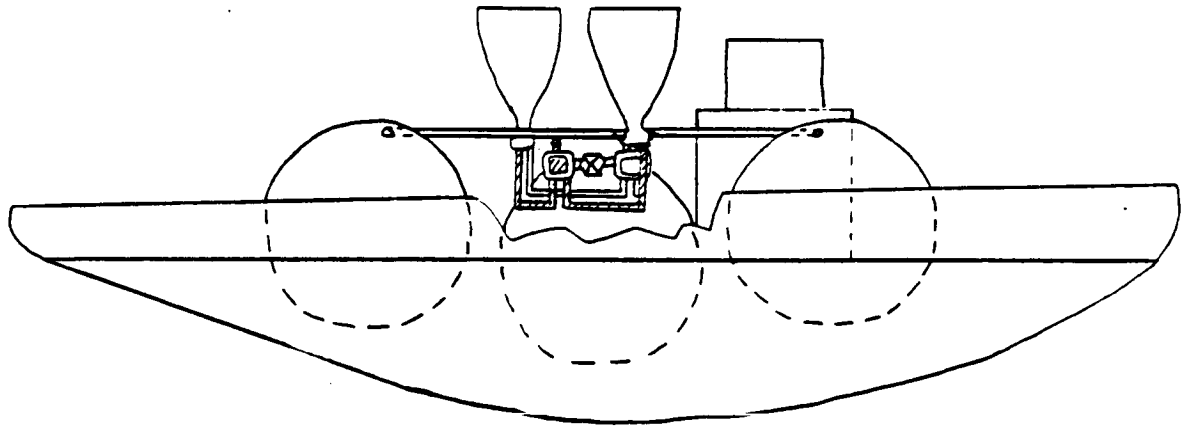
ⅢⅢⅢ LOX

═══ LH2

FIGURE 3.4.5

ENGINE FLOW SCHEMATIC
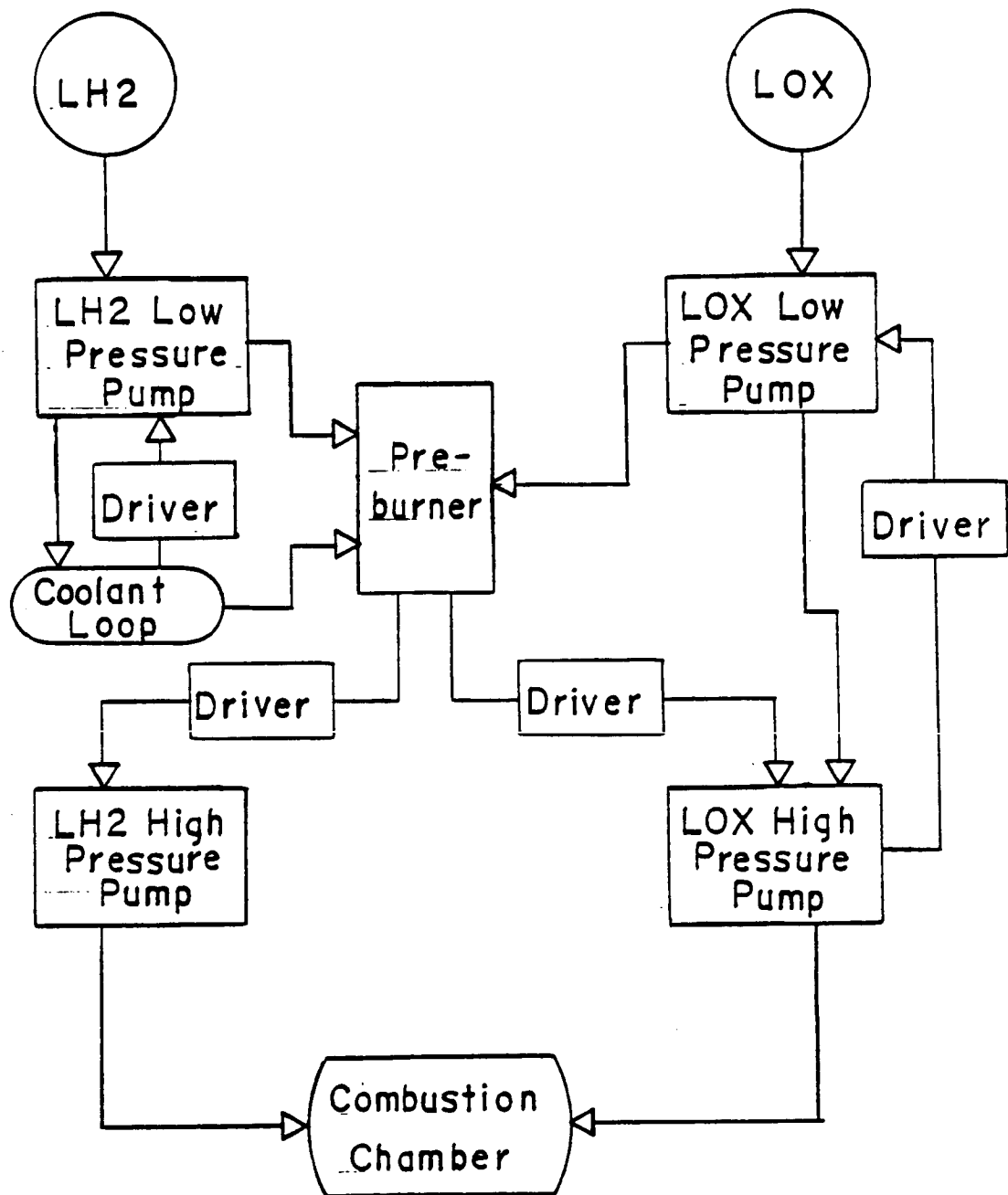
FIGURE 3.4.6

innovations in materials science may permit use of material that will serve the same functions as present materials but will be of lighter weight. Without this knowledge, however, these proven materials are the most likely to be used. Huzel gives more information.

A general scenario for the propellant system is as follows. Assumed is the existence of some start-up mechanism for the TAXI's engines. Before start, however, the propellants are forced to one side of the tanks by impulse settling, where the reaction control thrusters are first fired to cause the propellants to accumulate at the end where they feed into pipes. After startup, the cross-connection valves are kept closed while the collector inlet valves and the engine prevalves are wide open to accept propellant. The propellant is forced out of each tank by pressure into the pipe leading to the collectors. At the collector, a pump is used to force the propellant to the engine if needed. In all likelihood, this procedure is probably necessary since the collectors sit higher than the engine inlets so that the propellants need to be pushed back against the thrust vector. Once in the engines, the turbopumps there force the propellants through the engine. The cross-connection are used only if there is failure in one of the tanks; otherwise, they act only as a safety control factor.

3.4.3 Cryogenic Propellant Storage and Transfer Systems

Design Criteria and Objectives

Requirements for the cryogenic propellant storage system are as follows:
- minimal propellant loss due to boiloff
- minimum possible weight
- the system must allow for efficient and safe refueling
- the system must be easily maintainable

A nominal mission length of 146 days for the outbound leg and 636 days for the return leg is used.

Basic System Selection

The possible system options studied include passive open cycle, open cycle partial and total reliquification, passive open cycle with cooled shields, open cycle refrigeration, as well as closed cycle reliquification and refrigeration. Analysis of these systems is performed for an outer tank shell temperature of 460 degrees R (256 K). An overall assessment of initial mass in LEO versus mission time for each system concludes that reliquification and refrigeration would only be best for missions of 1.6 years or greater duration (based on studies performed by Martin Marietta Aerospace Company). Therefore, a passive system utilizing multi-layer insulation (MLI), vapor cooled shields (VCS), thermodynamic vent system (TVS), thermodynamic control system (TCS), low heat leak support struts, reflective outer shielding, and para-ortho hydrogen conversion is selected.

System Design

In this system, vented hydrogen vapor passes through a VCS made of honeycombed aluminum that surrounds the LH2 tank (see Figs. 3.4.7 and 3.4.8). The hydrogen vapor should absorb 50% of the heat leak

PASSIVE SYSTEM SCHEMATIC

FIGURE 3.4.7

59
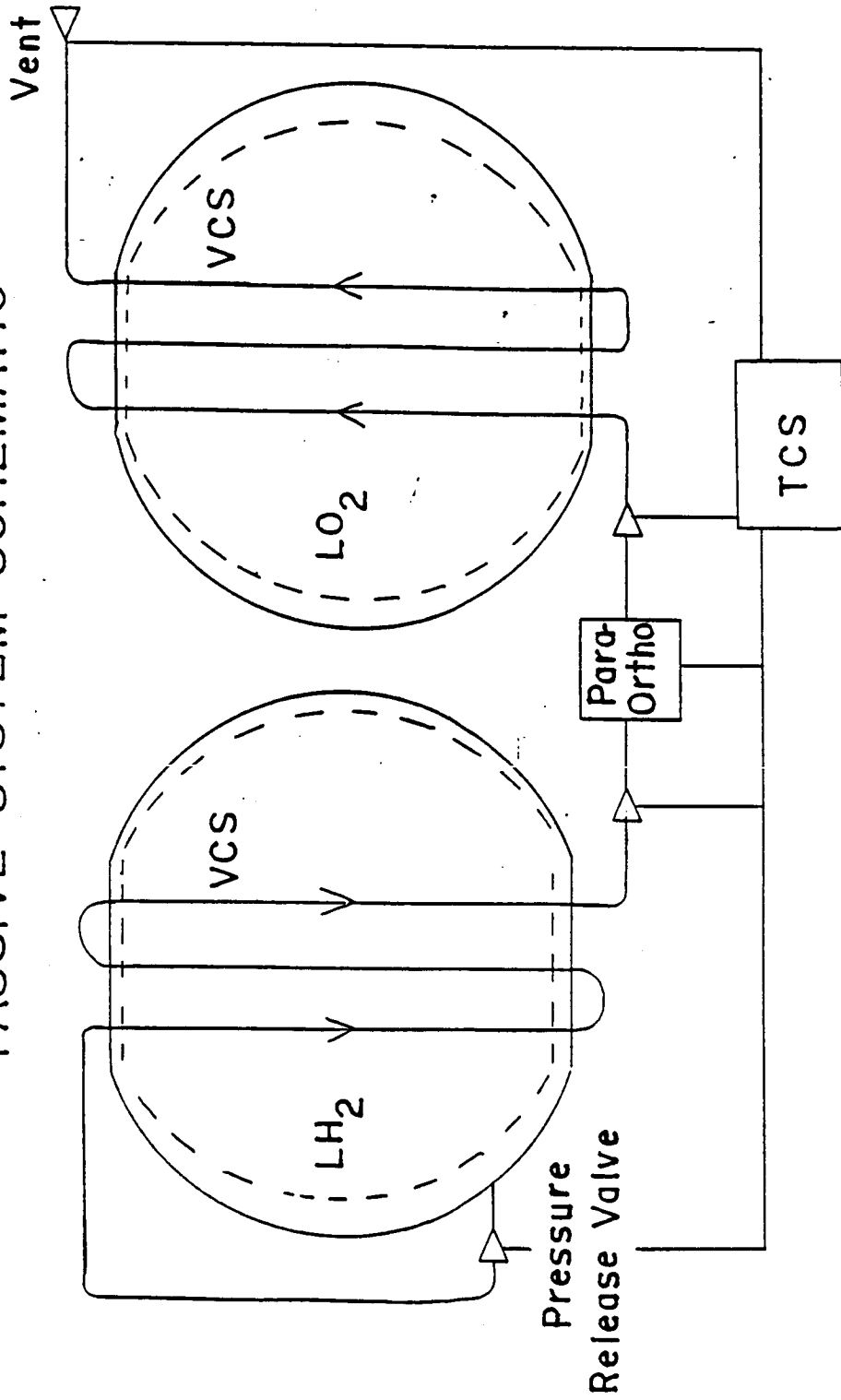
PASSIVE COUPLED TANK DESIGN
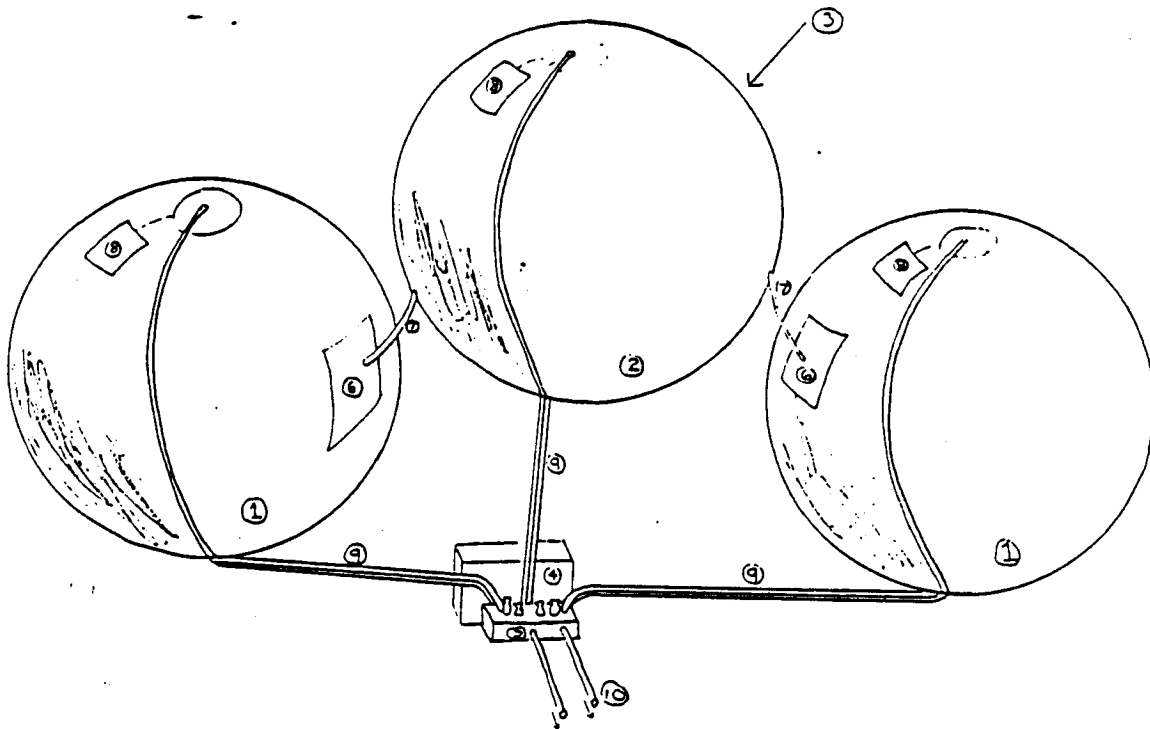
1	LH$_2$ Storage Tanks
2	LO$_2$ Storage Tank
3	H$_2$ Vapor Overboard Relief Valve on LO$_2$ VCS
4	Thermodynamic Control System
5	Propellant Transfer Connection Panel
6	Para-to-Ortho Converter
7	LH$_2$-to-LO$_2$ VCS Connect Line
8	Thermodynamic Vent System
9	Propellant Tank Vent/Fill Lines
10	Cross Feed Lines

FIGURE 3.4.8

encountered at the VCS. As it leaves the VCS, the hydrogen vapor then passes through a para-ortho converter. This converter speeds up the conversion of para-hydrogen (hydrogen with anti-parallel proton spins) to ortho-hydrogen (hydrogen with parallel proton spins). This conversion is an endothermic reaction and is used to absorb 15% of the total heat leak in the system.

The above conversion is performed by the addition of a catalyst, such as APACHI-1. The heat of conversion has a maximum of 400 J/g at 100 degrees K while an enthalpy change of 900 J/g gives a change in temperature from 20 to 100 degrees K. Therefore this conversion can reduce the temperature of the hydrogen vapor by 36 degrees K. The use of APACHI-1 would require about 100 grams of catalyst for each g/s of hydrogen vapor flow.

After leaving the para-ortho converter, the vapor passes through the VCS surrounding the LOX tank. A constraint is placed on the system such that the hydrogen vapor flow rate through the VCS surrounding the LOX tank is sufficient to intercept all heat leak to the LOX tank. The hydrogen vapor is then vented through an overboard relief valve on the LOX tank into the environment. A TCS and a TVS should control the flow of hydrogen vapor through the vapor cooled shields, as well as the para-ortho conversion. The TCS, TVS, and para-ortho unit should weigh approximately 800 lbs (363 kg) for the TAXI A version.

The VCS should be embedded in a two inch thick insulation blanket (see Fig. 3.4.9)(based on a study at Ames Research Center and a Boeing study). A study performed at NASA's Ames Research Center concludes that for a single VCS the shield should be located at 0.35 times the insulation thickness, or .7 inches (1.72 cm). The insulation blanket will consist of foam insulation, multi-layer insulation, and Dacron net spacers as described below.

The first layer of the blanket is an inner radiation shield. This should consist of a .00033 inch (.0076 mm) thick layer of double aluminized Kapton (DAK). DAK is selected because it is a state-of-the-art material and has been well tested. Double goldized Kapton provides slightly higher performance, but is not considered to be as cost effective as DAK.

The second layer of the blanket consists of a 0.7 inch (1.78 cm) thick layer of foam insulation. The foam insulation selected is Rohacell 31, which is a polymethacrylimide, and has a density of 1.9 lb/ft^3 (30.0 kg/m^3). This gives a lay-up density of .11 lb/ft^2 (.54 kg/m^2). It is selected because it exhibits similar properties as all other available insulation materials, yet has a lower density and is easier to apply. This insulation is applied in cut out layers which are staggered to reduce heat leak through the seams (see Fig. 3.4.10). This allows the insulation sections to be easily replaced, as opposed to spray-on insulation.

A Dacron net spacer is then placed between the foam insulation and the VCS. This helps to reduce layer to layer heat transfer.

MLI/FOAM INSULATION BLANKET
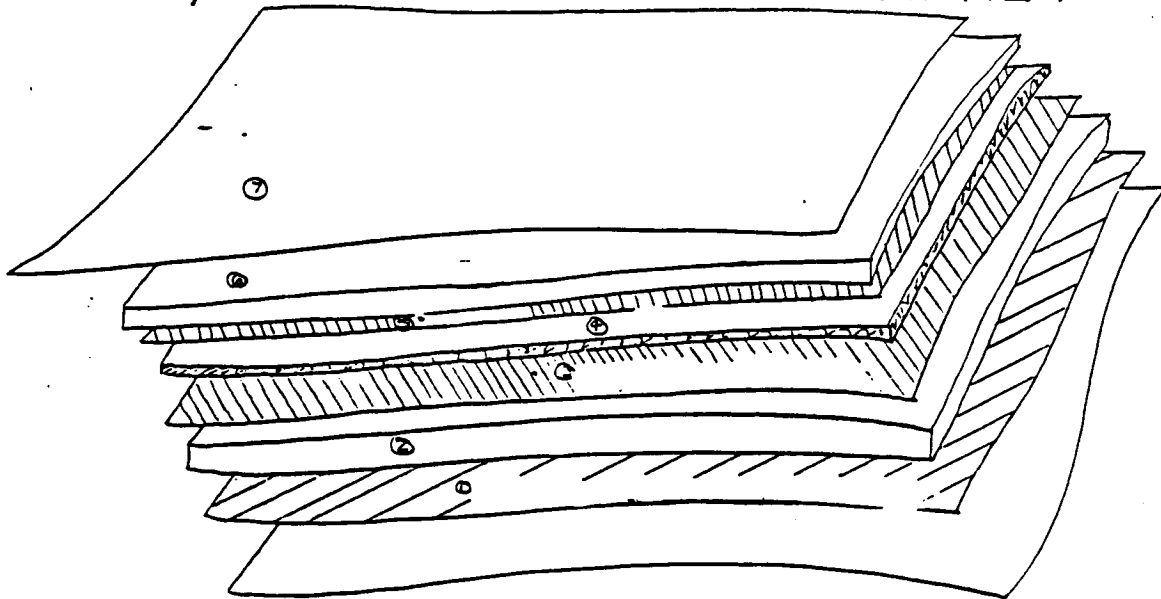
1   Inner Radiation Shield : 0.00033 in. (0.0076 mm)
        Thick Double Aluminized Kapton
2   Foam Insulation : 0.70 in (1.778 cm) Thick
        Rohacell 31 Foam Insulation
3&5 Dacron Net Spacers
4   Vapor Cooled Shield (VCS) 0.00512 in
        (0.130 mm) Thick Al Sheet Bonded To
        A 0.252 in (0.64 cm) Thick Al
        Honeycomb
6   Double Aluminized Kapton 1.30 in
        (3.302 mm) Thick
7   Laminated Double Alumined Kapton
        And Dacron Scrim 0.001 in (0.025 mm)
        Thick

FIGURE 3.4.9

INSULATION LAY-UP
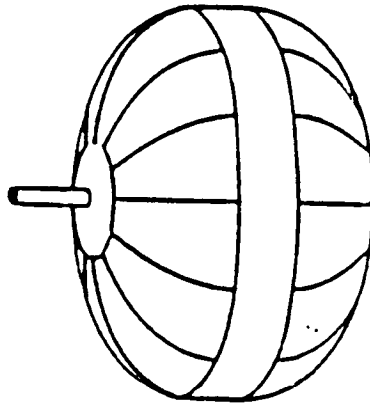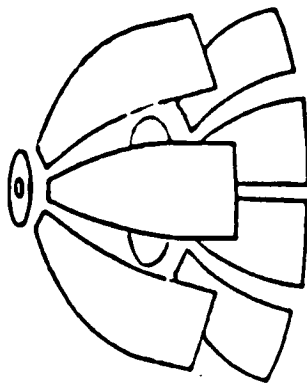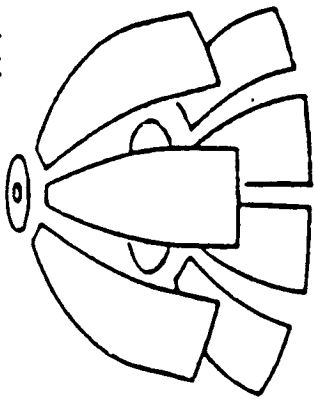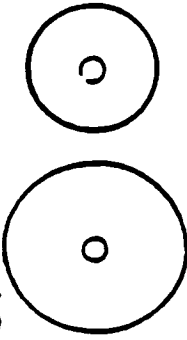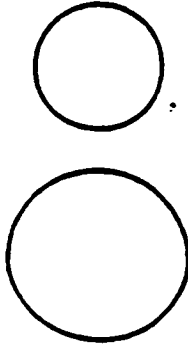
UPPER POLAR CAP

LOWER POLAR CAP
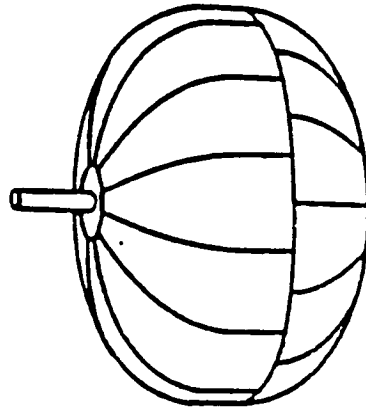
INSULATED TANK

TANK

FIGURE 3.4.10

The VCS is made of a .00512 inch (0.130 mm) thick aluminum sheet bonded to a .2520 inch (0.640 cm) thick aluminum honeycomb. The combination has a lay-up density of .237 lb/ft² (.57 kg/m²). A Dacron spacer is then placed between the VCS and the next layer of insulation.

The MLI consists of 1.30 inches (3.302 cm) of DAK. There are 60 layers of DAK per inch. The DAK is applied as the foam insulation was applied, in overlapping sections to reduce heat leak at the seams as well as give greater ease in replacement (see Fig. 3.4.10).

Finally an outer radiation/reflective shield is applied. The shield consists of a laminated DAK and Dacron Srim layer 0.001 inch (0.025 mm) thick. The DAK layers, Dacron spacers, inner and outer shields, as well as Velcro attachment tabs gives a density of 2.19 lb/ft³ (35.1 kg/m³) for a lay-up density of .238 lb/ft² (1.16 kg/m²). This gives a total blanket lay-up density of .463 lb/ft² (2.26 kg/m²).

Propellant Boiloff

For the TAXI B (LH2 tank diameter = 16.43 ft), the tank insulation system proposed here is expected to yield a boiloff rate of approximately 0.15 lbm LH2/hr per LH2 tank or a total of 14.4 lbm LH2/day for four tanks. It is assumed that this boiloff rate can be reduced to 75% of the stated value with 2020 technology. This will yield a boiloff of 10.8 lb LH2 for four LH2 tanks. Because well over 75% of the propellants will be used during the first few days of the trip, the maneuvering propellant needed for the propulsive maneuvers during transfer from the Cycling Ship to the planets may be stored in one LH2 tank. This will reduce boiloff during long trips when the TAXI is docked at the Cycling Ship. During the 146 days enroute to Mars system, the boiloff will be 394.2 lbm which represents about 1 1/3 percent of the total initial LH2 carried by the TAXI. This loss of propellant can be compensated by simply increasing the fuel reserve; as the tanks are sized for the return trip from Mars to Earth, they can easily accommodate extra fuel enroute to Mars. Enroute back to Earth (636 days), the boiloff may reach 1717.2 lb or 4.2 percent of the initial LH2 (40,814.3 lbm) carried by the TAXI. Perhaps the simplest way to compensate for such a loss of the propellant is to adopt the following scheme. Each TAXI departing from LEO would carry additional 2000-3000 lbm of LH2 and deposit it in Cycling Ship tanks while enroute to Mars. This propellant would then be supplied to the Earth bound TAXI shortly before the latter leaves the Cycling Ship.

Significant reductions in heat leaks could be achieved with specially designed low leak support struts made of composite materials with high strength and low thermal conductivity, and orbital disconnect struts which connect to the tank structure only during periods of high structural loading and should be considered in the future. During vehicle transit the orientation of the vehicle to the sun will also be critical in order to allow the minimum possible tank area to be exposed to the solar flux.

Additional situations exist in which the vehicle is subjected to higher than normal heat flux. The most important of these is the heating during aerobraking maneuvers. It is estimated that this maneuver will

result in a worse case heating of 5 watts/cm^2 of exposed tank area. However this heating condition will only exist for a maximum of 150 seconds and will be mostly radiated heat energy. Because we can expect that the reflective outer shielding will reflect well over half the heat flux, and due to the limited duration of the heating, we can expect that the increased boiloff rate can be easily accounted for with propellant reserves. Additionally, problems will be experienced in LEO and Mars orbit due to albedo effects from solar reflections on the surface of the Earth and Mars. This problem will also require careful·vehicle orientation to help keep heat flux to the tanks to a minimum.

Propellant Transfer Systems

Initial requirements of the propellant transfer system are that the system must offer reasonable transfer times, low system weight, and simplified operation. The system must also be adaptable to a number of different environments as it will be necessary to transfer fuel from orbital tankers in the Earth-Moon and Mars-Phobos systems as well as to and from the cycling vehicle.

Attached and tethered depots were considered and a tethered system is selected because it meets the above requirements. The first advantage of the tethered system is that it settles fluid. This allows for an Earth-like environment where the liquid is over an outlet and the vapor is over a vent so that operations can be performed as normal with the tanks coupled together and continuously vented during fill (see Figs. 3.4.8 and 3.4.11). A propellant transfer connection panel connecting the two sets of 3 tanks is located next to the LOX tank in each tank set. This connection panel has quick-disconnect line connectors with lines for both vent and fill operations, as well as cross feed lines to connect to the tank set fill systems. This eliminates the need for extensive pressure control and driving systems as well as storage for pressurizing gases. The tether also allows for separation between the vehicles to protect from contamination and explosive hazards (Kroll, 1985 and 1986). Furthermore, if performed correctly, tether operations could reduce delta-V requirements for subsequent operations when operating between the TAXI vehicle and an orbital tanker (Carroll, 1985)(see Fig. 3.4.12).

In zero-g loading conditions, as in the case of the attached depot, fluid location in the propellant tanks becomes uncertain and therefore requires some means to prevent gas pockets from interfering with propellant extraction. Attached depots must therefore achieve fluid settling through positive expulsion methods. Positive expulsion is achieved through the use of movable metal and elastomer diaphrams and pistons as well as pressurant gases. These systems add weight to tankage and require that pressurant gases be available wherever a propellant transfer is to take place. This adds a substantial weight penalty and complicates the propellant transfer system (Huzel, 1971). As attached propellant transfer techniques will be necessary if refueling is performed at the cyclic vehicle, pressurizing systems will have to be made available on the cyclic craft itself. The TAXI vehicle will not be equipped with propellant driving pressurization systems.

OFF-LOADING PROPELLANT
FROM TAXI VEHICLE
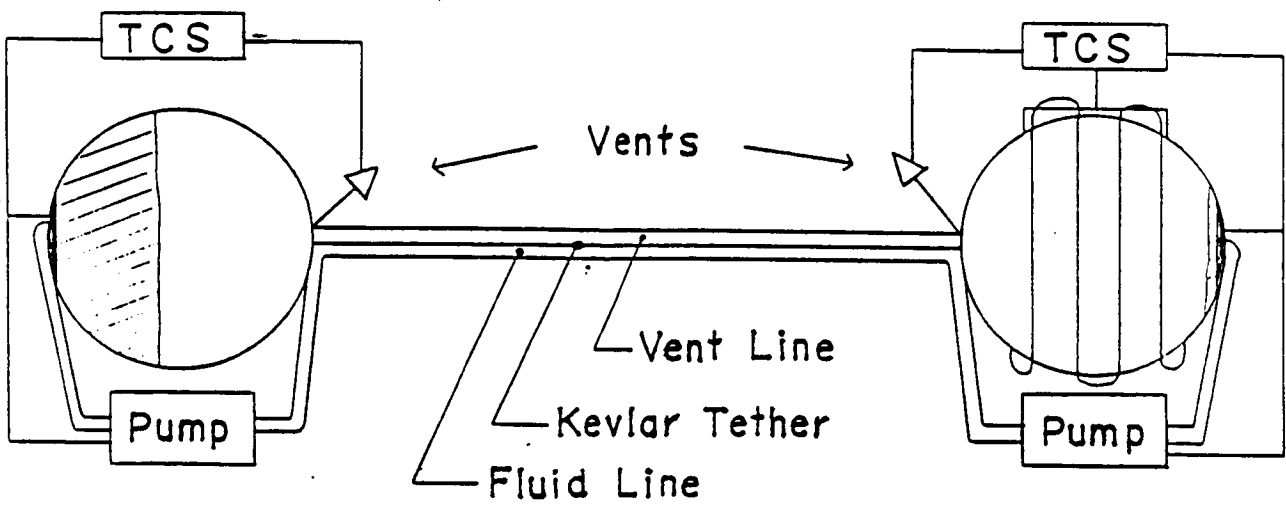
ON-LOADING PROPELLANT
TO TAXI VEHICLE
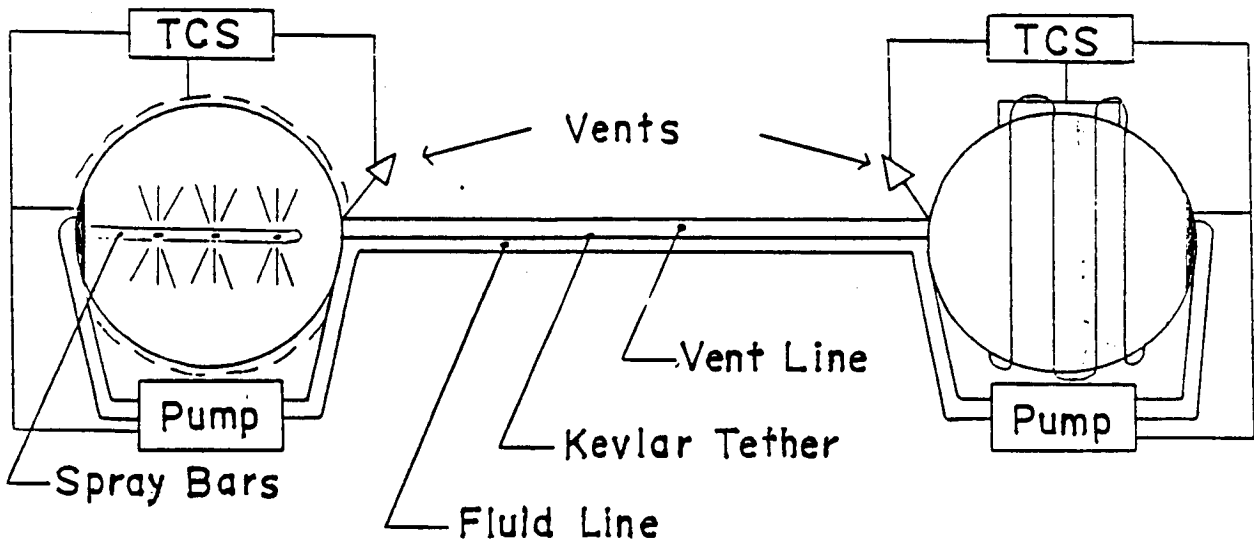
FIGURE 3.4.11

BOOST/DEBOOST OPERATIONS

Tanker to Fuel
Production Site

Taxi Vehicle
to Cyclic Craft
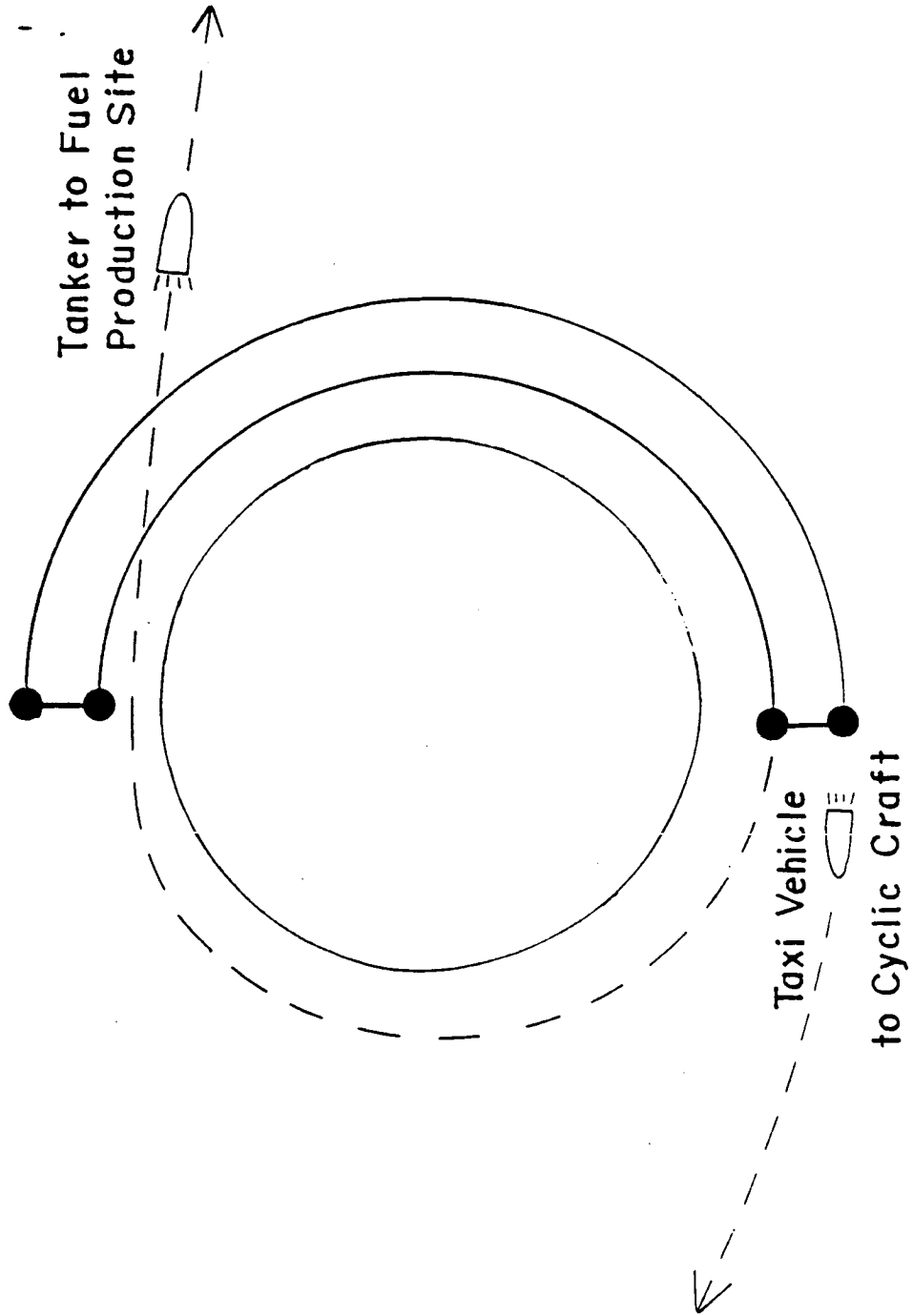
FIGURE 3.4.12

A problem that tethered refueling does have is that of keeping vapor from dipping into the outlet due to suction from propellant outflow. This "suction dip" phenomena becomes the limiting factor in flow rate during refueling. The flow of propellant must be stopped before the vapor reaches the outlet to avoid problems in the propellant feed system. This can cause a large residual propellant mass to be left in the tanks. Tether lengths versus LH2 tank diameter, transfer times for various tether lengths, tank sizes and mass flow rates for various suction dip heights have been calculated for both LH2 and LOX assuming an angular velocity of the tank combinations of .2 rpms. LH2 cases are shown as they are the limiting cases due to liquid properties (Figs. 3.4.13 and 3.4.14). It is concluded from these calculations that reasonable transfer times with residuals as low as 1% can be achieved by varying mass flow rate (Kroll, 1985).

The lines used for tethering the propellant transfer facilities should be made of high strength Kevlar or other high strength polymers and could be housed on large reels onboard the cyclic vehicle (Kroll, 1986 and NASA N85-17006, 1985).

While conducting propellant transfer operations from a storage facility or tanker craft to the TAXI vehicle it will be necessary to "chilldown" the propellant tank walls before pumping. This is accomplished by successively spraying liquid propellant into the tank, and allowing the propellant to vaporize and cool the tank's walls, and then immediately venting it into space (Kroll, 1985). The process will be repeated until the receiving tank's walls are at a sufficiently low temperature to accept the liquid propellant (see Figure 3.4.15).

Tether Length vs. LH2 Tank Diameter

(length for minimum fluid settling)

tether length (feet)

tank diameter (feet)

FIG 3.4.13

69
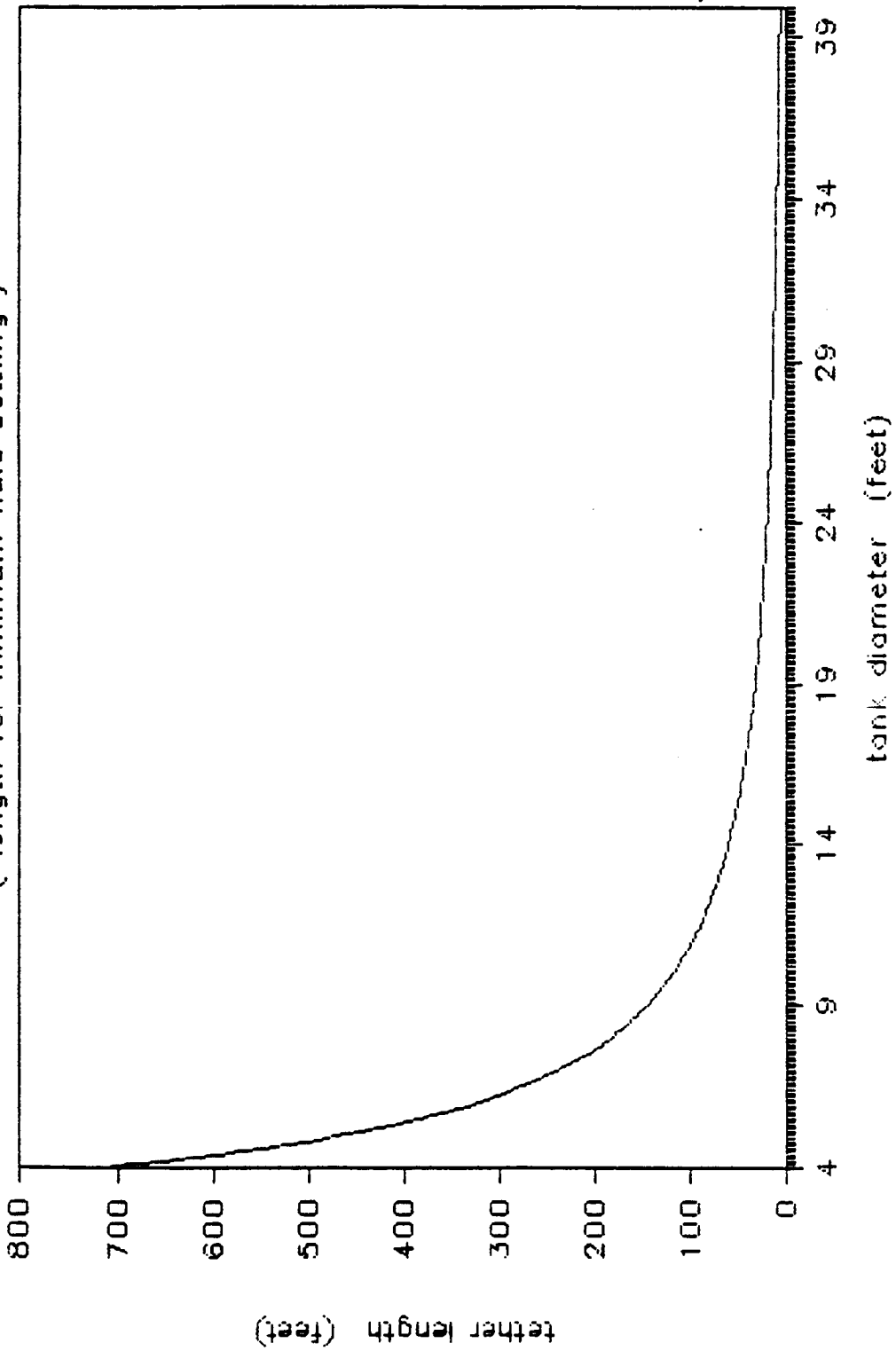
LH2 Transfer Time vs. Tether Length
(8351 lbs. LH2, Dt=19.5 ft., Dl=4 in.)

FIG 3.4.14

70
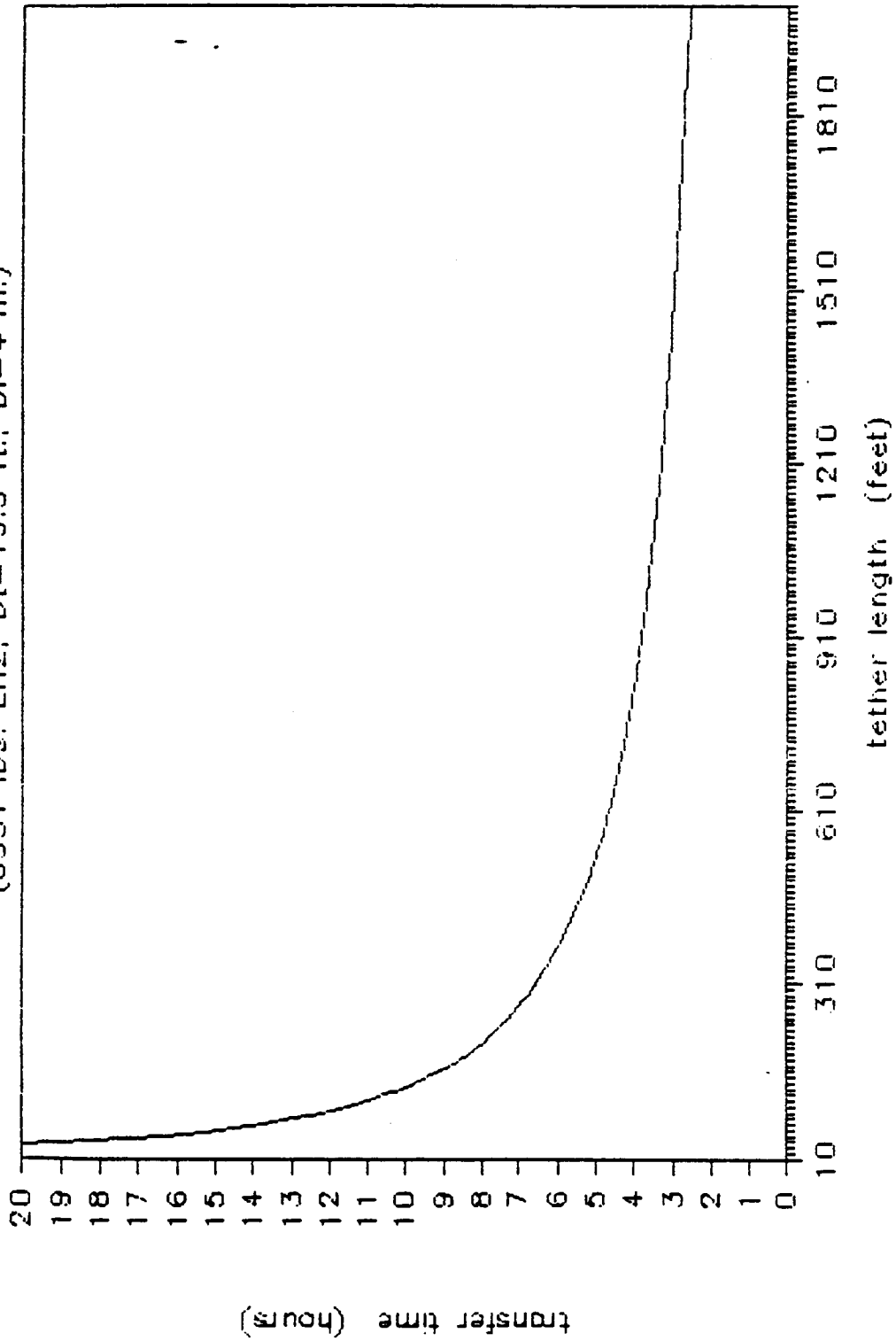
TANK THERMODYNAMICS
DURING CHILLDOWN
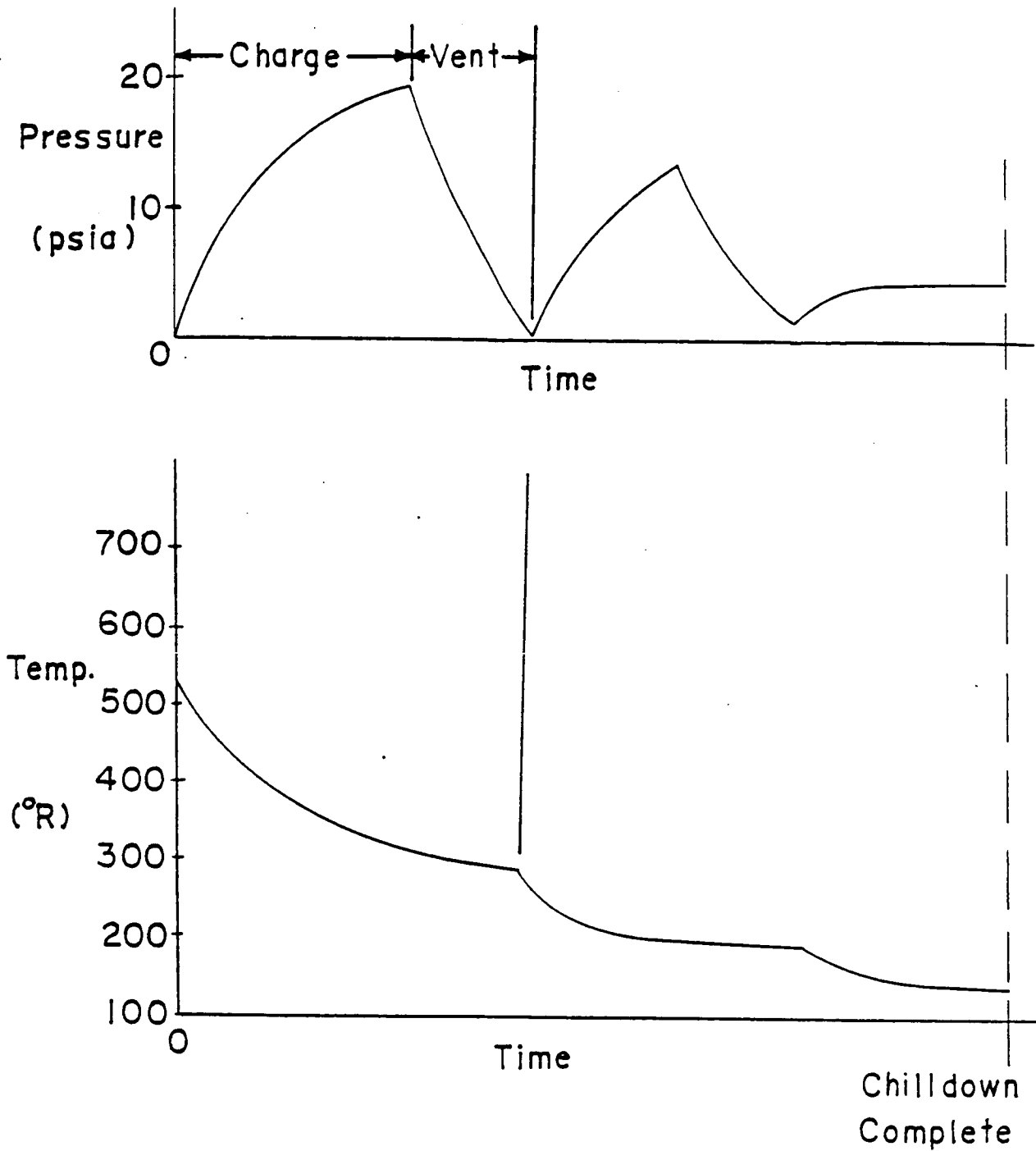
FIGURE 3.4.15

REFERENCES

"Advanced Propulsion Systems Concepts for Orbital Transfer Study", Vol. I, Seattle: Boeing Aerospace Co., 1981.

Bialla, P., P. Rizzo, J. Schuster, C. Torre, and K. Whitehead, "Orbital Transfer Systems Studies & Technologies," December 1986, General Dynamics Aerospace Division.

Blount, D. H. and J. L. Tuttle, Perfect Bell Nozzle Parametric and Optimization Curves, NASA Reference Publication 1104, 1983.

Brown, Norman, "Mars Transit Vehicle Thermal Protection System: Issues, Options, and Trades," NASA-MSFC.

Carroll, Joseph A., "Guidebook for Analysis of Tether Applications," Martin Marietta Corporation, March 1985, Contract no. RH4-394049.

Eagle Engineering, Manned Mars Mission Study Group, "Conceptual Sketches for an Aggressive Man in Space Program," November 1985, NASA Contract no. NAS9-17317.

Eberhardt, Ralph N.,"Propellant Transfer: Attached Depot," Martin Marietta Denver Aerospace, NASA Report no.N85-17005.

Eqorov, P. R., "Fuels for Rocket Engines," NASA Report N67-25155.

Faget, Maxime A., "The Space Shuttle," The Space Shuttle--Its Current Status and Future Impact.

General Dynamics Convair Division, "Definition of Technology Development Missions For Early Space Station-Orbital Transfer Vehicle," San Diego, California, Report no. GDC-SP-83-052. Contract no. NAS 8-35039.

Hastings, Leon J., "Cryogenic Fluid Transfer - Orbital Transfer Vehicle," Marshall Space Flight Center, NASA Report no. N83-11197.

Hill, P. G., and C. R. Peterson, Mechanics and Thermodynamics of Propulsion, Reading, Mass., Addison-Wesley, 1970.

Huzel, Dieter K., D. H. Huang, Design of Liquid Propellant Rocket Engines, NASA SP-125, Washington, D.C., 1971.

Kittel, Peter, "Passive Storage Technologies," NASA Report no. N85-17003.

Klein, Gail A., "Active Cooling Requirements for Propellant Storage," NASA Jet Propulsions Laboratory, NASA Report no. N85-17004.

Kramer, T. J., E. W. Brogren, B. L. Siegel, "Evaluation of Propellant Tank Insulation Concepts For Low-Thrust Chemical Propulsion Systems - Executive Summary," Boeing Aerospace Company, Contract no. NAS3-22824.

Kroll, Ken,"U.S. Gravity Utilization of Tethers Activity," Johnson Space Center, NASA Report no. N86-28417.

Kroll, K., "Propellant Transfer - Tethered Depot," NASA Johnson Space Center, NASA Report no. N85-17006 -- 85-109C.

Lewis Research Center, "Storage and Handling Of Cryogenic Fluids," NASA Report no. N66-33674.

Lindstrom, Robert E. and Judson A. Lovingood, "Status of Space Shuttle External Tank, Solid Rocket Boosters, and Main Engine," The Space Shuttle--Its Current Status and Future Impact.

NASA Space Shuttle News Reference, NASA Press Release Kit, Fourth Space Shuttle Mission, NASA, 1982.

Pederson, Erik S., Nuclear Energy in Space, New Jersey: Prentice-Hall, Inc., 1964.

Perini, L. L., "Thermochemical Code for a Personal Computer", Johns Hopkins Applied Physics Laboratory, 1986.

Peters, Dr. Robert L., Design of Liquid, Solid, and Hybrid Rockets, Hayden Book Company, Inc., New York, 1965.

Quentmeyer, R. J., H. J. Kesper, and J. M. Kazeroff, "Investigation of the Effect of Ceramic Coatings on Rocket Thrust Chamber Life", NASA Lewis Research Center, 1986.

Rysavy, Gordon, Thomas G. Rogers, Michael L. Davis, Robert K. Allgeier Jr., "The Development of Cryogenic Storage Systems for Space Flight," 1970 NASA, Washington, D.C.

Sanchini, D. J. and H. I. Colbo, "Space Shuttle Main Engine Development," The Space Shuttle--Its Current Status and Future Impact.

Sarner, Stanley F., Propellant Chemistry, Reinhold Publishing Corporation, New York, 1966.

"Structural Integrity and Durability for the Space Shuttle Main Engine", NASA-TM-87280.

Stuhlinger, E. A., "Ion Propulsion for Space Flight," McGraw-Hill, New York, 1964.

Sutton, G. P., Rocket Propulsion Elements, New York, John Wiley & Sons, 1956, 1976.

Walburn, Allen B., "Development of a Reusable Flightweight Cryogenic Storage System," AIAA Paper No. 74-726.

Warren, Francis A., Rocket Propellants, Reinhold Publishing Corporation, New York, 1958.

4. Aerobrake Design

As part of the scenario for the Manned Mars Mission, aerobraking will be used to decrease the energy of the   TAXI   at both Earth and Mars. Any configuration considered for the TAXI must therefore be able to achieve the required velocity changes without exceeding heating or deceleration limits. Since 1961, there has been interest in finding a way to accomplish orbital and velocity changes using aerobeaking systems (Walberg, 1982). The drive behind this is the reduction in the amount of weight, namely fuel, that has to be lifted from the earth's surface. For instance, 10 kg must be lifted from earth to place one kilogram in orbit at Mars.

Because the vehicle will be space-based and manned, a design with high reliability that needs little or no refurbishment is desired. Therefore, ablative thermal protection systems (TPS) are undesirable, whereas a flexible, reusable aerobrake structure is desirable.

4.1 Aerobrake Types Considered

Three classifications of aerobraked vehicles have been designated in the literature.[4] The first of these is a variable area type, whose ability to adjust drag is limited by the maximum and minimum brake areas. This type has no lateral plane control: it cannot change the angle of its orbit around the planet.

The second type is a biconic craft with fixed area and variable angle of attack (see figure 4.1.1). A low volumetric efficiency characterizes this kind of vehicle, making it somewhat unsuitable for our project.

The third type considered consists of a large fixed area shield, with a fixed angle of attack and variable bank angle. This vehicle flies a deceleration profile indirectly, with the lift vector moving the craft to a higher or lower density regime to adjust the drag.

A moderate to high L/D aeromaneuvering vehicle was dismissed as a possibility.[3] It weighs much more than other designs for a given payload volume, is more difficult to construct, and its high ballistic coefficient necessitates a heavier heat shield.

Based on mission requirements, three aerobrakes were examined: a symmetrical aeroshell (figure 4.1.2), an extendable web mesh behind or in front of the ship (figure 4.1.3), and a raked-off elliptical cone (figure 4.1.4). Blunt symmetric aeroshells have been studied extensively, and were presented for the NASA Manned Mars Mission Report.[7] The latter two designs were investigated in more detail.

The webbing design has two possible configurations (Ehricke). The first consists of a rigid outer frame with ribbons of Teflon-covered steel mounted in tension between the sides of the frame. This configuration weighs more than the second design which is simply a mesh of ribbons. The cables are held in tension during aerobraking by forward-running cables and aerodynamic forces. These cables would be highly susceptible to flutter.

BICONIC LIFTING CRAFT

FIGURE 4.1.1

SYMMETRIC AEROSHIELD

fuel tanks

symmetric aeroshield

crew module
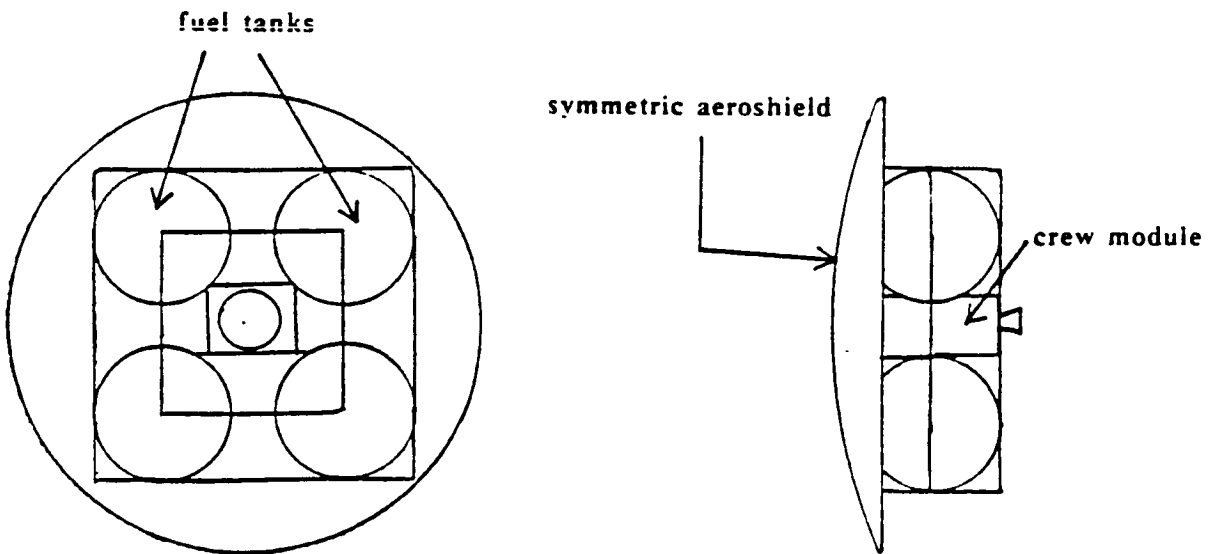
FIGURE 4.1.2

FLEXIBLE MESH BRAKE
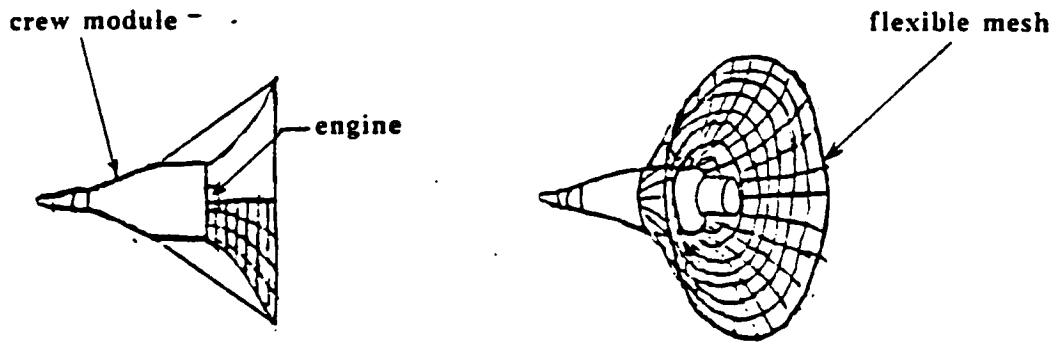

FIGURE 4.1.3

RAKED-OFF ELLIPTIC CONE
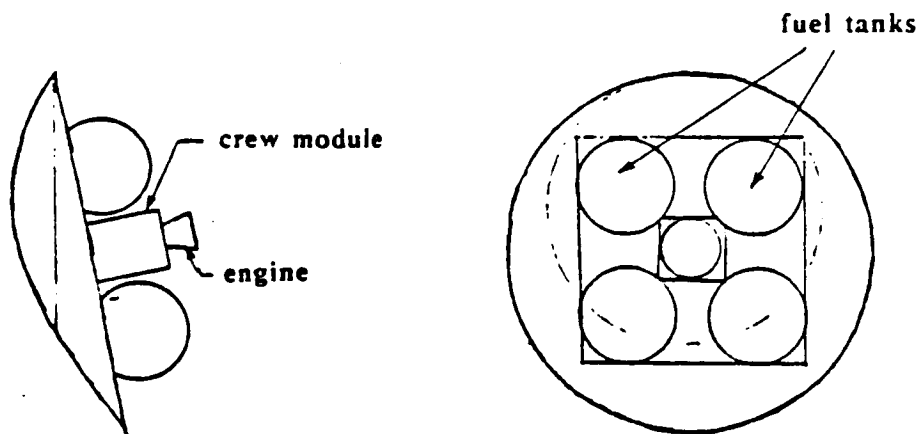
FIGURE 4.1.4

The advantages of this type of design are the ability to radiate heat from both the inner and outer surfaces, very low weight, variable brake deployment (allowing adjustment to drag requirements), and the fact that the use of large, high-drag surfaces reduces the need to enter high density atmospheric regions for velocity reduction. Unfortunately, literature searches revealed only two papers which examined this design; they pointed out many technological barriers to a brake of this type, leaving more questions than this level of investigation could answer.

The following section describes the chosen configuration, an ellipsoidally-blunted raked-off elliptic cone (EBROEC), mounted in front of the crew module, payload and engine systems. Next, trajectory simulations and aerothermodynamic analysis of the aerobrake (sections 4.3 and 4.4) are discussed followed by presentation of a preliminary structural design of the aerobrake and its supporting structure (sections 4.5 and 4.6). All these sections refer to the TAXI version A. The main design paremeters of the aerobrake for the TAXI versions B and C are given at the end of this chapter.

4.2 Aeroshield Geometry Analysis

The heat shield designed for the TAXI is basically a modified elliptic cone, with a coordinate system setup which has its origin at the vertex of the cone(figure 4.2.1). The half-angle along any given meridional cut (φ=constant) is called θ. Specifically, the half-angle in the x-y plane is designated θ_{xy} and in the x-z plane θ_{xz}. From these angles the cone ellipticity is defined as $\varepsilon = \tan\theta_{xy}/\tan\theta_{xz}$. A reference plane is chosen normal to the x-y plane and raked at an angle δ with respect to the x-z plane. The requirement that the intersection of the cone and the reference plane be a circle for easier shape definition determines the angle θ_{xz}, and hence ε, for a given δ and θ_{xy}.[2] For our selection of θ_{xy} =60 degrees, we will have a cone ellipticity of 0.9377 in order to have a circle as a base.

To reduce nose heating, the nose is replaced with an ellipsoid which is tangent to the cone at every point. The shape of the ellipsoid is determined by the ellipticity ε_b. The region of the elliptic cone between the ellipsoid and the reference circle is a function of φ, the angle about the x-axis describing the y-z location, and the equation for the elliptic cone.

In each plane of constant φ, a circular skirt of radius R is fit to the reference circle. This will reduce the trailing-edge heat flux and provide greater dynamic stability. The center of rotation for the arc (x_{os}, r_{os}) is a function of φ. The rear of the body is defined by a base plane parallel to the reference plane. The angular extent τ of the circular arc defines the distance between the reference plane and the base plane. Note that the resulting base plane is no longer a perfect circle. A shape of this form is then completely characterized by specifying δ θ_{xy}, ε_b, R, and τ.

The conical afterbody is raked off at angle δ to provide lift at zero angle of attack. The base of the heat shield in the rake plane is circular for packaging efficiency and to ease the joining of the shield and payload. The heat shielding under consideration would have a nominal diameter of 120 ft (36.5 m).

With a suitably placed center of gravity, this design produces lift and trim at zero angle of attack. One other advantage of high rake and cone angles is that it permits a greater latitude in the placement of the center of gravity; i.e. the c.g. can be placed farther aft.

77

FIGURE 4.2.1

FIGURE 4.2.2

PRECEDING PAGE BLANK NOT FILMED
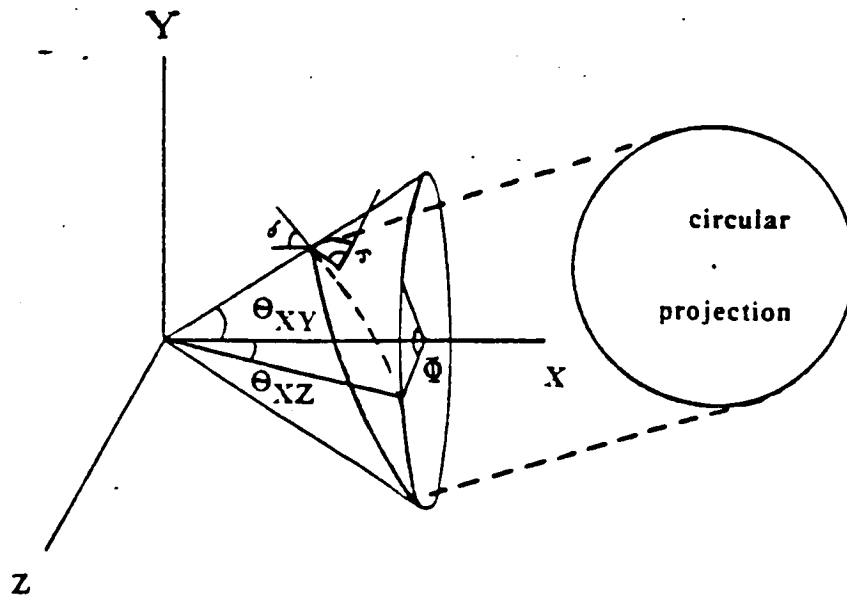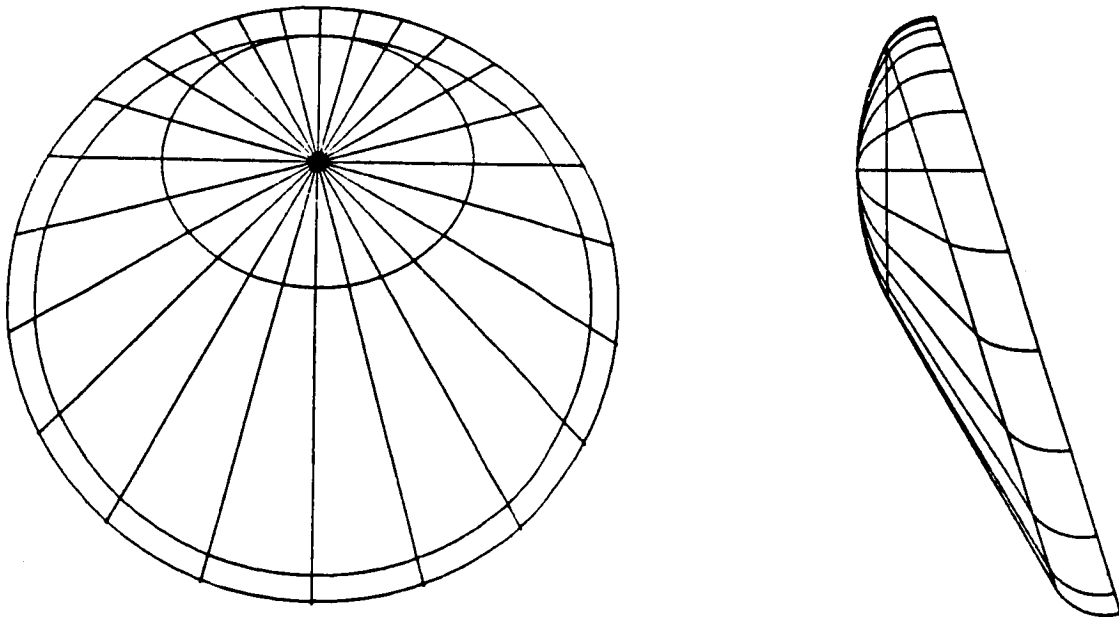
Our current design utilizes a rake angle of 80 degrees. For a given rake angle there will be an optimal radius of curvature, R_o, at the nose in order to reduce maximum heat flux. This radius is a measure of the bluntness of the ellipsoid at the Newtonian stagnation point in the x-y (pitch) plane. Larger values of R_o are possible for a given δ and θ_{xy} by increasing the nose ellipticity ε_b. As ε_b increases the nose becomes flatter. An optimum ε_b is possible from a standpoint of a uniform heat flux on the blunt surface, and will be discussed further in section 4.4. In this design we will use an ellipticity ε_b of 2.0, resulting in a moderately flat nose with low heating rates[1].

The shape of the heat shield has been computed and is shown in figures 4.2.2 and 4.4.1. Its main advantage is its lift at zero angle of attack relative to its x-axis. See the paper by Cheatwood, et al. for a complete geometrical derivation of the shield.

4.3 Aerobrake Trajectory

4.3.1 Introduction

Aerobraking uses the planet's atmosphere to dissipate energy to affect orbital changes. The velocity decrement is accomplished through the aerodynamic properties of the vehicle, mainly drag. A plane change is desirable, but not a requirement. The vehicle in this design is classified as one with a fixed area and fixed angle of attack with variable bank angle and roll rate (Dauro, 1979). This means that lift moves the craft to higher and lower density regions to keep the ship on the design deceleration profile. This differs from a direct profile, which would be flown by changing angle of attack, thus changing lift and drag.

The type of trajectory to be flown is a skip trajectory, defined by Eggars and Allen as having three parts: atmospheric entry, maneuvers, and atmospheric ejection. Figure 4.3.1 is a sketch of the flight path. Also included in the sketch is a diagram of the forces acting on the vehicle throughout the passage. The equations of motion for this ship are written in terms of coordinates parallel and perpendicular to the flight path. The resulting equations are generally nonlinear, second order differential equations which cannot be easily integrated (Chapman, 1957). The simplified equations were derived by Miele, who assumed a flat, nonrotating planet. He further simplified the equations by assuming $D/W \gg 1$, $L/W \gg 1$, and flight in two dimensions. These equations will be integrated numerically in time so that the flight profile can be determined. After a description of the mission and the computer programs, the results of the programs will be discussed in terms of whether or not aerobraking can accomplish the required velocity changes.

4.3.2 Mission Requirements

The entry state of the vehicle is important in determining whether or not the vehicle can achieve its mission. Dauro and Boobar defined the entry state by latitude, longitude, altitude, velocity azimuth, flight path angle, aerodynamic characteristics, and the ship's physical constraints, which include limits on aerodynamic heating, aerodynamic pressure, and deceleration. In order to achieve the required velocity decrement, the only parameter that may be varied is the flight path angle. Table 4.3.1 provides an overview of the relevant parameters.
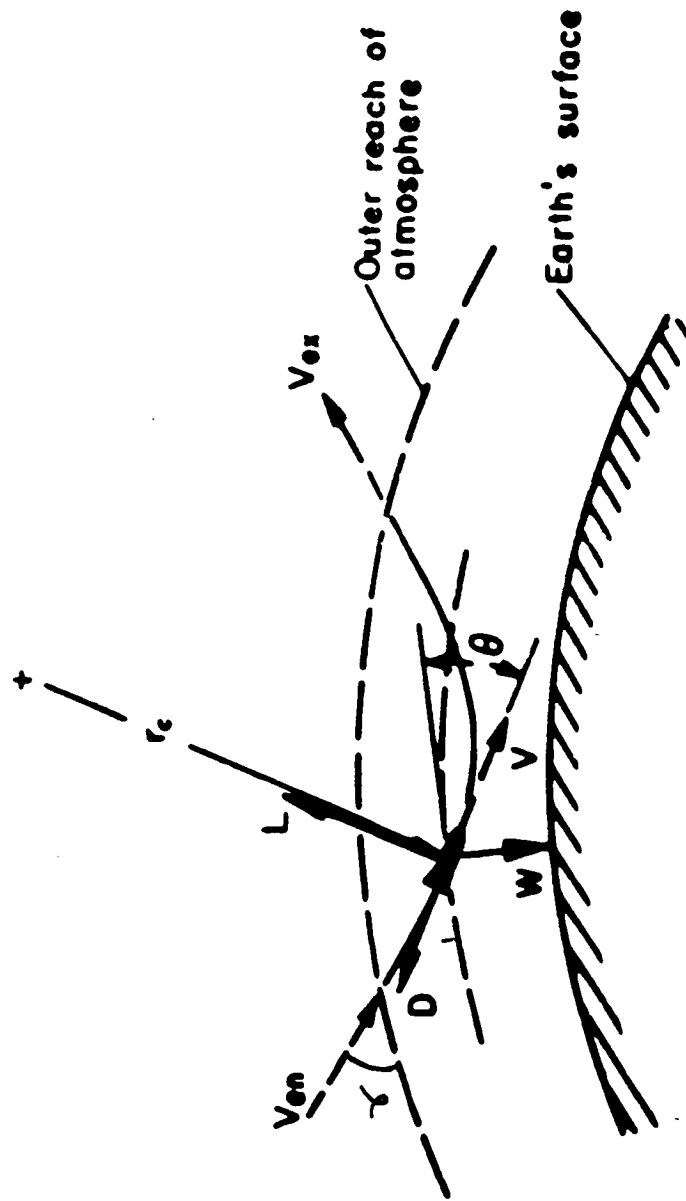
FIGURE 4.3.1 (Ref. 4)

Table 4.3.1 Physical Parameters (TAXI A)

Reference area, A	11602.4 ft^2 (1078 m^2)
Vehicle mass at the beginning of the aeroassisted maneuver near Earth, M_{BAM}	114,347 lbm (51,855 kg)
C_D	1.574
Ballistic coefficient $M_{BAM}/C_D A$	6.26 lbm/ft^2 (30.56 kg/m^2)
L/D	0.1526
Maximum heating rate, $\dot{q}_{max}$	30 W/cm^2
Maximum acceleration	5 g
Initial inclination	23 deg.

Latitude, velocity, and velocity azimuth were prescribed by the orbital mechanics group. At both Earth and Mars, the ship enters the atmosphere with its velocity vector at an angle of 23 deg to the plane of the equator. In order to dock with the space station in LEO, and Phobos orbit, the ship must be in the plane of the equator, so that whatever plane change cannot be accomplished during the atmospheric pass will have to be done by propulsion. Aerodynamic characteristics are calculated in section 4.4.1 using Simplified Newtonian Theory. The reference area is the area perpendicular to the free stream. Nicalon, the flexible thermal protection material, defines the limit on aerodynamic heating. The deceleration limit was imposed by the maximum that the crew can be subjected to. The use of a low L/D and low ballistic coefficient makes it possible to stay in the viscous region of the atmosphere, which keeps heating and deceleration rates low since most of the aerobraking will occur near perigee (Dauro, 1979, Walberg, 1982).

The exit state is defined by the same parameters as the entry state. The final velocity is determined by the velocity change. The other parameters are important in determining corrections needed beyond the atmosphere to place the ship in its final orbit.

4.3.3 Computer Programs

Computer programs simulate trajectories by using numerical techniques to integrate the equations of motion. The accuracy of the simulation depends on the assumptions made in the governing equations and the accuracy of the numerical method. Two programs, one simple and the other complex, were used. A simple model can be run quickly and cheaply on a personal computer.

Simplified

Using Miele's equations and the further assumption that density varies exponentially with altitude, a FORTRAN code using Euler integration was written and run on an IBM Personal Computer. The trajectory was purely ballistic, with no bank angle modulation. This means that the results will be the most severe that can be expected. The program outputs velocity, acceleration, and altitude as funtions of time, as well as the magnitude and point of maximum dynamic pressure. Heating rates were not determined within this program; instead, a code that solved the Euler equations for an axisymmetric shape was used to solve for the heating rates at the perigee of the trajectory.

POST

The second simulation was the Program to Optimize Simulated Trajectories, POST, which was written at NASA Langley in 1971 and is updated continuously. The program can be run for either 6 degrees of freedom (DOF), or 3 DOF. In 3 DOF it assumes that the vehicle is a point mass, limiting its motion to vertical, forward, and lateral directions. The program optimizes entry angle using heating rates and deceleration as limiting parameters. The trajectory is controlled by bank angle, with rolls considered instantaneous. POST outputs include velocity, altitude, acceleration, dynamic pressure, heating rate, and bank angle as functions of time. The heating rate is based on Chapman's heat equation, which accounts for the incident convective heat on the shield. It does not account for the shield's ability to reflect incoming heat, nor does it take into account radiation, which may be important, especially at Mars.

4.3.4 Results of the Simulations

Both codes were run at Earth and Mars. Initially, POST was run at Mars because the acceleration and thermal environments were expected to be more severe. However, this did not appear to be the case when the simulation results were fully analyzed.

Earth

For the first pass at Earth, the ship will enter the atmosphere at 41393.6 ft/sec (12.62 km/sec) requiring a loss of 6133.6 ft/sec (1.87 km/sec). Figures 4.3.2 through 4.3.4 show the velocity, acceleration, and altitude from the PC simulation for three different entry angles: -0.5, -1.0, and -1.5 deg. From figure 4.3.3 it is apparent that an entry angle close to -.75 deg should be chosen. This results in a maximum acceleration of 1 g which is well below the 6 g limit. The altitude plot shows that the craft will reach perigee still in the viscous region of the atmosphere.

POST, however, found -4 deg to be the best entry angle (Figure 4.3.5). A gamma higher than -4 deg caused skipping into a hyperbolic orbit. The resulting maximum acceleration and heating rates are 3.5 g's acceleration and 20.5 W/cm^2 Fig. 4.3.6 & 4.3.7).

The second pass begins at a velocity of 35 686.4 ft/sec (10.88 km/sec). Figure 4.3.8 shows that an entry angle of approximately -1.25 deg. will result in the necessary loss of 9184 ft/sec (2.80 km/sec). The associated values of maximum acceleration, 1.84, and minimum altitude, 280,085 ft (85.37 km), are shown in figures 4.3.9 and 4.3.10 respectively.

POST again required a steeper entry angle than the PC simulation to avoid skip-out to a hyperbolic trajectory. The entry angle is about the same as for the first pass, -3.72 deg, (Figure 4.3.11), but the acceleration is higher, 4.0 g (Figure 4.3.12). The heating rate is 14.5 W/cm^2 (Figure 4.3.13).

Mars

The results of the PC simulation at Mars reveal that an entry angle of -2.5 deg will enable the ship to lose 19 122.4 ft/sec (5.83 km/sec). However, it has been calculated that at this entry angle the acceleration exceeds the 6 g limit. Without checking the results against POST, this would lead to an erroneous conclusion that either the ship needs to be redesigned or rockets must be used.

POST required an entry angle less than -6.0 to avoid skipout to a hyperbolic trajectory , and greater than -7.5 degrees to avoid impact with the planet. Figure 4.3.14 shows that an entry angle of -6.5 is the optimum. These angles are much larger than those in the PC simulation, yet the maximum acceleration is three Earth g's (fig. 4.3.15). This can be attributed to the control of the flight path through roll and the fact that POST integrates the complete governing equations. Figures 4.3.16 and 4.3.17 show a maximum heating rate of 18.9 W/cm^2 and a maximum dynamic pressure of 240 N/m^2. Both of these values are below the upper limits.

The second pass at Mars was not simulated because of the small velocity decrement required.

4.3.5 Conclusions and Recommendations

In its present configuration the ship can achieve all of the specified velocity decrements, eliminating the need for propulsive maneuvers. Table 4.3.2 summarizes the results of the trajectory simulations. The passes at Earth do not present any problems in terms of stress on the ship, crew, or modeling. Mars, however, requires more sophisticated modeling. Because of the narrow entry corridor, complex adaptive control laws will be necessary, which was expected (Walberg, 1982). Because the ship will fly in the free molecular and viscous regions of the atmosphere, degradation of L/D will have to be taken into account, and analysis of rarefied flow, which is difficult to simulate in ground test facilities, must be improved. In further studies a better model of the heating environment at Mars will be required, and the 6DOF POST simulation should be run.

Table 4.3.2 Trajectory Summary

	Earth		Mars	
	Pass 1	Pass 2	Pass 1	Pass 2
V_{enter}(kft/sec)	43.33	35.69	33.88	16.07
delta-V(kft/sec)	6.13	9.18	7.81	2.07
V_{exit}(kft/sec)	35.19	26.50	16.07	14.00
Gamma$_{initial}$(deg)	-4.0	-3.72	-6.50	
Initial Inclination(deg)	23.0	?	23.0	
Plane Change(deg)	1.12	2.0	6.65	
Perigee Altitude(kft)	311.60	301.76	229.60	
Passage Time(sec)	130.0	247.0	160.0	
Maximum Acceleration(g)	3.52	4.06	2.9	
$\dot{q}_{max}$ (W/cm^2)	20.5	14.50	18.9	

Velocity vs Time

First Pass
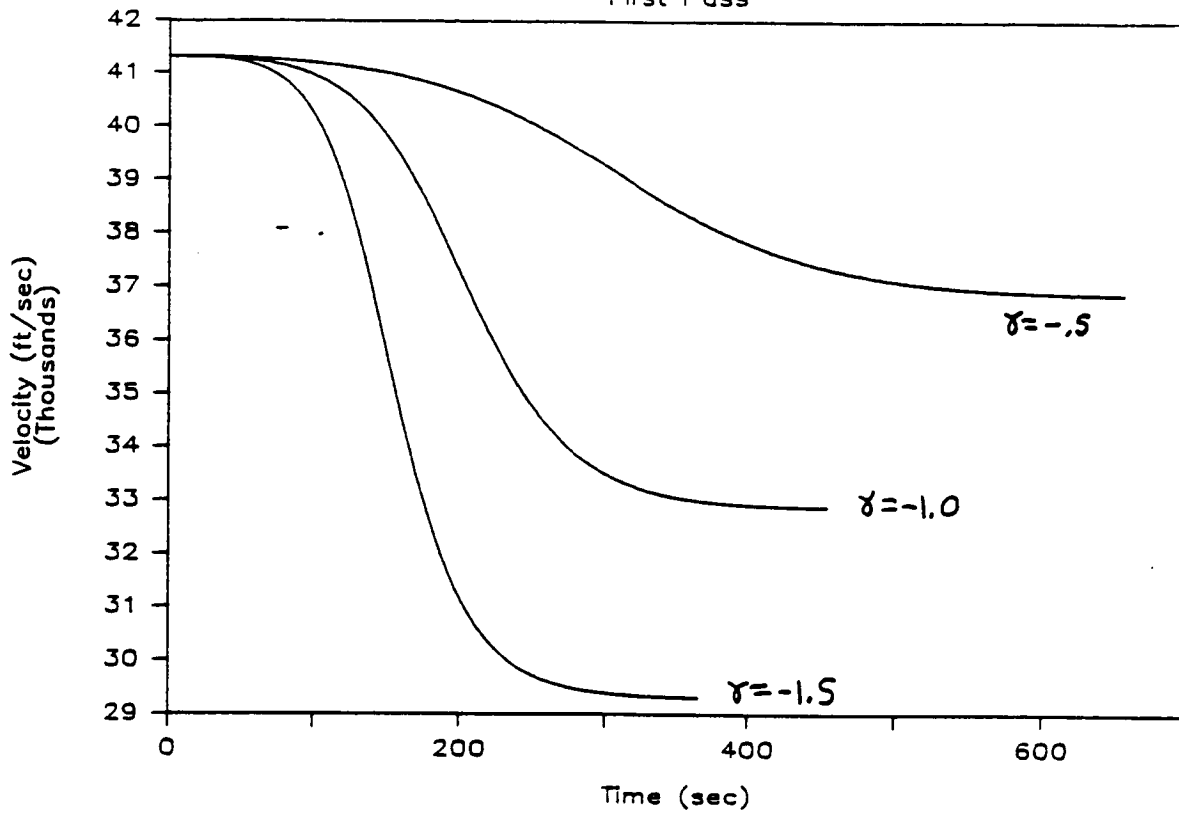
FIG 4.3.2

Acceleration vs. Time

First Pass
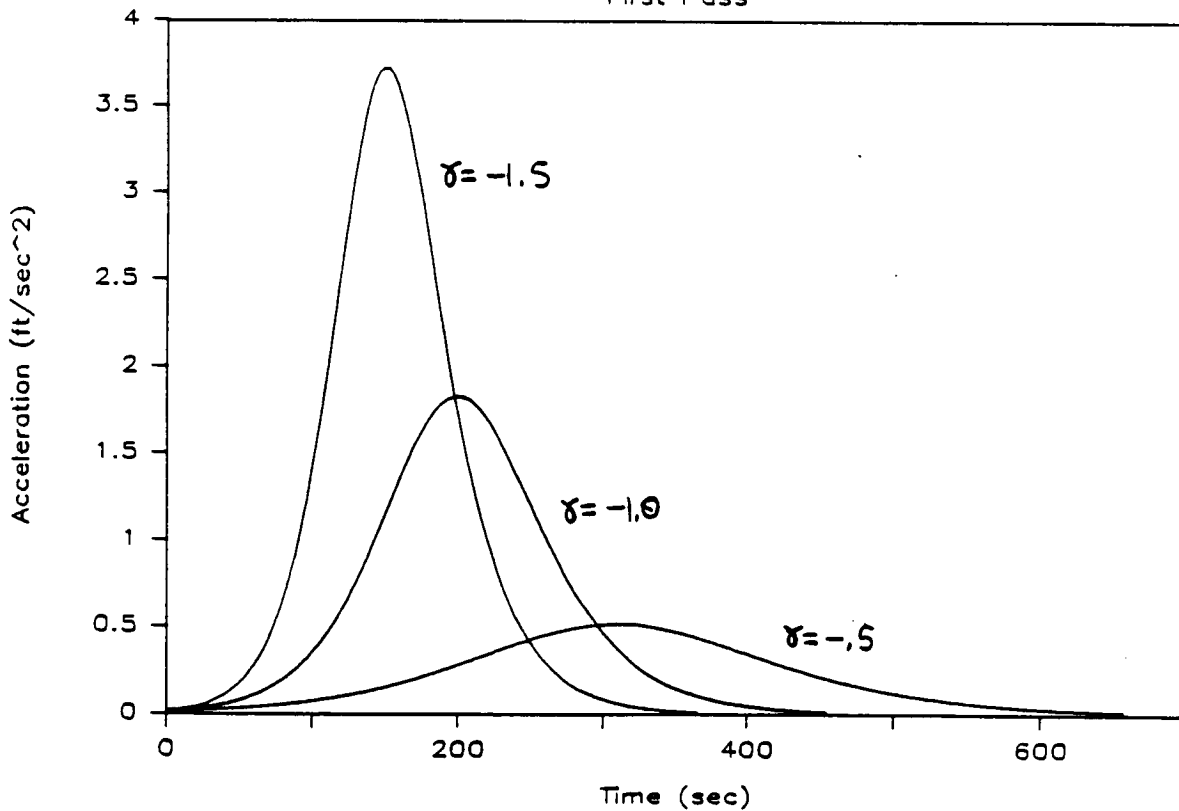
FIG 4.3.3

Altitude vs. Time

First Pass
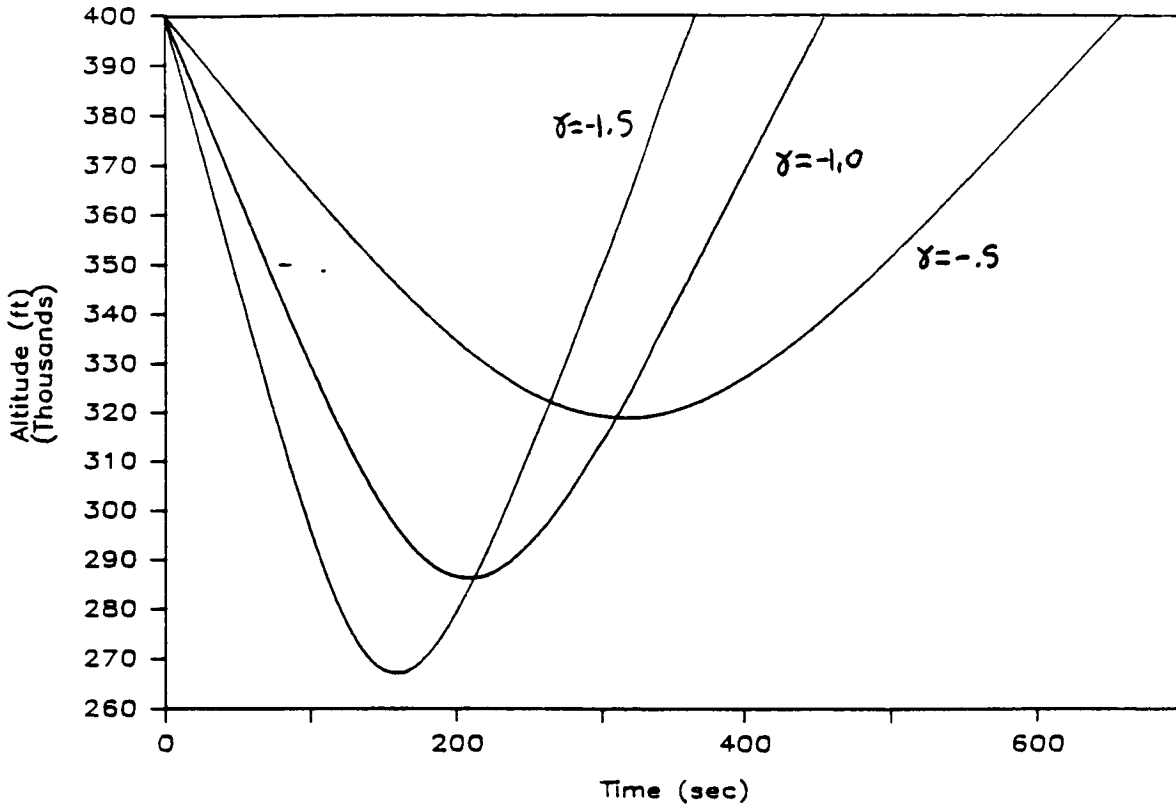
FIG. 4.3.4

FLIGHT PATH ANGLE

EARTH AEROBRAKING, FIRST PASS
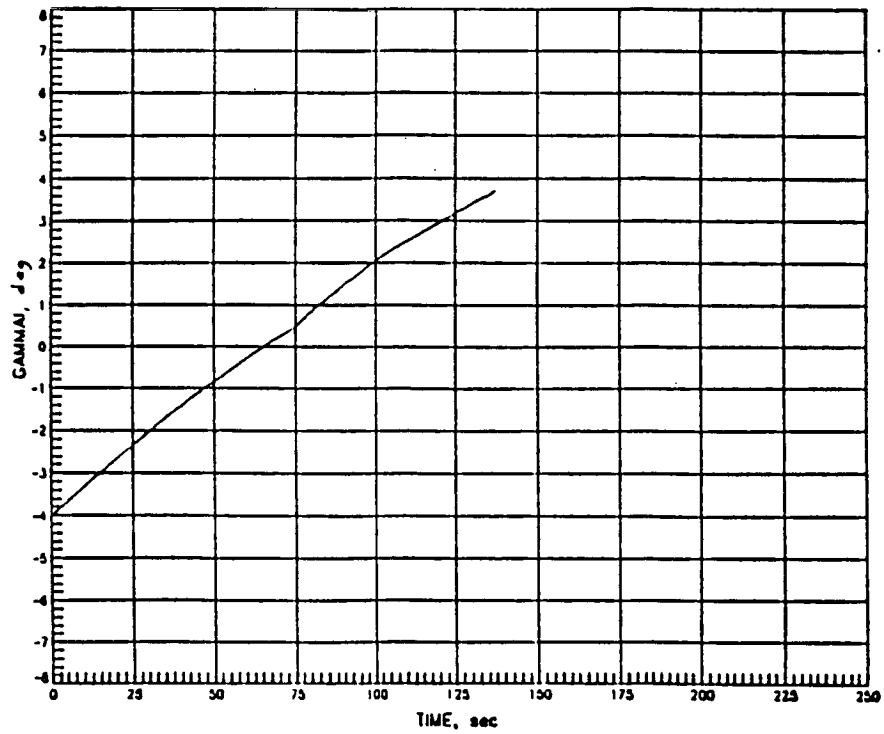
FIG. 4.3.5

85
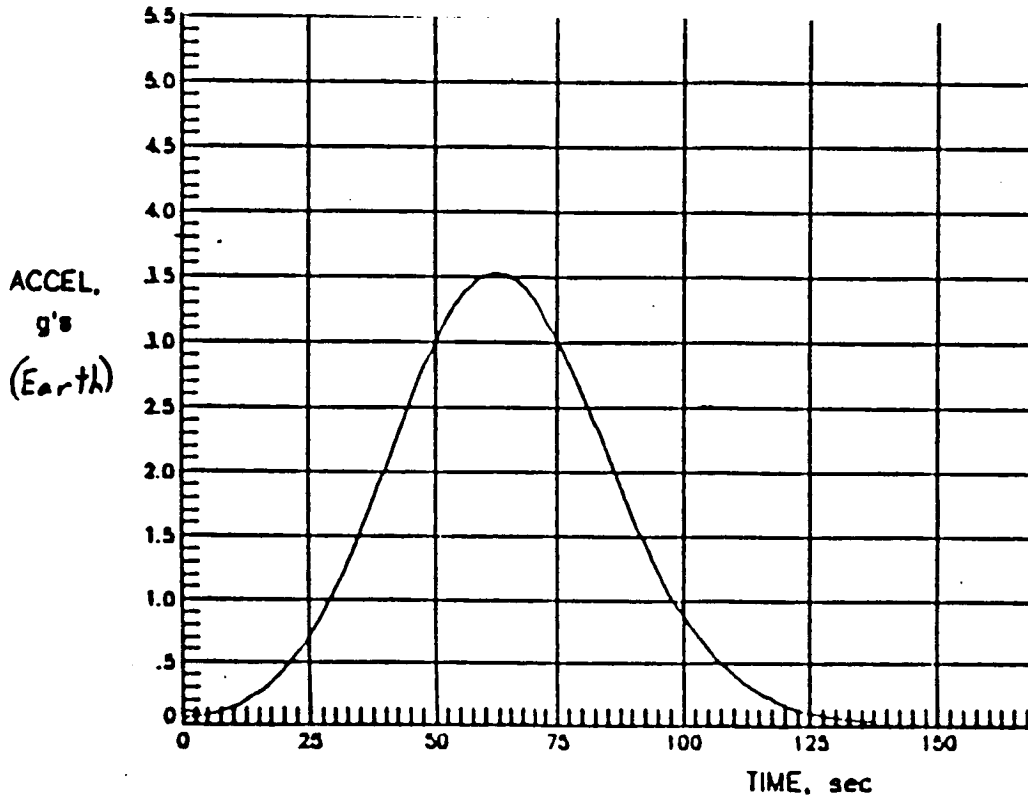
ACCELERATION

FIGURE 4.3.6

FIGURE 4.3.7

86
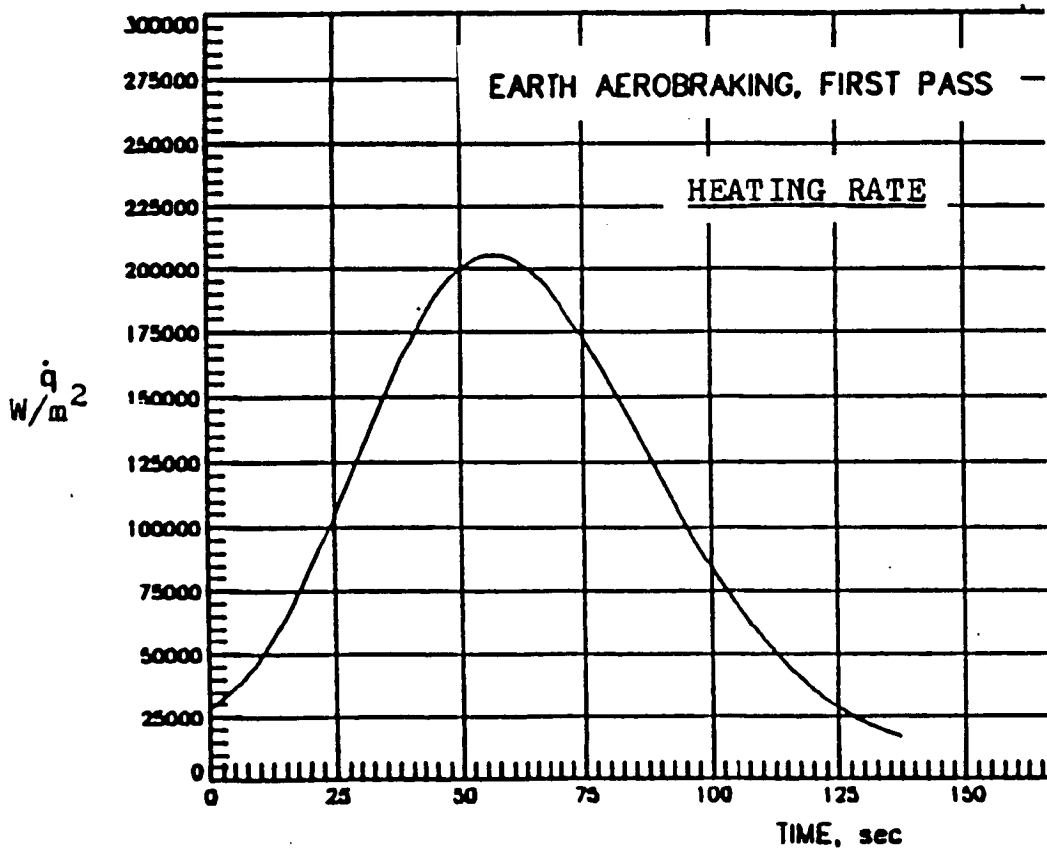
Velocity vs Time
Second Pass

$\gamma=-1.0$

$\gamma=-1.25$

$\gamma=-1.5$
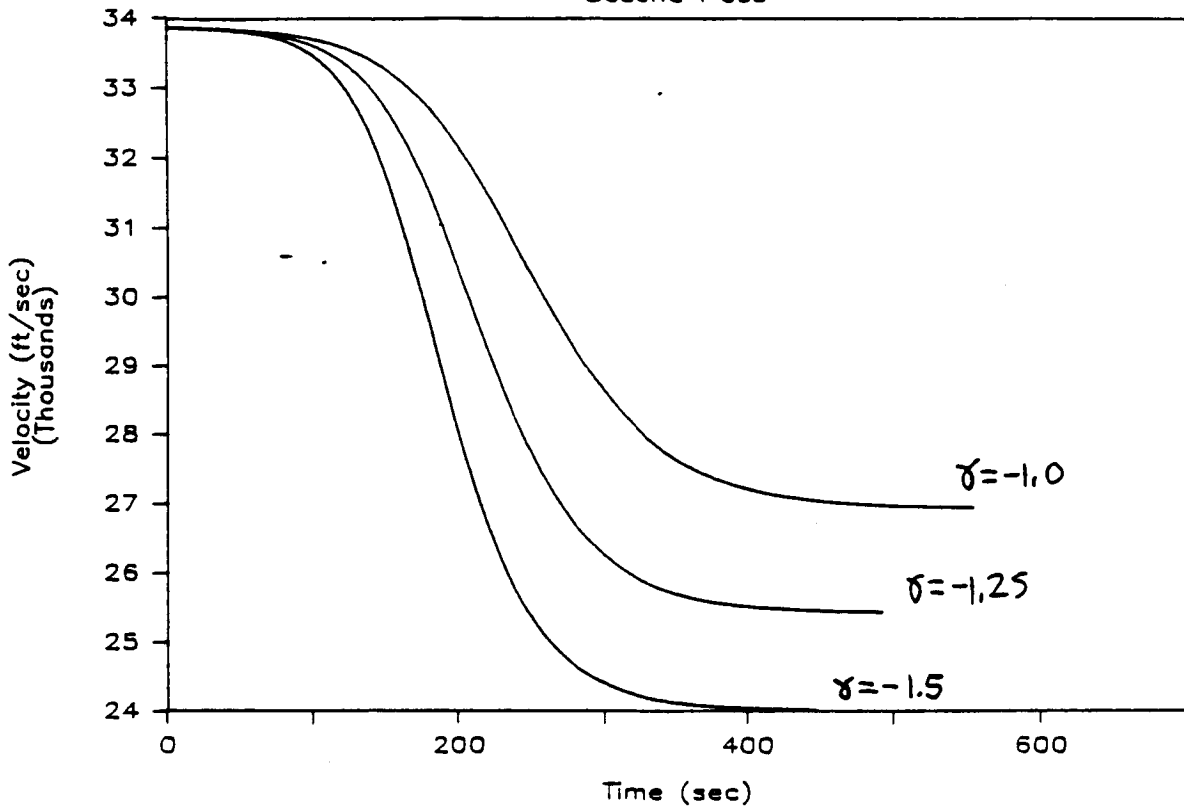
FIG 4.3.8

Acceleration vs. Time
Second Pass

$\gamma=-1.5$

$\gamma=-1.25$

$\gamma=-1.0$
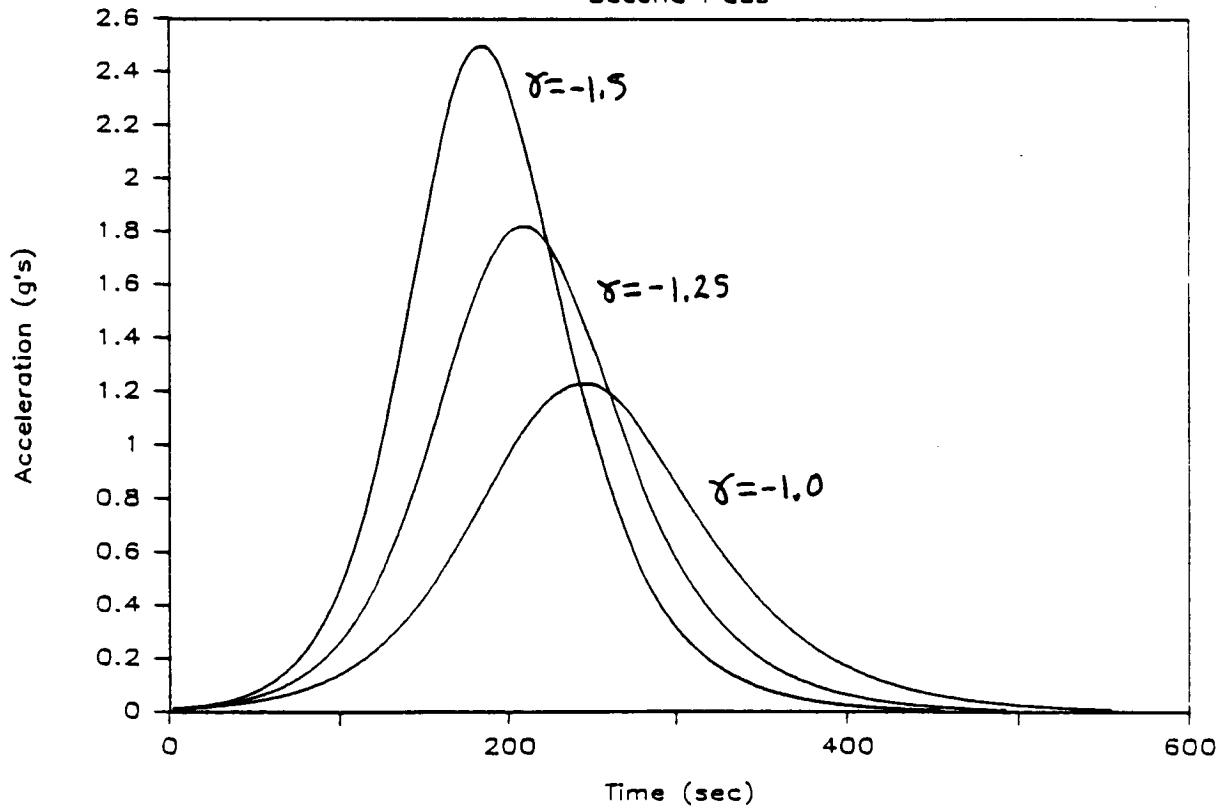
FIG 4.3.9

Altitude vs. Time
Second Pass
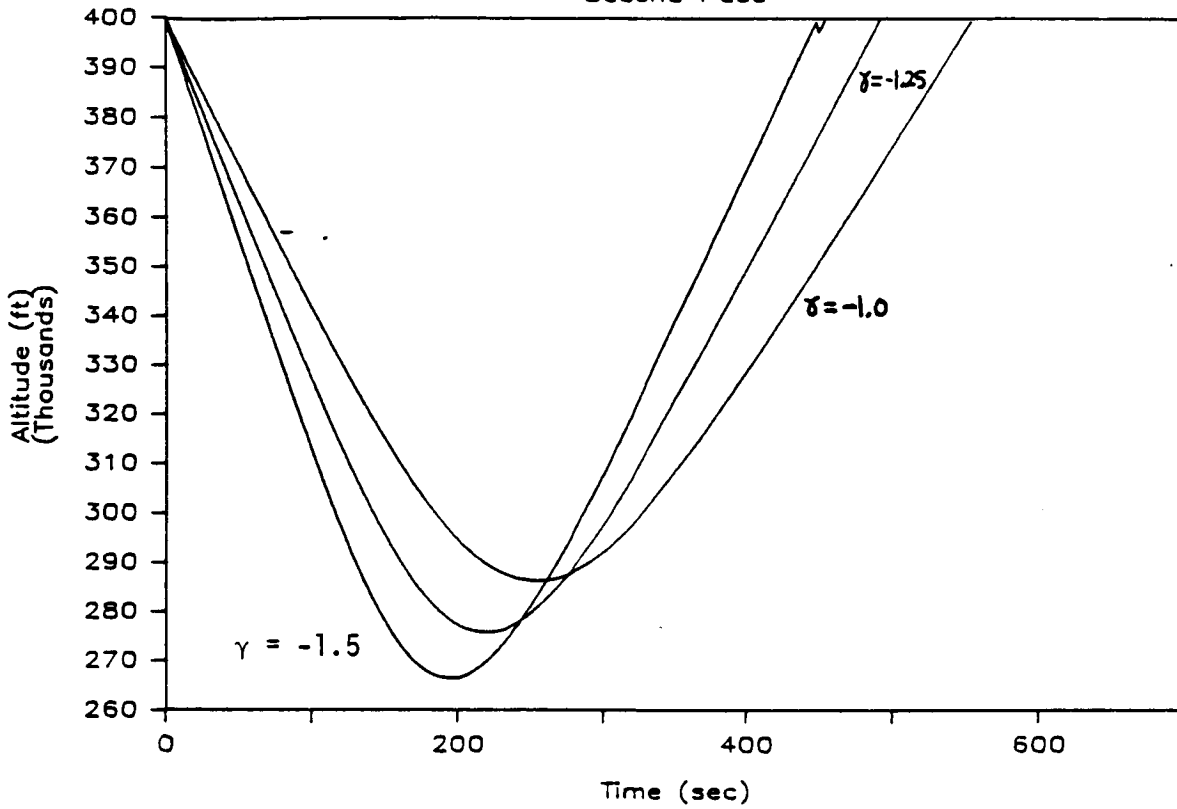
FIG 4.3.10
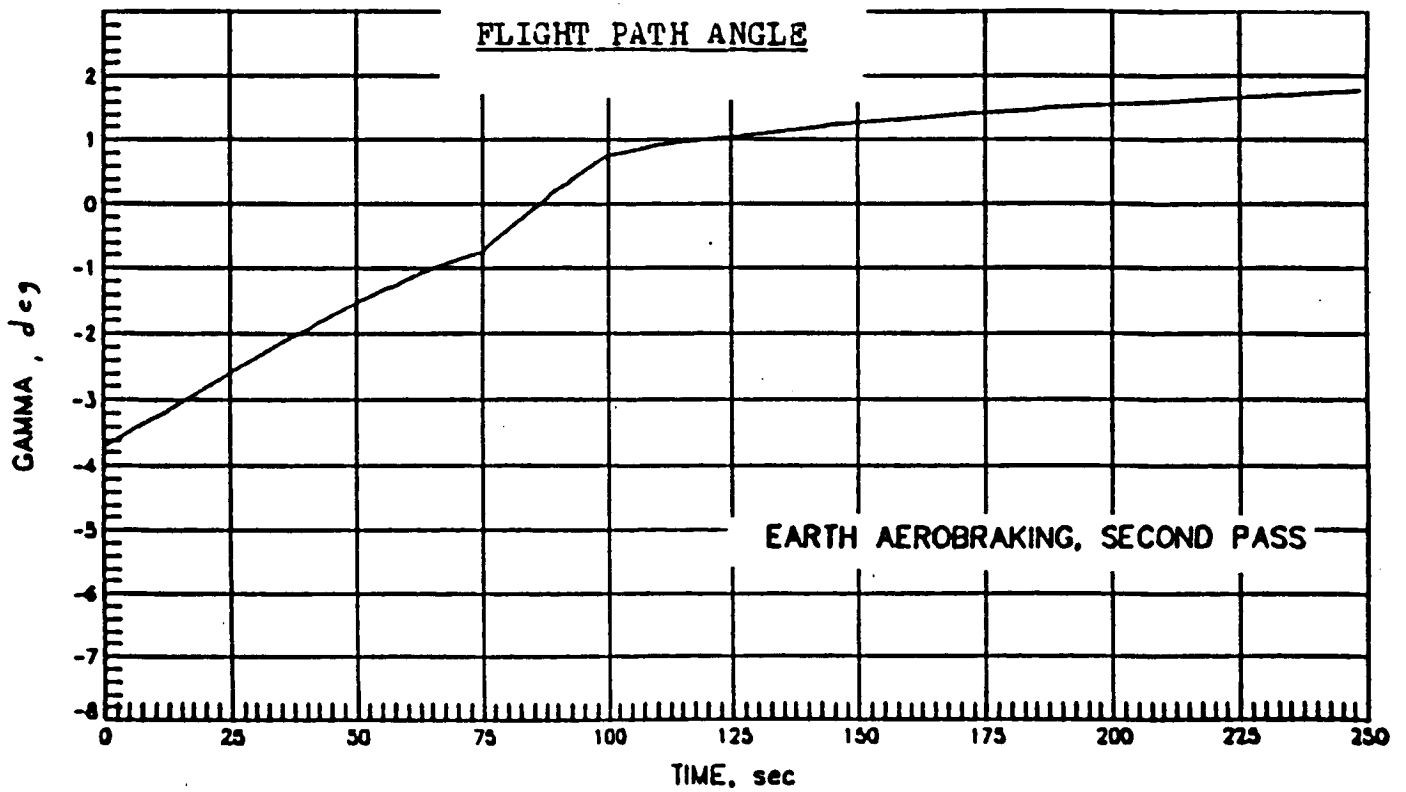
FIGURE 4.3.11
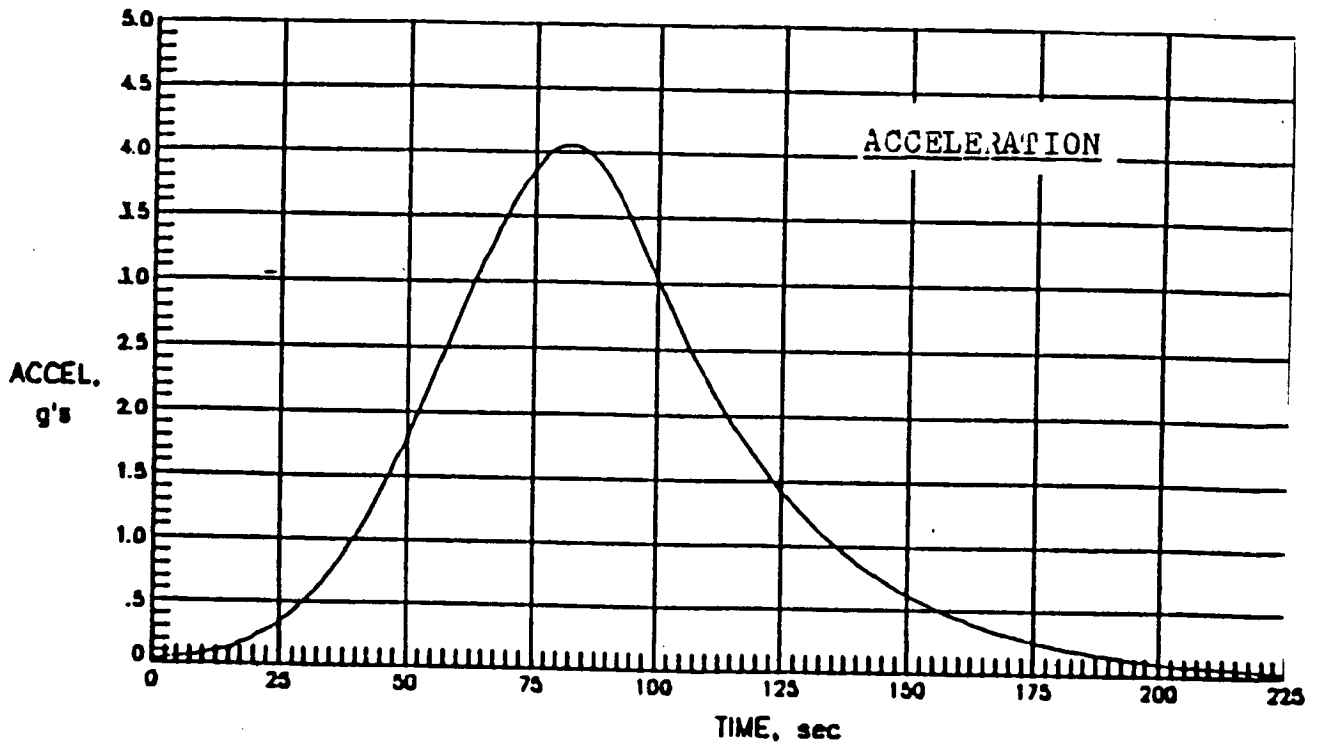
FIGURE 4.3.12
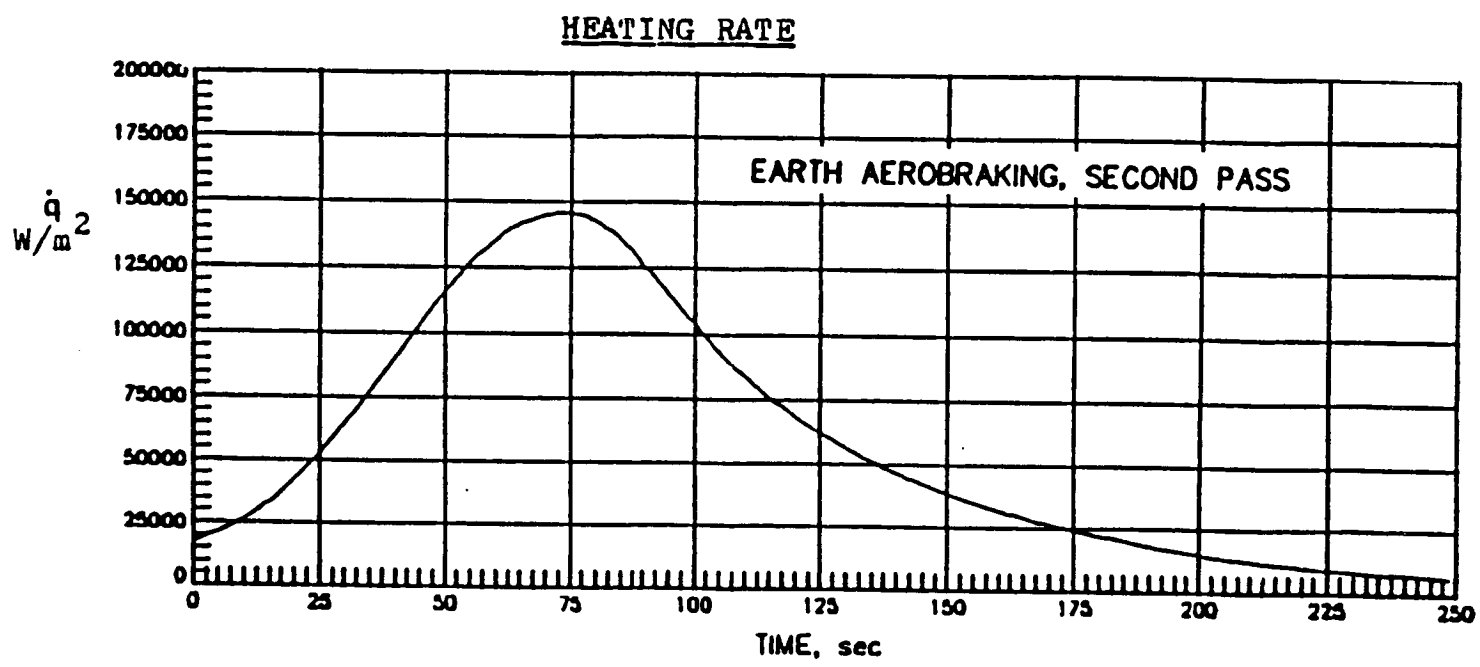
FIGURE 4.3.13

FLIGHT PATH ANGLE

MARS AEROBRAKING

FIGURE 4.3.14

ACCELERATION

FIGURE 4.3.15

90
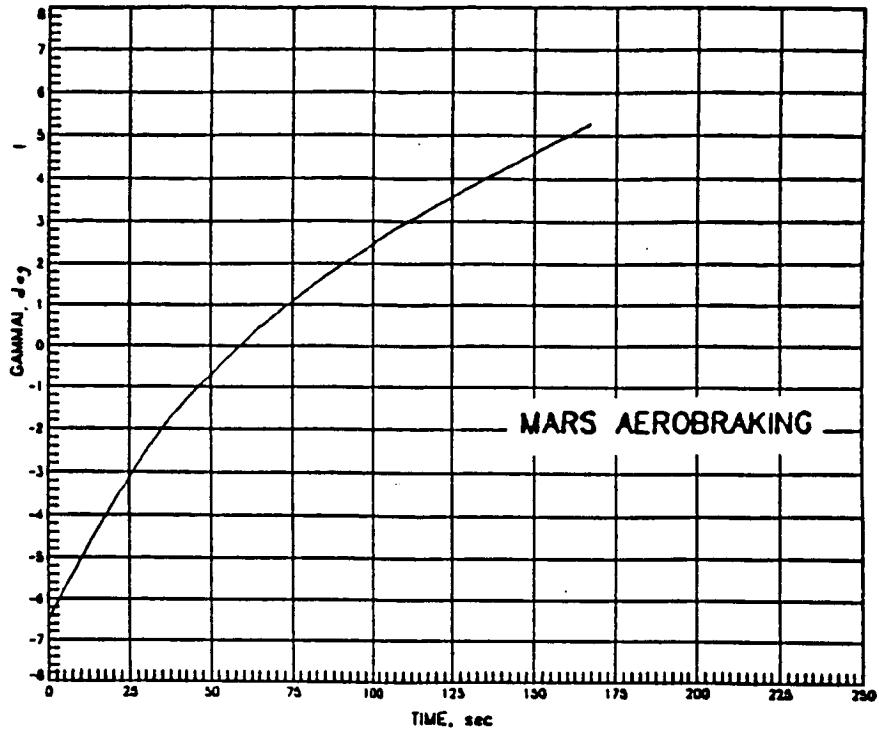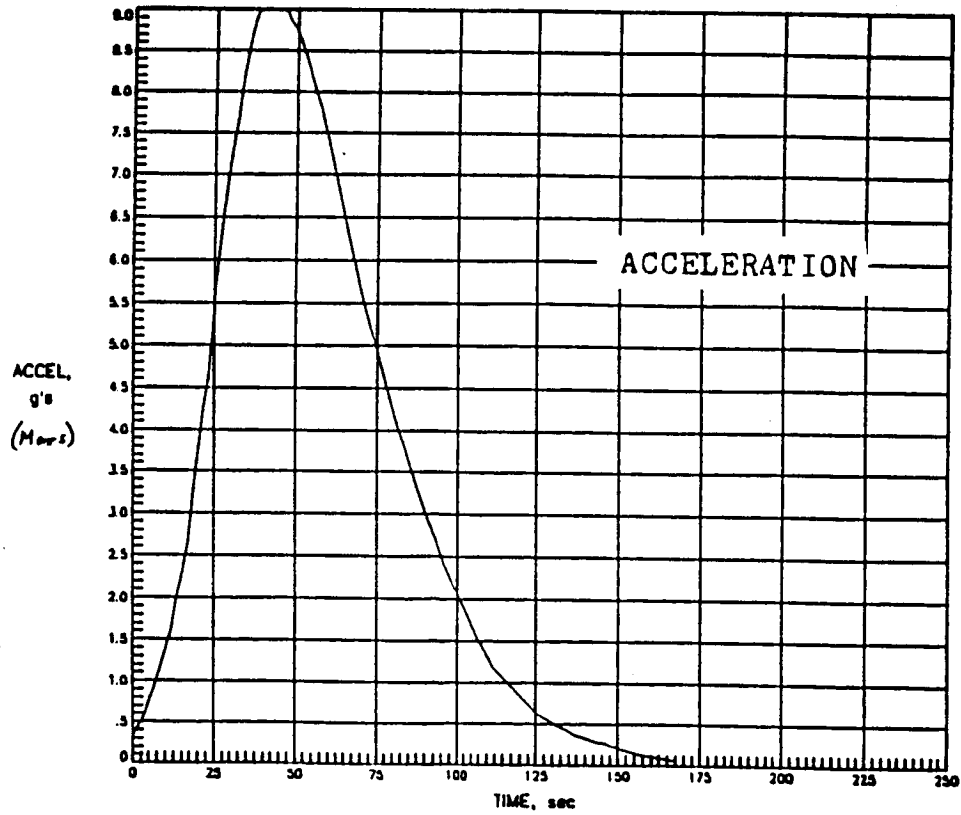
HEATING RATE

FIGURE 4.3.16

DYNAMIC PRESSURE
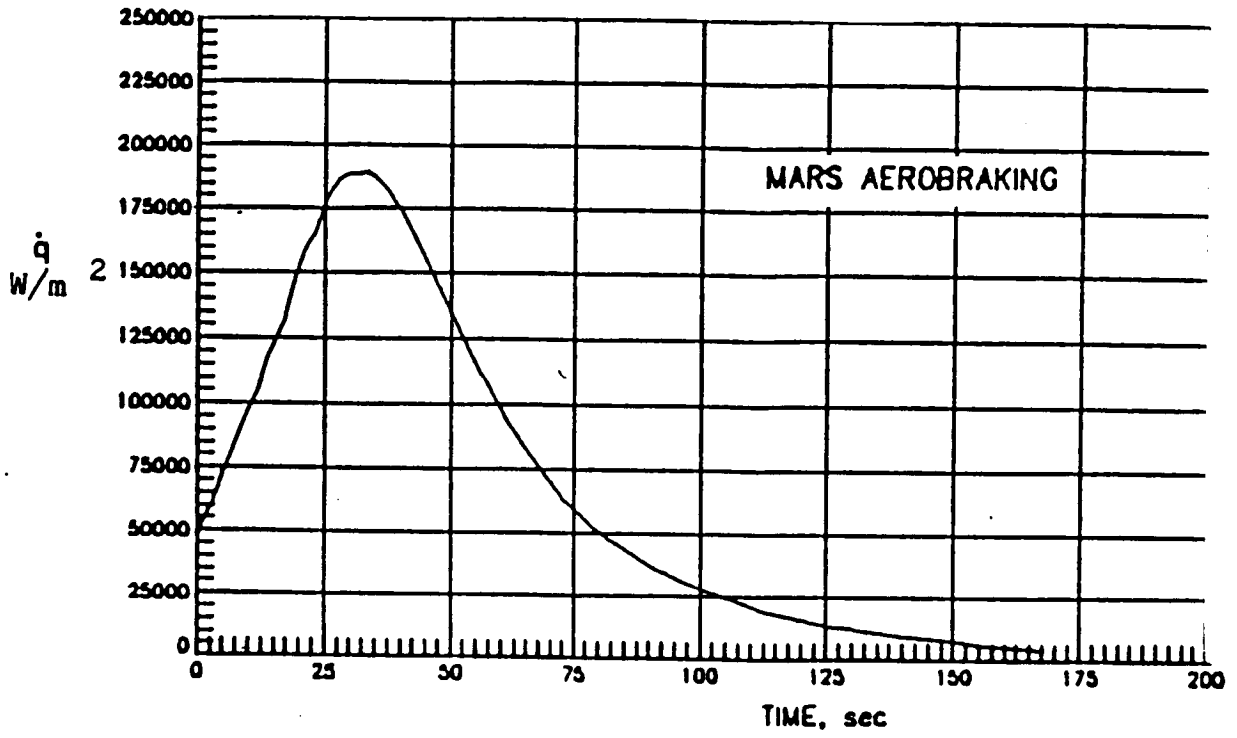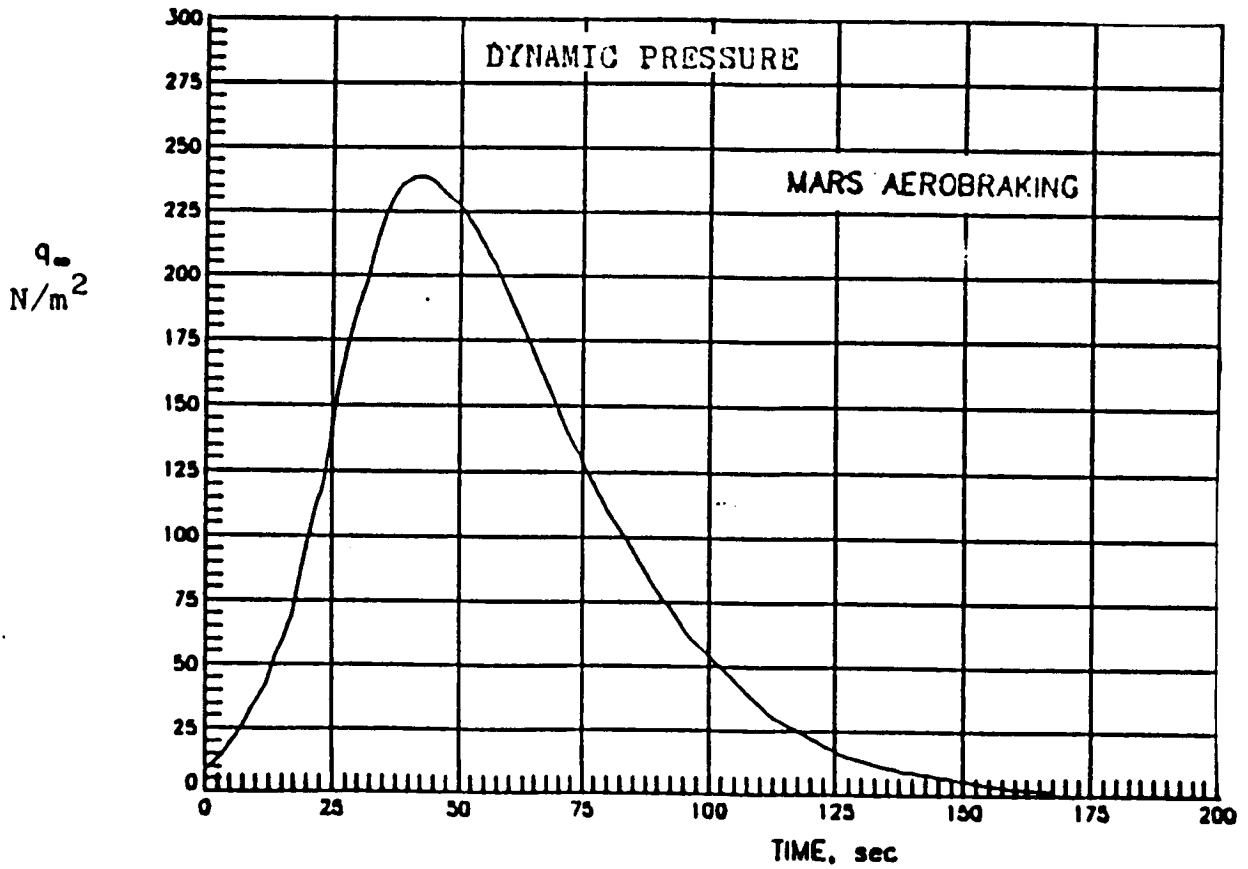
FIGURE 4.3.17

4.3.6 References

1. Boobar, M. G., Chapel, F. G., and Repic, E. M., "Aerobraking as a Potential Planetary Capture Mode," Journal of Spacecraft and Rockets, Vol 5, Aug 1968, pp 921-926.

2. Chapman, D. R., "An Approximate Analytical Method for Studying Entry Into Planetary Atmospheres," NACA TN 4276, 1956.

3. Dauro, V. A., "Aerobraking," Marshall Space Flight Center, 1979.

4. Eggars, A. J., Allen, H. J., Neice, S. E., "A Comparative Analysis of the Performance of Long-Range Hypervelocity Vehicles," NACA TH 4046, 1957.

5. Loh, W. H. T., "Reentry and Planetary Physics and Technology, Vol. II," Springer-Verlag, New York, Inc., 1968.

6. Miele, A., Theory of Flight Mechanics, Vol.1, Addison-Wesley Publishing Company, Inc., Reading, Massachusetts, 1962, pp 301-307.

7. Walberg, G. D., "A Survey of Aeroassisted Orbit Transfer," AIAA 82-1378.

4.4 Aerothermodynamic Analysis

In evaluating the heating and pressure characteristics of a hypersonic re-entry vehicle several methods may be used. Of these, Newtonian or modified Newtonian methods are useful in approximating Cp's and aerodynamic coefficients. Also, Euler codes are used to evaluate the region behind the bow shock and are coupled with either integral or finite difference boundary layer solutions.

The region aft of the shock is generally transonic with the shield being fully wetted with subsonic flow. When using blunt, low L/D shield configurations, a skirt is usually employed on the out-flow edges to ensure supersonic flow leaving the shield. This will help diminish the thickness of the viscous shear layer in the wake region, thus, creating a larger zone of protection and lower heating behind the shield.

A pressure, temperature, and heating analysis is presented that is coupled with the trajectory maximum loading conditions. A Simple Newtonian method is used to establish the Cp distribution, and aerodynamic characteristics of the shield. An axisymmetric Euler and Integral Boundary Layer solution is employed on a cross-section of the shield in order to establish the stagnation temperature, pressure, and heating on the shield.

4.4.1 Aerodynamics

Simple Newtonian Theory offers a useful approximation for surface pressure distribution in hypersonic flows. The pressure coefficient, Cp, is calculated by $2*\sin^2\theta$, where θ is the angle of the surface to the free stream direction (Figure 4.4.1). Figure 4.4.2 shows the pressure coefficient distribution over the shield surface at zero angle of attack. This distribution is used in a later section to develop the support structure. By varying the shield's orientation to the flow and integrating pressures over the surface, the shield's aerodynamic coefficients are computed.

Reference Area (area projected on y-z plane):
$$A = 11602.4 \text{ ft}^2 \ (1078 \text{ m}^2)$$

Reference Diameter: (the circular projection in Fig. 4.2.1):
$$D = 115 \text{ ft} \ (35.1 \text{ m}).$$

The total shield area is 14090 ft^2 (1310 m^2)

Calculated values at $\alpha = 0$:

$$C_D = 1.5743 \qquad\qquad C_L = 0.2402$$
$$L/D = 0.1526 \qquad\qquad C_M = -0.2854$$

$$C_{L\dot\alpha} = -0.01924/\text{deg} \quad C_{D\alpha} = 0.01263/\text{deg}$$
$$C_{M\dot\alpha} = -0.00783/\text{deg} \quad C_{Y\alpha} = -0.00825/\text{deg}$$
$$C_{N\dot\alpha} = 0.00617/\text{deg} \quad C_{Z\alpha} = -0.000081/\text{deg}$$

The coefficient curve slopes listed by Mayo et al for a shield without a skirt are lower, revealing the increased stability due to the skirt.

FLIGHT GEOMETRY

← reference area

V_∞

X

Y

Z

α

da

Θ

$\tilde{n}$

V_∞

($\alpha = 0$)

51.8 ft (15.8 m)

line of action of forces
- stable C. G. locations

8.68°

D = 115 ft (35.1 m)
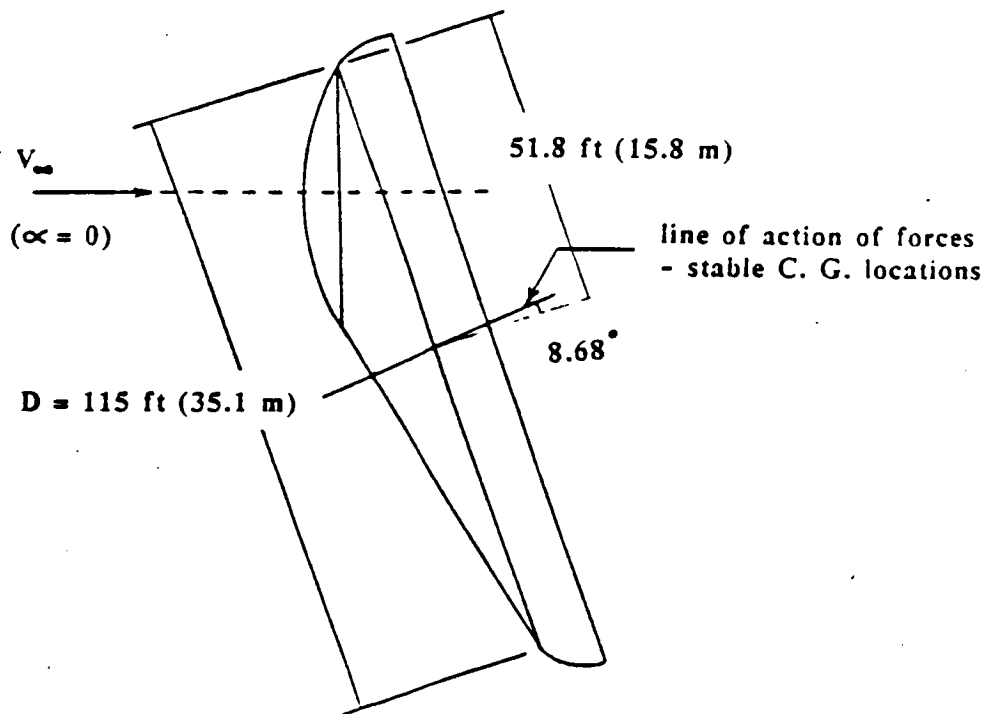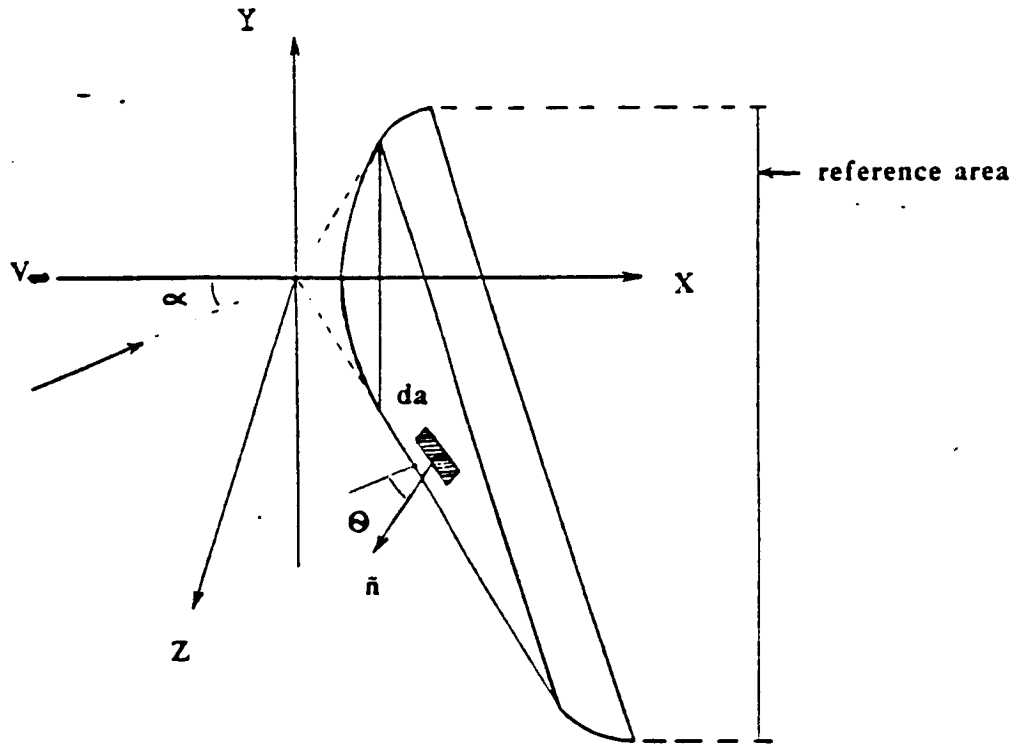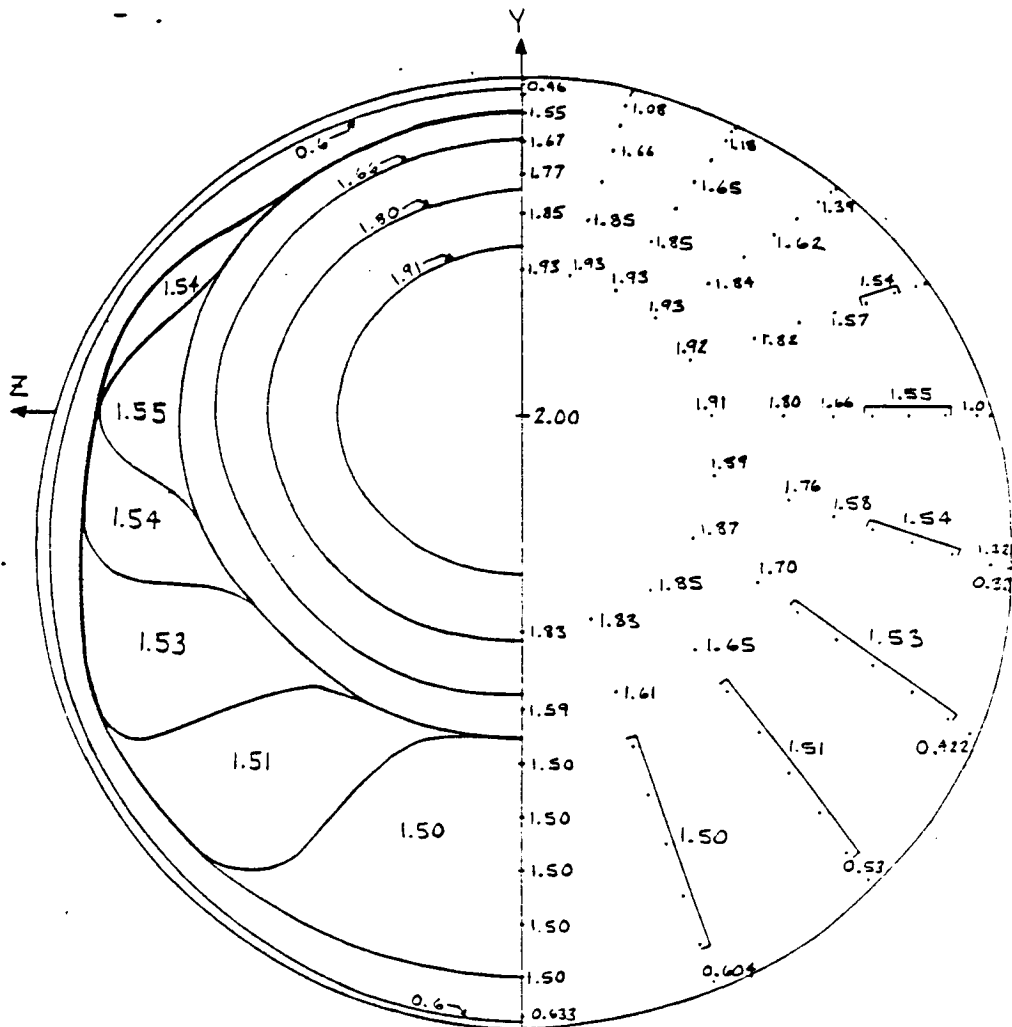
FIGURE 4.4.1

C_p Distribution (symmetric about the y-axis)

$\frac{1}{50}^{th}$ scale

FIGURE 4.4.2

95

Alpha is defined in Figure 4.4.1. Aerodynamic coefficients are plotted vs α in Fig. 4.4.3. Note, however, that C_M is referenced to the vertex of the cone, not the C.G.

The position of the line of zero moment (C.G. position line) is found by dividing C_M by C_D, and its slope is given by tan $\theta = C_L/C_D$ (Figure 4.4.1).

4.4.2 Numerical Results

Upon completion of the trajectory calculations, the point of maximum heating for Earth was determined to occur at an altitude of 280,000 ft (85,366 m). The corresponding flight regime is specified by the following quantities:

P_∞ = 0.38717 N/m² M_∞ = 41.87

T_∞ = 180.65 deg K V_∞ = 11280.4 m/s

ρ_∞ = 7.468 E-6 kg/m³ a_∞ = 269.45 m/s

A numerical axisymmetric solution is set up using integral boundary layer equations. A slice of the shield through the stagnation point (Figure 4.4.4) was chosen to give a good representation of the shield behavior and was used to create a numerical grid for calculations (Figure 4.4.5). The shield was tested for thicknesses of 0.5 to 1.5 inches and plots of pressure, temperature, and heating were developed.

For the encountered Mach number of 41.87, the stagnation point pressure rise P/P_∞ (Figure 4.4.6) is about 2300, which drops to 1800 near the shield edge. Cp_{max} is 1.874 with a dynamic pressure of 475.1 N/m².

The heat transfer (Figure 4.4.7) will be mostly convective for the altitude and shield parameters involved. At the stagnation point $\dot{q}$ is 11.27 W/cm² convective heat flux. The heat transfer drops to 9.01 W/cm² towards the shield edge. An expected hump occurs near S of 22 m where the flow accelerates over the edge (S = distance along the surface from the stagnation point). The heat conducted through the surface can now be calculated. The shield surface temperature reaches a stagnation value of 1249 deg K and stays nearly constant until the boundary is reached. Similarly, the backface temperature also stays constant along the surface. Small discontinuities arise near the corner of the shield.

The effect of shield thickness on pressure, heat transfer, and outside wall temperature is negligible (Figs. 4.4.8-4.4.10); however, its effect on inside wall temperature is significant (Figure 4.4.1). Since the graphite polymide aerobrake support structure cannot endure temperatures exceeding 600 deg K, the backface temperature must be kept moderate. For Earth, a 0.5 inch thick shield would accomplish the required protection; however, since there remains uncertainty about Mars environment, a 1.0 inch shield is selected. The backface stagnation temperatures are 541.3, 461.1, 418.8 deg K for 0.5, 1.0, and 1.5 inches, respectively.

Aerodynamic Characteristics of Shield

FIGURE 4.4.3

Angle of Attack

□ Cl   + Cd   ◇ Cm   △ L/D

Aerodynamic Coefficient
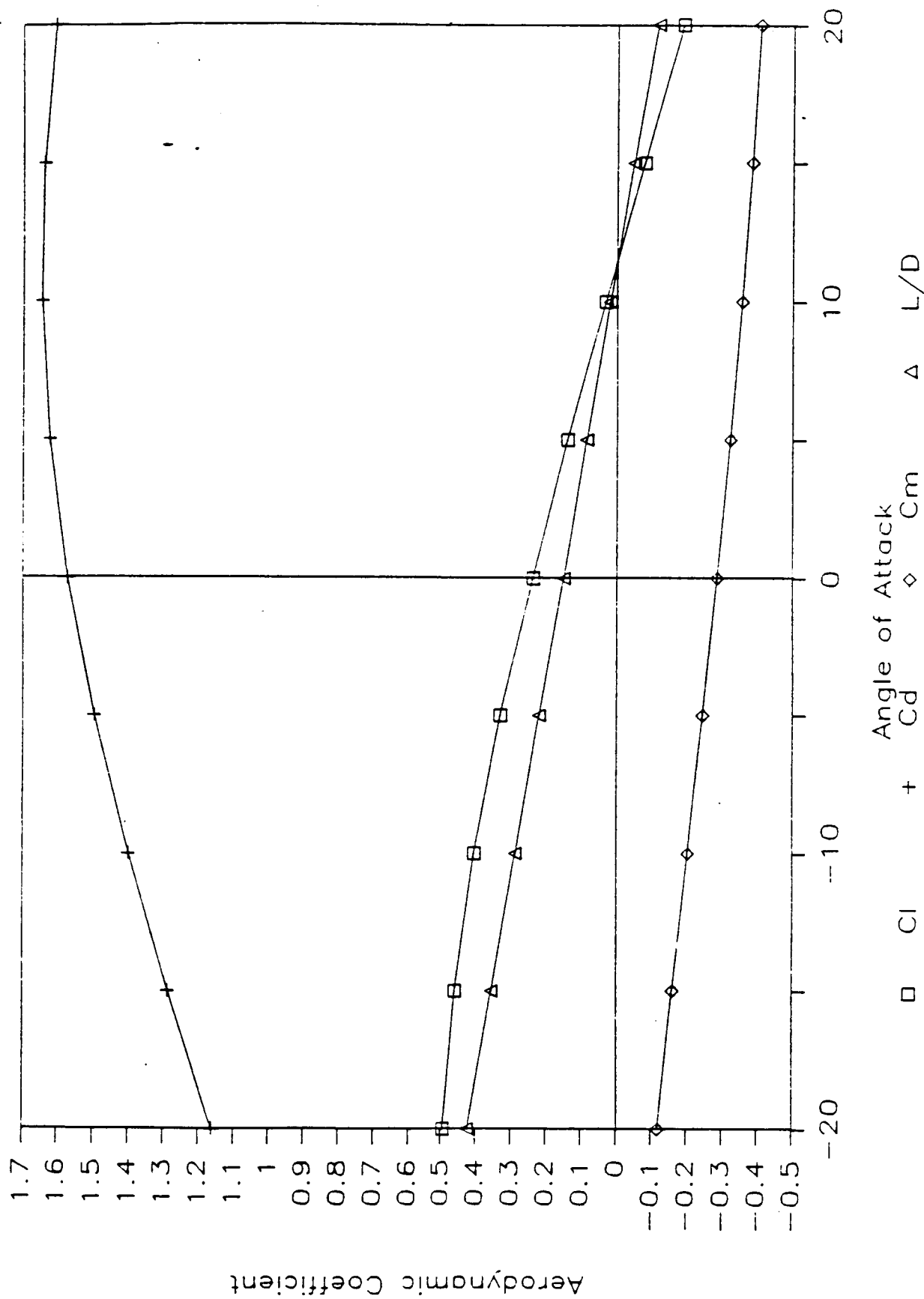
plane
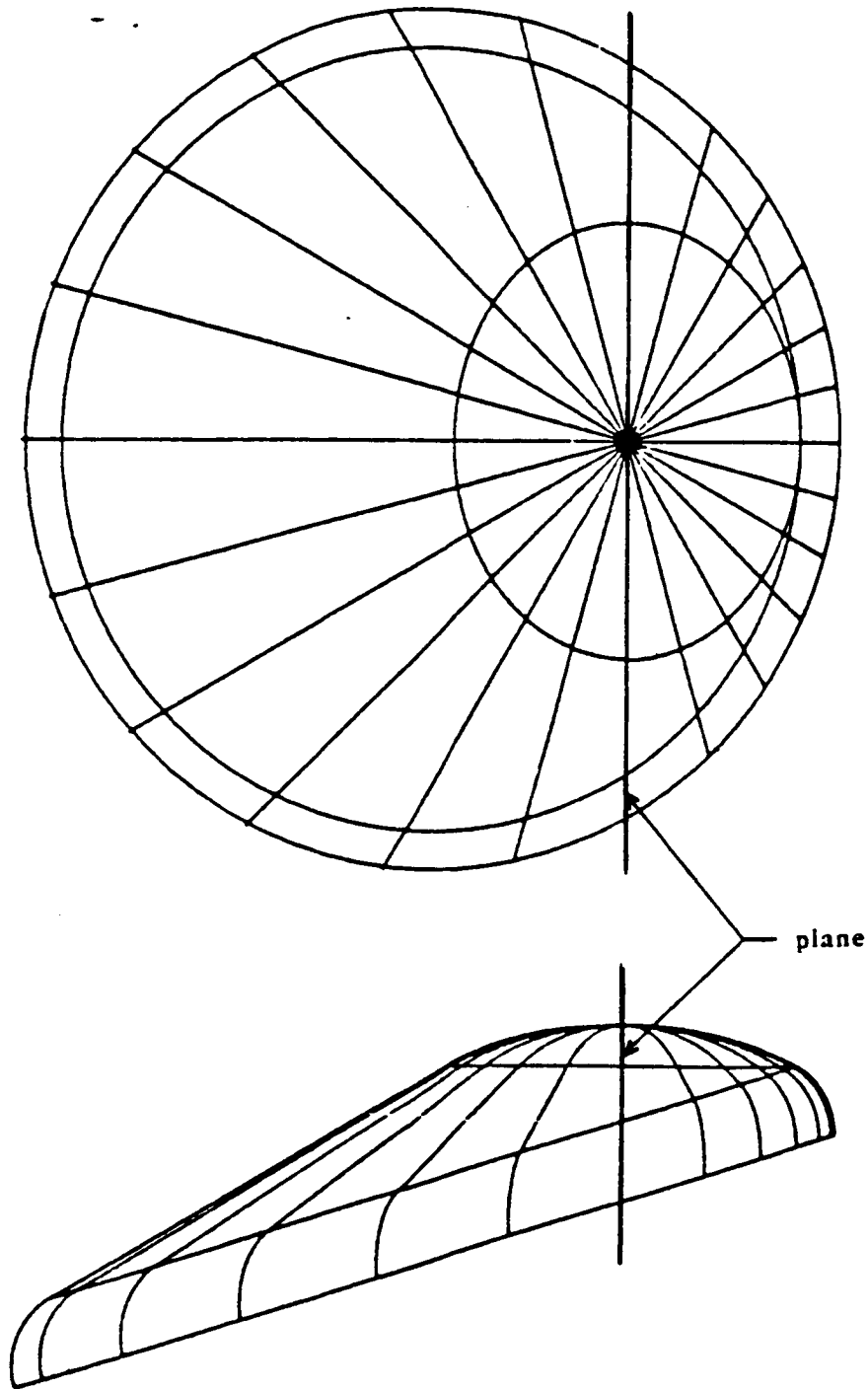
FIGURE 4.4.4

GRID

FIGURE 4.4.5

99

SURFACE PRESSURE

Mach 41.87

$\frac{P}{P_\infty}$

S,m

FIG. 4.4.6

SURFACE HEAT TRANSFER (t = 1.0in)

Mach 41.87

$\dot{q}$
W/m^2

S,m

FIG. 4.4.7

SURFACE TEMPERATURE
(t = 0.5in)

M = 41.87

Outside wall

Inside wall

T,°K

S,m

FIG. 4.4.8

SURFACE TEMPERATURE
(t = 1.0in)

M = 41.87

Outside wall

Inside wall

T,°K

S,m

FIG. 4.4.9

SURFACE TEMPERATURE
(t = 1.5in)

Outside wall

M = 41.87

Inside wall

T,°K

S,m

FIG. 4.4.10

INSIDE WALL TEMP vs
WALL THICKNESS

Mach 41.87

T,°K

t,in

FIG. 4.4.11

102
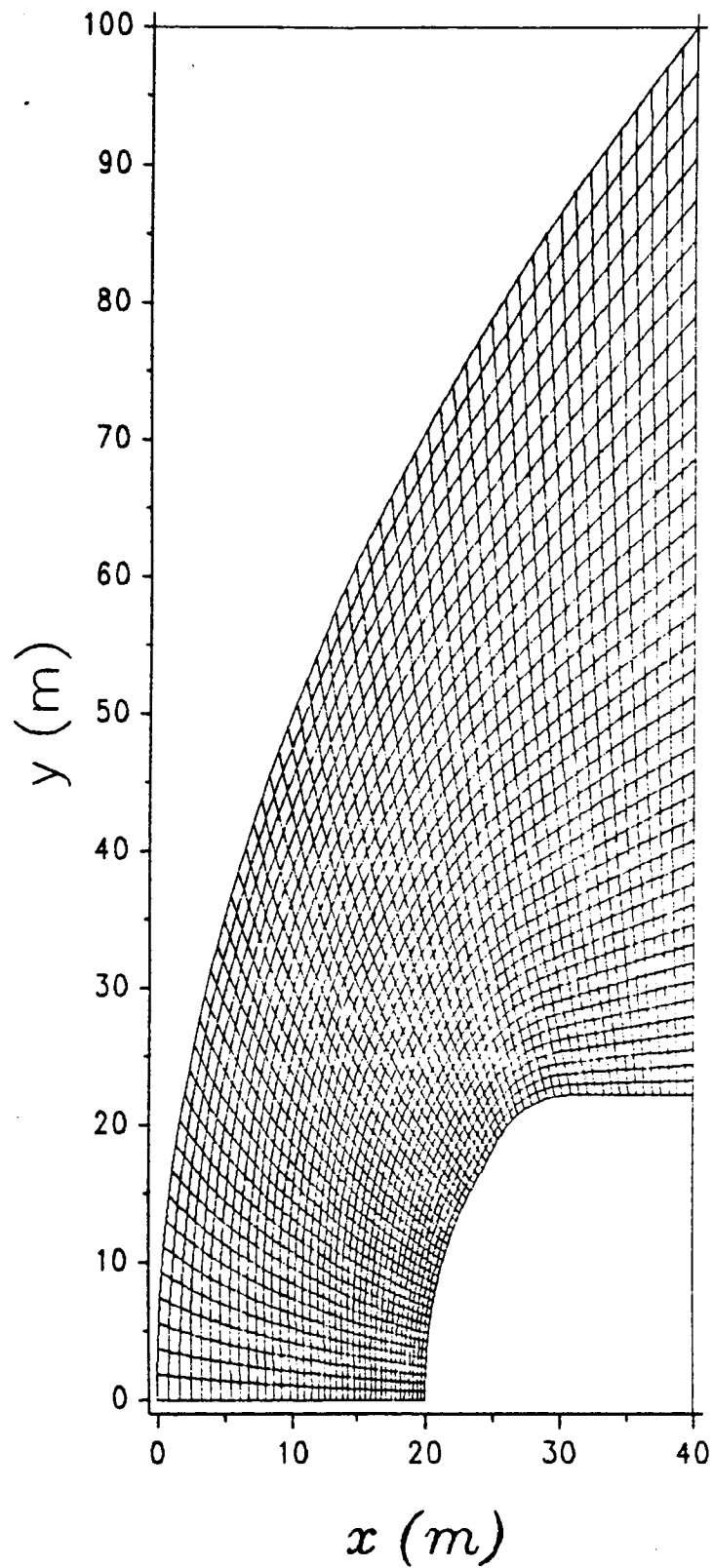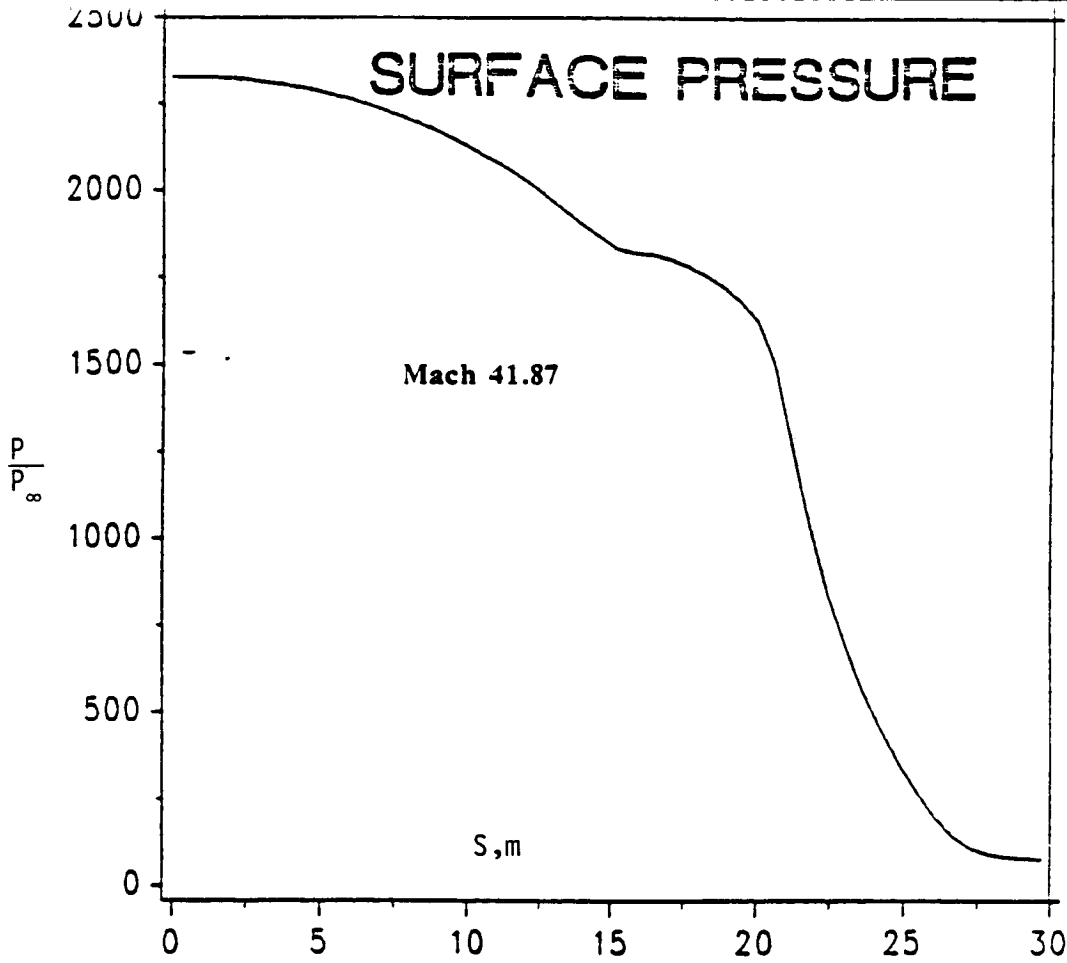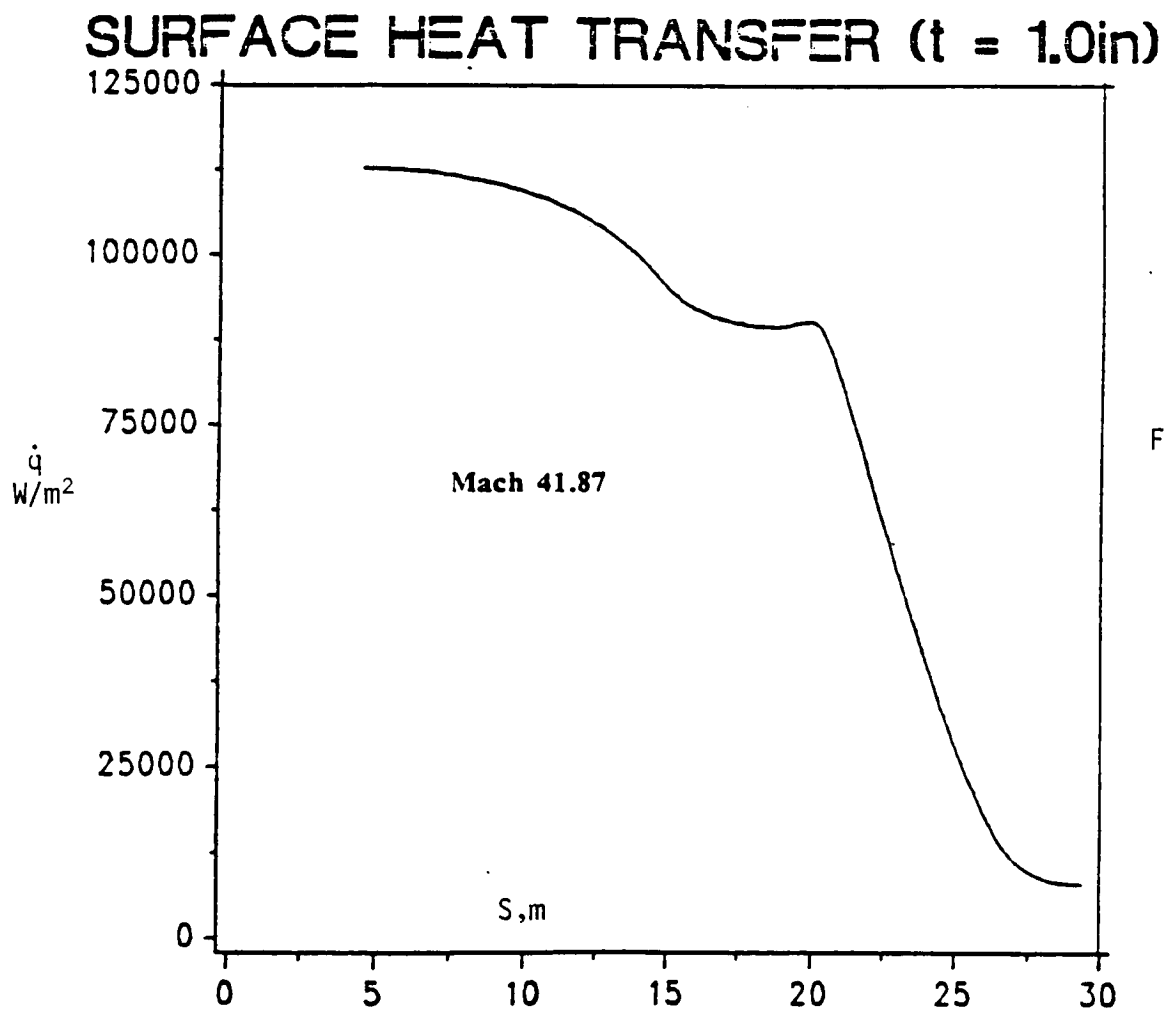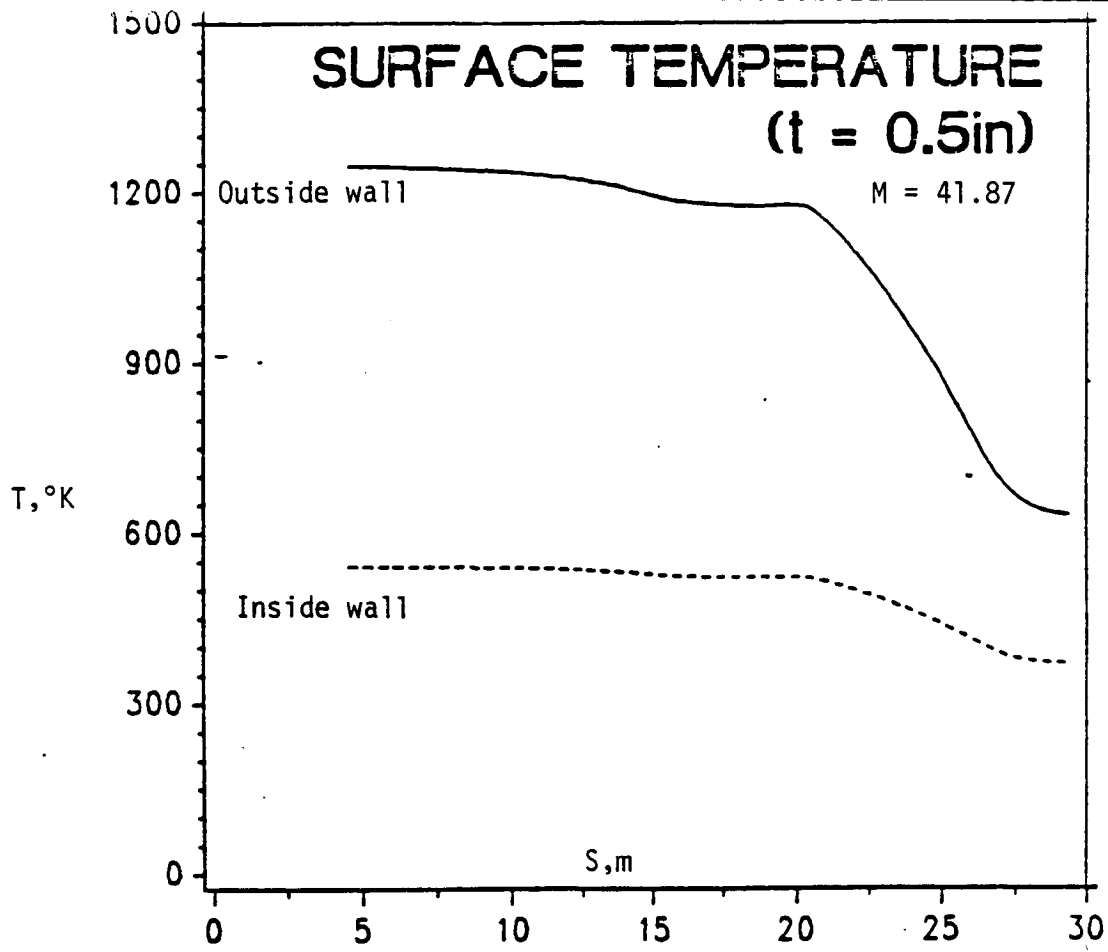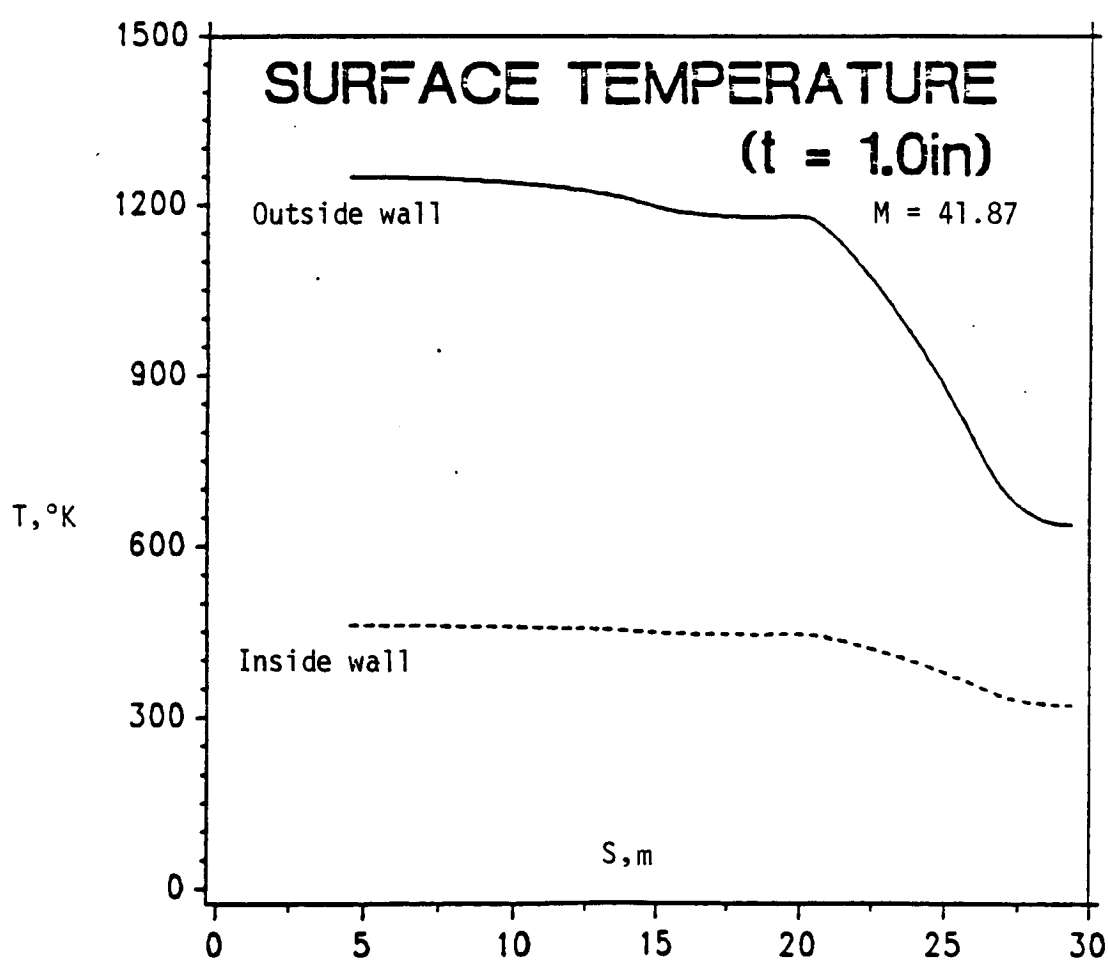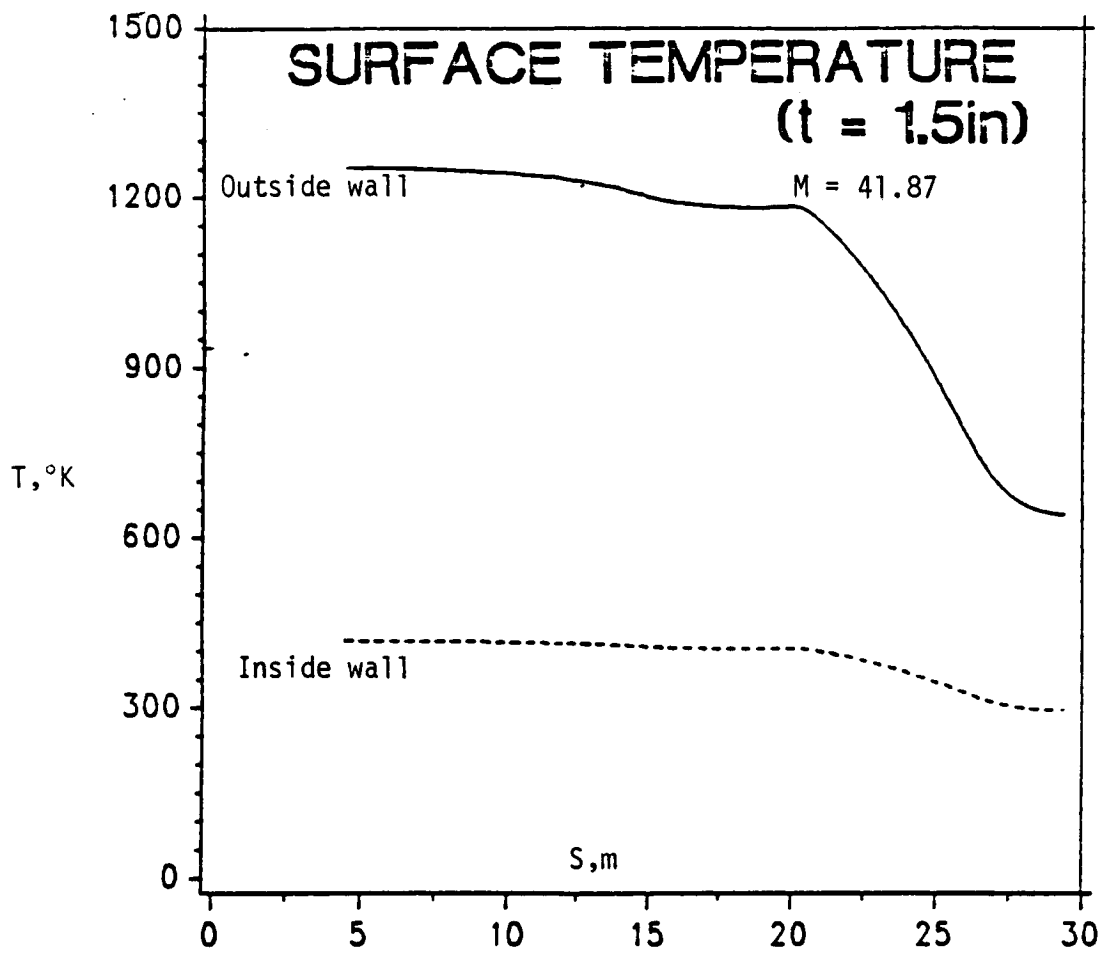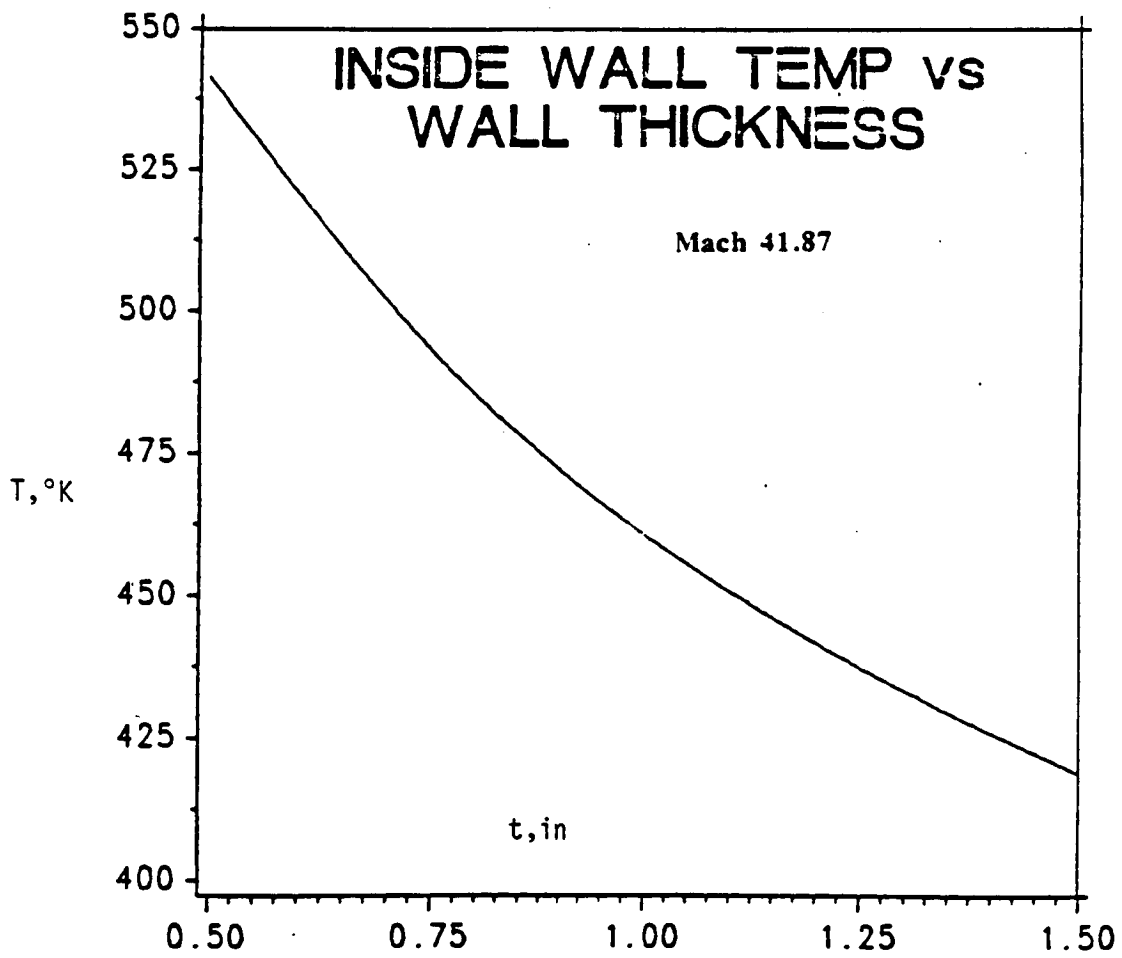
4.4.5 References

1. Weilmuenster, K. James and Hamilton, H. Harris II. "A Comparison of Computed and Experimental Surface Pressure and Heating on 70 Degree Sphere Cones at Angles of Attack to 20 Degrees." AIAA Paper 86-0567, 1986.

2. Hamilton, H. Harris II and Weilmuenster, K. James. "Calculation of Convective Heating on Proposed Aeroassist Flight Experiment Vehicle." AIAA Paper 86-1308, 1986.

3. Menees, Gene P., et. al. "Aerothermodynamic Heating Analysis of Aerobraking and Aeromaneuvering Orbital Transfer Vehicles." AIAA Paper 84-1711, 1984.

4. Menees, Gene P., Chul Park, and John F. Wilson. "Design and Performance Analysis of a Conical Aerobrake Orbital Transfer Vehicle Concept." AIAA Paper 84-0410, 1984.

5. DeJarnette, F. R., et. al. "A Review of Some Approximate Methods Used in Aerodynamic Heating Analyses." AIAA Paper 85-0906, 1985.

6. Scott, Carl D., Robert C. Ried, et. al. "An AOTV Aeroheating and Thermal Protection Study." AIAA Paper 84-1710, 1984.

7. Zoby, E.V., et. al. "Approximate Convective-Heating Equations for Hypersonic Flows." AIAA Paper 79-1078, 1979.

8. Menees, Gene P. "Thermal Protection Requirements for Near-Earth Aeroassisted Orbital Transfer Vehicle Missions." AIAA Paper 83-0919, 1983.

9. Scott, Carl D., et al., "An AOTV Aeroheating and Thermal Protection Study", AIAA-84-1710.

10. Cheatwood, F.M., et. al., "Geometrical Description for a Proposed Aeroassist Flight Experiment Vehicle", NASA Technical Memorandum 87714, July, 1986.

11. Letts, W. R.," Aeroassisted Orbital Transfer Mission Evaluation", AIAA-82-1380.

12. Walberg, G.D., "A Review of Aeroassisted Orbit Transfer", AIAA-82-1378.

13. Menees, G.P., "Thermal-Protection Requirements for Near Earth Aeroassisted Orbital-Transfer Vehicle Missions", AIAA-83-1513.

14. Mayo, E.E., et. al., "Newtonian Aerodynamics for Blunted Raked-off Circular Cones and Raked-off Elliptical Cones", NASA Technical Note D-2624.

15. Duke, M.B., ed., "Manned Mars Missions", Working Group Summary Report, NASA, May 1986.

16. Pitts, W.C. and Murbach, M.S., "Thermal Design of AOTV Heat Shields for a Conical Drag Brake", AIAA-85-1052.

17. Pitts, W.C. and Murbach, M.S., "Thermal Response of an Aeroassisted Orbital-transfer Vehicle with a Conical Drag Brake", AIAA-84-1712.

18. Finch, T.W., "Aerodynamic Braking Trajectories for Mars Orbit Attainment", AIAA-Preprint-64-478.12. Regan, Frank J.,Re-Entry Vehicle Dynamics, AIAA Education Series, AIAA Inc., 1984, pp. 219-234.

The aeroshield supporting structure is designed to be the main load carrying element of the TAXI. Three major loads, aerobraking, thrusting, and inertial, are supported and transferred throughout the vehicle. Some of the design criteria are minimum weight, ease of assembly, ease of integration with other components, and support of the complex geometry of the aerobrake surface. The structure itself is composed of two distinct assemblies. The first is the 3 dimensional truss structure (Fig. 4.5.1) which bears and distributes the forces. The second, the ribbing (Fig. 4.5.2) which defines the shape of the insulation and transfers the aerobraking pressure loads to the truss structure. The ribbing is attached to the truss network at the lower 32 node points of the truss network (Fig. 4.5.3). The tanks, engine mounts, payload and crew module all have their truss work attached to node points of the truss structure (Fig. 4.5.3). The weights and moments of this design are given in Table 4.5.1.

4.5.1 Truss Selection

A few alternate truss structures were considered but were rejected for various reasons. A radial truss network (Figure 4.5.4) was refused on two points. The nature of a radial design made a high density of supports near the center but left large areas unsupported near the periphery. An originally simple truss network geometry was complicated when the trusses had to be re-routed around the tanks and crew module units. Another structure system considered was one in which each unit (tanks, engine, crew module) has its own truss work which attaches directly to the shield ribbing (Figure 4.5.5). This resulted in a complicated geometry of crossing members and also required stronger ribbing to provide adequate support against bending. The truss network which was adopted (Figure 4.5.1) is simple in geometry, very weight efficient, and avoided the aforementioned problems of the other alternatives. Certain cross-sections of the truss are taken to show dimensions. The dimensions are given in Figure 4.5.6. The truss network allows the removal of individual members to facilitate replacement of parts or repair work. Furthermore, the simple geometry lends itself to analysis more easily.

Table 4.5.1 Weights and Moments of Inertia - TAXI A

Truss frame

Mass	6,000 lbm
I_{xx}	4.02×10^6 lbm-ft^2
I_{yy}	4.00×10^6 lbm-ft^2
I_{zz}	8.03×10^6 lbm-ft^2

Ribbing

Mass	2,600 lbm
I_{xx}	6.82×10^6 lbm-ft^2
I_{yy}	6.80×10^6 lbm-ft^2
I_{zz}	4.20×10^6 lbm-ft^2

Total mass   8,600 lbm

3-D TRUSS NETWORK
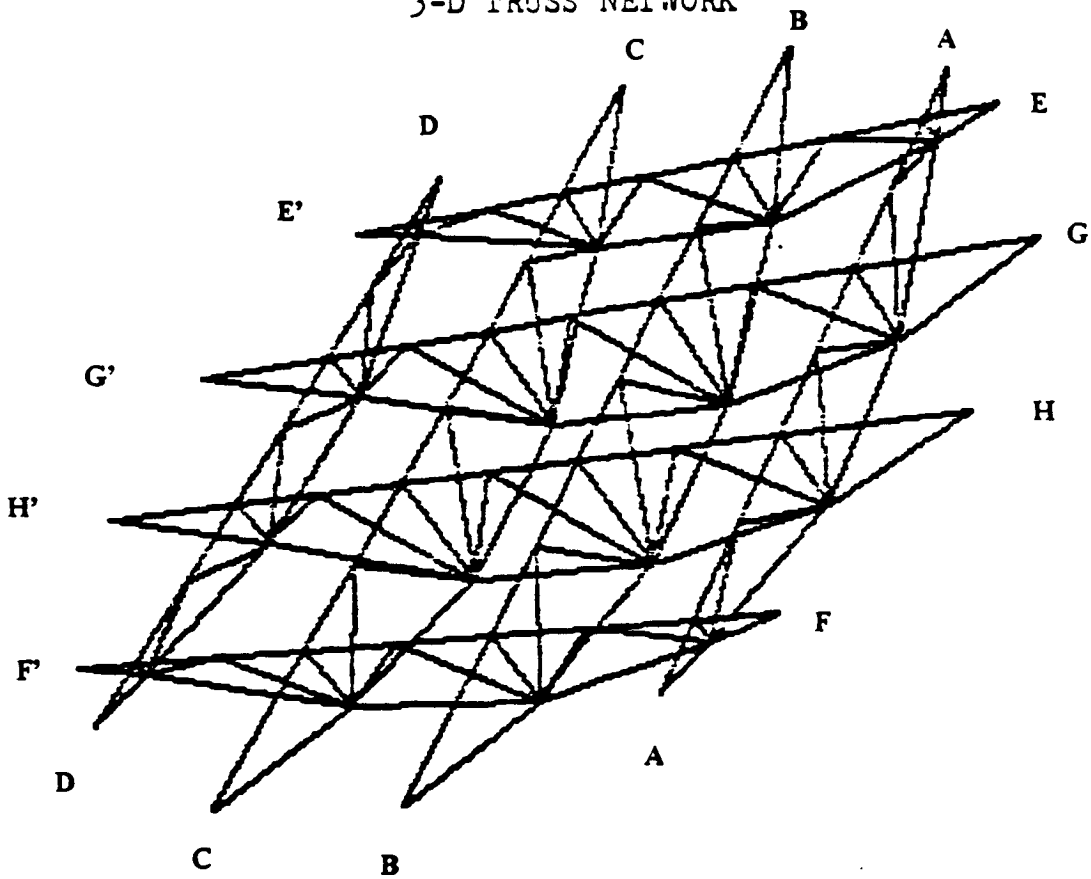
FIGURE 4.5.1

Ribbing and its Assembly Pattern
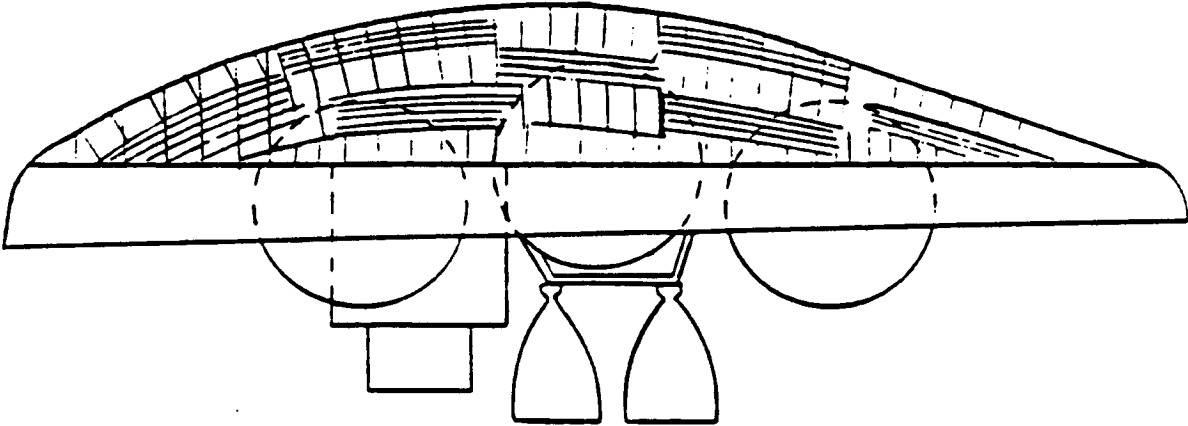
FIGURE 4.5.2

TRUSS CROSS-SECTION LOCATION
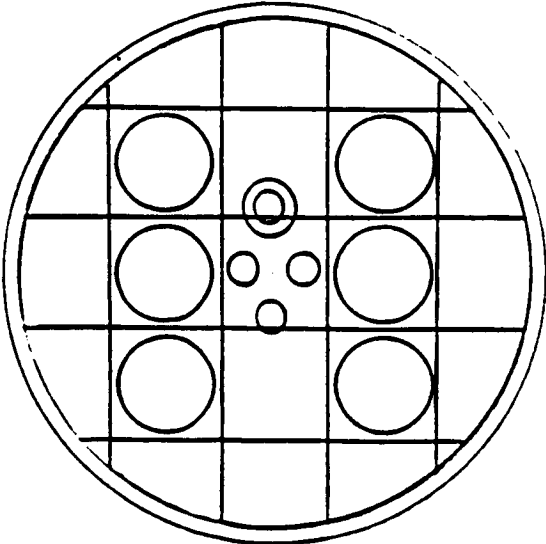
FIGURE 4.5.3

RADIAL TRUSS NETWORK
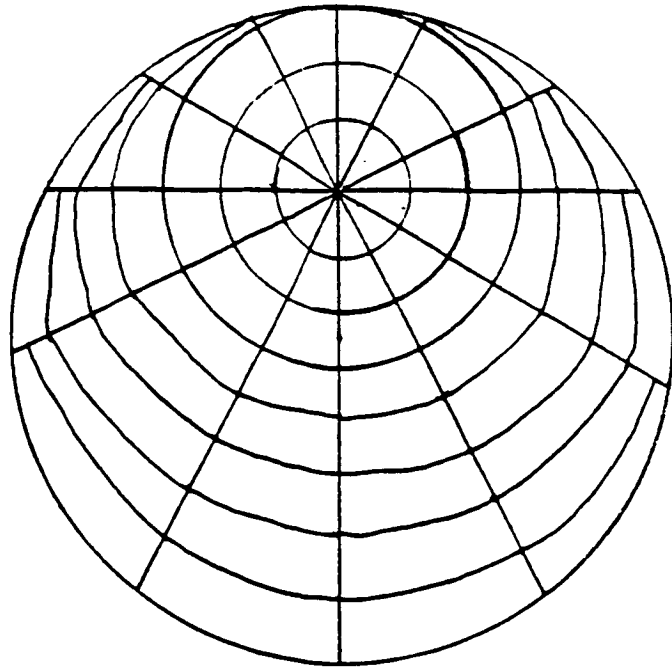
FIGURE 4.5.4

THE MEMBERS CONNECT
MODULES TO RIBBING
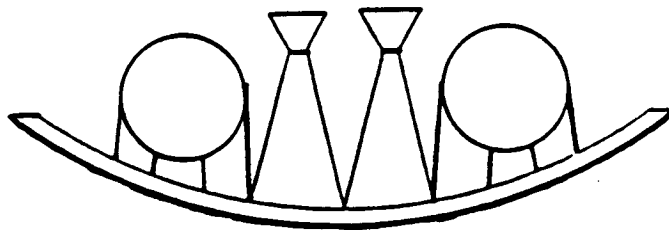
FIGURE 4.5.5

Truss Network Cross-Section Dimensions

A 8.8'   12'   8.8' A
          10.1'   10.1'
2.9'   2.9'

B   20.2'   12'   20.2' B
          9.6'   15.8'   15.8'   9.6'

C   20.2'   12'   20.2' C
          8.6'   15.3'   15.3'   8.6'

D 8.8'   12'   8.8' D
                  6.7'   6.7'
1.9'   1.9'

F'   F
E'   E
    8.8'   12'   8.8'
          8.6'   9.6'
1.9'   2.9'

H'   H
G'   20.2'   12'   20.2' G
          6.7'   15.3'   15.8'   10.1'
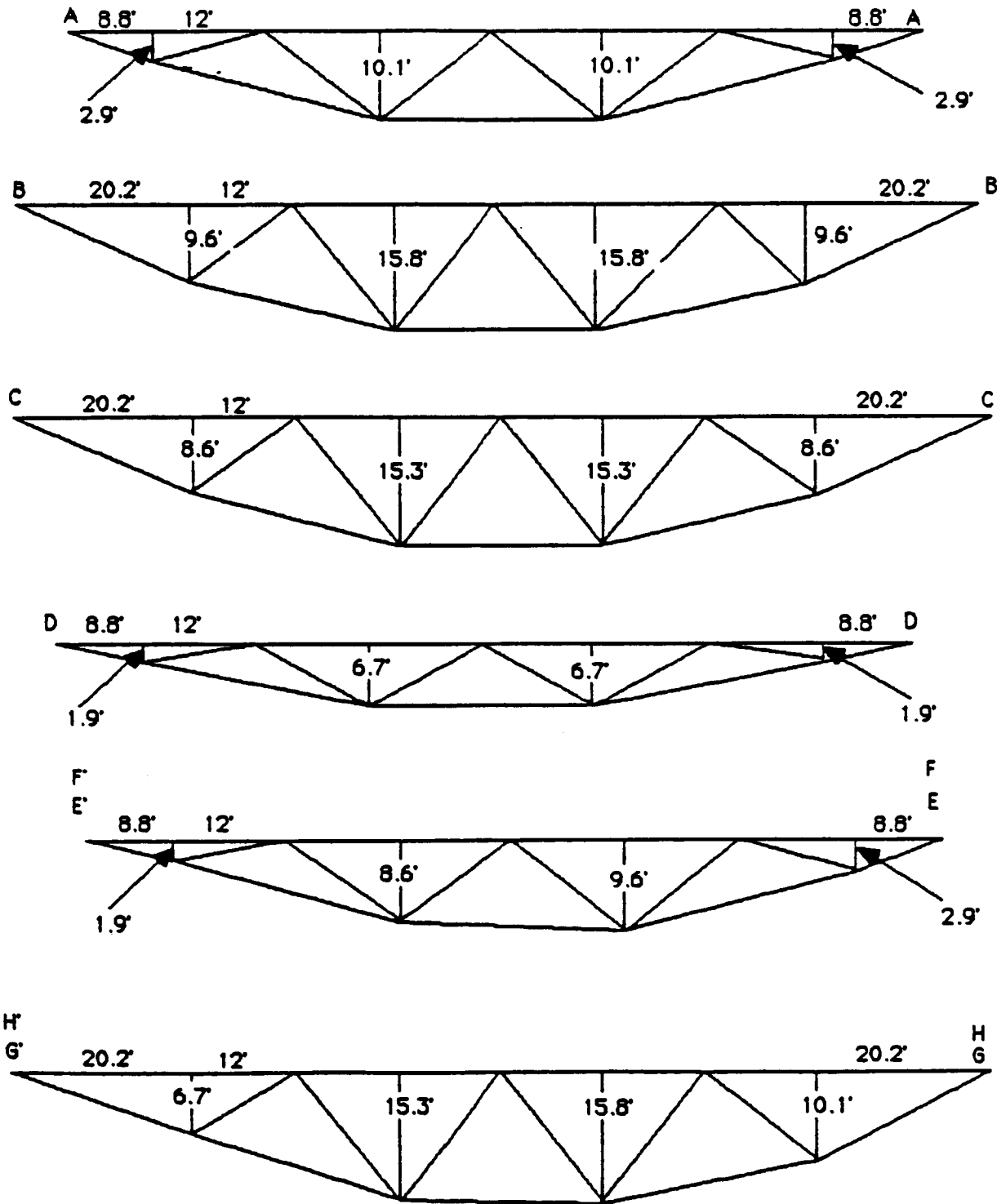
FIGURE 4.5.6

4.5.2 Truss Design

The forces on the structure are the main considerations of the design process. There are two major loading conditions to model, aerobraking and thrusting. Each condition has an inertial loading which is the sum of the inertia loads of the tanks, crew module, payload and other parts. The inertia load for each component is the product of its mass and the vehicle's acceleration. For thrusting, the maximum inertial loading occurs under an acceleration of 4 g's when there is 120,000 lbm of oxygen left and 20,000 lbm of hydrogen left in the tanks. During aerobraking the maximum inertia loading occurs at 3 g's when the tanks are essentially empty. The other loads are the pressure drag encountered during aerobraking and the thrust from the engines.

The pressure loads from aerobraking were calculated using the Cp distribution on the surface of the shield and the dynamic pressure at the time of maximum deceleration. This gives a maximum dynamic pressure loading of 52.4 lb/ft^2. The resulting pressure distribution was integrated over discrete areas centered on individual node points. The resultant pressure forces were then applied at each respective node point. With the forces and the truss geometry, an analysis of the truss work was done to determine the forces in the individual members.

4.5.3 Truss Element Description

The 3-dimensional truss structure is pictured in Figure 4.5.1. In selecting the number of truss elements and their relative configuration the simplest design was chosen. The truss members were assumed to be two-force members made of graphite poly mide. Because of the similarity in loading from aerobraking and thrusting, some members are only loaded in tension while others are only loaded in compression. Since buckling is the dominant failure mode, it was used to find the minimum cross-sectional area required for the members in compression. The largest radius was designed to give standard size wall thicknesses. In compression this design criteria gives a cross-sectional area of 0.06 ft^2 with a 1/2 in. wall thickness. There can be a considerable weight savings by reducing the cross-sectional area of members that are always in tension. A thickness of 5/32 in. was necessary to keep the tensile stress below the yield stress. This results in a cross-sectional area of 0.02 ft^2. Typical individual truss elements for both tension and compression are shown in Fig. 4.5.7. The truss network receives its stiffness against shear loading from the tank and engine support structure which attaches to the aerobrake structure.

4.5.4 Joint Description

Each truss member has a titanium end fitting (Fig. 4.5.8) to attach to its two ends. The end fittings are shaped to slip into and over the ends and are held in place by adhesive. The other end of the end fittings are made to work as pin connections. The titanium end fittings were chosen over just shaping the graphite polymide pieces into the proper form because the titanium has isotropic properties and allows for easier design of stress concentration. At the node points where several members come together, another titanium piece (Fig. 4.5.9) called a joiner is used to join the members together. Since each node in the truss network has its own unique geometry a separate joiner has to be made for each node. All of the connections are done by means of pins. Pins only allow one degree of freedom as opposed to ball-and-socket joints which allow two degree freedom. However, the ball-and-socket joints are difficult to design to adaquately take tensile forces. The pin joints take tensile forces into account and they will be oriented so that what deflections might occur will be in the plane of freedom.

Typical Truss Element Designed for Tension

5/32 in.

A-A

6 in.

24 ft

A   A

1/2 in.

B-B

6 in.

12 ft

B   B
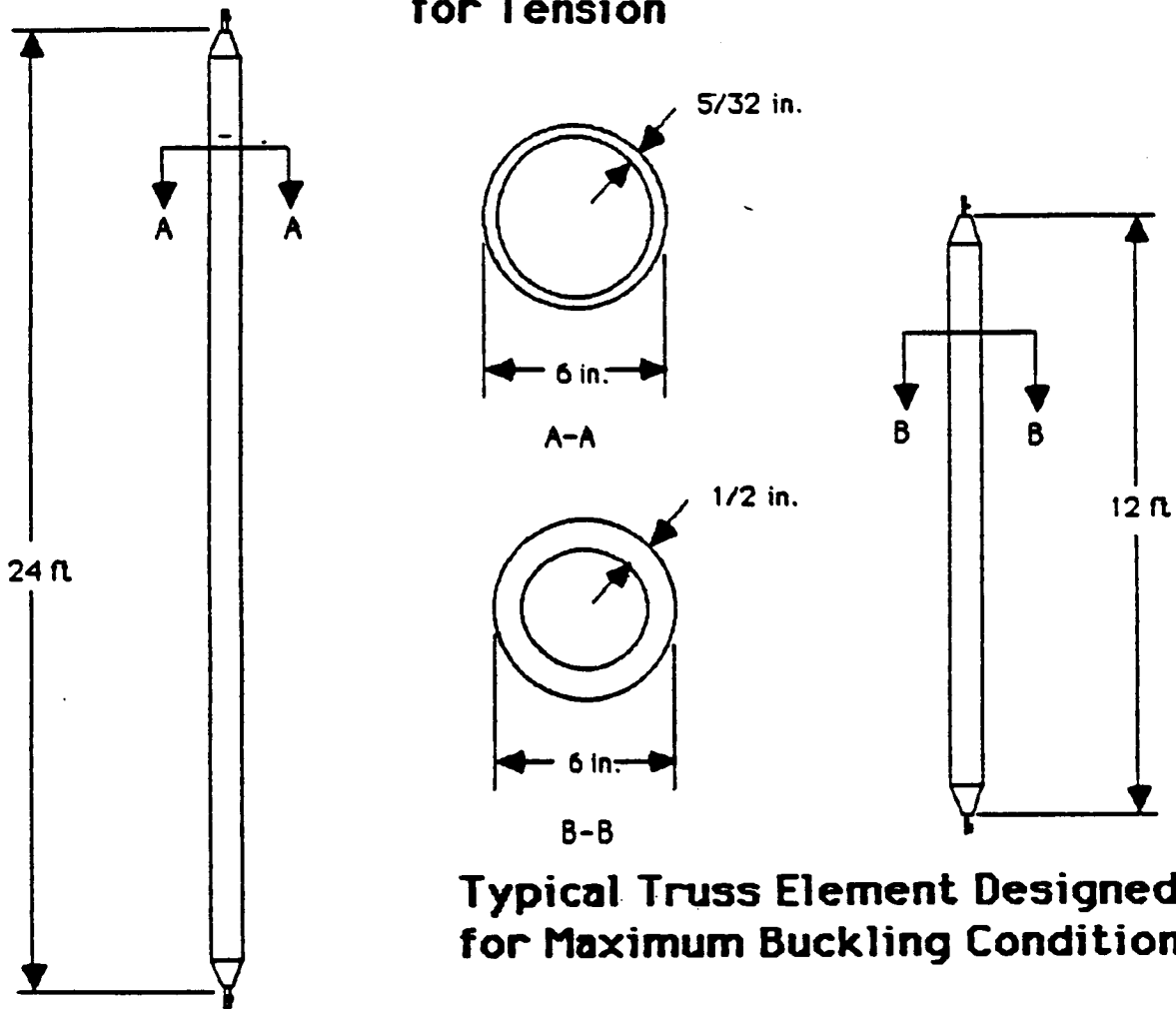
Typical Truss Element Designed for Maximum Buckling Condition

FIGURE 4.5. 7

Titanium End Fitting

Titanium End Fitting

Titanium

Graphite Polyimide Truss Element

Graphite Polyimide
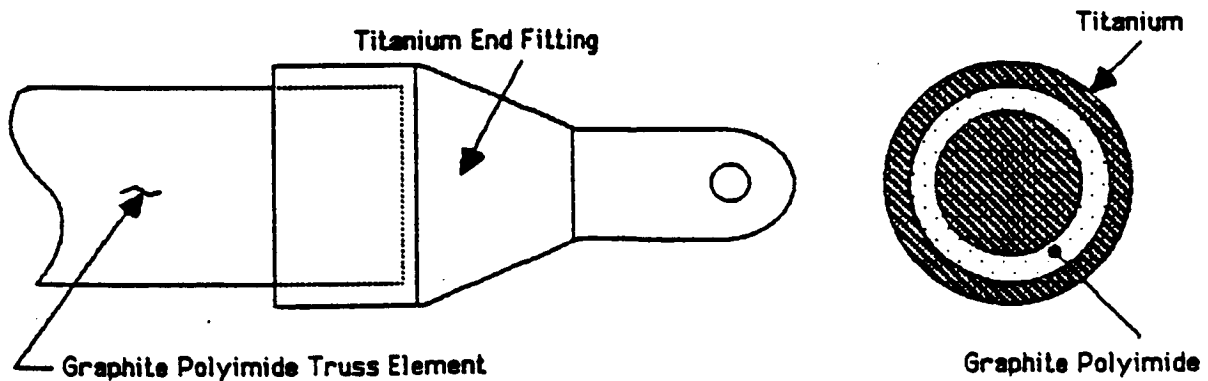
FIGURE 4.5. 8

TITANIUM JOINER
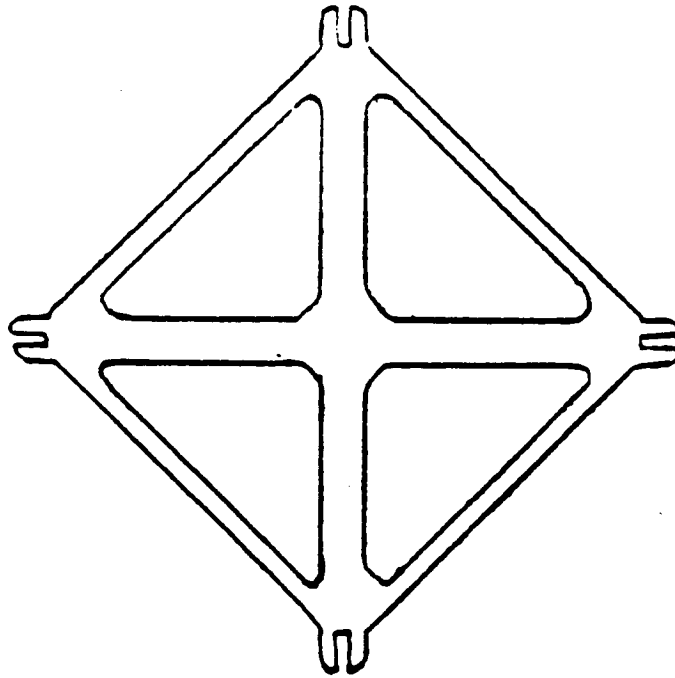
FIGURE 4.5.9

4.5.5 Ribbing Selection

The ribbing is designed to shape and support the TPS. The ribs must support pressure loads during aerobraking. The ribbing configuration is a grid of equally spaced squares (Figs. 4.5.2, 4.5.10) and was chosen over a radial one and one with a hexagonal grid pattern (Figs. 4.5.11, 4.5.12) for its simplicity. The beams were designed to support uniform loading (Fig. 4.5.13a). Out of all the options examined ribbing one was chosen. Rectangular cross-section and I-beams were two of the options considered (Figs. 4.5.13b,c). It was found that the I-beams would give adequate support at less weight than rectangular cross-section. However, these straight beams could not be assembled to give proper support. The beams chosen for ribbing look like ladders from a top view (Fig. 4.5.14a). These were chosen over I-beams because they offer ease of assembly and because they better support and shape the TPS. They are also easier to transport because they can cut the number of beams by a factor of four when compared with I-beams.

4.5.6 Ribbing Design

The cross-sectional dimensions of the beams were determined by a structural analysis which took into account the aerobraking loads of 52.4 lb/ft^2 as maximum. The design analysis was carried out assuming that the beams are simply supported and carry a uniformly distributed load. Most beams have a projected length of 24 ft and an actual length of no more than 25 ft (Fig. 4.5.14a). The thickness, b, of the beams was taken to be 0.15 in. to allow for stresses due to weaving them directly into the TPS (Fig. 4.5.14b) to give enough area for adhesive application, and sufficient thickness to resist buckling loads. The maximum tensile and compressive stresses of the ribbing material set the height of the beams at 3.75 in (Fig. 4.5.14c).

4.5.7 Arrangement of Ribbing

The ribbing has also been arranged in a pattern which prevents buckling and better supports the TPS (Fig. 4.5.15). This arrangement pattern gives more integrity to the ribbing system. The ribbing has several connections all of which are made of titanium. The beam members parallel to each other are connected together at 12 ft intervals to reduce assembly time while preserving the integrity of the system (Fig. 4.5.16). The beam members perpendicular to each other are connected at the corners of the smaller dimension using L-shaped links. These links are easy to manufacture and are the simplest connection between two perpendicular members (Fig. 4.5.17). The beam members supporting the edge of the shield all run perpendicular to the edge. The beams giving support at the edge are cut-off sections of actual 24 ft long beams (Figure 4.5.18). The TPS itself is connected to the ribbing by an adhesive and by weaving the structure to the TPS. It has been assumed that an appropriate adhesive will be available when this project is initiated.
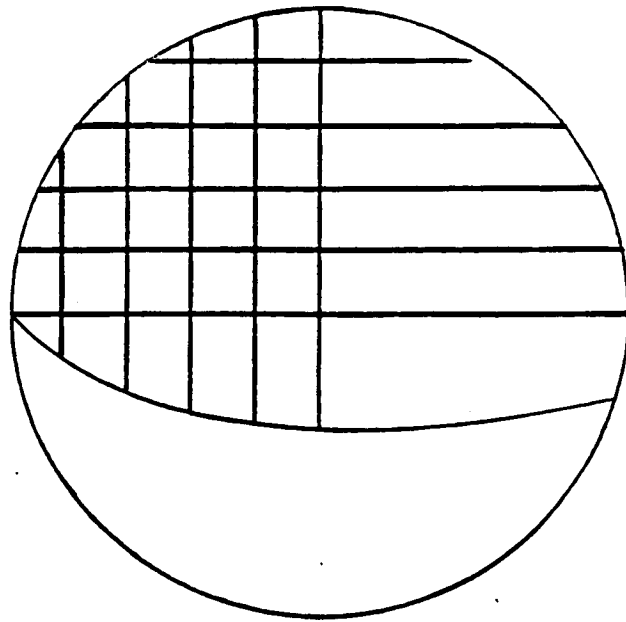
FIG. 4.5.10 Ribbing with Square Grid Pattern
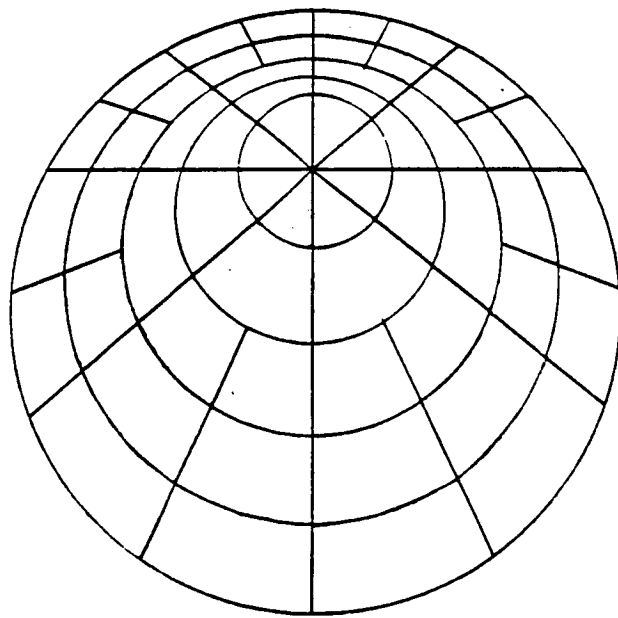
FIG. 4.5.11 Ribbing with Radial Grid Pattern

FIG. 4.5.12   Ribbing with Hexagonal
              Grid Pattern

UNIFORM LOADING DESIGN CRITERIA

FIG. 4.5.13a

RECTANGULAR CROSS SECTION BEAM

FIG. 4.5.13b

I-BEAM
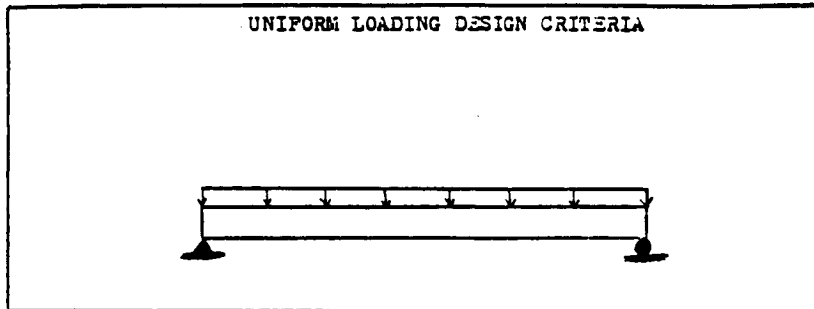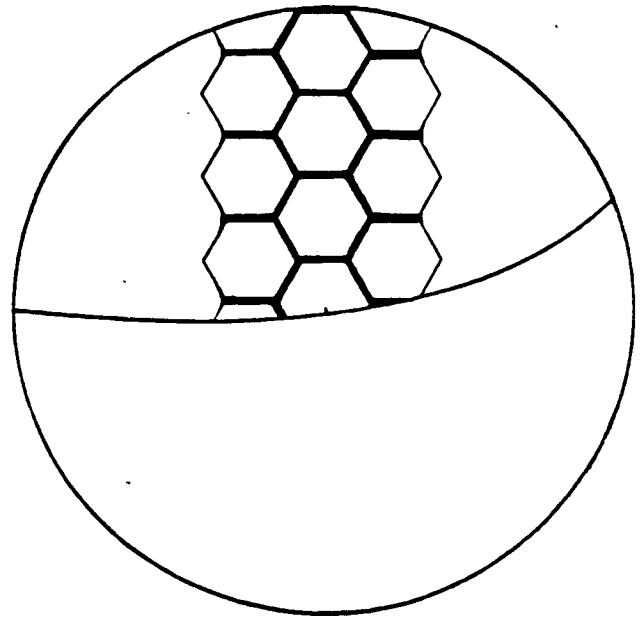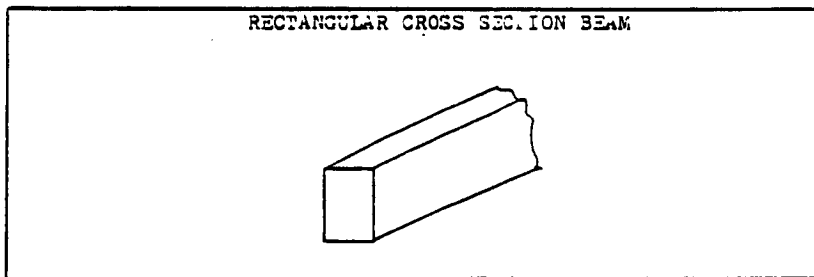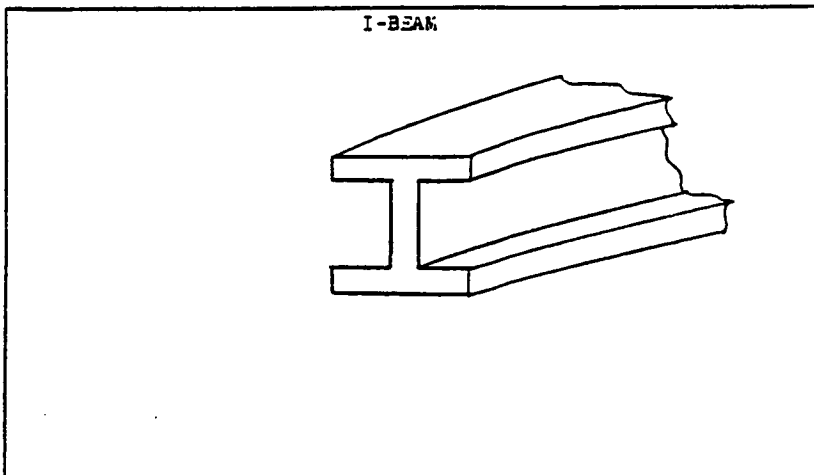
FIG. 4.5.13c

RIBBING BEAMS

Top View

24 ft.

3 ft.
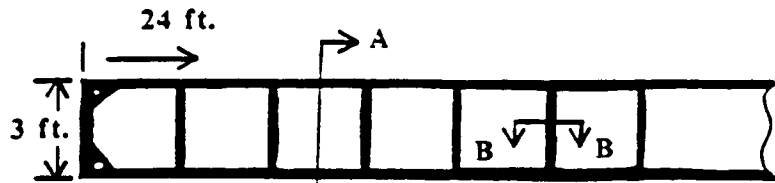
FIGURE 4.5.14 a

RIBBING BEAMS

Section AA

.15 in.

3.75 in.

3 ft.
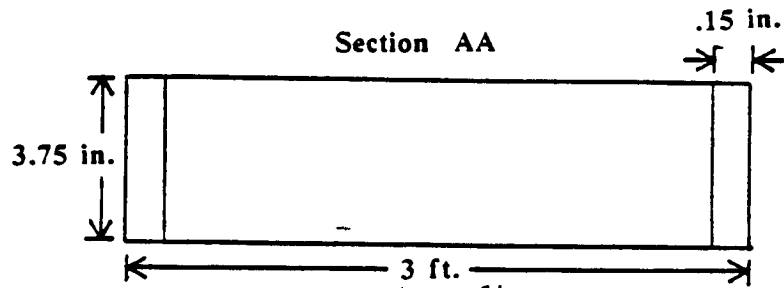
FIGURE 4.5.14 b

RIBBING BEAMS

Section BB

3.75 in.

.15 in.

FIGURE 4.5.14 c

3 ft.
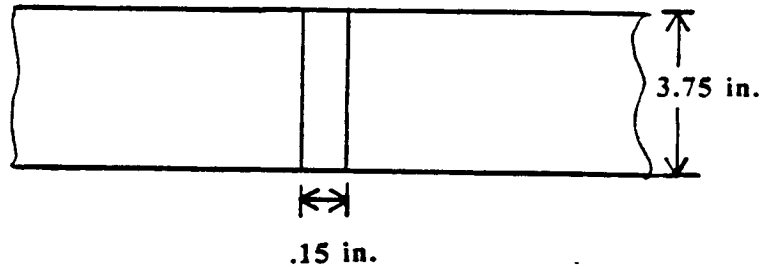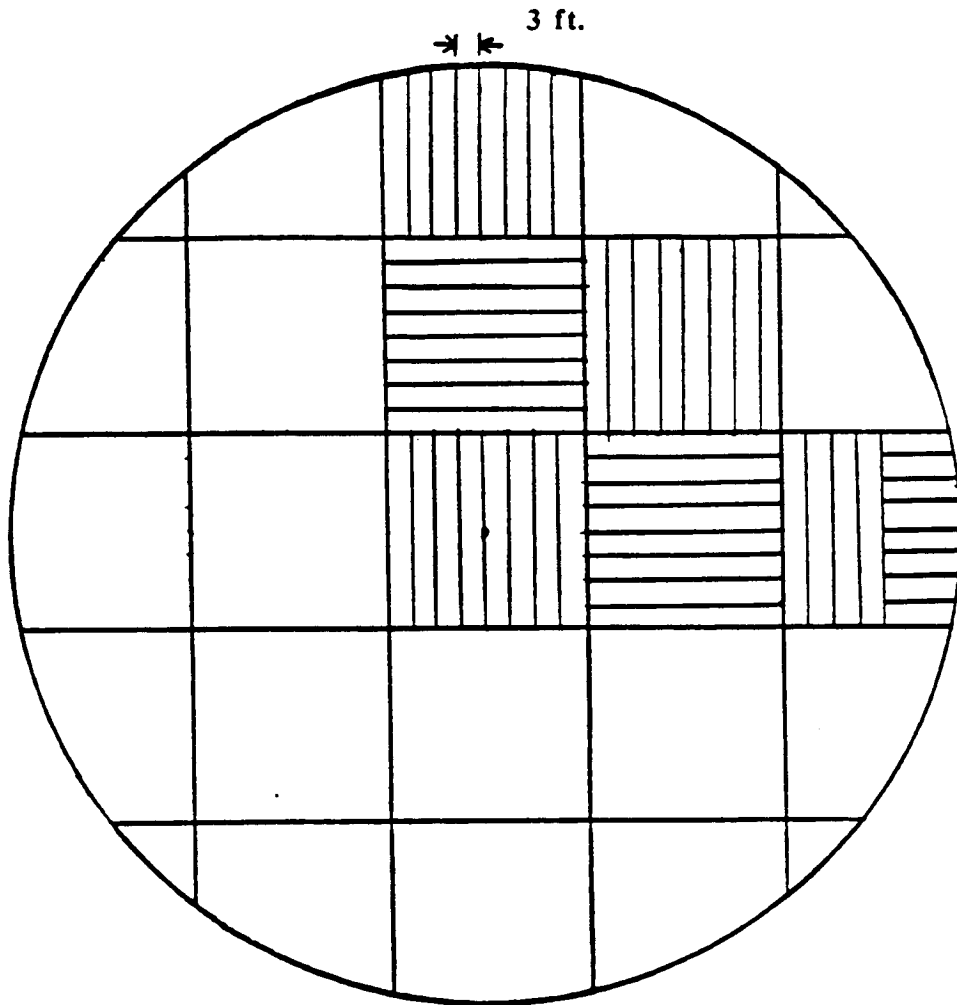
FIGURE 4.5.15

RIBBING BEAM ASSEMBLY PATTERN

Connected by L-links
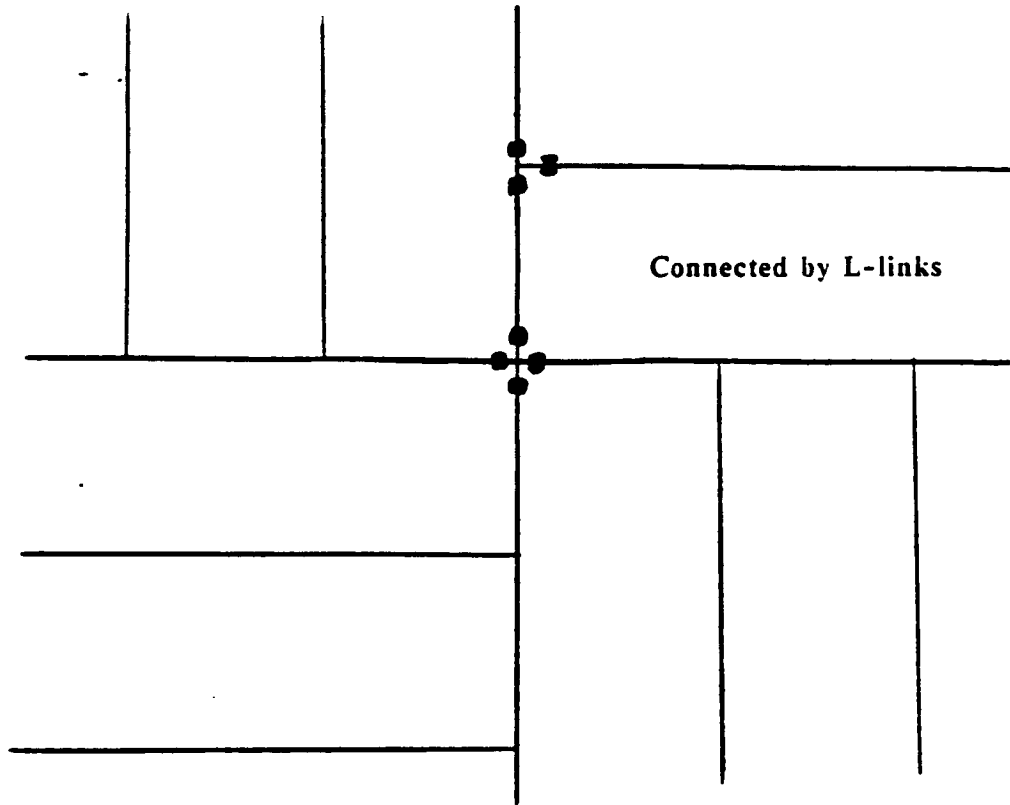
L-LINKS CONNECTING PERPENDICULAR MEMBERS
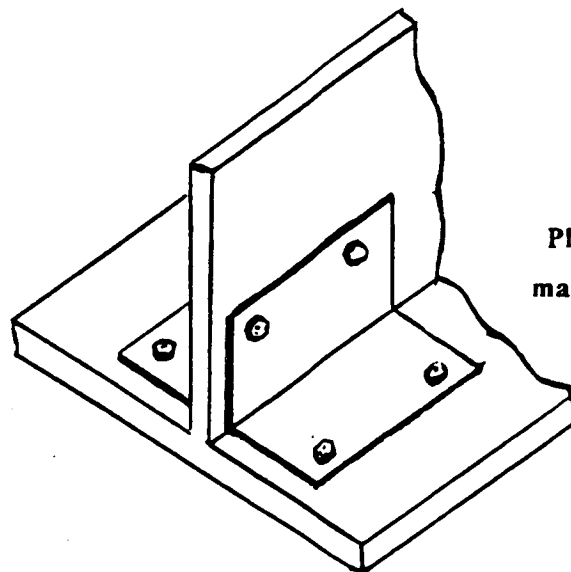
Plate and Bolts
made from Titanium

FIGURE 4.5. 16

RIBBING SUPPORT AT EDGES

12 ft.

Edge of Shield
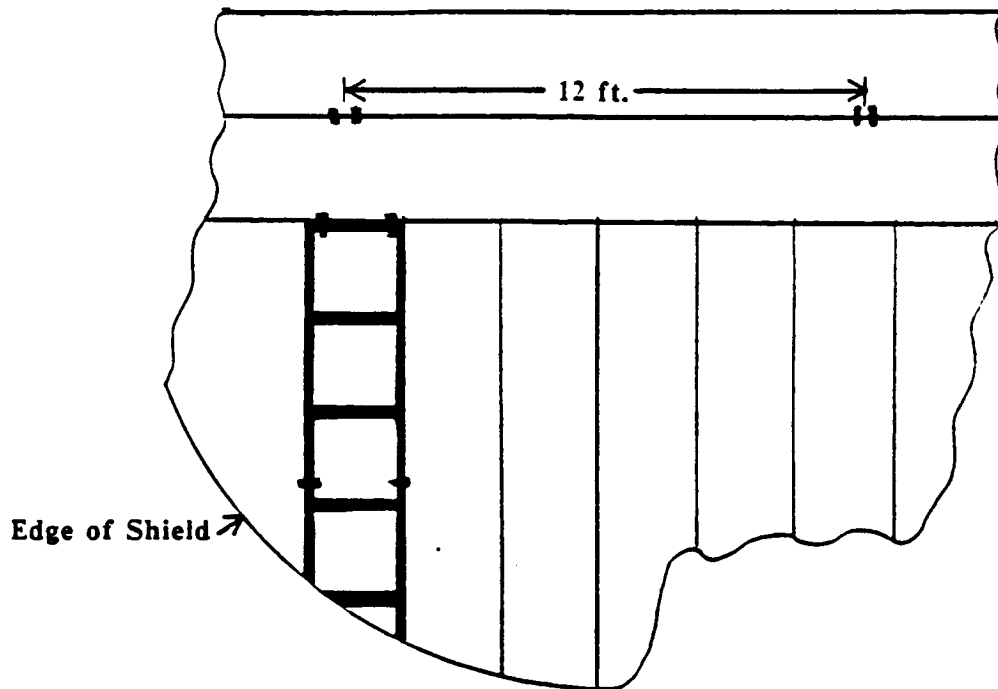
FIGURE 4.5.17

ATTACHING TPS TO RIBBING
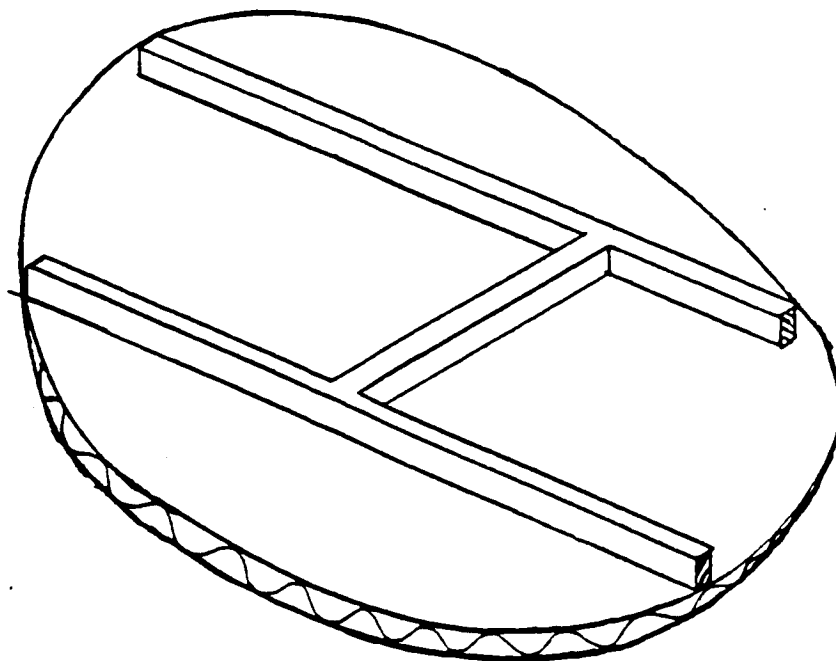
FIGURE 4.5.18

The connections by weaving are done at 10 ft intervals. It is unnecessary to weave the entire length of the beam. Weaving at 10 ft intervals reduces TAXI assembly time while keeping the shield structurally sound. At points where the ribbing connects to the truss network, a plate with four bolt like extensions is used as a connector. The plate is weaved and glued to the TPS (Fig. 4.5.19). The bolt like extensions fit through holes at the corners of the beams. A plate of titanium is added after the beams to provide additional support. A second plate is also added which is attached to a truss joiner. These plates serve to connect the truss frame to the ribbing. The rib structure is extended to support the shield skirt. The supporting ribs are open cut-off sections of the longer beams (Fig. 4.5.20a). The skirt rib structure is attached to the rest of the rib structure by bolted links and adhesive (Figure 4.5.20b).

4.5.8 Transport to Orbit and Assembly

The four main trusses E-E', F-F', G-G', H-H' (Figure 4.5.6) will be divided in half giving eight assemblies that are all less than 56 ft x 15 ft. The other four trusses A-A, B-B, C-C, D-D are divided into 20 sub-assemblies by the four main trusses. The 20-sub assemblies have dimensions of approximately 24 ft x 24 ft. The ribbing will be broken into seven units approximately 70 ft x 24 ft (Figure 4.5.21).

Once the sub-assemblies are in orbit, the truss structure is assembled first. Note that this only requires the alignment of the truss members and the insertion of pins in the joiners. The ribbing is then attached to the truss structure. When the ribbing is in place, the insulation will be stretched over the ribbing and the skirt will be secured to the outer edge of the remaining ribbing.

4.5.9 Materials Selection .

Minimizing weight is the most important factor in choosing a material. Three choices were available: Aluminium, Titanium, and Graphite composite. Graphite polymide was chosen over aluminium because of its lighter weight and greater strength. The composite is chosen over titanium because of its lower cost. However, in areas of greater stress or higher temperature titanium is used. The graphite polymide has a temperature limit of 600 deg F and titanium has a temperature limit of 800 deg F. The properties of graphite polymide are as given below:

Property		
Tensile Strength	203.3 kpsi	(1401 MPa)
Tensile Modulus of Elasticity	18.3 Mpsi	(18.3 GPa)
Compressive Strength	206.1 kpsi	(1420 MPa)
Compressive Modulus of Elasticity	18.7 Mpsi	(129 GPa)
Density	1.6 g/cm^3	

Titanium
Joiner

Plate

Rib

Connector
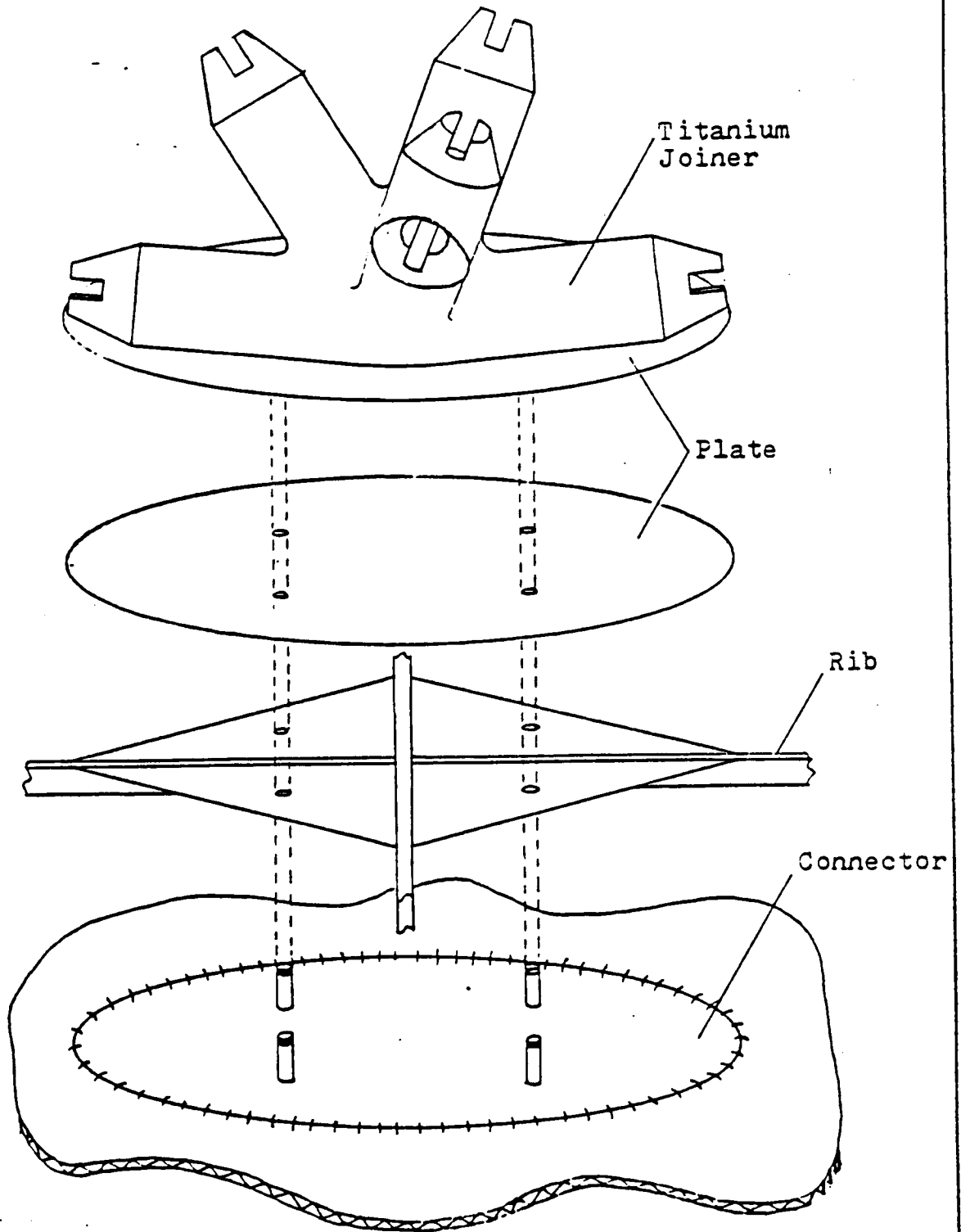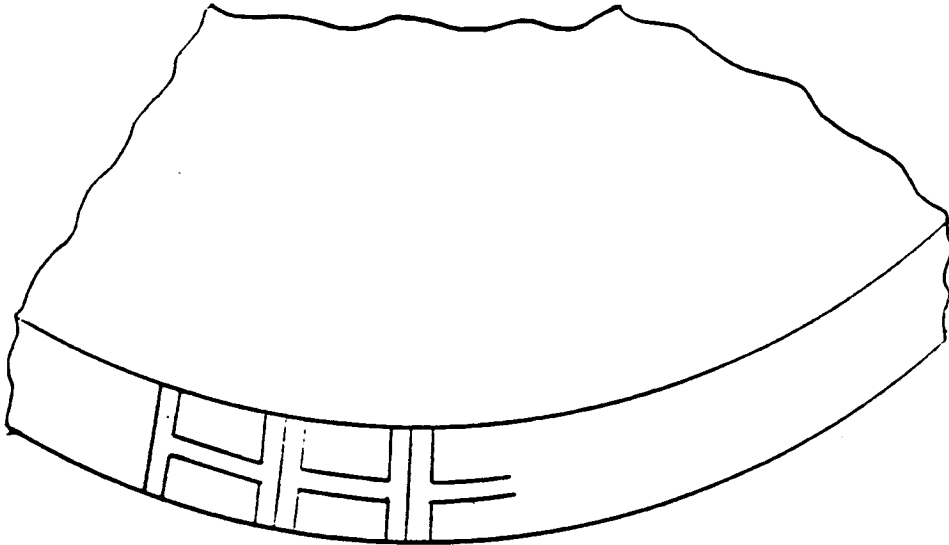
FIGURE 4.5. 19

FIGURE 4.5.20a
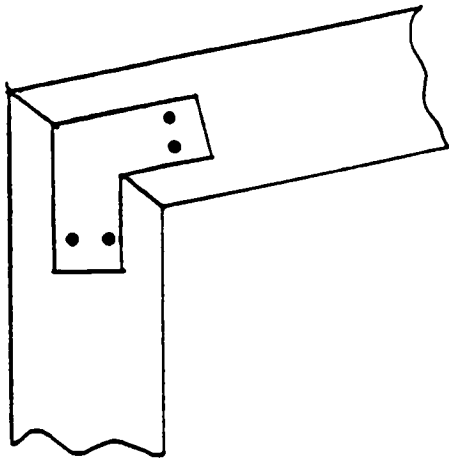
FIGURE 4.5.20b

Each subsection approx. 70 ft. by 20 ft
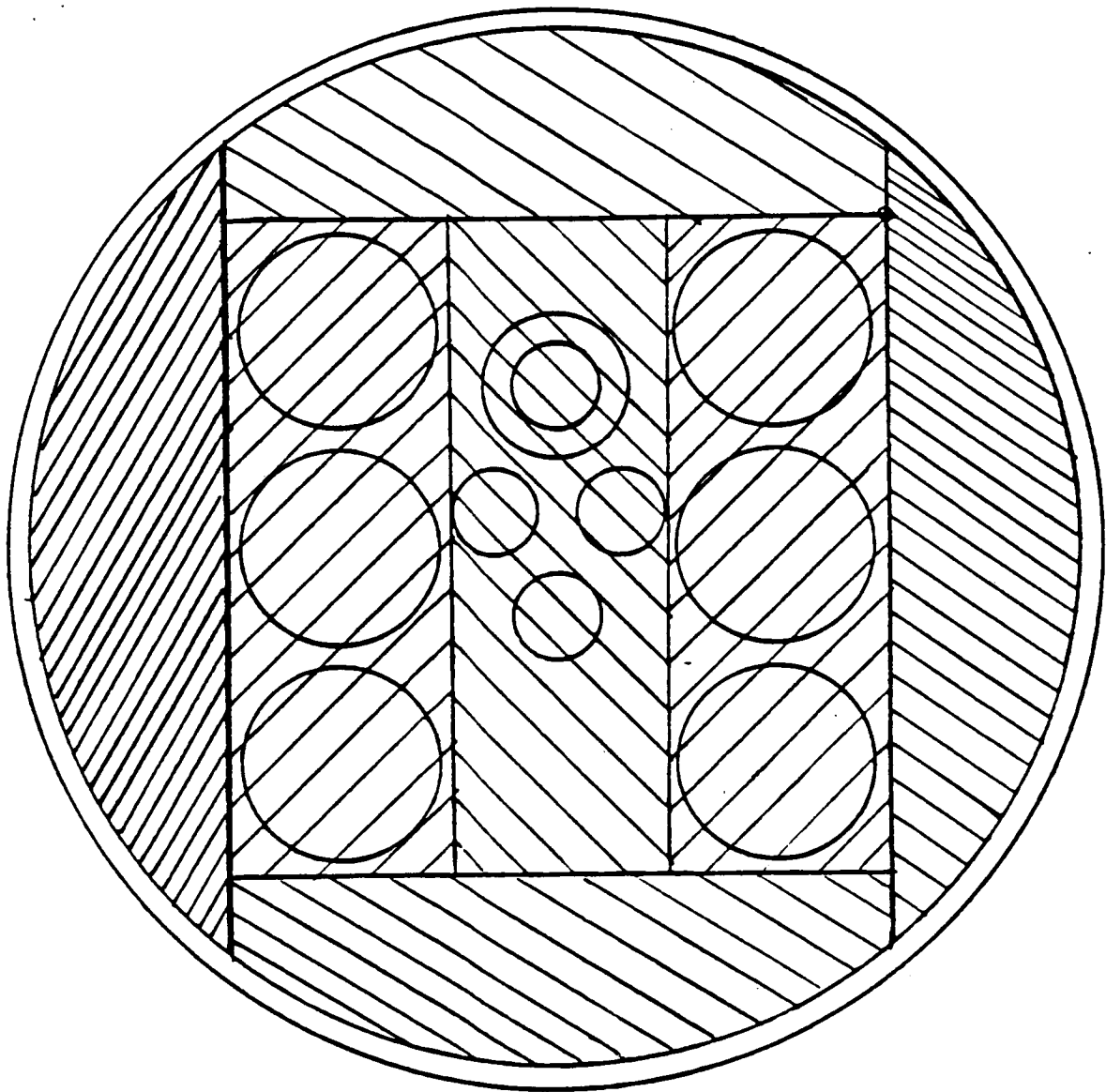
FIGURE 4.5.21

4.6 TPS Material Selection

The design of an aerobrake for atmospheric entry requires a load-bearing structure operating under adverse heating conditions. Temperatures of 1600 K and heat fluxes on the order of 19 W/cm^2 at Mars to 22 W/cm^2 at Earth will be present on the aerobrake surface. The outer layer, or TPS, must prevent most of this heat from reaching the inner structure and must transmit aerodynamic loads to that structure. Numerous studies have been done on aero-assisted orbital transfer vehicles. Results of studies of AOTV's have been used extensively in this report due to their similarity to the TAXI aerobrake.

Ceramics are the chosen materials for the TPS. Of current materials, they have the highest operating temperatures, are lightest in weight, and can be designed for specific properties such as reflectivity and resistance to heat shrinkage. A major advantage is their low catalycity (Menees,1983, Savage,1984). As gas molecules pass through the high temperature regions behind the bow shock, they tend to dissociate and ionize. Catalycity is the tendency of a TPS surface to cause the recombination of those dissociated molecules. Since this recombination process releases additional heat energy to the flow, low catalycity is desired to mimimize the heat flux onto the TPS surface.

Three major designs were looked at:

1) rigid thermal protection system
2) flexible TPS mounted on a rigid load-bearing surface
3) flexible TPS mounted on a frame and carrying the load itself.

A rigid design consists of a stiffened plate overlying an inflexible structure (Figure 4.6.1). A rigid ceramic system similar to shuttle tiles is attached to the shell. If the supporting layer flexes during aerodynamic loading, the inflexible tiles can easily pop off of their clips or other bonding material. Although a rigid system would be feasible, the lighter weight, ease of intallation and manufacture, increased panel size, and the better response to temperature-induced shock of the flexible designs (Savage,1984), encourage the use of those systems where conditions allow it. For example, rigid ceramic tiles would have to be individually sculpted and fit into place. The usefulness of a flexible TPS is seen in its replacement of rigid tiles on low temperature regions of the shuttle orbiters. As discussed below, current and projected advances in flexible shield materials will allow their use in higher temperature regions.

For the reasons listed above, flexible ceramics have been chosen for the surface of the TPS. The next decision involves the method of supporting the aerodynamic loads on the shield. The second design also has a rigid shell of graphite polyimide (GR-PI) transmitting the loads from the aerobrake surface into the shield support structure (Figure 4.6.2). Ideally, this layer would be extremely thin, but this results in a low resistance to buckling. Therefore, the shell must be either fairly thick or it must be supported by an extensive system of stiffeners (Blosser). A sample calculation reveals that a 1/16 inch layer of GR-PI over the entire surface results in a mass increase of 13,182 lbm over a flexible load-bearing layer, as in the chosen design.As a shield material, aluminum is even heavier than GR-PI.

123

RIGID DESIGN

rigid ceramic tiles

rigid backing
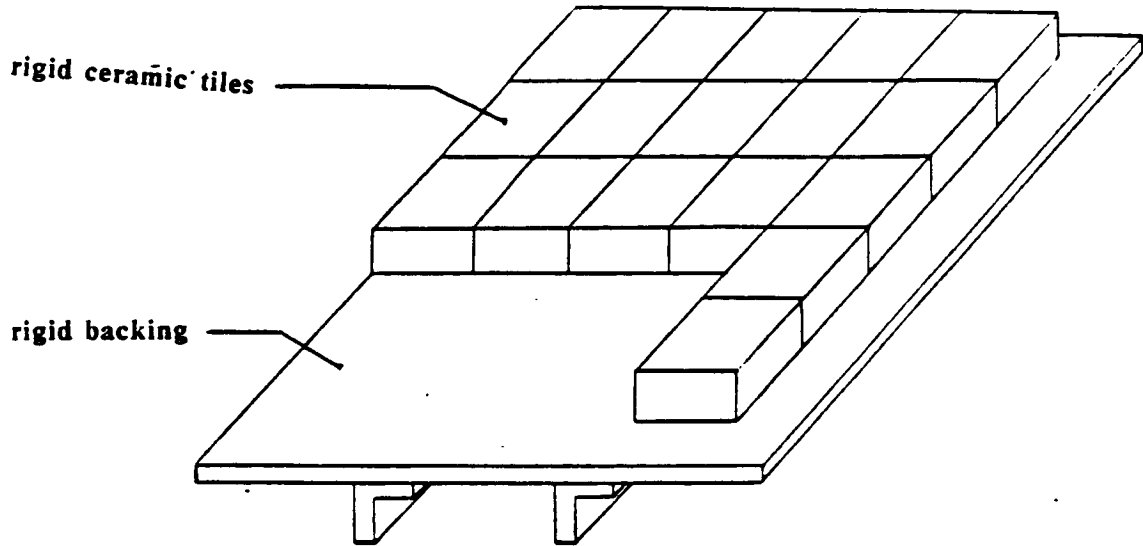
FIGURE 4.6.1

RIGID/FLEXIBLE DESIGN

flexible ceramic surface

rigid backing
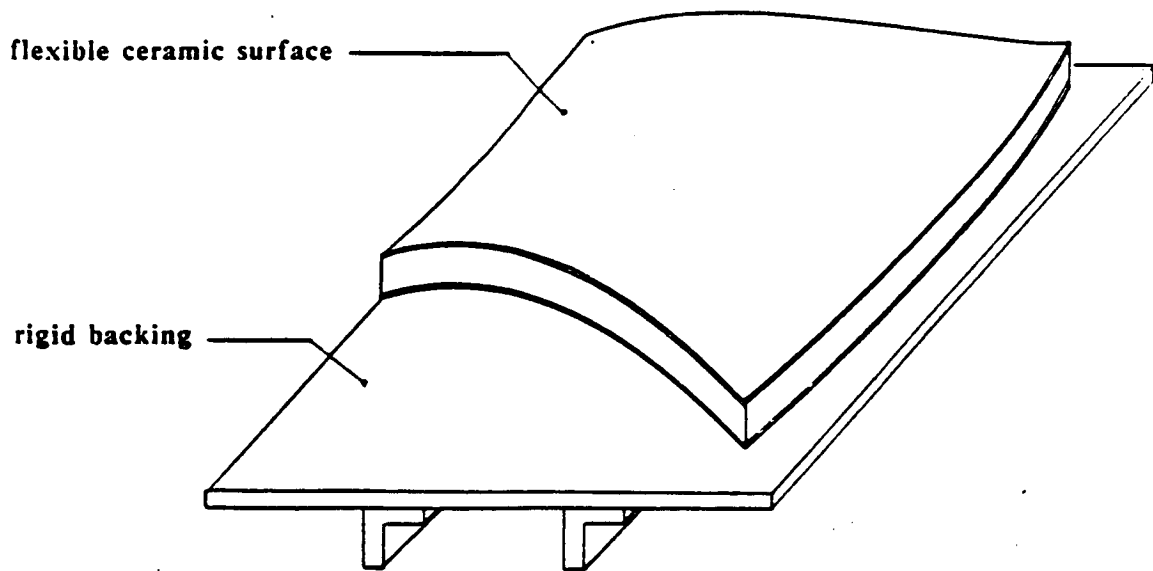
FIGURE 4.6.2

4.6.1 Chosen Configuration

The chosen design is shown in figure 4.6.3. It is a multilayer concept designed to allow each component to perform a specific task. The outer coating must survive the highest temperatures. It should have high reflectivity (about 0.8) in wavelengths emitted by the dissociating and ionizing gases behind the bow shock. There is disagreement over the magnitude of the radiative heat flux. In general, in the mission flight environment, radiation is considered significant but of a lesser magnitude than convective heat transfer. Highly reflective materials are used to reject the radiative heating.

This layer should be smooth and noncatalytic to minimize convective heating. The colloidal silica particulate coating used on the space shuttle is such a material. Currently, it is limited to temperatures of 1260 K and has a reflectivity up to 0.7 (Goldstein). The temperature limit and reflectivity of this material are inadequate for the TAXI aerobraking environment; however, development over the next forty years should alleviate those shortcomings. The weight of each layer is 0.0362 psf, resulting in a total weight of 460 lbm (209 kg).

The next layer protects the inner insulation and is the foundation of the surface coating. Possible materials are Nicalon, Nextel, and silica cloth. Nicalon is the chosen surface material for several reasons. Of all the flexible ceramics found in the literature, it has been tested at the highest heat flux. When tested at a heat flux of 36.1 W/cm^2, Nicalon was unaffected while Nextel stiffened when exposed to about half that heat flux. Silica surface sheets (AFRSI) do the same at even lower heating rates (Savage,1984). Nicalon can operate at temperatures over 1640 K. In addition, silicon carbide, as in Nicalon (Pitts,1984), is projected to be able to withstand 65 W/cm^2 (Menees,1981).

The major way Nicalon reduces heating to the shield is through reradiation of the heat to the flow. The average emittance of Nicalon is 0.8 and absorptivity is also 0.8 at 0.1 to 0.01 atmospheres. This means that Nicalon will radiate effectively when its temperature rises. One half of this, which would otherwise conduct through the shield, radiates outward. The weight of a standard thickness of Nicalon is 0.0694 lb/ft^2 (Goldstein),giving a total weight of 978 lbm (444 kg).

The major drawback of Nicalon is its low reflectivity, about 0.05 (Covington,1986), which is much lower than that of other materials, including Nextel and silica cloth. Since the resistance of Nicalon to thermal degradation is needed at Mars (heating rate about 20 W/cm^2), this material must be used, although most of the radiative heat flux must still be reflected. The solution is in the use of surface coatings, as mentioned before.

The next layer is the primary protection of the inner structure from the aerodynamic heating. Additionally, it relieves the thermally-induced shear stresses between the inner and outer layers. The insulation is required to have low thermal conductivity to protect the support structure and concentrate the highest temperatures in the Nicalon face sheet. This second function causes much more heat to radiate to the environment than to enter the insulation. Two possible materials are Nextel felt and Q-felt (General Dynamics,1986, Savage). Q-felt (silica fiber) has been chosen because it is less porous than Nextel felt (Savage). This is important because porosity increases convective heat transfer to the material (Menees, 1983, Engel,1983).

125

* detail

colloidal particulate coating

Nicalon

Q-felt

Nicalon membrane
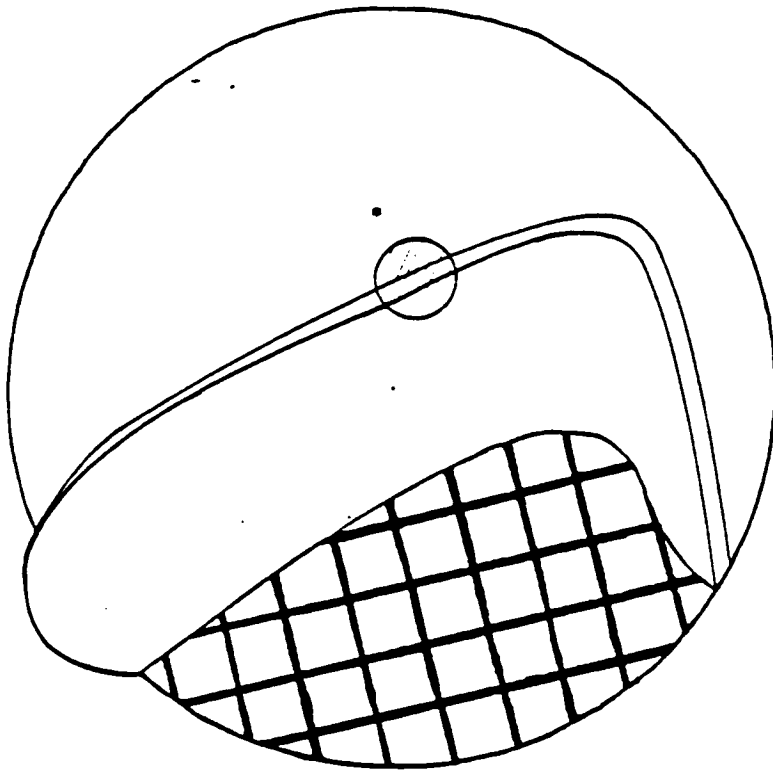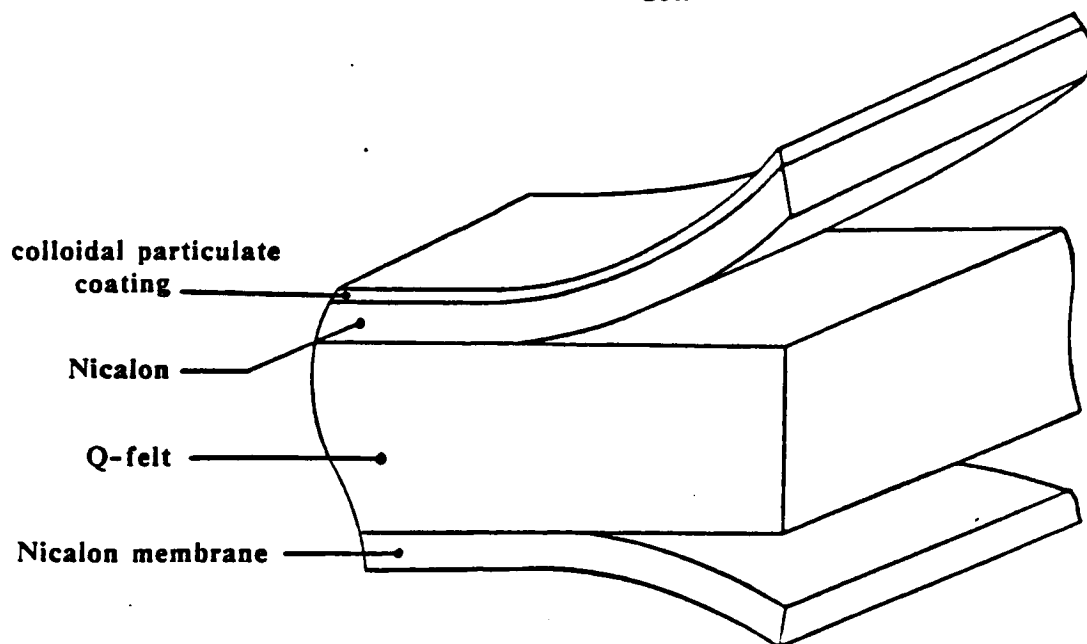
FIGURE 4.6.3

The insulation thickness, one inch, is determined by the need to limit the temperature of the supporting structure and bond line to 600 K, the maximum operating temperature of current bonding agents and GR-PI (Fig. 4.4.11). This maximum temperature is reached when the shield is unloaded and cooled in space after the atmospheric pass. Q-felt has a density of 6 lb/ft^3 (General Dynamics,1986) for a total weight of 7045 lbm (3196 Kg) and is by far the greatest weight of the shield surface.

The backing layer consists of a flexible membrane stretched taut over the supporting frame. This layer of Nicalon composite carries the loads of the aerobrake and must maintain strength while receiving conducted heat from the Q-felt and radiative heating from the wake. It has a density of 0.20 psf producing a total mass of 2818 lbm (1278 Kg). The total weight of the shield is then 11,300 lbm (5126 Kg).

4.6.2 Transportation to Orbit

Because the shield is very large, it cannot be shipped into orbit in its deployed state. Because of difficulties in working in orbit, however, the shield must be largely prefabricated. For this reason, the individual layers will be manufactured and sewn together on Earth. To withstand the heating of reentry, Nicalon thread is used to connect the layers. The surface coating can be added, as well, but should be flexible to survive handling, a problem with the current materials.

One possiblity for stowage on the launch vehicle is to roll the shield up, but this is likely to damage the shield. Our solution is to cut the shield into eight large panels (Figure 4.6.4). These will fit in the 25' x 90' Shuttle-derived Heavy Lift Launch vehicle (see section 9.3). The bottom layer will extend beyond the rest and will have adhesive strips and clips. The correct shape of the pieces will preferably be preserved, but this may be unnecessary. When the shielding is reassembled in orbit, the clips will hold the pieces temporarily in alignment. A protective cover is then removed from the epoxy adhesive to permanently join the pieces. Finally, an epoxy resin bonds the shielding to the support structure.

4.6.3 Questions to be Addressed

In addition to improving the nominal performance of the colloidal silica particulate coating, its resistance to long-term environmental damage needs to be examined. Alternating exposures to the different chemicals of the planetary atmospheres may be a problem. In addition, materials such as thermal control paint and polished aluminum left on the moon for extended periods were found to have deteriorated reflectivity after retrieval by a later mission (Anderson,1971). Solar radiation was at least partially responsible, and its effects must be guarded against during the lifetime of the heat shield and structure.

SHIELD SURFACE CONNECTIONS
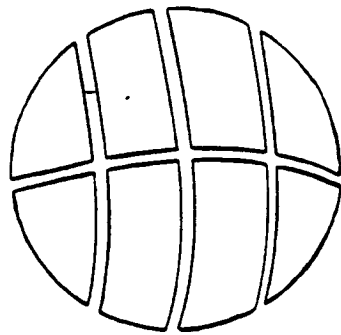
eight shield panels

nominally 30 x 60 ft (9.2 x 18.3 m)

adhesive strip

surface

Q-felt

backing

membrane

clips
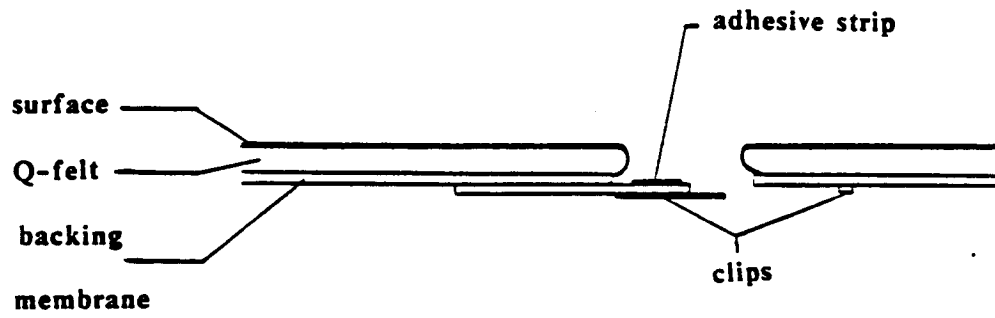
FIGURE 4.6.4

4.6.4 References

1 Menees, G.P., C.B. Davies, J.F. Wilson, and K.G. Brown, "Aerothermodynamic Heating Analysis of Aerobraking and Aeromaneuvering Orbital Transfer Vehicles", AIAA Paper 84-1711, June 1984 (also published in the 1984 Volume of the AIAA Progress Series).

2 Pitts, W.C. and M.S. Murbach, "Thermal Response of an Aeroassisted Orbital Transfer Vehicle with a Conical Drag Brake", AIAA Paper 84-1712, June 1984 (also published in the 1984 Volume of the AIAA Progress Series).

3 Pitts, W.C., and M.S. Murbach, "Thermal Design of AOTV Heat Shields for a Conical Drag Brake", AIAA Paper 85-1052, June 1985.

4 "Orbital Transfer Systems Studies and Technologies", General Dynamics Space Systems Division, Dec. 1986.

5 Menees, G.P., "Thermal-Protection Requirements for Near- Earth Aeroassisted Orbital Transfer Vehicle Missions", AIAA Paper 1513, June 1983 (also published in the 1984 Volume of the AIAA Progress Series).

6 Engel, C.D., "AOTV Low L/D Preliminary Aeroheating Design Environment Final Report", NASA Paper N83-36097, Remtech, Inc., Huntsville, Ala., Aug. 1983.

7 Savage, R.T., W. Love, and F. Bloetacher, "High Temperature Performance of Flexible Thermal Protection Materials", AIAA Paper 84-1770, AIAA 19th Thermophysics Conference, Snow Mass, Col., June 1984.

8 Menees, G.P., and C. Park, "Design and Performance Analysis of a Conical Aerobrake Orbital TRansfer Vehicle Concept", AIAA Paper 84-0410, Jan. 1984 (also published in the 1984 Volume of the AIAA Progress Series).

9 Scott, C.D., R.C. Ried, R.J. Maraia, C.P. Li, and S.M. Derry, "An AOTV Aeroheating and Thermal Protection Study", AIAA Paper 84-1710, June 1984 (also published in the 1984 Volume of the AIAA Progress Series).

10 "Aerothermodynamic Design Considerations of and Aerobraked Spacecraft", AIAA Paper 83-1510.

11 Hair, L.M., C.D. Engel, and P.R. Sulyma, "Low L/D Aerobrake Test at Mach 10", AIAA Paper 83-1509, 18th Thermophysics Conference, Montreal, Canada, June 1983.

14 "General Aerocapture Atmospheric Entry Study",NASA CR-164160, AIAAPaper 82-1378,General Electric and Jet Propulsion Lab, Oct. 1980.

15 Schwartz, M.M., Composite Materials Handbook, McGraw-Hill Book Co., 1984, pp. 2.21 and 2.53-2.55.

16 Anderson, D.L., B.E. Cunningham, and R.G. Dahms, "Radiation Degradation Analysis of Surveyor III Material", AIAA Paper 71-478, presented at AIAA 6th Thermophysics Conference, Tullahoma, TN, Apr. 1971.

17 Goldstein H., personal communication.

18 Blosser, M., personal communication.

19 "Air Force Composites Handbook", 1985.

21 Menees, G.P., "Thermal-Protection Requirements for Near- Earth Aeroassisted Orbital Transfer Vehicle Missions", AIAA Paper 1513, June 1983 (also published in the 1984 Volume of the AIAA Progress Series).

22 Covington,M.A. and P.M. Sewko, "Optical Properties of Woven Fabrics for Flexible Heat Shields", AIAA Paper 86-1281, June 1986.

4.7 Aerobrakes of TAXI B and TAXI C

Aerobrakes of the TAXI versions B and C use the same geometrical configuration and similar thermal protection system (TPS) as the aeroshield of the TAXI A (section 1.5). Reduced tank sizes of the TAXI B and C, along with reexamination of the required aeroshield surface led to selection of the aeroshield sizes. The physical and design parameters of the TAXI B and TAXI C aeroshields are listed in Table 4.7.1.

Table 4.7.1 Aeroshield Physical and Design Parameters

Parameter	TAXI B	TAXI C
Reference area, A	5157.2 ft²	8058.2 ft²
Vehicle mass at the beginning of the aeroassisted maneuver near Earth, M_{BAM}	74,300 lbm	102,100 lbm
C_D	1.574	1.574
Ballistic coefficient, $M_{BAM}/C_D A$	9.15 lbm/ft²	8.05 lbm/ft²
L/D	0.1526	0.1526
Max heating rate, $\dot{q}_{max}$	30 W/cm²	30 W/cm²
Max acceleration	5 g	5 g
Diameter	80 ft	100 ft
Mass: TPS	5,420 lbm	7,860 lbm
Support structure	4,370 lbm	6,260 lbm

5. Life Support Systems

5.1 Design Criteria

In choosing life support systems for our vehicle, several factors had to be considered. These are shown in Table 5.1.1 in order of importance.

Table 5.1.1 Design Criteria Considerations

1. Crew safety
2. Length of time crew needs to be supported
3. Number of crew members
4. Mass and volume of the system
5. Reusability of the system
6. Maintainability of the system
7. Crew adaptability

Once these factors were evaluated, systems were chosen for air supply, water, food, waste, thermal protection and radiation protection. Since the crew size and trip duration were essentially the same for the TAXI versions A, B and C, life support systems are the same for all these TAXI versions.

5.2 Human Factors Considerations

5.2.1 Crew Size

Based on the projected requirements for the Mars missions, a typical number of crew members to be transported by TAXI is assumed to be nine including an overall commander, a pilot and a doctor with medical and surgical capabilities. With some modifications, the crew module design will allow for a maximum crew size of eleven.

5.2.2 Living Quarters and Recreation

The living quarters volume of the TAXI occupies 3467 ft^3(98.2 m^3) of space. This divides into two main areas: sleeping quarters and an area for food preparation and vehicle control.

Recreational facilities consist of reading materials, audio equipment and computer generated games. Physical recreation has not been included because the short duration of the trip does not justify the additional space required by the equipment.

5.2.3 Zero-Gravity Effects

Since the TAXI trip will take place in a zero gravity environment, the problems associated with this must be considered. There are several changes that occur which necessitate special design considerations for the interior of the module. The first of these is that the human body changes from an upright position to a crouched position. This causes the new eye point to be approximately seven inches lower than normal and the limbs to be lower and in front of the body. These changes must be considered when designing controls for the ship and its systems. The second effect is that people float, so restraints must be provided whenever it is necessary to obtain leverage or stability to perform a task.

Many physiological changes also occur. In long duration flights, some of these changes may be irreversible. Due to the short stay on the TAXI the crew members should regain their normal body functions quickly after returning to an environment with gravity. There is one

physiological problem that will, however, have a substantial effect on the crew members. This is space motion sickness caused by disturbances in the functioning of the vestibular system. There is no known way to prevent this disorder, but it is treated with drug therapy and the symptoms usually disappear in two to four days. Astronauts afflicted with this condition will function with reduced efficiency for the first few days spent in this environment.

5.2.4 Medical Equipment and Training

Each crew member should receive a basic medical training, listed in Appendix 11.5.1. Since the TAXI is similar to the Space Shuttle in terms of length of flight and crew number, the ship will carry the Shuttle Orbital Medical System (SOMS). This will enable crew members and the doctor to adequately handle most medical problems until the ship docks.

5.3 Life Support Systems Design

5.3.1 Atmosphere System

In determining   means of providing a Controlled Environment Life Support System (CELSS), a choice had to be made between an open or closed atmosphere gas system. Due to the brevity of the mission, a completely open system is very feasible because its overall weight is less than that of a closed system. However, the difference in weight is not enough to merit its use. With an open system, there is always the chance of gas depletion in the event that travel time is longer than anticipated. In order to prevent this, extra gas must be carried on board, thus increasing

the weight . Another disadvantage of an open system is that it requires more maintenance. Not only will the crew have to perform the necessary maintenance to keep it running efficiently, but they will also have to replace the used gases each time they rendezvous with the cycling ship. If the TAXI vehicle was to be used for just one trip, an open system would be more practical. But due to the circumstances of this mission, a completely closed system is preferred.

The ideal breathing environment is composed of 20% oxygen and 80% nitrogen, with a cabin or crew module pressure of 14.7 psi (101.4 kPa).

The gas recycle system, Figs. 5.3.1 & 5.3.2, consists of the separation of carbon dioxide and oxygen from atmospheric gas consisting of oxygen, carbon dioxide, and nitrogen.

Chemical absorption and desorption will be used for the separation of carbon dioxide gas. Solid amine, a regenerable CO_2 absorber, is used to separate and concentrate carbon dioxide from the atmosphere. Once separated, the gas is then compressed and stored in the CO_2 gas bottles.

Chemical absorption and desorption will also be used for the oxygen gas separation. The zirconia oxygen pumping method, which uses zirconia as a solid electrolyte, separates oxygen from the atmosphere. It is then compressed and stored in the O_2 gas bottles. Once separated, the gases are mixed properly and supplied to the various utilities.

Gas Recycle System Requirements

Flow Rate (for one man life support)

Item	
O_2	30 l/hr
CO_2	25 l/hr

Purity

O_2	% > 90
CO_2	% = 90
N_2	% = 90

Block Diagram Explanation

The blower draws 951.1 gal/hr (3600 l/hr) of inlet gas. The filter, containing activated charcoal and hophalite, removes all contaminants such as CO, odor, dust, crumbs, and other particles.

At the CO_2 concentrator of solid amine, about 10.6 gal/hr (40 l/hr) of CO_2 is obtained. The concentrator compresses and stores it in the CO_2 gas bottle.

The system returns 887.7 gal/hr (3360 l/hr) to the cabin atmosphere.

The residual flow of 52.8 gal/hr (200 l/hr) is led to the next process, salcomine O_2 concentration.

At the salcomine O_2 concentrator, about 10.6 gal/hr (40 l/hr) of O_2 is obtained, compressed and stored in the O_2 gas bottles.

Gas Recycling System Functional Diagram

C - compressor
B - bottle
CN - concentrator
BL - blower
F - filter
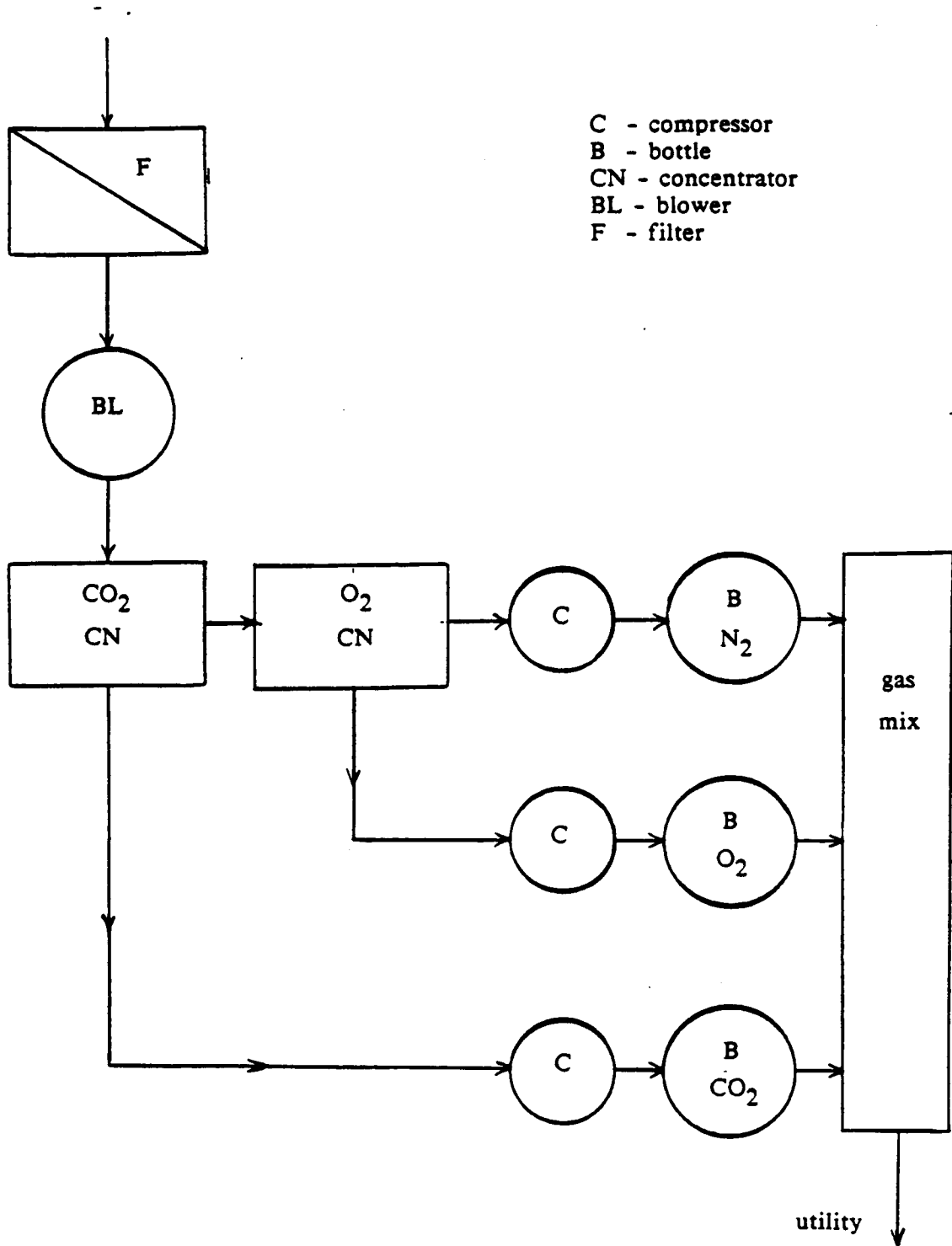
Figure 5.3. 1

Gas Recycling System Block Diagram

887.7 gal/hr

$O_2 + N_2$

42.3 gal/hr N_2

951.1 gal/hr

10.6 gal/hr O_2

O_2

10.6 gal/hr CO_2

CO_2

R - resevoir
SA - solid amine
S - salcomine
C - compressor
B - blower
CN - controller
F - filter

Figure 5.3. 2
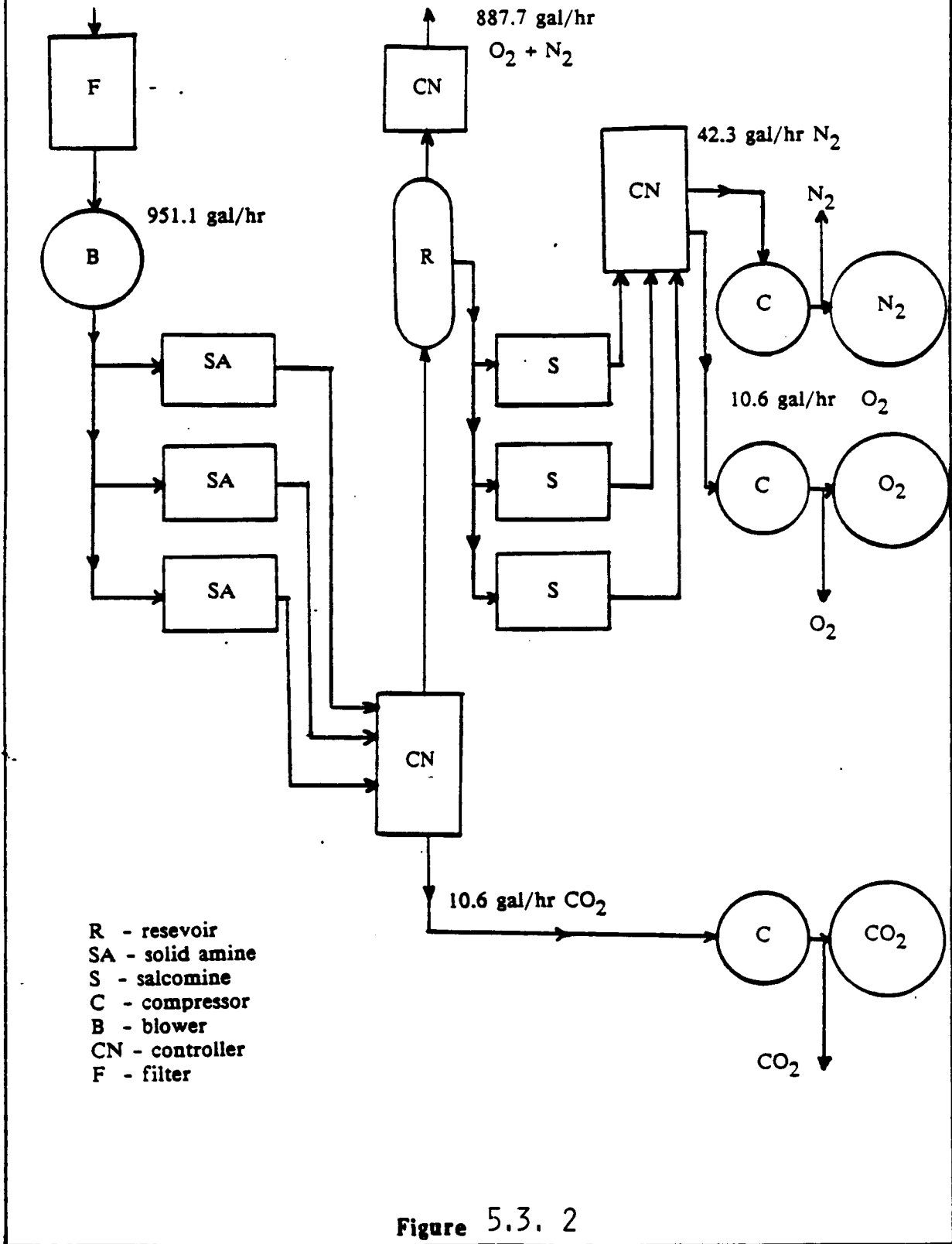
The residual flow, 42.3 gal/hr (160 l/hr) of N_2 gas is compressed and stored in the N_2 gas bottles.

5.3.2 Water Systems

Various methods which can be used to supply the crew with water are as follows:

1. Using water derived from hydrogen-oxygen fuel cell product
2. Using water supplies in combination with regeneration of drinking water from atmospheric condensate
3. Using water regenerated from liquid and solid wastes on board the spacecraft

The water supply on the TAXI will be a combination of onboard storage and fuel cell by-product. On board storage consists of 220 lb (100 liters) of water for emergency purposes only. The main water supply will come from a fuel cell located in the avionics module. This fuel cell will operate at 20 kW and produce 1.91 gal/hour (7.2 l/hr). The excess water will be stored on the TAXI and then removed to the cycling ship after docking.

5.3.3 Food Systems

The food system on board the TAXI must provide for the needs of the crew while :

1. meeting dietary goals
2. maintaining health and safety standards
3. providing potable drinking water
4. minimizing waste in packaging and food processing
5. appealing to the crew

Because of the short duration of the flight, a special food inventory and diet monitoring device is not essential to crew survival.

Three forms of cooking or thermal processing are available for space travel.

1. Fluid immersion (pressure cooking)
2. Roasting and baking (with a combination forced convection/microwave oven)
3. Direct contact and/or radiant heat (grilling)

The form most suited for the transport vehicle is an oven using microwave and forced air convection. This system is the simplest to design and operate and it is the most flexible in food preparation.

Food stuffs must be planned and preserved so as to be most beneficial to the crew. The present meal guidelines follows the four basic food group rules. Food preservation methods available include:

1. dehydration
2. thermostabilizing by canning and/or retort pouch
3. irradiation
4. intermediate moisture
5. freezing

Dehydration and thermostabilizing by retort pouch are the best methods because of their lightweight packaging and they allow for storage at room temperature. A hot and cold water dispenser can also be addded to increase food preparation variety.

Foodstuffs will be stored in cabinets in the crew module. Two separate locations for storage will be used in the event that if one becomes inaccessible an emergency food supply will be available. One location is inside the safe haven. A food supply emergency requirement is alotted for 50 % of the total trip duration time and will equal 60 % of the normal supply.

The crew requires 2600-3000 calories per man-day(Compton)[7]. Stowage space for food is 3.53 ft^3 (0.1 m^3) and the weight is 550 lb (250 kg).

This system is best suited for the transfer vehicle because of its light weight, simplicity and ease of storage. It will offer the crew a "mix and match" variety in meal selection, preparation and equipment operation is simple and waste is kept to a minimum.

5.3.4 Waste Management Subsystem

Human Body Waste Collection

A waste collection assembly consisting of one fecal tank, two wipes tanks, bag liners for each tank, a urine collection assembly, and a vacuum actuated piston type compactor will be used. This is shown in Figure 5.3.3. The sytem has a total storage capacity of 4.48 ft^3 (0.127 m^3) and a total weight of 170 lb (77.27 kg). It necessitates main DC power (28 V) and inverter AC power (400 Hz, 115 VAC). This assembly is taken from Reference 9.

This system was selected due to its compact size and its design and operation simplicity. The collection, drying and storage is carried out in one process. There will be absolutely no handling of body waste, other than the wipes used in cleaning one's person.

Solid waste will be collected in the fecal and wipes tanks, dried by vacuum, and stored in the bag liners within each tank.

Waste water will cause little problem since it will be transported by air flow to the liquid waste storage tank, instead of being recycled or cleansed aboard the TAXI.

Waste will be stored until junction with the space station or cycling ship. It will then be transferred to their waste management system . Due to the short duration of the mission, storage of body waste poses no threat of contamination and therefore, jettisoning of waste from the TAXI will be limited to radioactive or otherwise hazardous materials which must be removed immediately.

5.3.5 Thermal Control Systems

The thermal balance of the vehicle includes the following

      1. Heat absorbed from thermal radiation (direct solar
         radiation and albedo radiation)
      2. Internal heat generation (crew members and electronic
         equipment)
      3. Heat loss through radiation to space

Wake heating during aerobraking is not expected to be significant due to the large diameter of the shield.

Waste Collection Assembly

left wipes tank

right wipes tank

fecal tank

split tank

urinal

vacuum pump

close

open

to vacuum

2 FS 1

FS 2

FS 1

off

legend

cabin

odor bacteria filter

to waste storage tank

open

closed

closed/open

FS fan separator
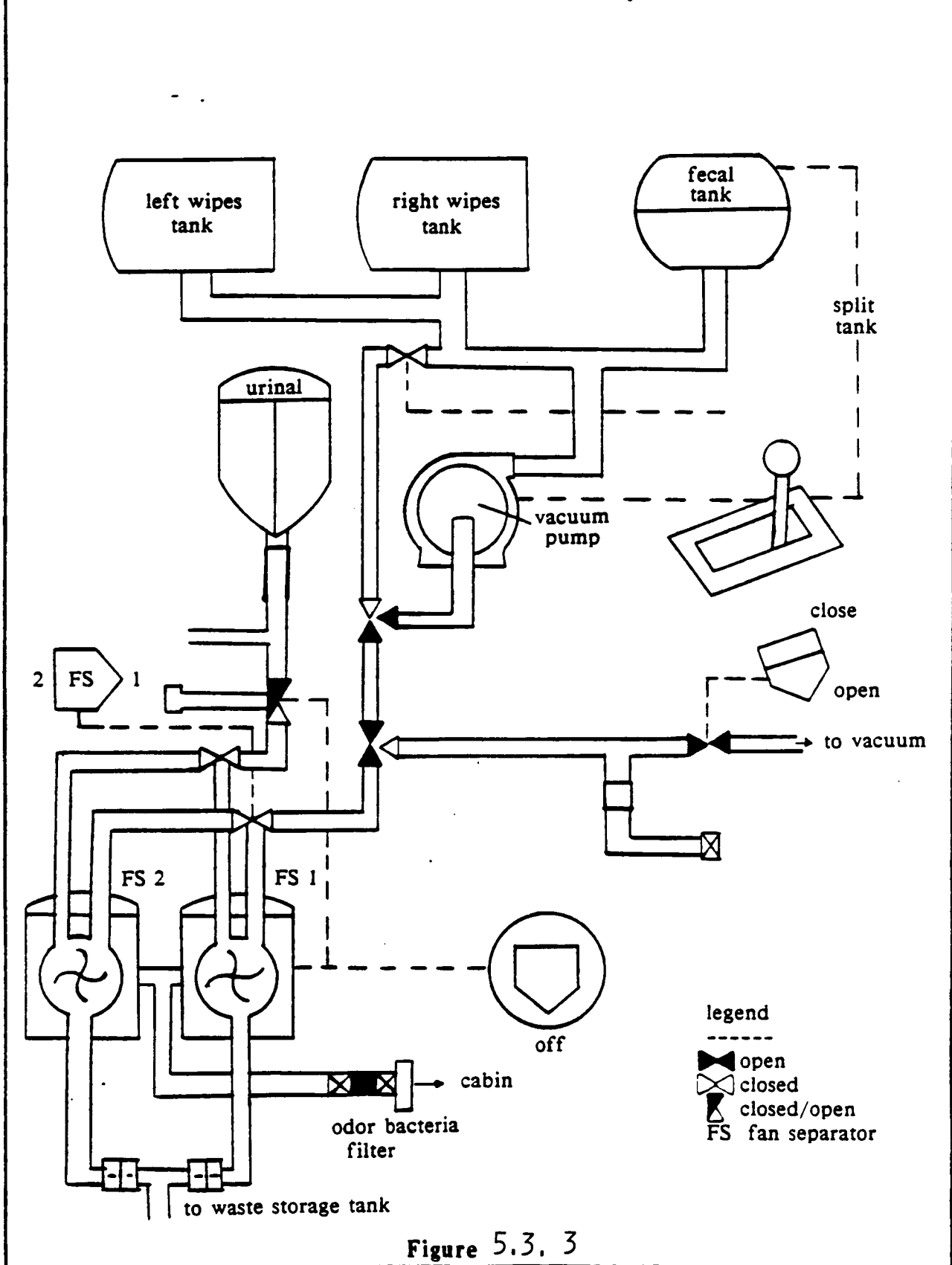
Figure 5.3.3

While docked, the cycling ship and the base stations are assumed to act as heat sinks for the TAXI.

A thermal control system can include both active and passive methods. The following table lists several types of each.

Active and Passive Methods of Thermal Control

-Passive	-Active
-insulation	-radiators in conjuction
-multi-layer walls	with heat exchangers
-thermal control coatings	and fluid heat pipes
	-variable absorbance/
	emittance panels

An active thermal control system consisting of two radiators and a heat exchanger was chosen because it is more versatile than a passive system. A passive system cannot be controlled, whereas an active one can. An active system also weighs less and is more easily maintained than a passive system. Rapid heating was not a concern since this occurs during reentry.

The radiators and heat exchanger are mounted on the hull near the docking system. This location was chosen because it is the outermost point on the vehicle and eliminates any possibility of radiating into the tanks or aerobrake structure. The radiators weigh 44 lb (20 kg) each and the heat exchanger weighs 88 lb (40 kg).

5.3.6 Radiation Protection

Radiation Sources

During transfer from LEO to the cycling ship, radiation can be encountered from the Van Allen belts, cosmic radiation and solar flares.

The Van Allen belts consist of electrons and protons trapped in a geomagnetic field occupying a volume of space about the earth from approximately 700 to 7000 miles. In an unprotected spacecraft a crew would receive a dose of 10 rads/hour or more while passing through these belts. With shielding the vehicle receives negligible cosmic radiation beyond the Earth's atmosphere. Solar flare particles consist of protons, alpha particles and a few heavier nuclei. As many as 10^{30} of these particles may be emitted during a single flare lasting up to one hour. The sun follows a semi-regular eleven year cycle; eleven years of a solar minimum followed by eleven years of a solar maximum during which time flares may or may not occur.

Limits and Effects

Solar flare radiation hazard is compounded due to the effects of the doses received over the mission. Limits on radiation exposure are set by the U. S. Nuclear Regulatory Committee at 1.5 Sv (150 rems) for astronauts. The effect radiation will have on cells depends on the size of the dose received at one time, the condition of the person, and the area of the body exposed.

There is a variation in opinion as to the hazard posed to astronauts by solar flares because quantitative data on their occurrence and information on the response of the human body to space radiation is limited.

Safe Haven·Pros and Cons

Since the Mars missions will span over many years, a solar maximum may be encountered sometime during TAXI trips.

A radiation shielding system must satisfy these requirements:
1. Provide adequate protection for the crew
2. Not interfere with the normal functioning of the spacecraft
3. Be relatively light in weight.

Either bulk shielding or a safe haven shield effectively. Bulk shielding requires a very large added mass and, therefore, is not recommended for our TAXI. Safe have introduces certain restrictions of the crew activities during the flare, ruling out normal flight and scientific duties for the flare duration. A safe haven was chosen because a solar flare is generally unlikely for the period the crew will be in the TAXI. The shielding density thickness for the 99.0% reliability, adequate, given the odds of a flare, is listed in Table 5.3.1 for the polyethylene and aluminum materials. Polyethylene has been chosen over the aluminum due to its lighter weight.

Table 5.3.1 Solar Flare Protection Materials

Reliability	Material	Density Thickness	
		$16/ft^2$	kg/m^2
99.0%	polyethylene	20.44	100
	aluminum	34.75	170
99.9%	polyethylene	110.37	540
	aluminum	149.20	730

The safe haven will be a cylinder 16.4 ft (5.0 m) in diameter, 6.6 ft (2.0 m) in length with a volume of 932.0 ft^3 (26.39 m^3) and a surface area of 524.0 ft^2 (48.68 m^2). This will also be the crew's sleeping quarters which will further reduce their radiation exposure. Enough food and water to sustain the crew for up to 24 hours will be stored in the safe haven. The weight of the polyethylene shielding is 10709.6 lb (4868.0 kg) and it has a thickness of 4.13 in (0.105 m).

References

1. Adams, James L.. Space Technology-Spacecraft Mechanical Engineering, Volume II. NASA 1965.

2. Benedikt, Elliott T.. Weightlessness-Physical Phenomena and Biological Effects. Univelt, Inc., SanDiego, CA 1960.

3. Bluth, B> J.. Socio/Psychological Issues for a Mars Mission. NASA Headquarters, Washington, D.C..

4. Brodsky, Allen B.. CRC Handbook of Radiation Measurement and Protection. CRC Press, Inc., Boca Raton, FL.

5. "Celss Experiment Model and Design Concept of a Gas Recycle System". NASA Report N86-19909. National Aerospace Lab, Tokyo.

6. Cheston, T. Stephen and David L. Winter. Human Factors of Outer Space Production. AIAA Selected Symposium. Westview Press, Inc., Boulder, CO 1980.

7. Compton, W. David and Charles D. Benson. Living and Working in Space-A History of Skylab. NASA History Series, NASA SP-4208 1983.

8. Conors, Mary M.. Living Aloft Human Requirements for Extended Spaceflight.

9. "Design Concept Definition Study for Improved Shuttle Waste Collection Subsystem". NASA-Cr 171834 1985.

10. Gofman, J. W.. Radiation and Human Health. Sierra Club Books, San Francisco 1981.

11. Haffner, James W.. Radiation and Shielding in Space. Academic Press 1967.

12. Hall, Eric J.. Radiation and Life. Pergamon Press 1976.

13. Helmreich, Robert L., John A. Wilhelm and Thomas E. Runge. Psychological Considerations in Future Space Missions.

14. Hord, R. Michael. CRC Handbook of Space Technology: Status and Projections. CRC Press, Inc., Boca Raton, FL 1985.

15. Horton, T. E.. "Spacecraft Radiative Transfer and Temperature Control". Technical Papers from AIAA 19th Conference, January 1981.

16. Lyndon B. Johnson Space Center. Space Shuttle. Washington, D. C. 1970.

17. Moore, Berrien III, Robert A. Wharton, Jr. and Robert D. MacElroy. "Controlled Ecological Life Support System". NASA Conference Publicaiton 2247 1982.

18. Murray, Robert W., John K. Manglialardik and John D. Schelkop. AIAA Paper no. 71-865, "Engineering Aspects of Zero Gravity Perosnal Hygiene and Waste Management Systems". Weightlessness and Artificial Gravity Meeting 1971.

19. Natani, Kirmach. Future Directions for Selecting Personnel.

20. Nicogossian, Arnauld E. MD and James F. Parker, Jr. PhD. "Space Physiology and Medicine". Nasa SP-447, Scientific and Technical Informaiton Branch, Septmeber 1982.

21. Oberg, James E.. Mission to Mars. Meridian Books 1982.

22. Pearson, Albin O. and David G. Grana. "Preliminary Results from an Operational 90 Day Manned Test of a Regenerative Life Support System". prepared by Langley Research Center.

23. "The Physiological Basis for Spacecraft Environmental Limits". NASA Reference Publication 1045, November 1979.

24. Santy, Patricia A.. Manned Mars Mission Crew Factors. Johnson Space Center, Houston, TX.

25. Santy, Patricia A.. Manned Mars Mission Psychological Issues. Johnson Space Center, Houston, TX.

26. Steinberg, Florence S.. "Aboard the Space Shuttle". NASA Report N81-23179. NASA-Division of Public Affairs 1980.

27. Van Vliet, Robert M.. Passive Temperature Control in the Space Environment. 1965.

28. Vaughn, Robert L.. "Space Shuttle-A Triumph in Manufacturing". SME 1985.

29. Weast, Robert C.. CRC Handbook of Chemistry and Physics, 62nd Edition. CRC Press, Inc., Boca Raton, Fl.

6. Vehicle Structures

6.1 Design Criteria

The primary consideration in the design of the TAXI was crew safety. Most of the systems and structural limits were set to insure the well being of the crew. Throughout the TAXI design a safety factor (SF) of 1.5 was used to provide an additional margin of protection.

Structural design criteria were established to maintain vehicle integrity and likewise crew safety:

1. sufficient structural strength and stiffness to withstand short duration (less than ten minutes), high force loads and smaller cyclic loads with no impairment to function, minimal deflections, and no significant degredation of material properties

2. structure and material durability to provide for an operating life of at least 5 missions allowing for minor repairs between missions.

3. a reliable docking system to connect with both space stations (LEO and Mars orbiting space station) as well as the cycling spacecraft.

The first of these requirements refers to the various loading situations the TAXI vehicle will have to endure. High force loads occur during aerobraking and during engine firings. A maximum force not exceeding 6 Earth g's is expected during engine use. Maximum aerobraking loads are somewhat less, not exceeding 4 g's, but these loads are also accompanied by high temperatures, 1080 R (600 K), and larger thermal gradients.

The second load type encountered involves small cyclic loads over long periods of time. These forces arise during normal operations and may be caused by small velocity or attitude changes, temperature induced stresses, or vehicle vibrations. Velocity changes will vary with the trajectory of the mission. Surface temperature gradients depend upon the orientation of the vehicle with respect to the sun. Temperature gradients and differences in thermal expansion coefficients between joined materials cause residual stress loads. In general, it will be assumed that these small cyclic loads will not restrict the TAXI design.

Another important consideration in the module design is the selection of materials. Materials used must not only be able to carry the required loads, but must also be lightweight, resistive to radiation damage, and practical from a cost and fabrication standpoint. These materials must be usable over a wide temperature range, 0 to 1080 degrees R (0 to 600 K). In addition, materials exposed to space should be relatively stable in a vacuum (low offgassing coefficients), and be resistant to micrometeriod and charged particle bombardment.

The vehicle docking system was chosen so that under a small misalignment the locking mechanism would guide the ship to the proper orientation. This feature saves on fuel needed for making many small adjustments in attitude and simplifies the docking process.

Some general assumptions made in the TAXI design include the following:

1. aerobraking loads along or very close to the vehicle central axis (parallel to the crew module axis)

2. relatively small loads on the TAXI when docked to the cycling spacecraft and space stations (so that these loads pose no restrictions on the overall design)

3. thermal stresses and fatigue are not limiting design factors.

6.2 Configuration

The TAXI consists of a two section conical aerobraking shield, a cylindrical crew module, payload module, three main thrusting engines plus smaller engines for attitude control, six liquid propellant tanks (4 hydrogen and 2 oxygen), guidance, navigation and control modules, power system, and truss supports for all these systems. The overall configuration and dimensions of the TAXI A, B, and C are shown in Figs. 6.2.1, 6.2.2, and 6.2.3, respectively. The "dry" masses (without LOX and LH2) of the TAXI A, B, and C are approximately 83,400, 65,100, and 77,600 lbm, respectively.

6.3 Crew Module Design

The crew module (the same for all three TAXI versions) is a short cylinder with an outer radius of 8.7 ft (2.65 m) and a length of 26.1 ft (7.95 m), including the 1.97 ft (.6 m) deep elliptical endcap and 7.4 ft (2.25 m) long docking/airlock section. (see Fig. 6.3.1). The crew module consists of an aluminum shell stiffened by sets of graphite rings and stringers. Over the entire module is another thin layer of aluminum which acts as a micrometeriod shield or bumper. The inside of the crew module measures 16.4 ft (5.0 m) in diameter by 16.4 ft (5.0 m) in length. The section nearest the aerobrake shield, 6.56 ft (2 m) long, of the module contains the sleeping area and solar flare safe haven. The other 9.84 ft (3 m) long section of the crew module contains the control and kitchen areas. The total mass of the module fully loaded is 20,000 lb (9090 kg).

6.3.1 Layout - CG and Moment of Inertia Calculations

Fig. 6.3.2 shows some of the basic features of the crew module layout. A better view of the layout can be seen in Fig. 6.3.3. The main concern of this section is the systems placement, shown in Figs. 6.3.4 and 6.3.5, and how it relates to the module CG location and mass moment of inertia. Reasons for the systems placement used here include use of available space, ease of access (according to the probability of access being required), and equal distribution of weights. Some of the systems like waste and medical were required to be within the safe haven area. The water system was placed underneath the safe haven to reduce the length and weight of the piping to the waste system. The atmospheric system was placed underneath the main control/living area where it could be easily accessed. The water and atmospheric systems are of approximately equal weights and so were placed on opposite sides of the x axis to balance each other. A complete table of the major system masses, locations, and volumes (where appropriate) appears in Table 6.3.1. The table does not include the masses of supplies, furnishings and other miscellaneous items. These items are assumed to have little affect on the CG and moment of inertia calculations.

Crew Module
8.7 ft   4.2 ft

10.88 ft

H_2

H_2

12 ft

9.6 ft

O_2

Nozzles

O_2

Payload Area

H_2

H_2

X

X

Nozzles

Nozzle Length = 13 ft

Crew Module

7.38 ft

Payload Area

16.4 ft

12 ft

3.9 ft

H_2

O_2

H_2

3.9 ft
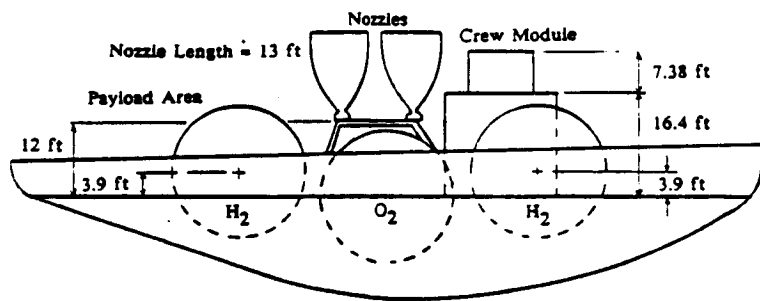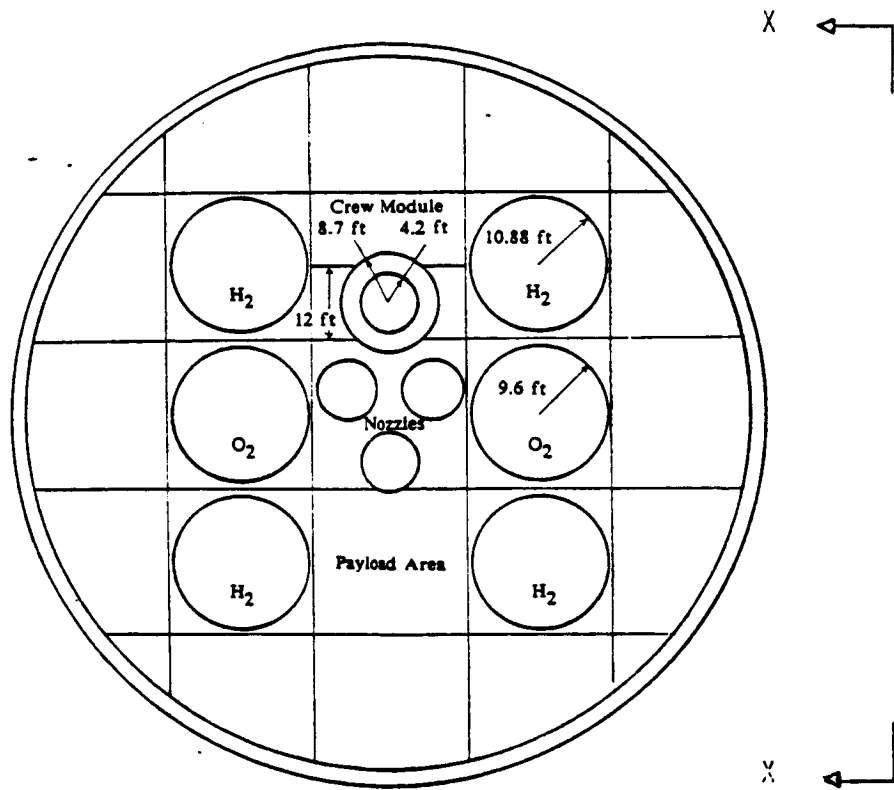
View X - X

Nozzle Exit Diameter = 9.63 ft
Shield diameter = 115 ft
Skirt Diameter = 120 ft

FIG. 6.2.1 TAXI A

146

FIG. 6.2.2   TAXI B

Dimensions in ft

147

Dimensions in ft

FIG. 6.2.3   TAXI C

148
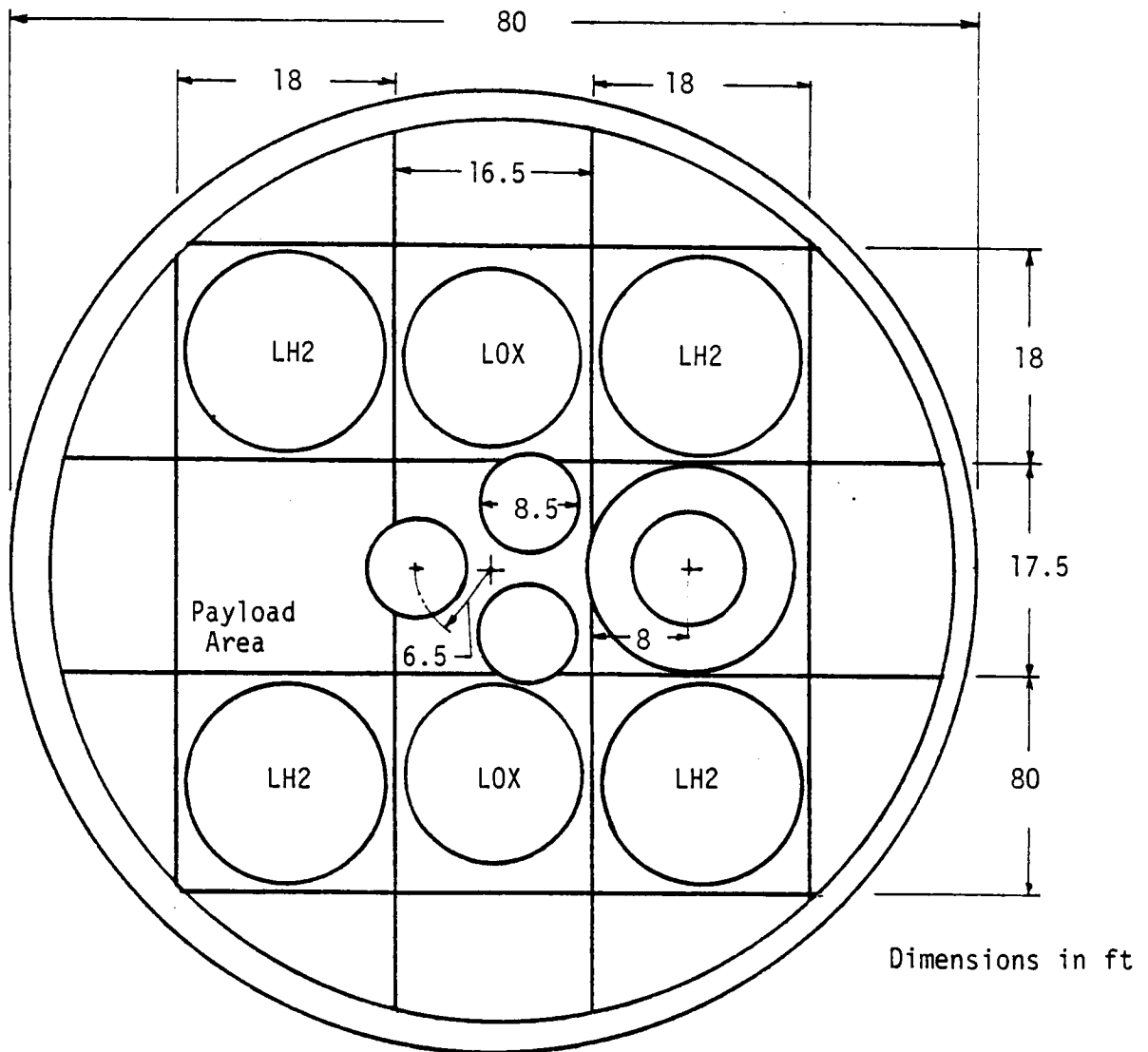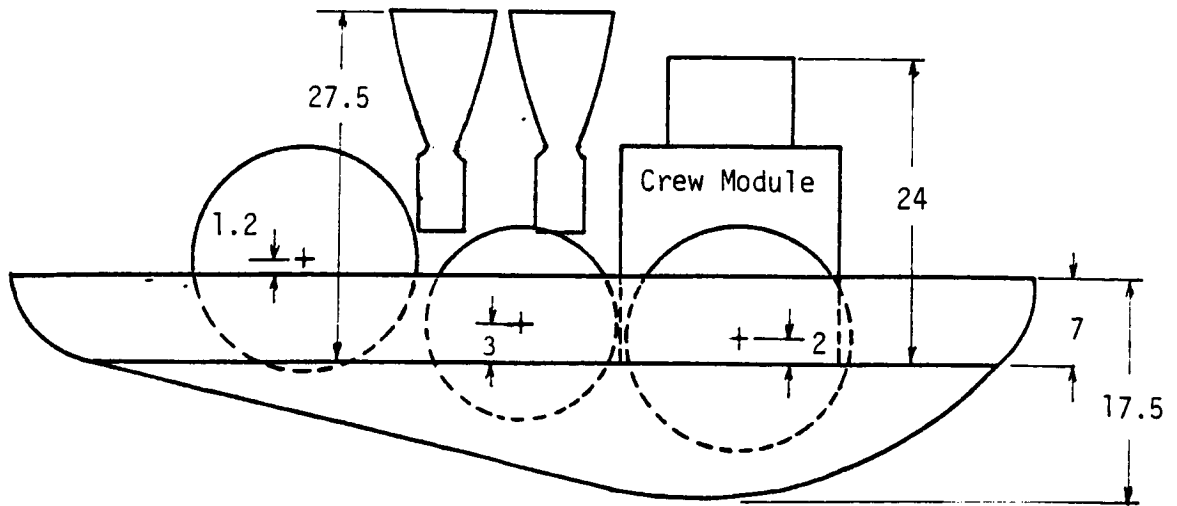
Crew Module, Airlock, Docking Assembly
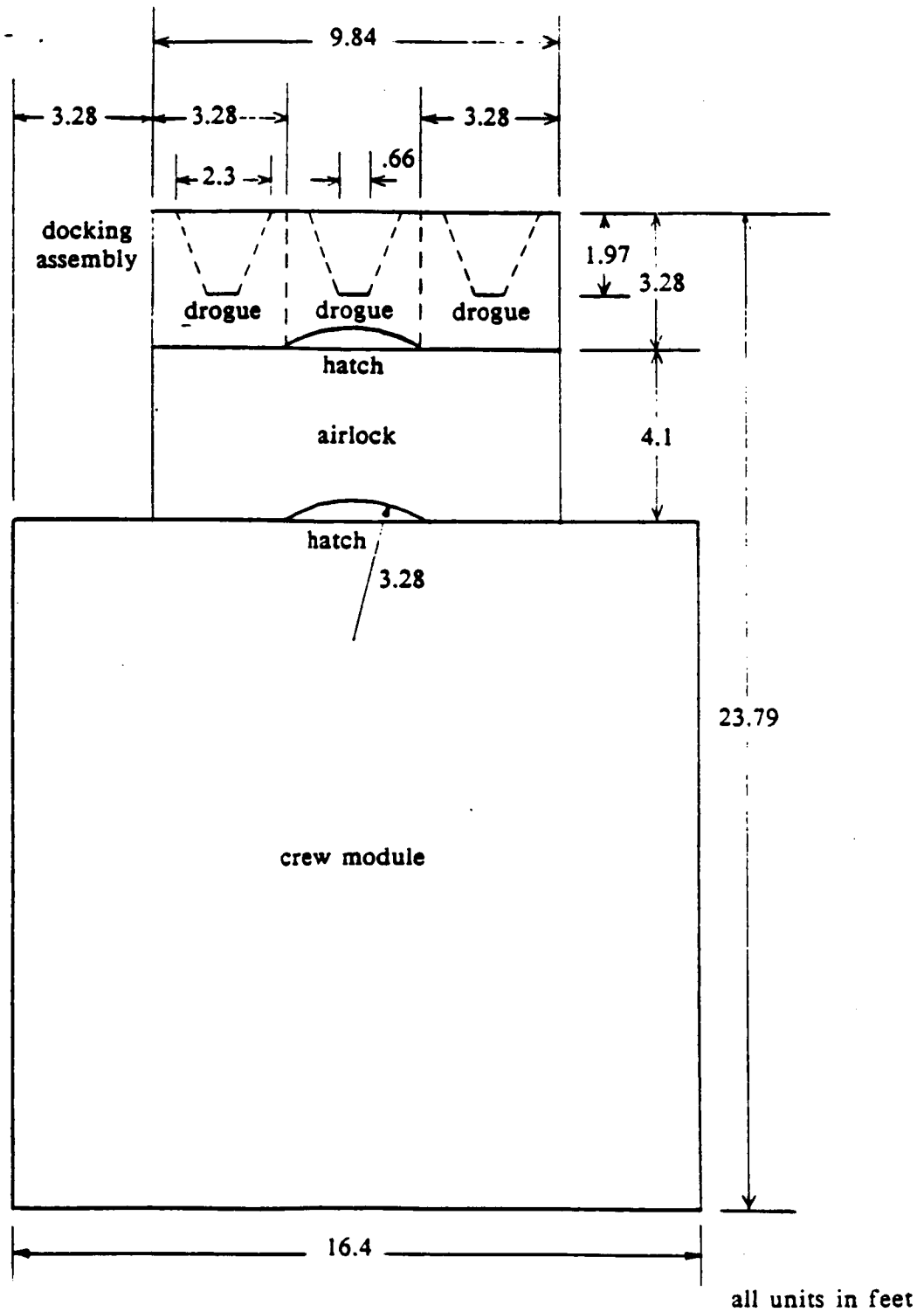
Figure 6.3.1

all units in feet

Crew Module Interior View
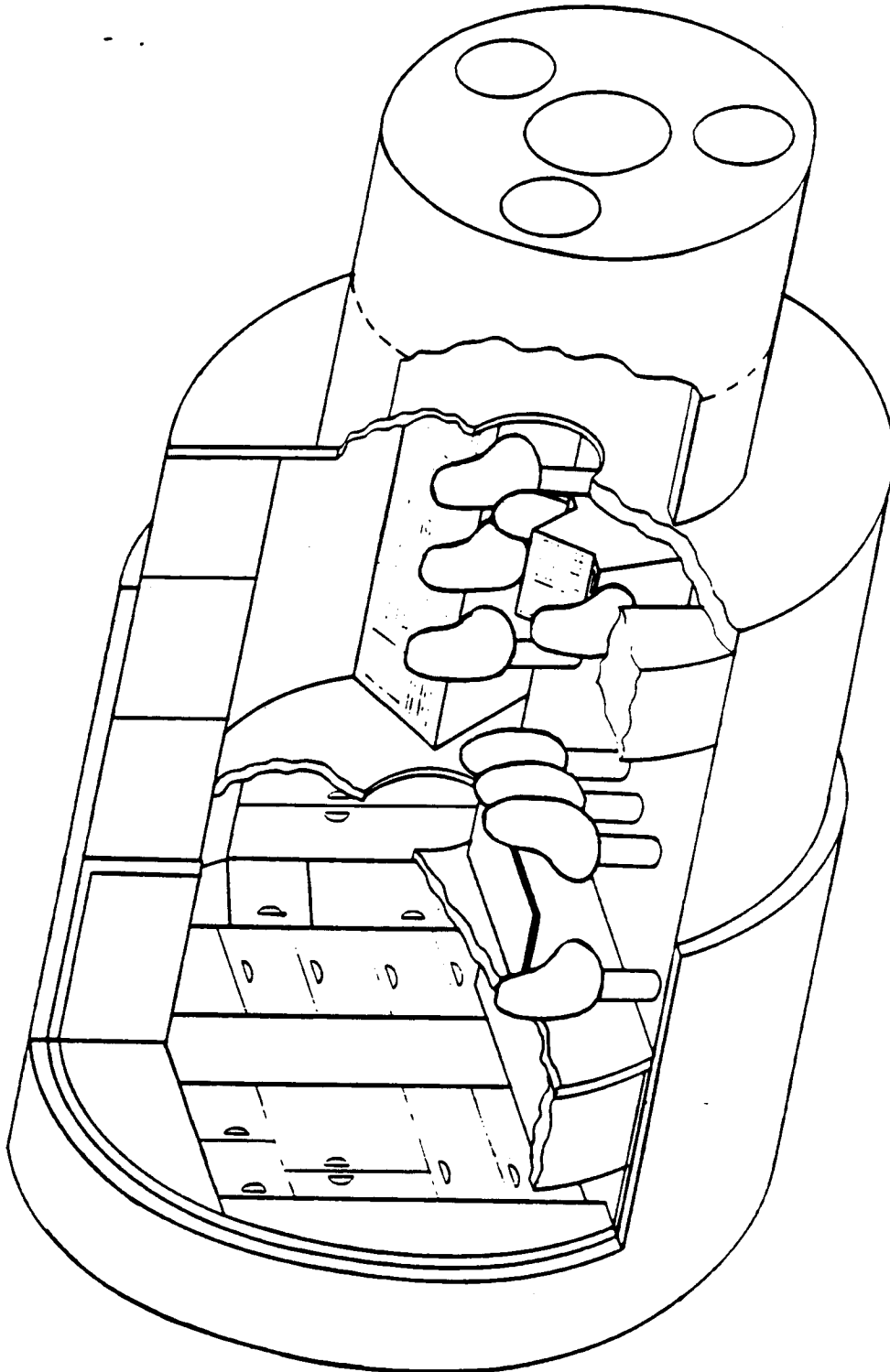
Figure 6.3.2

Crew Module Floor Plan
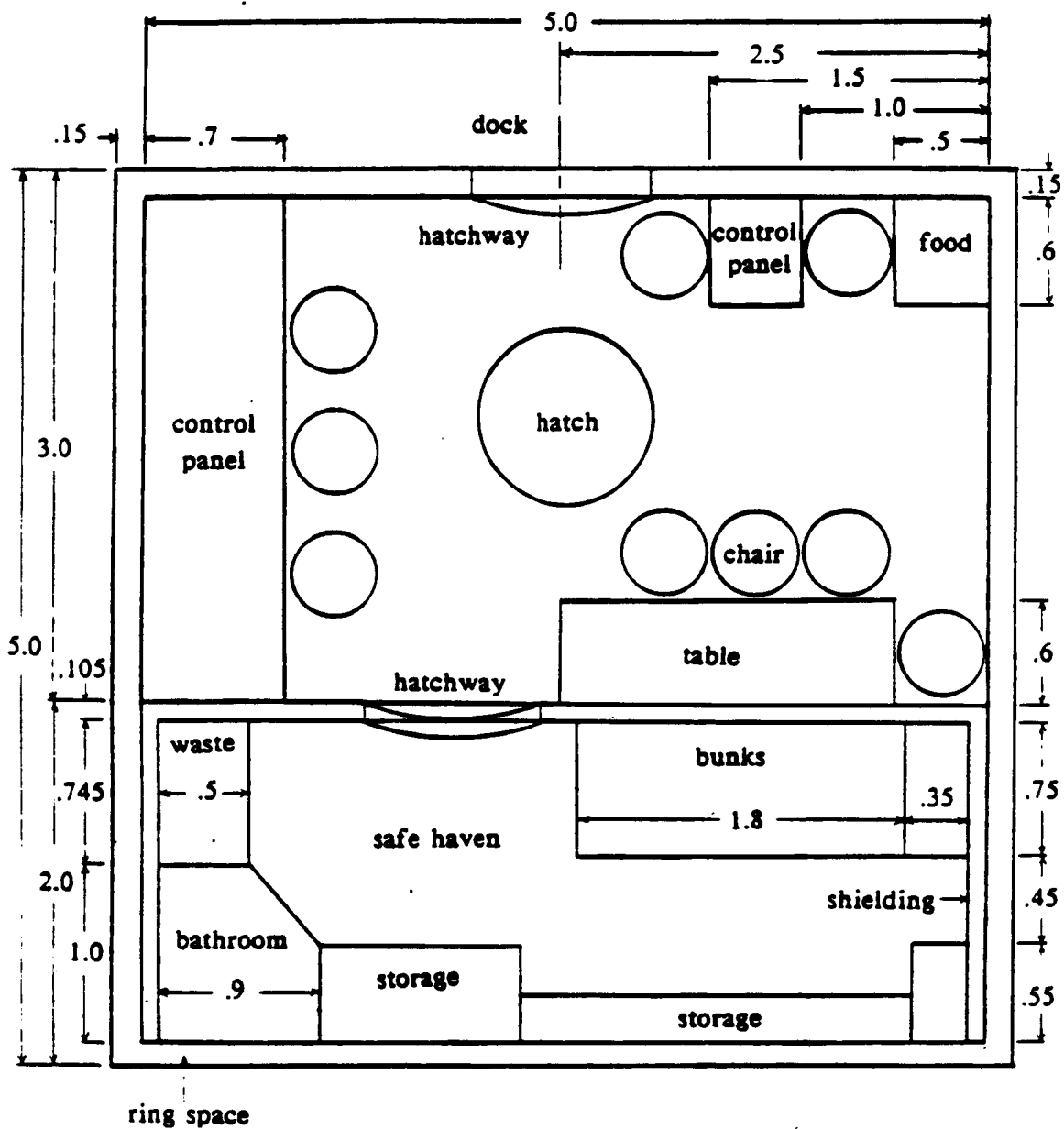
Figure 6.3.3

all units in meters
scale: 1 inch = 1 m

ring space

System CG Location Top View
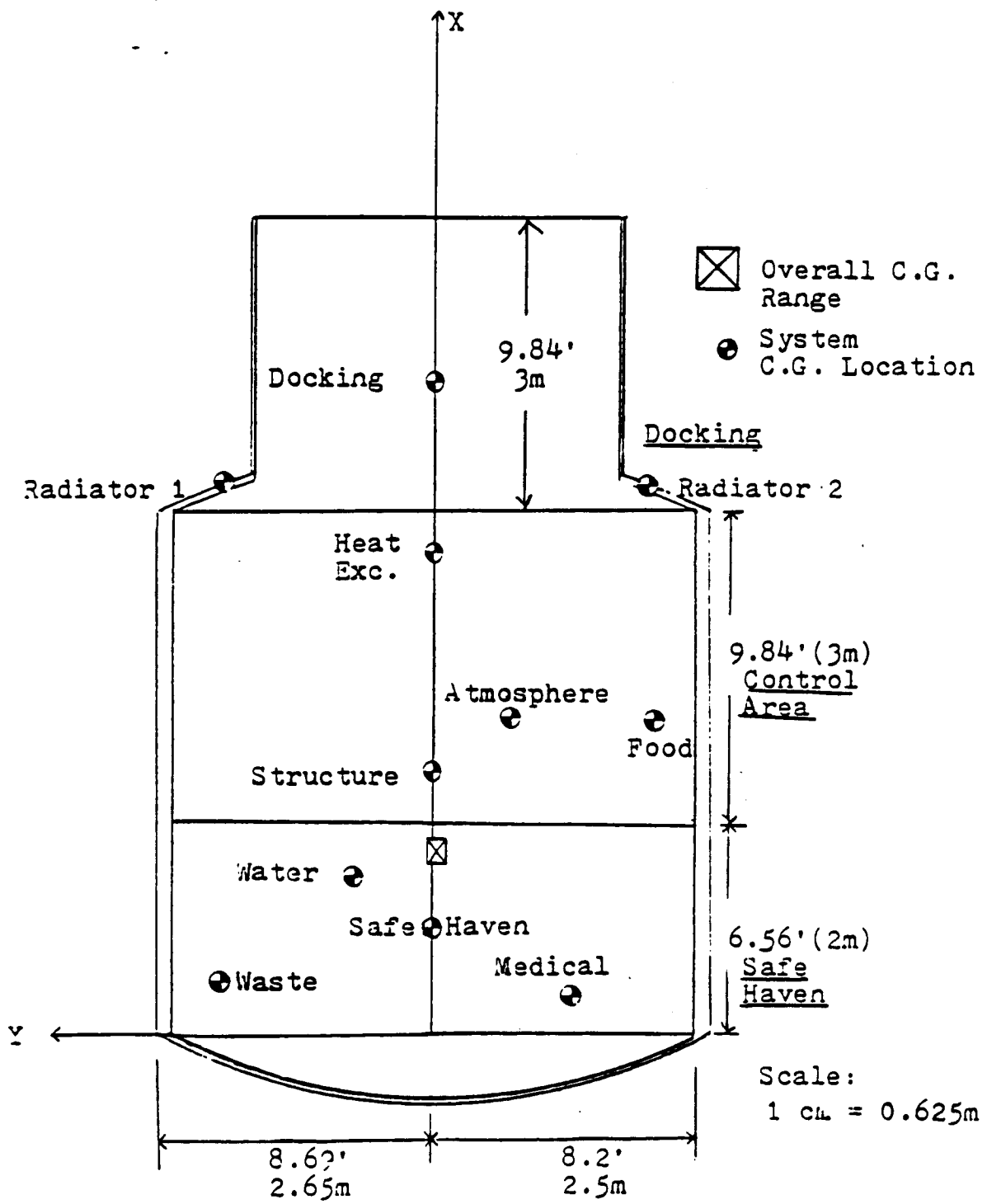
Figure 6.3.4

System CG Location Side View

Overall C.G. Range

System C.G. Location

Docking

Radiators

Floor · Heat Exc.

Atmosphere

Food

Structure

Water

Safe Haven

Waste

Medical

Scale:
1 cm = 0.5m
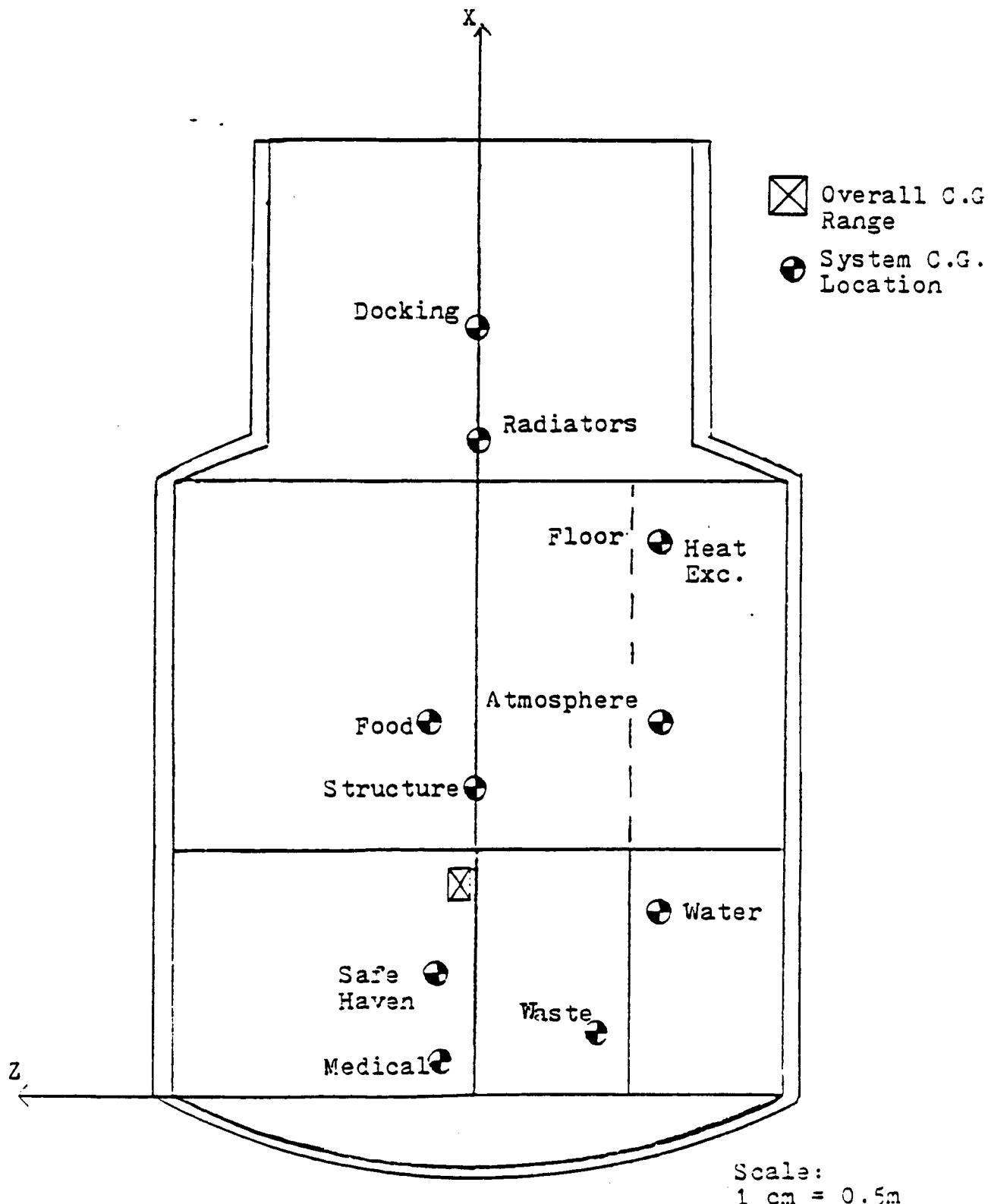
Figure 6.3.5

Table 6.3.1 CREW MODULE SYSTEM PLACEMENT

SYSTEM	MASS (kg)	VOLUME (m^3)	CG LOCATION (m)
Haven Shield	4870.		(1.0,0,.3)
Rings	560.		(2.5,0,0)
Stringers	650.		(2.5,0,0)
Skin	495.		(2.5,0,0)
Bumper	355.		(2.5,0,0)
Docking	180.	15.9	(6.25,0,0)
Air	200.		(3.0,-.75,-1.7)
Water	100.	0.1	(1.5,.75,-1.7)
Food	250.	0.15	(3.0,-2.1,.4)
Waste	80.	0.3	(.5,2.0,-1.0)
Medical	30.	1.07	(.3,-2.35,.3)
Radiators	40.		(5.2,2.0,0) *
Heat Exchanger	40.		(4.6,0,-1.7)
People	825 max		x: 1 to 3.5
	(225 min)		y: -1 to 1
			z: -.5 to 1.5

Total 8675 (19,120 lbm)

*radiators attached to outside of hull

From these the CG coordinates and the mass moment of inertia were calculated. The CG range was found to be:

```
X:        1.6 to 1.85 m (5.25 to 6.1 ft)
Y:        -0.16 to 0.02 m (-0.5 to 0.07 ft)
Z:        0.06 to 0.25 m (0.2 to 0.8 ft)
```

The mass moments of inertia for the crew module were estimated from the following information (using point mass approximations when the system shapes were unknown).

Mass Moments of Inertia Of The Crew Module

Axial Distance (m) Moment of Inertia (kg m^2)

System	Mass, kg	X	Y	Z	Ixx	Iyy	Izz
Water	100.	1.86	2.27	1.68	346.	515.	282.
Waste	80.	2.24	1.12	2.06	401.	100.	339.
Food	250.	2.14	2.03	3.66	1145.	1030.	3349.
Air	200.	1.86	3.45	3.09	692.	2381.	1910.
Radiators	20.	2.00	5.10	5.48	80.	520.	601.
Fuel Cell	200.	3.00	0.50	3.04	1800.	50.	1848.
Heat Exc.	40.	1.70	4.90	4.60	116.	960.	846.
Medical	30.	2.37	0.42	2.37	169.	5.	169.
Haven shield	4870.				12134.	14599.	15547.
Al Skin	495.				5301.	6273.	6273.
Bumper	355.				4165.	4652.	4652.
Docking	180.				356.	695.	695.
Rings	560.				2607.	6431.	6431.
Stringers	650.				2937.	6691.	6691.
Total	8030				29312	44902	49633

6.3.2 Hull Structure

The module hull consists of two separate layers of aluminum: a pressure shell (skin module) and a meteoroid bumper. The layers of aluminum are stiffened by stringers, between the layers, and rings, inside the pressure shell. There are 16 stringers and 6 rings (Fig. 6.3.6).

The single skin thickness required to meet the criteria of a 90% probability of no meteoroid penetration for ten years would be greater than one inch. For this reason, an aluminum bumper is used for the meteoroid protection system. The purpose of the bumper is to slow down the meteroid and break it into smaller pieces, greatly reducing the speed and force with which it strikes the inner hull.

The bumper thickness required to meet the design requirement is 0.037 in (0.1 cm) with a void space of 4 in (10.2 cm). The required module skin thickness to withstand the impact is 0.057 in (0.15 cm). The module skin thickness required to withstand the internal pressure is 0.031 in (0.08 cm) using thin wall pressure vessel analysis. Therefore, the minimum module skin thickness is determined by the meteroid protection criterion. The module uses a meteroid shield thickness of 0.04 in (.1 cm) and a module skin thickness of 0.06 in (.15 cm) with a spacing of 6 in (15 cm). The masses of the bumper and skin are 772.42 lb (351.1 kg) and 1088.56 lb (494.8 kg).

In determining the minimum skin thickness, the hoop stress was found to be the limiting stress. For our module, the internal pressure is 14.7 psia (101.4 kPa), and the interior radius is 8.2 ft (2.5 m). The minimum thickness was found to be .031 in (0.08 cm) using a 1.5 factor of safety. Shear considerations alone give a skin thickness of .026 in (.07 cm.) using an allowable shear of $28\ kpsi(193.1\ MPa.)$ for aluminum. It is clear that the thickness is not limited by stress requirements, but rather meteroid protection criteria, as stated above.

The maximum loads on the crew module occur during 6 g acceleration. The axial force on the module will be greatest when the engines are thrusting straight back. This force is $138\ klbf(614\ kN)$. The axial deflection is found to be .0217 in (.000552 m) using the total cross-sectional area of stringers, 70.7 in^2 (.0456 m^2), (the area of the skin is neglected). Once this maximum axial deflection has been calculated, it is checked to determine if it is acceptable given the material properties of the stringers. For graphite polymide composite, the ultimate stress is 196.4 $kpsi$ $(1.354\ GPa)$. Simple stress analysis gives a i aximum deflection of 1.46 in. (0.037 m) which is much less than the maximum allowable axial deflection.

Crew Module Structural Design
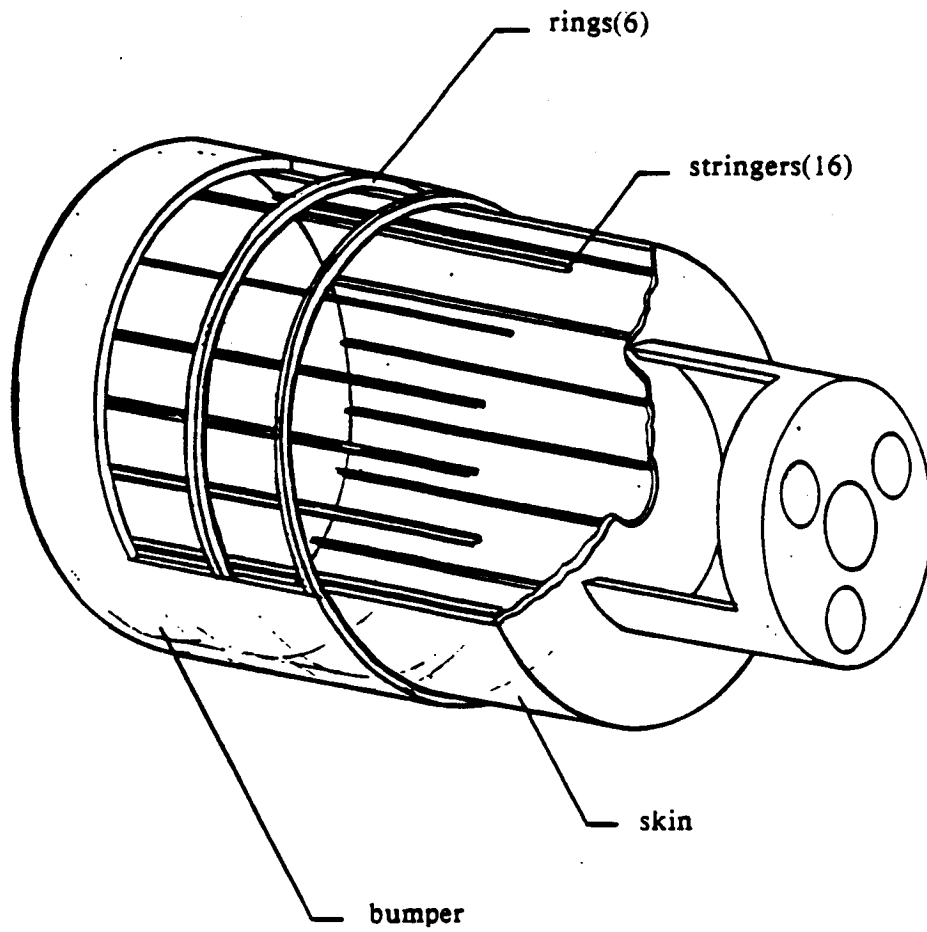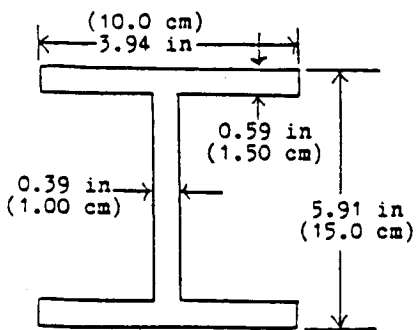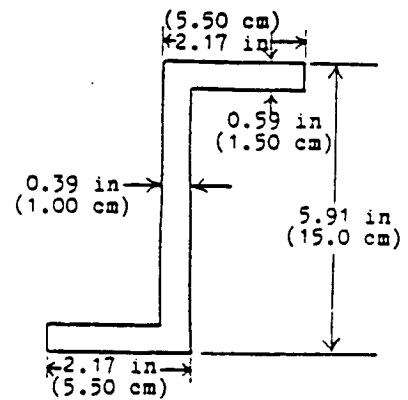
Figure 6.3.6

To analyze shear and bending moment, the maximum side force is first determined. The side force is greatest when the engines are thrusting at the maximum angle of 15 degrees Figs. 6.3.7a and b. This force is 35.7 kips (159 kN) and acts through the center of gravity roughly 5.74 ft (1.75 m) from the secured end of the module. This gives a maximum bending moment of 205.2 lb-ft (278.25 kN-m). To analyze the stress, the bending moment equation is used with a maximum y of 8.7 ft (2.65 m). The mass moment of inertia is found using a lumped mass skin stringer approximation as shown in Fig. 6.3.7c. This yields a maximum bending stress of 594.6 psi (4.1 MPa) which is much less than the material's ultimate strength of 10.9 kpsi (75 MPa).

6.4 Docking / Airlock System

This mission requires a docking apparatus to connect the TAXI with the Cycling Ship and the orbiting Space Stations. The docking process will be a "hard" docking procedure with misalignment capability, since exact alignment cannot be maintained. The following criteria were used in the docking design:

1. axial velocity of .1 to .5 ft/s (.003 to .152 m/s)

2. radial velocity of 0 to .2 ft/s (0 to .061 m/s)

3. angular velocity of 0 to 1 deg/s

4. angular misalignment of (+/-) 5 degreees pitch and yaw and (+/-) 2 degrees roll

5. radial misalignment (+/-) 2 inches (5.08 cm)

The apparatus chosen is comprised of three elongated probe members and three drogue (receptacle) assemblies (Chandler,1982). The probe members, the passive mechanisms in the docking process, are mounted on the Cycling Ship and Space Stations. The drogue assemblies, the active mechanisms of the docking system, are mounted on the TAXI (see Figs. 6.3.1 & 6.4.1). The drogue assemblies capture the probe members upon being maneuvered into close proximity with each other. The drogue assembly, shown in Figure 6.4.1, carries a cone subassembly having inwardly tapered conical surfaces for receiving the probe member, shown in Figure 6.4.2. Three latch members, located symmetrically around the cone subassembly extend and retract to lock the probe members in place. An operator assembly controls the latches.

The docking process begins with the remote or manual movement of the TAXI so that the probe and drogue assemblies are roughly aligned. Docking is completed using television cameras, radar, and attitude thrusters. Upon initial contact, the tapered drogue sides guide the probe to the axial center of the drogue assembly. To rigidly fix the probe member in position, the operator assembly is engaged. The TAXI docking system will use three drogue assemblies, each with a mass of approximately 50 lb (22.73 kg). The orientation to the crew module is shown in Figure 6.3.1. In docking, the majority of the initial shock of engagememt will be absorbed by spring loaded plungers and spirally wound springs which allow the cone subassembly to "float". This absorption significantly reduces the forces which must be taken by the crew module structure. For a more detailed discussion of the operator assembly, the dock and docking process, see reference 1.

A)

15° max. engine deflection angle

B)

$F = 6*m*g*\sin 15°$

x_{CG}

X

C)

$\bar{y} = 2.65*\sin \alpha$
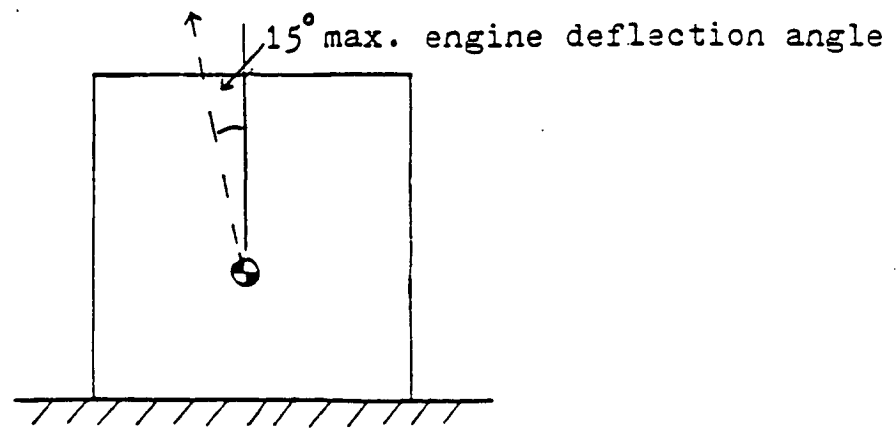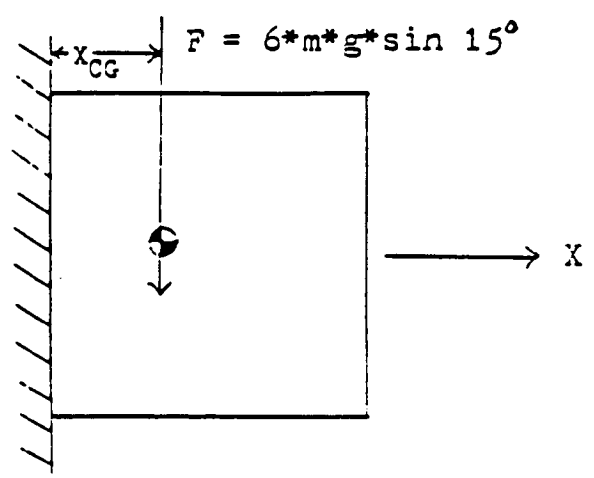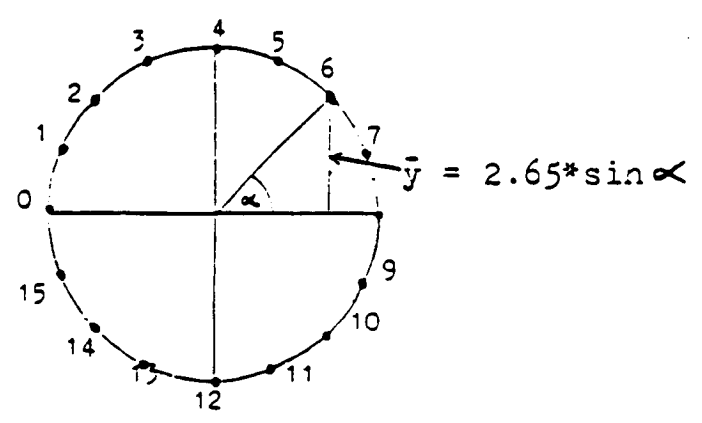
Figure 6.3.7

Drogue Assembly

tapered conical surface

latch member
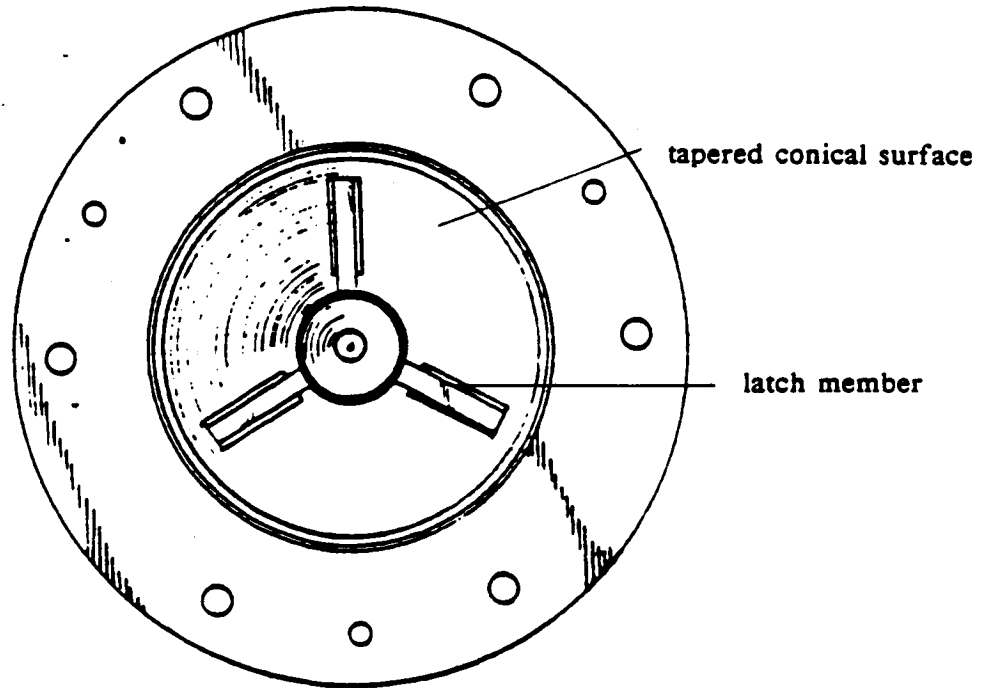
Figure 6.4.1

Probe/Drogue Link

probe

inwardly tapered conical surface

biasing spring

plunger

cone subassembly

latch member

coiled spring

operator assembly

housing

drogue assembly
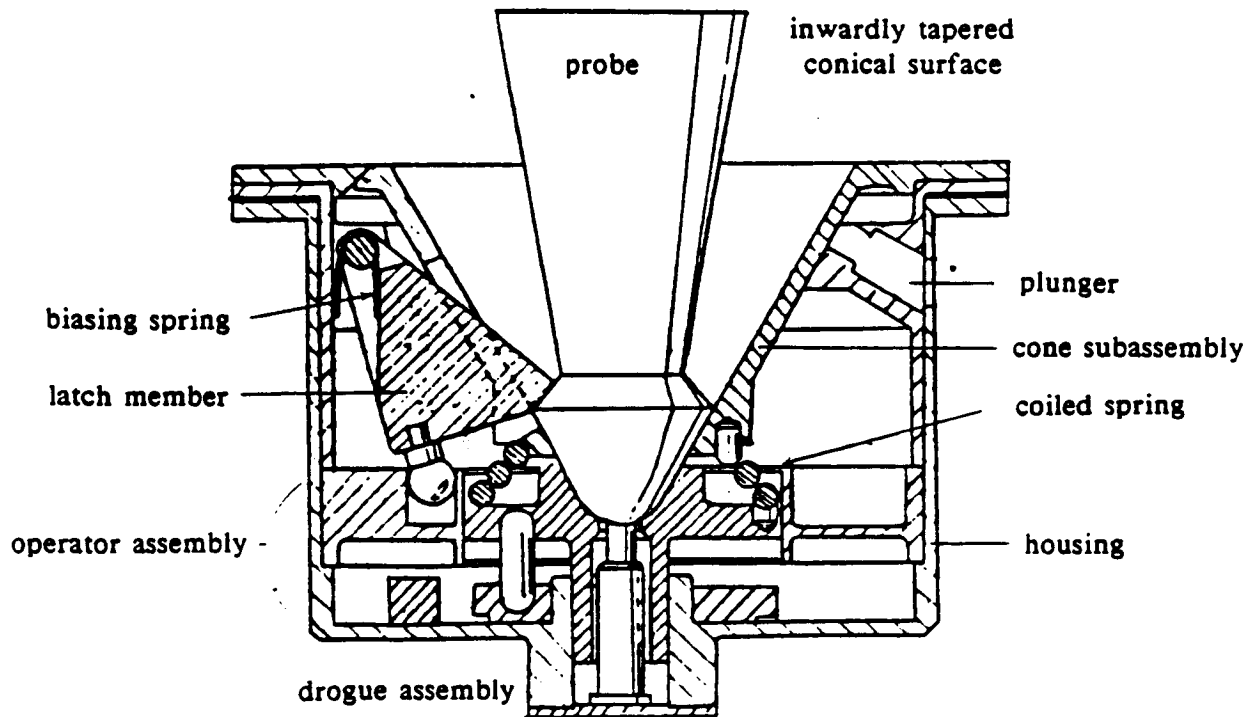
Figure 6.4.2

Attached to the crew module is a cylindrical airlock of diameter 9.84 ft (3.0 m) and a length of 4.1 ft (1.25 m). The airlock space allows several crew members to be in the airlock at the same time. The airlock is bound at each end by pressurized hatches 3.77 ft (1.15 m) in diameter (shown in Figure 6.4.3). The pressurized hatch has an outwardly concave surface of radius 3.28 ft (1.0 m) and a radius of curvature of 3.28 ft (1.0 m). This pressure vessel requirement gives an aluminum thickness of .0124 in (.0316 cm). Additional meteroid protection for the outer dock is provided by a bumper .04 (.1016 cm) thick. Four ribs line the inside of the spherical section for additional support during the locking process. Each hatch has an approximate mass of 75.0 lb (34.1 kg). Each hatch is circled by a 2.95 in (7.5 cm) flange portion which, in the closed position, contacts the hull section. The contacting surface of the hatch is fitted with a circular rubber washer which essentially seals the hatch under minimal contact force. The hatch locking assembly is shown in cross section in Figure 6.4.4.

Reference

1. J.A.Chandler, NASA Report # N82-28318, "Apparatus For Releasably Connecting First And Second Objects In Predetermined Space Relationship", April 14, 1982.

6.5 Module Support Structure

The module supports consist of two perpendicular contoured support beams (Figures 6.5.1 and 6.5.2). The beams are made up of graphite-graphite polyimide 103.4 lbm/ft^3 (1660 kg/m^3) in a 0/+45 layup. These beams have an ultimate tensile strength of 13.24x10^6 psf (634 MPa) and compressive strength of 12.82x10^6 psf (614 MPa). A simplified analysis of beam deflection was made using simple pinned-pinned beam theory. A conservative estimate of the moment of inertia was made by assuming that the beam is an I-beam of constant height. Each beam caried 1/2 the maximum axial load of 44606 kips (618 kN), uniformly distributed over the 17.4 ft (5.3 m) in contact with the crew module. The table below shows some of the variable I-beam parameters tried in an attempt to minimize weight. Thickness, t, was found to have the greatest affect on the support weight since the side supports do not contribute to axial stiffness. Various choices of t were examined but it was decided to use a mimimum thickness of 2.36 in (6.0 cm). This thickness was the smallest thickness that would give full contact with the 2.16 in (5.5 cm) thick stringer and still allow for some small misalignment in module assembly.

Module Support Reactions to Axial Load

Case	Web(m)	h1(m)	h2(m)	Area (m^2)	I (m^3)	Vol (m^3)
1	.03	.10	.30	.021	.000558	.173
2	.03	.10	.25	.0195	.000416	.1645
3	.03	.125	.20	.021	.000436	.172
4	.04	.10	.25	.022	.000430	.177

	Max. Deflection y (cm)	Buckling Stress (MPa)	Max. Bending Stress (MPa)
1	1.25	762	260
2	1.68	606	314
3	1.60	590	299
4	1.62	555	303

Case 2 was selected because its maximum stress, 6.56×10^6 psf (314 MPa), was well below both the critical buckling stress of 12.66×10^6 psf (606 MPa) and the material ultimate strength of 8.54×10^6 psf (409 MPa) with a 1.5 factor of safety, while still being light weight. The mass of both beams was found to be 1200 lb (545 kg).

6..6 Propellant Tank and Engine Support Structures (TAXI A)

The basic support structures for all propellant tanks and engines will be made of graphite polymide which allows for the greatest strength to weight ratio. Each support forms a cagelike structure consisting of tubular truss members; such members are easy to construct and can be tightly packed in shipping (if necessary). The support structures are connected to the aerobrake truss. The oxygen tank is set 9.6 ft deep into the shield. The hydrogen tank is placed 3.9 ft into the shield. Sketches of simple support structures and the results of some initial calculations are given in Appendix 11.6.1. Conservative estimates of support structures weights are given below.

	Mass, lbm	(kg)
LOX tank support structure	280	(127)
LH2 tank support structure	310	(140.6)
Total structural mass of tank supports	1800	(816.3)
Engine support structure	200	(90.7)

Hatch

all units in feet

Figure 6.4.3

Hatch

restraining arms

hinge

.16

gears

.3

.14

1.0

3.28

3.77
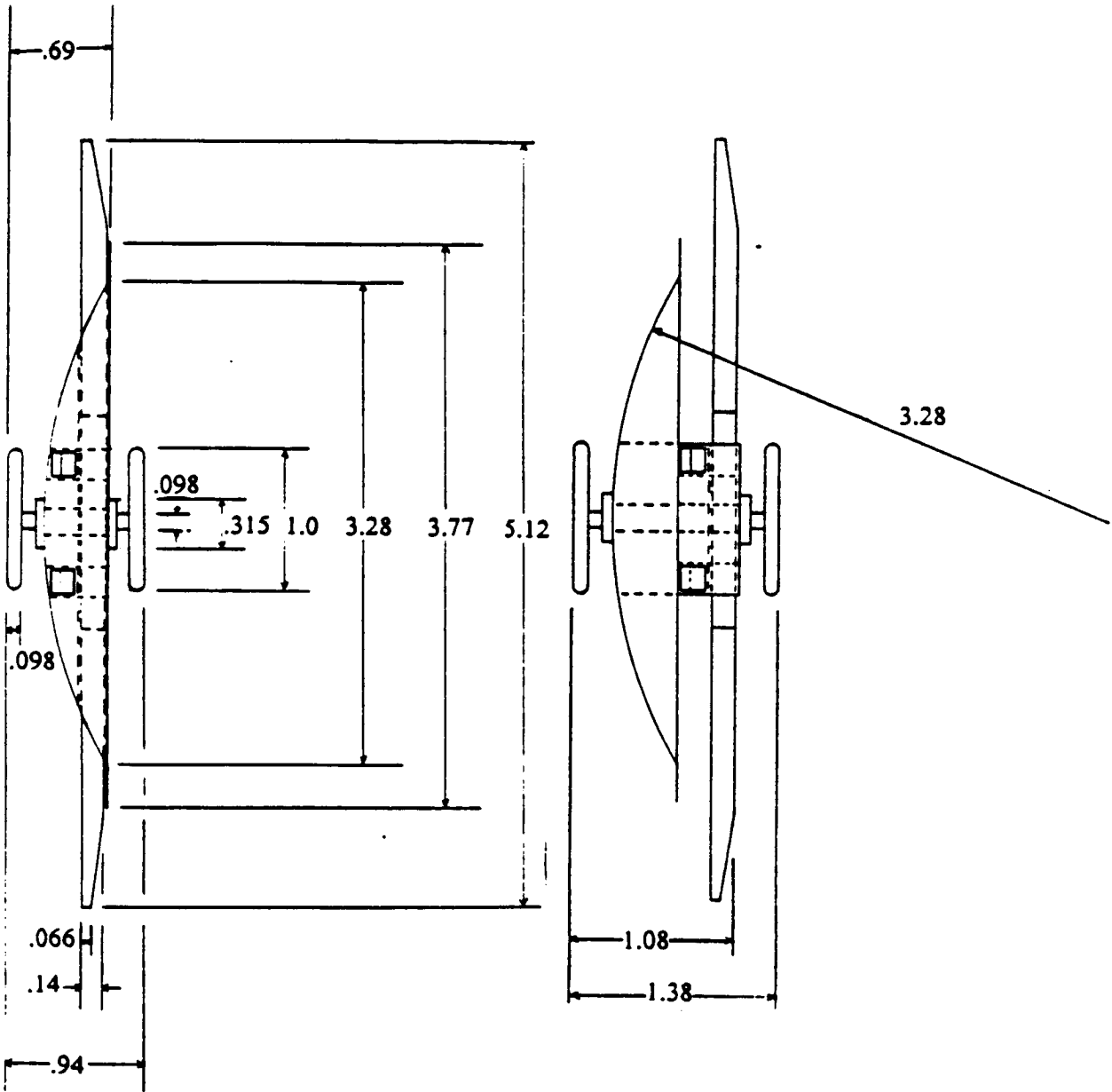
all units in feet
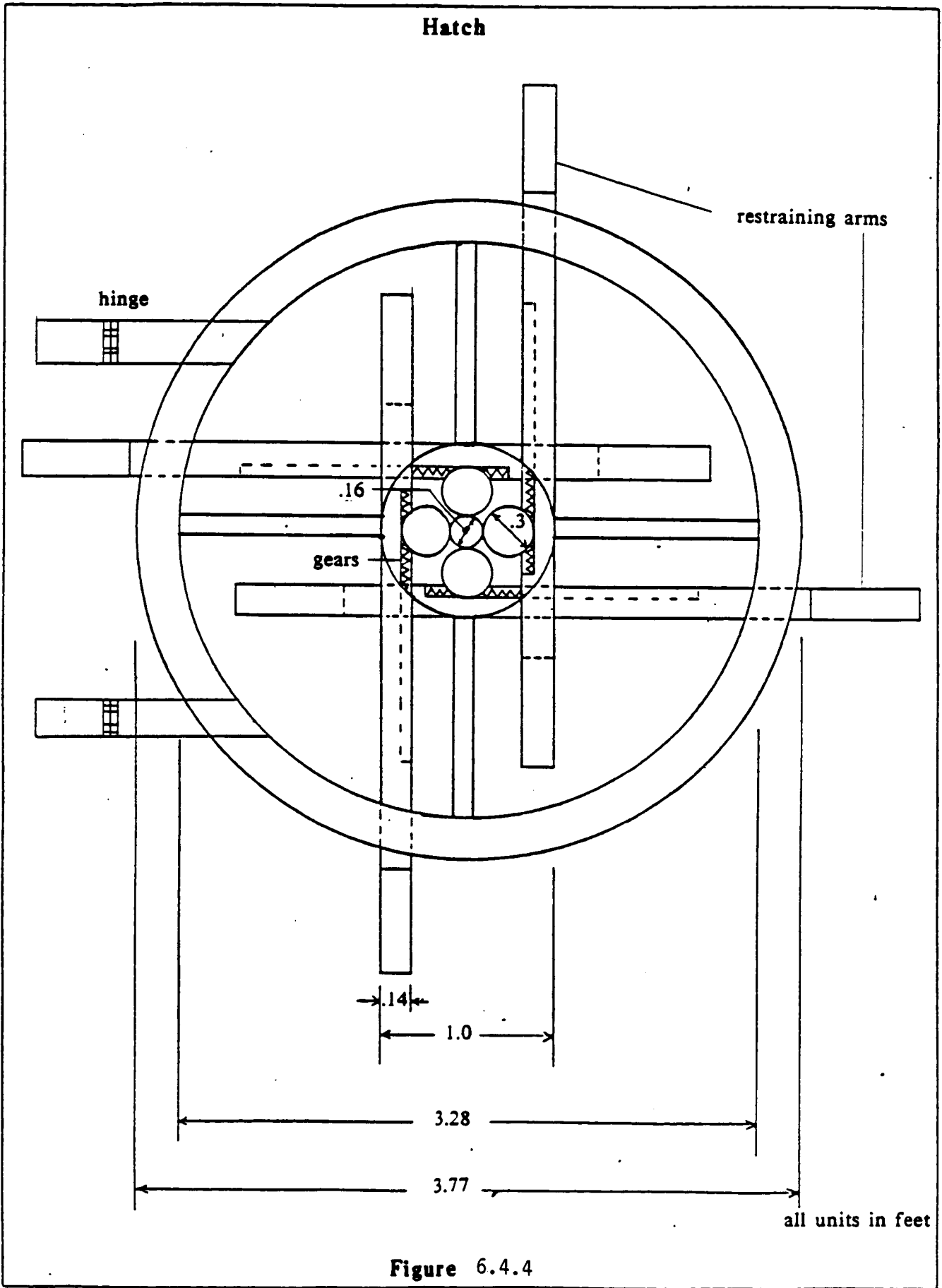
Figure 6.4.4

Partial
Module
Structure
Cross
Section

Stringers

Rings

Bumper
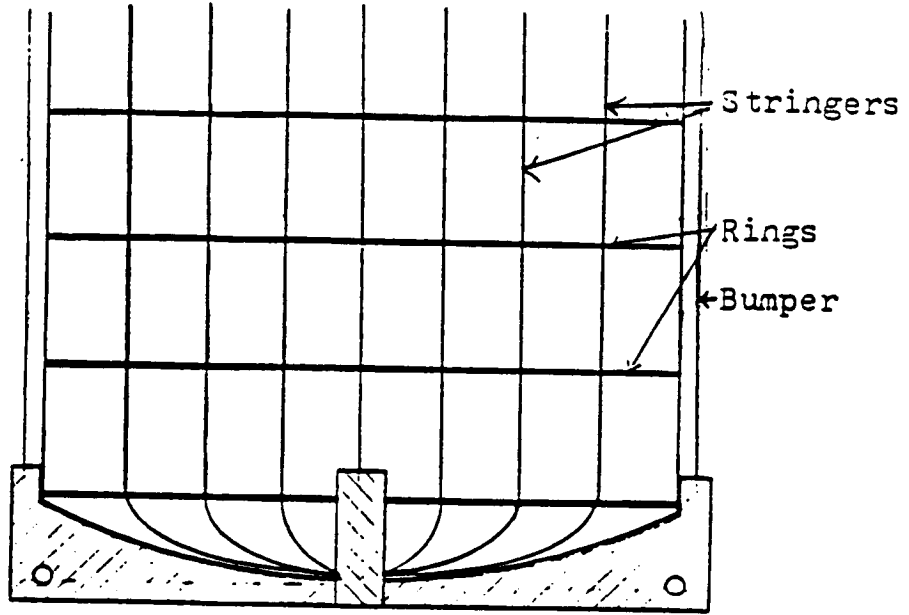
Basic Module Support Design
(not to scale)

.328'

1.97'

h

t

Shield Truss
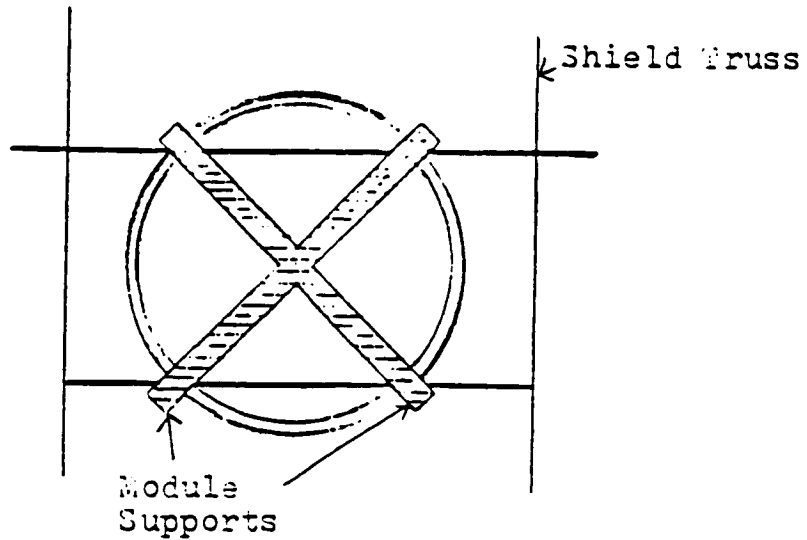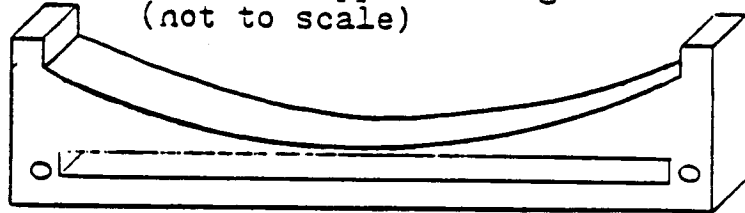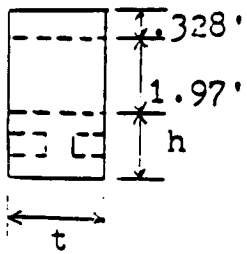
Module
Supports

Figure 6.5.1

Cutaway Showing Stringers and Module Supports

12'(3.66m)

Shield Truss

Support

9.01' (2.65m)

24' (7.32m)

Stringers

Rings

Bumper
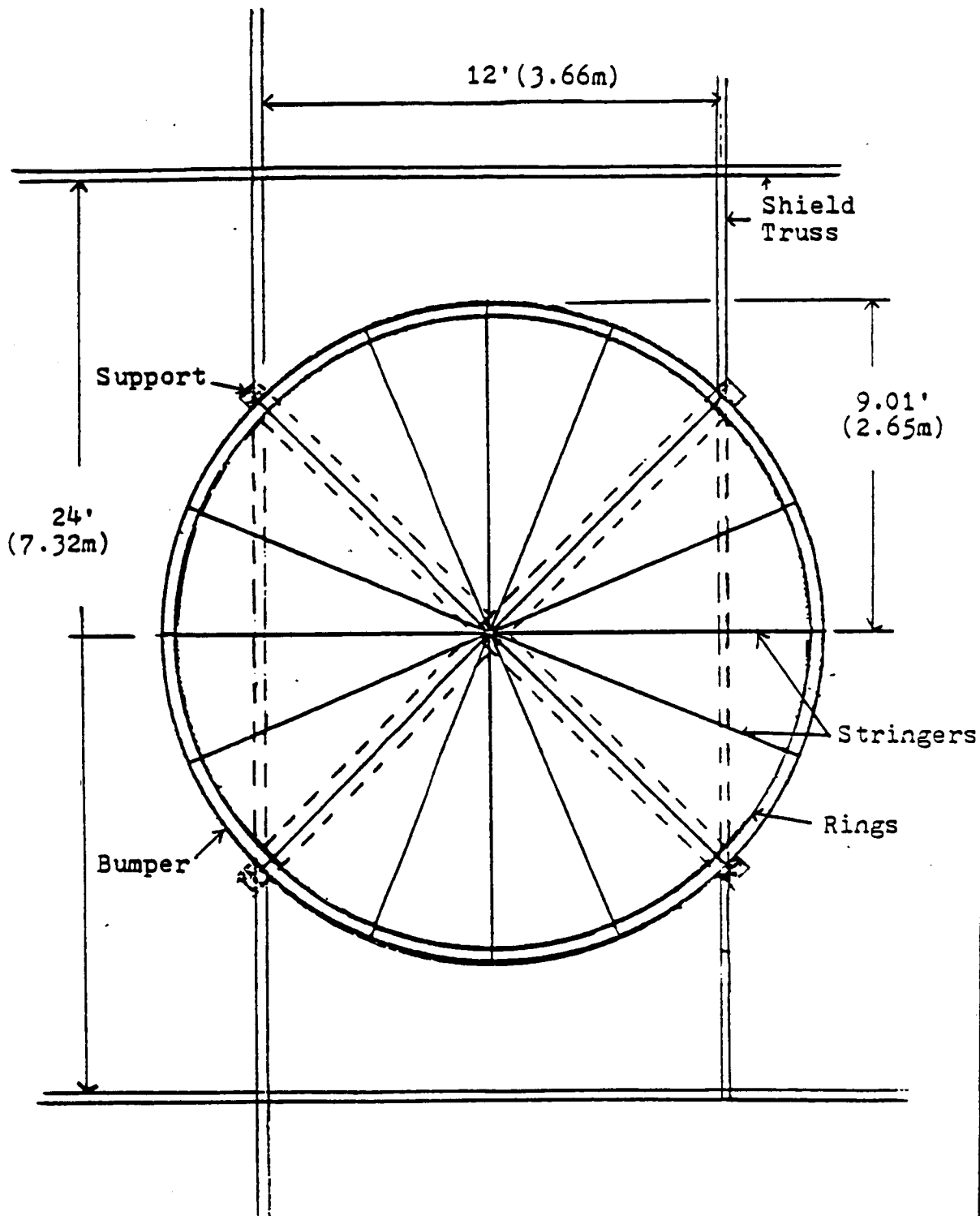
Figure 6.5.2

7. GNC and Communications Systems

7.1 Guidance, Navigation and Control

7.1.1 Guidance Concepts

The functions that are important for the guidance and control of the TAXI vehicle are: (1) acquiring long-term celestial references, (2) maintaining the spacecraft attitude throughout cruise periods, (3) reorienting the vehicle to perform various maneuvers (midcourse corrections and orbital insertion), and (4) maintaining control of the spacecraft during periods of occultation of the celestial references. In addition, midcourse correction and insertion maneuvers require attitude stabilization and thrust impulse control.

The guidance system finds the required thrust direction at any point in the flight needed to direct the ship's path towards a certain set of prescribed terminal conditions (i.e., rendezvous with the cycling ship or establishing an orbit). Varying end conditions for moving targets requires flexibility of the guidance system.

Since safety is of the utmost importance, an essential feature of the guidance system is redundancy. A fundamental requirement of the system is that no single electronic or electrical failure could cause a mission failure. This requires backup or redundancy for all critical guidance functions. Furthermore, this demands that failure detection and backup implementation be independent of Earth communications in either of two cases: (1) during critical phases of the mission, such as shortly prior to or during insertion maneuvers and (2) where the nature of the failure could have a serious or irreparable effect if not corrected before the time required for round trip Earth communications, such as a failure of an attitude jet in the "on" position. Techniques which avoid the use of complex means of failure detection, dissimilar means of backup, and do not require switching to accomplish backup have significant advantages in terms of simplicity, confidence, and protection against systematic failure.

Since safety is such an important feature of the guidance and control system, several methods of redundancy implementation were considered. Fig. 7.1.1 shows some of the basic methods of redundancy implementation for GNC components and the some of the pros and cons associated with the utilization of each.

For this mission, docking and rendezvous capabilities are also important aspects of the guidance system. These capabilities include: (1) GNC functions in two phases (relative to Earth in the initial phases and relative to another spacecraft in the terminal phases), (2) the joining, which involves either docking or berthing operations, and (3) monitoring and failure detection, which will require human control to actively monitor all flight operations.

Fig. 7.1.2 summarizes some of the major functions of the guidance system, the active periods of these functions, and system elements needed.

The Sun-Canopus celestial reference system is chosen for several reasons. The Sun is chosen as one of the major references because of its ease of identification and tracking. The second celestial reference is used for roll reference. The selection of Canopus is based on three factors: (1) the Sun is used as a primary reference, (2) most of the trajectories of the spacecraft lie near the ecliptic plane, and (3) for best attitude control, the roll reference object angle is near ninety degrees. Under these conditions, the roll reference star would have to lie near the ecliptic North or South Pole. A search for an easily distinguishable star in these regions yields the bright star Canopus as the obvious selection.

166

Mechanization Approach	Pro	Con
Two parallel systems	Simple, fewer parts	No control authority if one system fails - requires failure detection
Three redundant systems	High reliability - no degradation from single failure and protection against many second failures	Complex, many parts, high weight and power
Four parallel half systems	Failure detection avoids need for switching. Simple - relatively few parts	Reliability slightly lower than three redundant systems
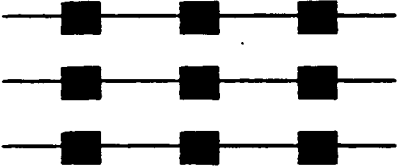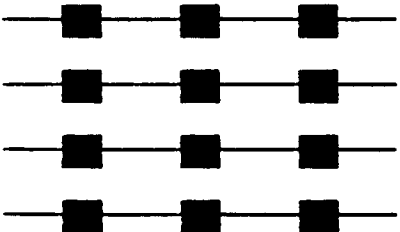
FIGURE 7.1.1

Function	Active period	System element
Celestial attitude reference	Cruise	Sun sensor and Canopus sensor
Inertial attitude reference	Acquisition, Maneuver, and Occulation	Gyros
Attitude control	Non-thrusting Midcourse Orbit insertion Aerobraking	Gas jets
Velocity measurement	Cruise Thrusting	Earth-tracking Accelerometer and timer
Integrating elements	Continuous	Onboard computer

FIGURE 7.1.2

7.1.2 Navigation and Instrumentation

The reference system chosen for the TAXI vehicle requires accurate sensors for both the Sun and Canopus. For each axis of the ship, the sun sensors consist of a pair of silicon photovoltaic or cadmium sulfide photoconductive cells which are connected in a bridge configuration. The physical arrangement of the cells in the instrument is such that a pointing error in one plane produces a difference in the amount of sunlight falling on the cells in that plane. This arrangement then produces a net output from the sensor which indicates an error in the orientation of the ship. The configuration of a typical sun sensor on the TAXI vehicle is shown in Figure 7.1.3.

Unequal solar cell aging, which creates an offset bias in the detector bridge, is a major problem in sun sensors. The application of radiation shields on the cells and the usage of light baffles are used to reduce aging. The problem of unequal aging is substantially reduced by choosing cells from a preirradiated lot, since continued degradation will follow the same exponential curve.

Roll attitude is maintained by using gimbaled star trackers to track the location of Canopus. Gimbaled star trackers are used since the vehicle must operate at various attitudes. This type of tracker has a very small field of view (FOV). The gimbal mounts serve to give the sensor a much larger effective FOV. The electronics assembly causes the gimbals to move so that the star image remains centered in the small FOV. The star's position is then given by the gimbal angle readout positions. The location of Canopus makes it especially useful for determining the rotation about the sunline. A serious disadvantage of unique star trackers is that they occasionally track either the wrong star or particles that scatter stray light, such as paint chips from the vehicle. The configuration of a gimbaled star tracker is shown in Figure 7.1.4.

During periods of occultation of the celestial references, the TAXI vehicle's attitude will be maintained with an inertial reference system. Orientation measurements are made by gyroscopes in this inertial system. Two types of gyros are used on the spacecraft (1) rate gyros (RGs) and (2) rate-integrating gyros (RIGs). Rate gyros measure spacecraft angular rates and are part of a feedback system for either spin rate control or attitude stabilization. Rate-integrating gyros measure the vehicle's angular displacements directly. The inertial navigation system requires three single-degree-of-freedom gyros in order to establish inertial coordinates in three dimensions. The quality of this inertial reference depends on the precision of the gyro instruments.

The output of a rate gyro is obtained by measuring the rotation of the gimbal about the output axis. The movement of the rate gyro's gimbal is inhibited by viscous damping and a spring restraint, where the spring constant is chosen so that it is large compared with damping effects. Rate gyros are the simplest and the least expensive gyros. Their accuracy is acceptable for spin rate control in the feedback system, but their integrated output requires frequent correction for precise attitude determination using other sensors such as the Sun sensors or the star trackers.

The rate-integrating gyro is the type used for vehicle attitude sensing because of its high accuracy and low drift. The gimbal is mounted so that its motion is essentially frictionless and without spring restraint. Since both the viscous damping and spring constants are small, the steady state solution indicates that a rate-integrating gyro's output (i.e., the rotation of the gimbal about the gyro's output axis) is proportional to the spacecraft's angular displacement about its input axis.

SUN SENSOR

Displacement
Angle

Sunlight

Detector 1   Detector 2

FIGURE 7.1.3

GIMBALED STAR TRACKER

Azimuth Axis
(Rotation Axis)

Elevation Axis

FIGURE 7.1.4
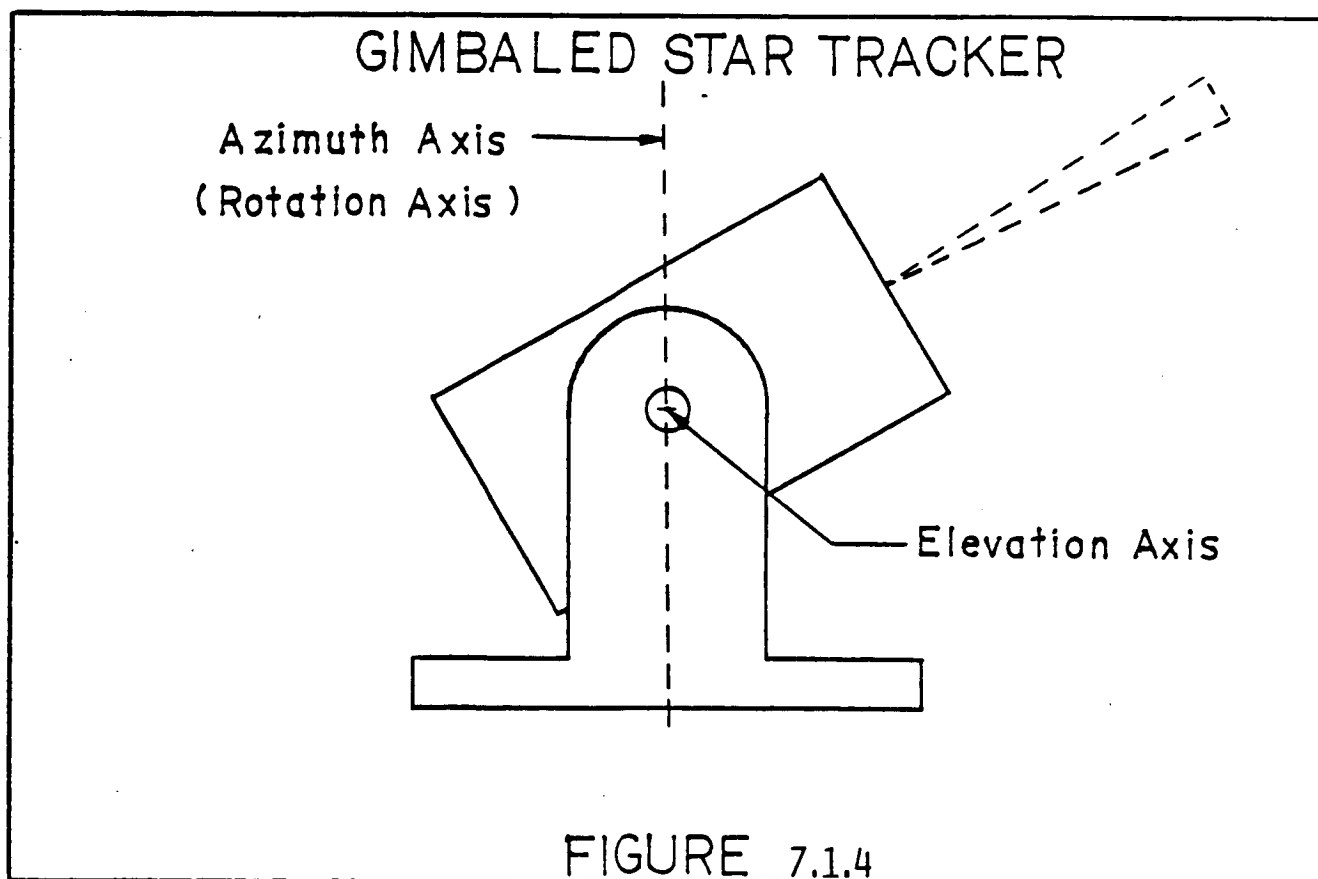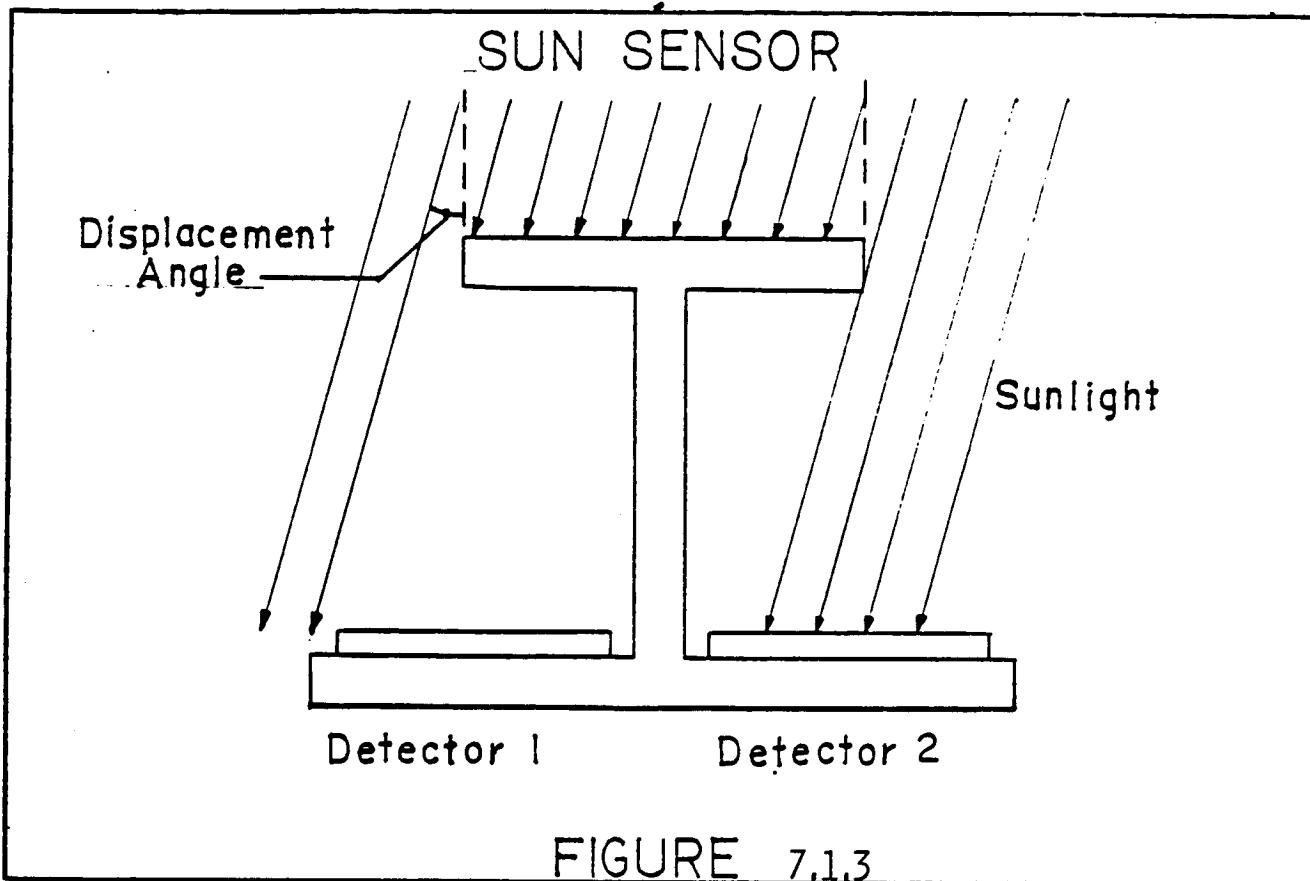
7.1.3 Vehicle Attitude Control Systems

A system of gas jets is used for attitude control of the TAXI vehicle. In orbits that are distant from the Earth, jets are the only practical means of exchanging momentum with the environment. Gas jets are classified as "hot gas" when the energy is derived from a chemical reaction or "cold gas" when it is derived from the latent heat of a phase change or the work of compression if no phase change is involved. Hot gas jets generally produce a higher thrust level and a greater time integral of the force. Cold gas systems operate more consistently because there is no chemical reaction which must reach steady state. Due to the large moments of inertia and strict performance requirements, high levels of thrust will be required for attitude control, which dictates the use of a hot gas system. Hot gas systems may be either bipropellant or monopropellant. Fuel and oxidizer are stored separately in a bipropellant system, and fairly high levels of thrust can be obtained (greater than those of a monopropellant system). The complexity of using a bipropellant system is justified due to the levels of thrust required.

The system of jets used to control the ship's orientation is referred to as the reaction control system (RCS). The main RCS engines are fueled by hydrazine (N_2H_4) with nitrogen tetroxide (N_2O_4) as the oxidizer. The fuel system for the RCS is independent of the fuel system for the main engines due to the possibility of a failure in the "on" position of one of the RCS engines. Maneuvering thrusters are aligned to lie as nearly as possible in the plane perpendicular to the axis of rotation so as to generate torques only about the axis of rotation.

RCS engines that produce 1000 lbs (4,540 newtons) of thrust each are used for rotations involved in major maneuvers. Smaller vernier engines that produce 25 lbs (110 newtons) of thrust each are used for precise adjustments and corrections. Fig. 7.1.5 shows a diagram of a typical RCS engine. These thrust levels were determined to meet the performance rates required and to distribute the loading on the truss structure. Appendix 11.7.1 gives calculation specifics and the locations and orientations of the RCS engines.

The four parallel half-system approach, which is a cooperative multichannel technique, is the simplest. It avoids the need for both failure detection and switching. Of the five critical G&C elements, protection against failure in three of the elements (Sun sensor, autopilot, and reaction control) can be accomplished with this technique. Only two of the elements (Canopus sensors and gyros) require block redundancy for implementation. Fig. 7.1.6 is a diagram of the four parallel half systems concept applied to the Sun sensor elements.

In the example shown, the problem is the "open" failure of the No. 1-Positive reaction control jet. The vehicle will begin to accelerate in the positive direction. The resultant error in position with respect to the Sun will be sensed by the two negative elements of the Sun sensor system (i.e., No. 1-Negative and No. 2-Negative). This will cause both of the two negative attitude jets to begin firing. Thus, the two stabilizing jets will have been activated by a mechanism that did not require error detection as such, but rather by a simple continuation of their normal operation function. The two jets have control authority over the malfunctioning jet so that the vehicle will be continuously maintained within the normal attitude range. If the failure continues, the system will continue to operate in this fashion until all the propellant in System No. 1 has been expelled. At this point , two-thirds of the propellant originally in System No. 2 will remain. The propellant supply is designed with a sufficient margin so that this portion will be adequate to complete the entire mission.

R.C.S. ENGINE

Fuel Inlet

Oxidizer Inlet

Combustion
Chamber

FIGURE 7.1.5

REDUNDANCY EXAMPLE

System	Sun Sensor	Autopilot	R C S
No. 1 Positive Negative		+ A/P - A/P	Failure
No. 2 Positive Negative		+ A/P - A/P	

FIGURE 7.1.6
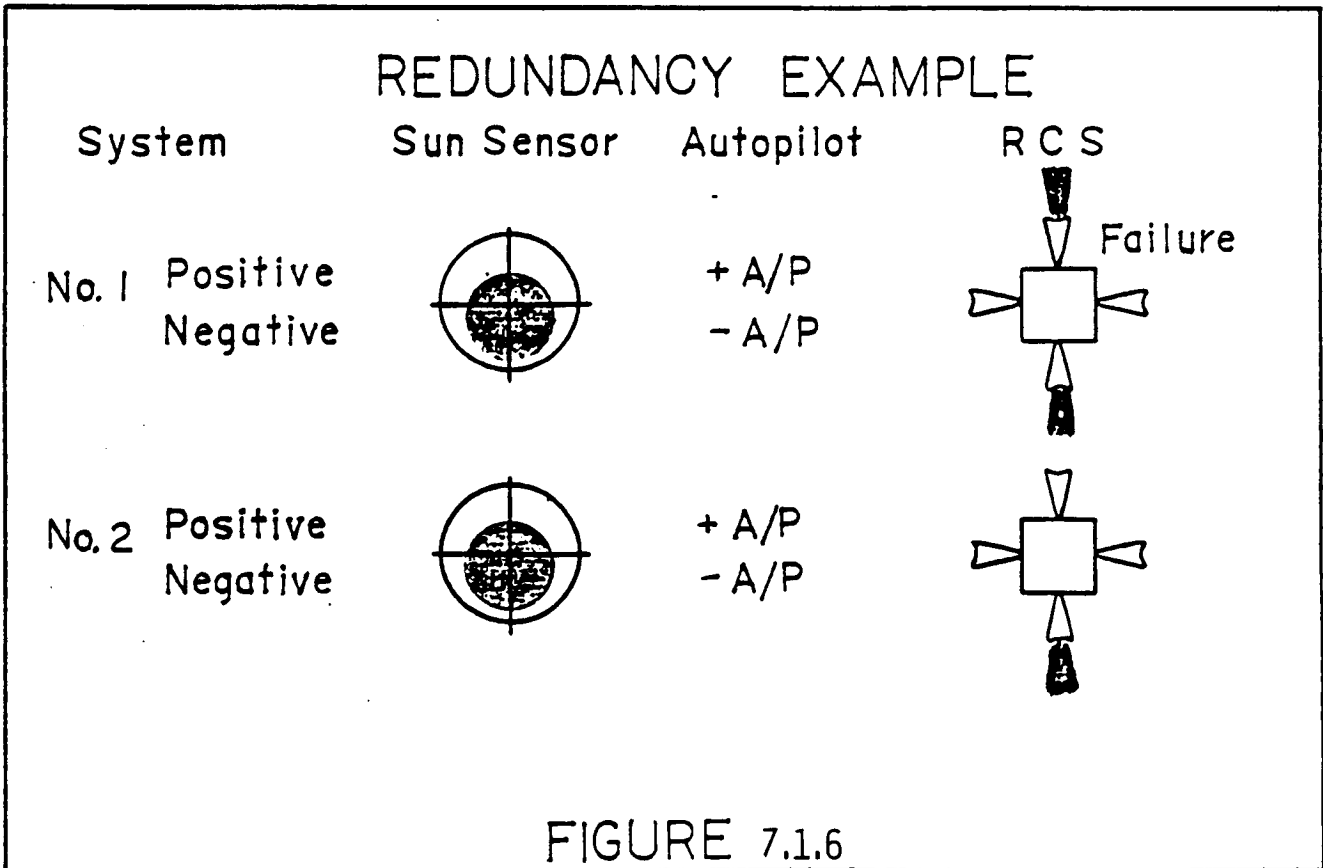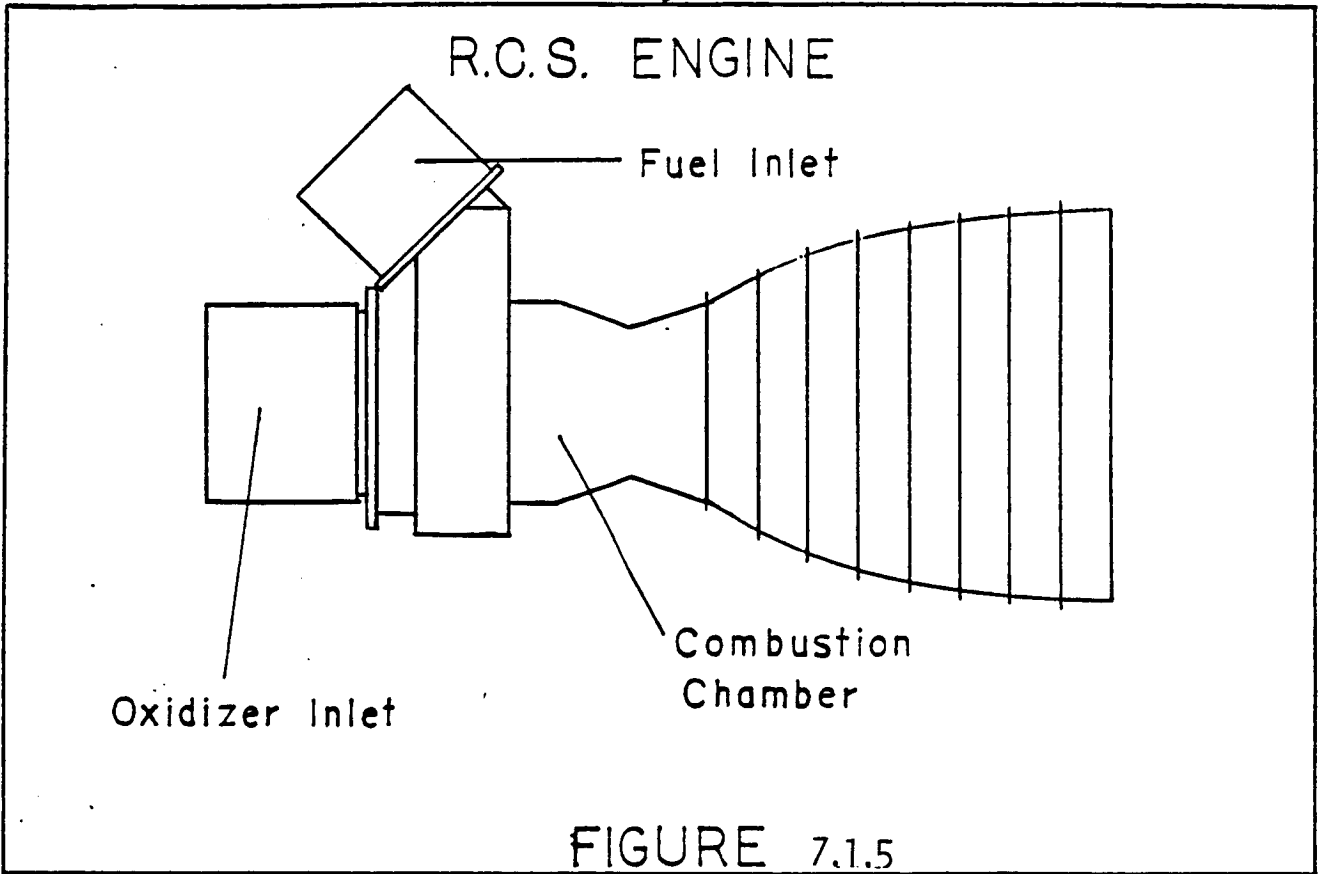
7.1.4 General GNC Topics

An orbital maneuvering system is required for rendezvous with the cycling spacecraft. The main engines of the TAXI can be throttled sufficiently to give levels of thrust suitable for relatively small maneuvers. The RCS engines are also capable providing translation for small changes in velocity.

Velocity measurements of the TAXI are made from the measurement of the Doppler shift of communications signals. Passing behind planet cuts off communication signals and permits precise determination of position at Mars which is useful for navigation and provides additional atmospheric data.

Attitude control is obtained by combining onboard sensors and torquers through a control law or control strategy which is implemented by the onboard computer. Major maneuvers are preprogrammed into the Digital Autopilot (DAP), but variations and adjustments can be programmed manually. An automated attitude control system responds to any change by the sensors. If the ship position drifts in relation to the Sun or Canopus, signals are sent to the RCS from the OBC to correct the ship's orientation. Fig. 7.1.7 shows a block diagram of the automated response system.

Path adaptive guidance permits a close approximation of optimal performance as it is defined ideally by the calculus of variations. The instantaneous state of the vehicle is represented by position, velocity, and acceleration, which is determined by the sensors of the G&C system. This state is used in the guidance scheme to define a thrust direction which gives an optimum path to specified end conditions. Path adaptive guidance corrects perturbations in the vehicle parameters occurring during flight by determining a new optimum trajectory. Direct computation of calculus of variations is not practical, so several adaptive schemes have been explored and developed to give a close approximation. These procedures are simple enough to be programmed into the flight computer of the vehicle.

In docking, sensors enable the TAXI to determine both the relative position and the relative attitude of the cycling ship. Relative position determination is fairly simple and places few constraints on the system. Relative attitude determination is calculated based on the relative position measurements of several reflectors placed in a known arrangement on the cycling ship.

The actual joining process involves mechanical guidance to cancel relative position and residual attitude misalignments. The dissipation of residual kinetic energy is allowed for by the use of shock absorbers in the hard docking mechanism. Interfaces for utilities are provided for electrical power, data transfer, and fuel transfer.

Fig. 7.1.8 summarizes the elements and numbers of the GNC system and the sizes, weights, and power required associated with each.

FEEDBACK SYSTEM

Sun Location → Sun Sensor

Canopus Location → Star Tracker

→ Onboard Computers → RCS System
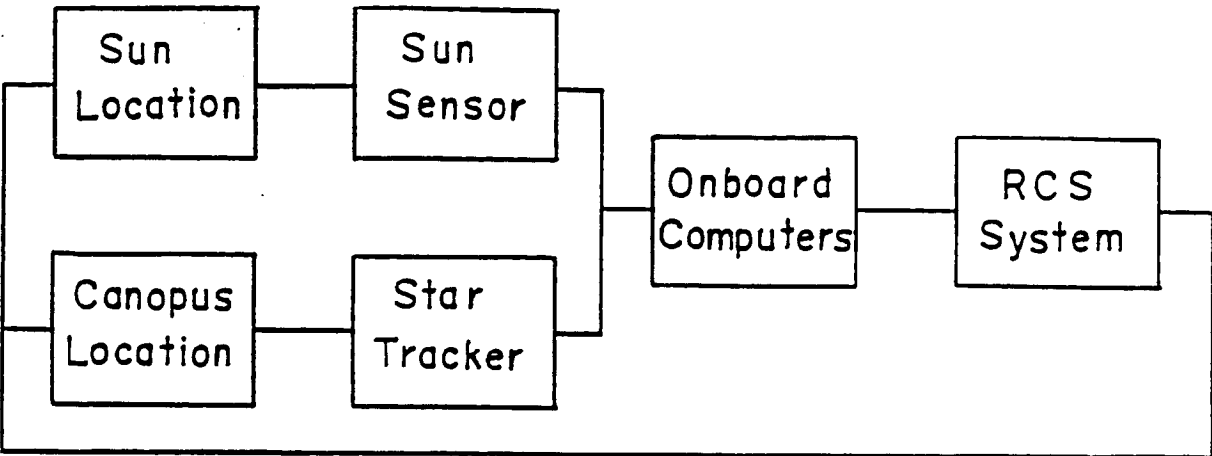
FIGURE 7.1.7

System element	Number required	Size	Weight	Power req'd
Sun sensor	six (redundancy of a three axis system)	.25 ft (.007 m) each	.26 lbs (.118 kg) each	100 mW each
Canopus sensor	two (one as an independent backup)	≈ 2 ft (.057 m) each	≈ 7 lbs (3.18 kg) each	1.5 W each
Rate gyros	three two-DOF gyros to provide complete redundancy	.5 ft (.014 m) each	.75 lbs (.341 kg) each	20 W max
Rate integrating gryos	as above	.75 ft (.021 m) each	1.7 lbs (.773 kg) each	20 W max
Onboard computer	two to provide redundancy	≈ 2 ft (.057 m) each	≈ 20 lbs (9.09 kg) each	500 W max

FIGURE 7.1.8

References

1. Chretien, J. P., _Automatic Control in Space_. Oxford: Pergamon   Press, 1986

2. Hatcher, N. M., _A Survey of Attitude Sensors_ for Spacecraft.   Washington D. C.: NASA, 1967

3. Joels, K. M., _The Space Shuttle Operator's Manual_. New York: Ballintine Books, 1982

4. Joels, K. M., _The Mars One Crew Manual_. New York: Ballintine   Books, 1985

5. Lunc, M.,   _Astrodynamics Guidance and Control_. Poland: Polish   Scientific Publishers, 1967

6. Lunc, M., _Guidance and Control_. Poland:Polish Scientific   Publishers, 1966

7. Wertz, J. R., _Spacecraft Attitude Determination and Control_.   Boston: D. Reidel Publishing Company, 1978.

7.2 Communications Systems

A predominant and essential function in every space mission is that of communication. An effective communication system is of vital importance to the success of the Earth / Mars manned missions.   This system sends all mission data back to Earth, reporting the condition of the TAXI and its crew to the cycling craft and the Earth.   The communication system also provides tracking and command transmissions capability to Earth-bound stations. The system is thus the crucial lifeline between the craft and Earth from the moment of launch throughout the duration of the mission.

7.2.1 System Requirements and Assumptions

The fact that this design is for manned space missions and not simply for an interplanetary probe adds to the complexity of the situation. A manned space mission has a greater data transmission load than an unmanned mission. Data transmission rates for a manned mission are required to be as high as possible, since data will be transmitted in multiple forms. For this design, the data transmission rates were set at 100 million bits per second. This is the current maximum data transmission rate attainable (Wolfe,1972). Since the area of communications and space-transmission is the fastest-growing area of space research at this time, projections for the future have been made using the current rate of development. The projected data transmission rate for the year 2025 A.D. is near 150 million bits per second. The data will be transmitted in many forms: digital data from telemetric tracking systems, voice channel communication and radio data, television data, and analog data from systems-monitoring processes on board the TAXI.

The communication system has the additional requirements of high reliability, multiple direction broadcasting, and multiple band broadcasting. Equipment used for this mission will be able to account very accurately for the Doppler Shift and highly accurate directional beaming needed to cover the long distances inherent in a mission to Mars (NASA,1974).

The weight of the communication system was not considered a primary factor in its design, since it is negligible compared to the total weight of the TAXI.   However, the weight of the system was reduced as much as possible after the system requirements were met. The communication system must be extremely reliable during the transfers because of the severe danger involved with a communication failure. The communication system environmental requirements are listed in Table 7.2.1 (Heitchu,1968;NASA,1979):

Table 7.2.1 Environmental Requirements

Humidity	95% for 50 hrs (max)
Temperature	0 to +180 deg. F
Vibration, g's	7.5 (all axes)
Sinusoidal,cps	5-3,000
Variation, g^2/cps	0.03
Shock, g's	30 (all axes)
Acceleration, g's	12 (all axes)
Vacuum, mm Hg	$1(10)^{-5}$

By the year 2025 A.D. it is expected that the components chosen for this system will be able to withstand greater forces and harsher environments than those listed here. Future systems should be able to withstand temperatures up to 225 deg. F, and accelerations, vibrations, and shocks on the order of 1.3 times greater than those listed.[4,12] It should also be noted that a heat dissipation problem is attendant with all designs of communication packages, because of the necessity of dissipating about 65 watts of heat. In order to meet the thermal requirements, the design required that all of the components generating a significant amount of heat are placed such that they are directly linked with the heat sink, so that the thermal resistances which exist between the heat sources and the heat sink are small. The components which generate significant amounts of heat are listed below:

D-C converters (2)	[approx. 8 watts]
Power transistors (3)	[approx. 7.5 watts]
Frequency doubling circuits	[approx. 7 watts]
Frequency Multiplexers (5)	[approx. 6 watts]

The total heat generation when the unit is operating will be about 66 watts.[7] At a design heat-sink rate of 1 watt/cm^2, nearly 600 cm^2 heat sink area , allowing for a 12% duty cycle, will be required. The heat dissipation requirement is easily taken care of by the communication module structure through direct contact with the generating components. Since all of the transistors are silicon transistors and high reliability circuits (non-temperature-sensitive) are used, all components are rated for 225 deg. F or greater at operation. All large heat-generating components are able to be bolted to the module structure directly, with the shock absorbing necessity taken into account by the casings and the packing of the components. The resulting interface conductance is a minimum of 2.0 watts/deg.F cm^2. The structure of the transmitter casing will be one piece of aluminum in order to minimize the thermal resistance between the heat sink and the other parts of the unit. The overall structural design incorporates large damping in order to protect the components from high resonance frequencies. The design objective was placed at 150 cps maximum (Yuen,1982).

Range And Power Requirements

Prominent among the many factors governing the communication system is the great distance which must be traversed by communication signals received and transmitted by the vehicle. These distances create a need for powerful and highly advanced directional capabilities in the communication system. The required area of coverage of the transfer vehicle is determined by the distance to Mars and the orbit chosen to reach this target, as well as the availability of relay devices which might boost and retransmit the transmitted signal. For the purposes of this project, it has been assumed that the standard requirement for communication in space is line-of -sight alignment. The ship will need to be able to broadcast to Earth, Mars, and the cycling spacecraft simultaneously. The system to be used for the TAXI will incorporate transducer which will convert physical parameters to voltage differences. These varying voltages are to be sent to the frequency modulator, which will alter the carrier wave of the radio broadcast (Doc #108,1976;Faget,1965). This signal will then be transmitted to the receivers at the various signal destinations. The process is reversed for received signals, going from the receiver to the demodulator and transducers, which produce the information in analog, digital, video- graphic, or voice signal information. Figure 7.2.1 is a block diagram of the general elements of the communication system.

Communication System Elements

raw information

↓

```
┌─────────────────────────┐
│       transponder       │
└─────────────────────────┘
             │
             ↓
┌─────────────────────────┐
│       modulator         │
├─────────────────────────┤
│       transmitter       │
└─────────────────────────┘
             │
             ↓
         ⏜ antenna ⏜


         ⏝ antenna ⏝
             │
             ↓
┌─────────────────────────┐
│        receiver         │
├─────────────────────────┤
│       demodulator       │
└─────────────────────────┘
             │
             ↓
```

digital ← ┌─────────────────────────┐ → analog
          │   display   │
          └─────────────────────────┘
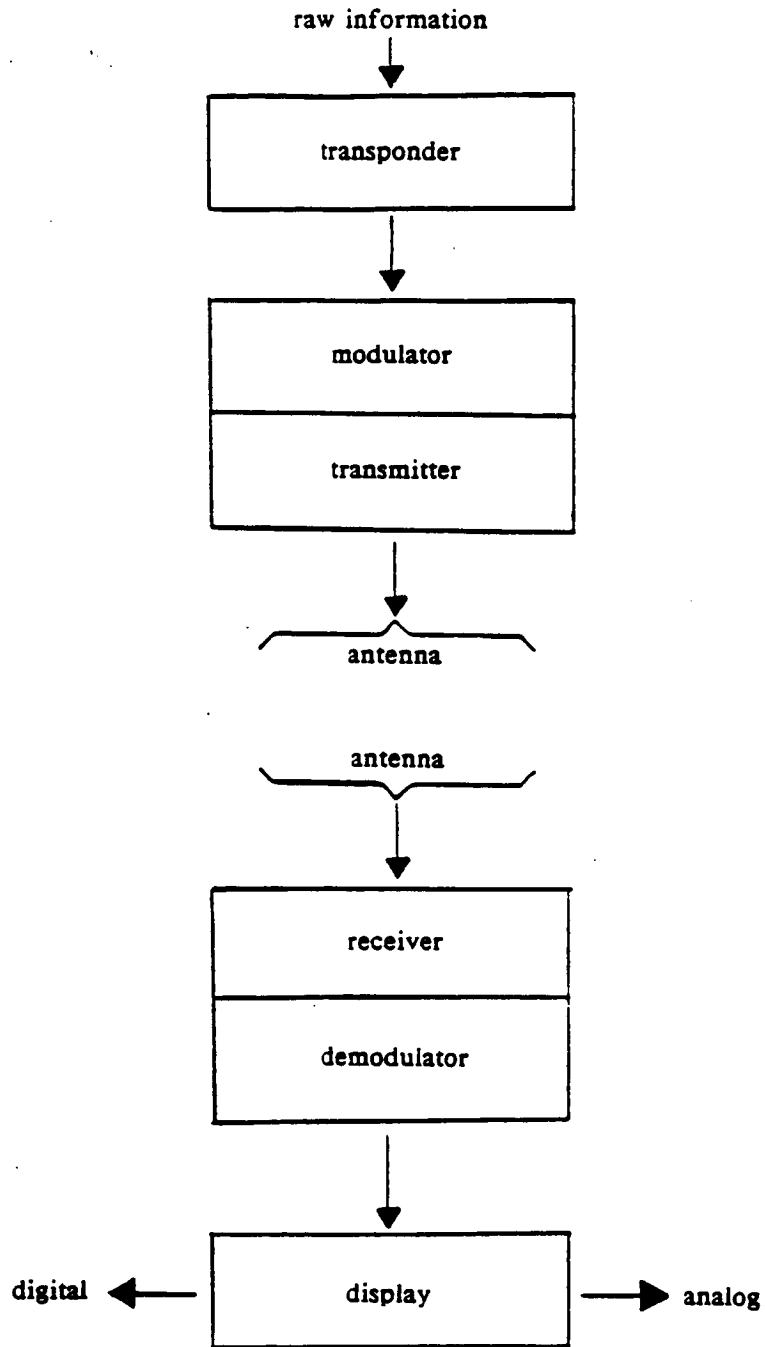
Figure 7.2.1

A problem which arose from the necessity of transmitting large quantities of information over such long distances was the amount of power required to generate the needed carrier waves and transmission modulations. In order to achieve the desired data transmission rates and frequencies, there were constraints and requirements which were made upon the power supply and the antenna system structure. The required transmitting power was derived from the Communications Range Equation (May,1986;Yuen,1982):

$$P_t = \frac{16(pi)^2 \times R^2 \times kTB(S/N)}{G_t \times G_r \times lambda^2}$$

where:

P$_t$ = power transmitted
G$_t$ = gain of the transmitter antenna
G$_r$ = gain of receiver antenna
lambda = wavelength
R = distance from source to receiver
S/N = avg. signal power/ avg. noise power
B = bandwidth
k = Boltzmann constant
T = avg. noise temperature

The power drain from the power source is related to the power of transmission, as well as the necessary power required for amplification, frequency modulation, and the transmitter/receiver functions as related to raw data (NASA,1969;NASA,1979;U.of Cal,1973). Some of the system loads required by the communication system of the vehicle power supply are given in Table 7.2.2:

Table 7.2.2 Power System Load Requirements

LOAD	watts
Continuous	12
15 watt transmitter	56
150 watt transmitter	475
210 watt transmitter	611
Transducer-modulator system	560
Receiver-demodulator system	620
Amplifiers	24
Videographic equipment	110
Other system functions	200
Total system requirements	2569

The use of the three levels of transmitters facilitates the separation of the different destination transmissions, while the multiple transmissions for a single destination are applied through the use of a multiplexer in a single antenna and transmitter.

7.2.2 Communications System Design

Modulation and Frequency Band Allocation

Among the many types of signal modulation which are effective within the constraints of this mission were frequency, phase, amplitude, and pulse-code modulation. Because of the multiple-destination, multi-media transmissions required by the TAXI vehicle, as well as the fact that the greatest improvements are expected in this area., frequency modulation has been chosen for this mission. This system provides a wide variety of available frequencies, tight bandwidths and high degree of signal reliability required for this mission (NASA,1979; NASA, 1980). The use of low-noise receivers at both the ground station and the transfer vehicle also aids in the elimination of external and internal noise and radio interference. Radio frequency modulation is used for every mission aspect in order to attain the necessary redundancy of the system to insure the safety of the crew members.

At this time, the communications industry does not have the capability necessary to allow transmission or reception of radio signals during the aerobraking procedure. During the approximately 250 seconds of atmospheric penetration, in which the plasma sheath will encase the _ vehicle, there will be a period of communication blackout. This is, however, of little importance, since the period of blackout is very short and communication can be re-established immediately following the break-down of the plasma sheath (Faget,1965;Wolfe,1972).

One of the most important parameters of a communications system is bandwidth. Successful radio communication between the TAXI and Earth stations depends upon the use of appropriate radio frequencies and freedom from as much interference as is possible. Radio frequency ranges used in this report are listed in Tables 7.2.3 and 7.2.4.

Table 7.2.3   Frequency Band Nomenclature

Frequency Range	Band Name	Abbreviation
3-30 kHz	Very Low Frequency	VLF
30-300 KHz	Low Frequency	LF
300-3000 kHz	Medium Frequency	MF
3-30 MHz	High Frequency	HF
30-300 MHz	Very High Frequency	VHF
300-3000 MHz	Ultra High Frequency	UHF
3-30 GHz	Super High Frequency	SHF
30-300 GHz	Extremely High Frequency	EHF

Table 7.2.4   Microwave Band Nomenclature

Frequency Range	Identification Band
390-1500 MHz	L
1550-5200 MHz	S
5.2-11 GHz	X
11-33 GHz	K

Since atmospheric and lunar interference are considerable below the frequency of 100 MHz, and the atmospheric attenuation and galactic noise are considerable above 10 GHz, the frequencies for this mission were necessarily chosen to lie within the 100 MHz to 10 GHz range (May,1986). The maximum beamwidth was set at one degree, due to significant information losses at wider beamwidths. It was found that beamwidths of near 10 MHz allowed for the greatest amount of data to reach its destination without severely affecting the weight of the necessary equipment. The transmission frequencies of this mission were chosen at 8400-8450 MHz and 2290-2300 MHz down-links, which are in the UHF range, in order to keep external noise interference to a minimum. The uplinks, also in the UHF range, were chosen at 2110-2120 MHz and 7145-7190 MHz for the same reason. Tables 7.2.5 and 7.2.6 show the band allocations available (by international treaty) for deep space missions[14], and the frequency bands chosen for this mission.

Table 7.2.5 Band Allocations for Deep Space Missions

BAND	DIRECTION	
2110-2120 MHz	Earth to Space	(up-link)
2290-2300 MHz	Space to Earth	(down-link)
7145-7190 MHz	Earth to Space	
8400-8450 MHz	Space to Earth	
12.75-13.25 GHz	Space to Earth	
16.6-17.1 GHz	Earth to Space	
31.8-32.3 GHz	Space to Earth	
34.2-34.7 GHz	Earth to Space	

Table 7.2.6 Mission Bands and Channel Frequency Ratios

BAND PAIR	CH. FREQ. RATIO	
2110-2120 MHz	uplink	221/240
2290-2300 MHz	downlink	
7145-7190 MHz	uplink	749/880
8400-8450 MHz	downlink	
2290-2300 MHz	uplink	3/11
8400-8450 MHz	downlink	

There are more downlink frequency bands than uplink because larger amounts of data will be sent to Earth than command data sent from the Earth or the orbiting spacecraft.

The radio frequency signal for deep-space communications includes a carrier wave and two sets of data sidebands. The two sets of data sidebands used in this mission are the combined telemetry and ranging signals on a downlink, or the combined command and ranging signals on the uplink. Channel selection was based on calculation and analysis of the interference-to-signal power ratios (ISR) as a function of time for each two possible interfering transmitters. The worst case ISR was then compared to the criterion of acceptable interference. The acceptable interference to signal power is called the interference protection ratio. The required protection ratio for this mission was considered to be -20 dB during critical mission phases and -15 dB at all other times (Springett,1981). The ratio is the maximum interference power with respect to the power of the desired signal. A -15 dB ratio will produce a negligible effect on carrier tracking performance, a 0.4 dB degradation of telemetry performance, and a 1.0 dB degradation of command performance, since both the telemetry and command are operating at an error rate of $1(10)^{-5}$ to 1. Of course, the -20 dB allowance gives even greater protection, which is necessary at critical stages of the mission. From the protection ratios, the frequency channel ratios can be effectively chosen to augment the system reliability.

Radio Tracking System

The radio tracking system has a dual purpose for this mission. First, the system obtains information concerning vehicle position, radio propagation, and solar system properties from radiometric functions. This information is important in the navigation of the   vehicle, which relies on star-trackers and sun-sensors. The tracking system also provides radio frequency carriers and additional reference signals that are used for telemetry and command functions.

The two-way system used in this design begins with a Deep Space Station frequency standard (DSS) modulation system linked to an exciter system and transmitter, which are used to generate an S-band carrier signal. The signal, after modulation and amplification, is then collimated and directed to the vehicle by a 113 or 213 foot parabolic antenna and associated pointing system at the ground station (McKinney,1981;Springett,1981). The 12.3 foot (3.7 meter) parabolic antenna on the transfer vehicle will intercept and focus this radio wave. The spacecraft receiver uses the phase-locked loop data capture system to lock on to and track the uplink carrier. The reference signal produced demodulates the ranging and command signals from the carrier. These signals are passed through a bandpass filter (bandwidth = 1.5 MHz), and the downlink exciters which coherently multiply the receiver reference frequency to obtain S- and X-band carrier signals which are higher in frequency than the received carrier signals (by the ratio 240/221 for S-band, and 880/221 for X-band). Unrelated fixed frequencies are used to generate the downlink carriers, which can be obtained from the crystal oscillators. The computer used in the guidance and navigational controls will be capable of handling the communication system needs. Figures 7.2.2 and 7.2.3 show block diagrams of the ground and TAXI tracking systems.

Block Diagram - Ground Tracking System

Figure 7.2.2

Block Diagram - TAXI Orbiter Tracking System

Figure 7.2.3
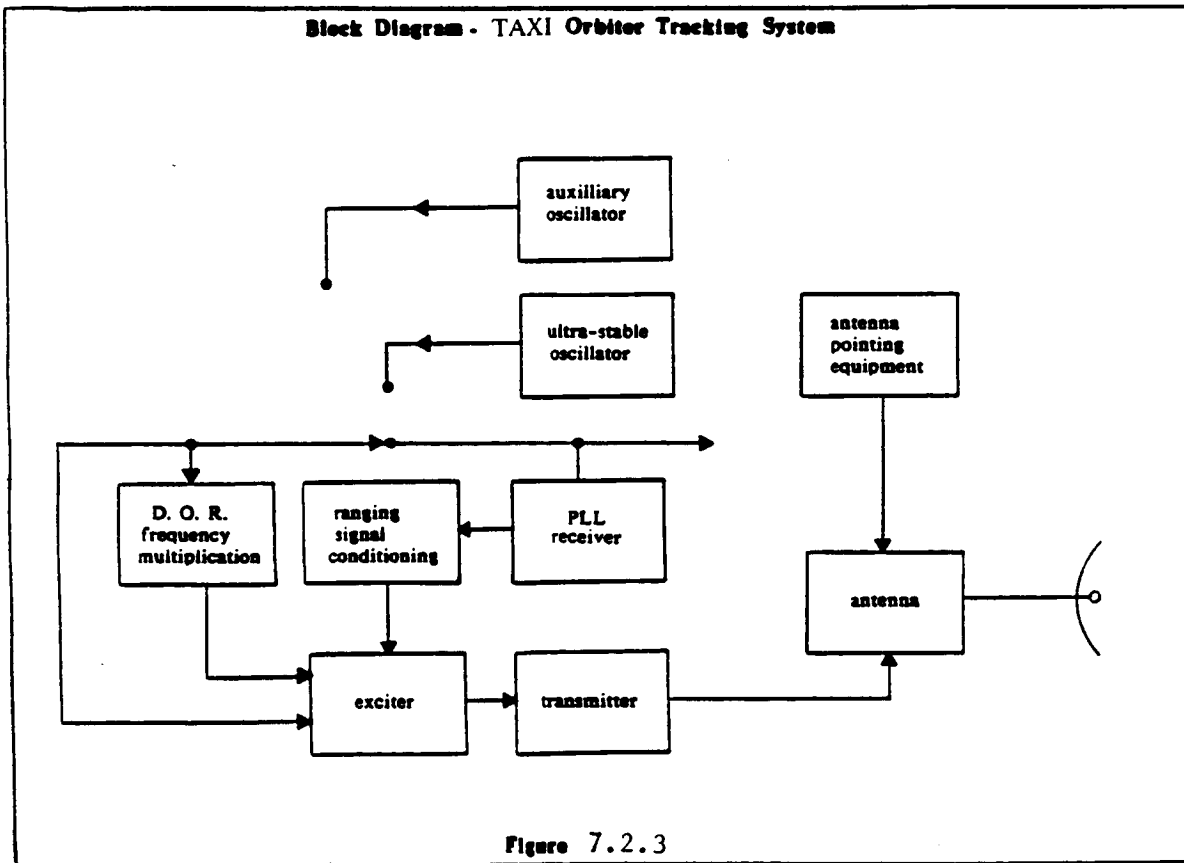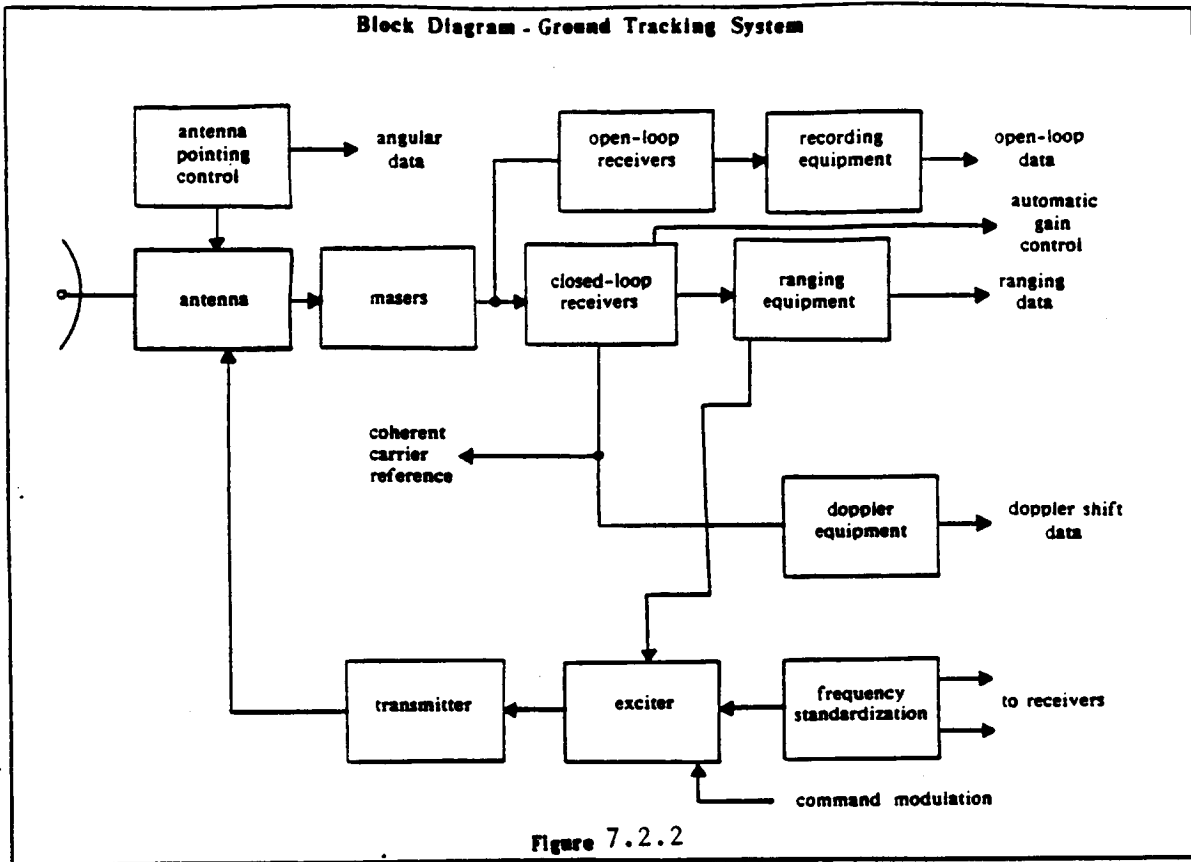
System Receiver

There are two basic types of deep space communications receivers: the phase-locked loop (PLL) receiver and the Costas loop receiver. For the purposes of this manned mission, the phase-locked loop receiver is being used in conjunction with a residual carrier transmission system. The first receiver stage has very high gain, and thus is responsible for a large percentage of the receiver noise. The most recent developments and future trends show that receivers which have better noise-damping systems will be available, allowing for higher gain with less noise interference. The heterodyne design is employed to translate the radio frequency signal down to a frequency for which stable phase detectors have been built. Automatic gain control is required to provide a signal whose amplitude is within the dynamic range of the intermediate frequency (IF) amplifier stages (U.of Cal.,1973). The bandpass limiter minimizes the total mean-square ratios, while the phase-locked loop system allows for a greater information capture rate. This configuration provides near-optimum PLL performance. Figure 7.2.4 shows a block diagram of the PLL system designed for the TAXI

Transfer Vehicle Antennas

One of the most important features of TAXI antennas considered for this design was size, and due to this, weight. Higher gain antennas are usually larger in size, and heavier than lower gain antennas. In a weight-critical vehicle, it is necessary to decide upon antenna gain or transmitter power as the route to optimum performance. For this mission, a tight beamwidth is necessary and can be achieved by either of the above methods. To meet the mission requirements as well to minimize weight , two parabolic directional antennas were chosen for the vehicle. In addition to these, an "omni-directional" spike-cone antenna will be used for short-range communication.

Maximum spacecraft telecommunications performance is obtained when the target is aligned with the maximum-gain point of the antenna, but this is nearly impossible to maintain. An acceptable pointing error is specified at 1.0 degrees deviation, as previously mentioned. The tracking system chosen will adjust the orientation of the antennas to compensate for the movement of the TAXI and the Earth.

The two parabolic antennas will be 12.3 feet (3.7 meters) in diameter, and will be capable of multiple-band, multiple frequency transmission and reception. Close-range communication needs will be taken care of by the 2.0 foot (0.6meter) spike-cone antenna, which will be used during EVA and docking procedures. The spike antenna will be retractable and one of the parabolic antennas will be able to be pulled into a storage compartment in the communications/GNC module, while the other will be folded to a position near the structure of the fuel tanks. The antenna is capable of withstanding the temperatures of aerobraking, and, in the folded position, the forces inherent in that maneuver. For mid-flight communication, the ship will be rotated through an angle of approximately 65 degrees to allow the widest communication line-of-sight spectrum available. The two parabolic antennas will be placed at opposite ends of the TAXI vehicle in order to achieve communication with both the Earth and Mars, as well as the cycling spacecraft with the least amount of interference from the structure of the TAXI vehicle and its aerobraking/heat shield. One will be situated 15-20 feet behind the heat shield in the truss structure which supports the fuel tanks, while the other will be supported by the communications module itself, located beside the crew module.The transmitter system and the parabolic antenna design for this mission are shown in Figures 7.2.5 and 7.2.6.

Figure 7.2.4

Block Diagram - Mission PLL Receiver System

coherent AGC

coherent amplitude detector

LPF

BPF (46 MHz)

I.F. amplifier

LPF (20 MHz)

I.F. amplifier

limiter

BPF (9 MHz)

BPF (10 kHz)

I.F. amplifier

loop phase detector

BPF (120 MHz)

diviser (one-half)

24.5 MHz oscillator

diviser (one-half)

loop filter

8x multiplier

S.A.W. BPF

S.A.W. BPF

13x multiplier

VCO

S.A.W. BPF

LPF: low-pass filter
BPF: band-pass filter
VCO: voltage control oscillator
AGC: automatic gain control

Figure 7.2.5

Block Diagram - Transmitter System

modulation inputs

input summation

voltage controlled oscillator

buffer

3x multiplier

power amplifier

4x multiplier

low-pass filter

crystal oscillator

4x multiplier

mixer

D-C amplifier

frequency disc

I.F. amplifier

band-pass filter

voltage output

DC-DC converter

ground

Geometric Layout of TAXI Parabolic High Gain Antenna

S-X coaxial feed

linear-to-circular hybrid circuitry

coated graphite-epoxy reflector

x-band waveguide

handling fixture

0.15 ft

S-band coaxial

5.28 ft

0.32 ft

5.64 ft

3.03 ft

waveguide and coaxial

4.05 ft

12.14 ft

64.3°
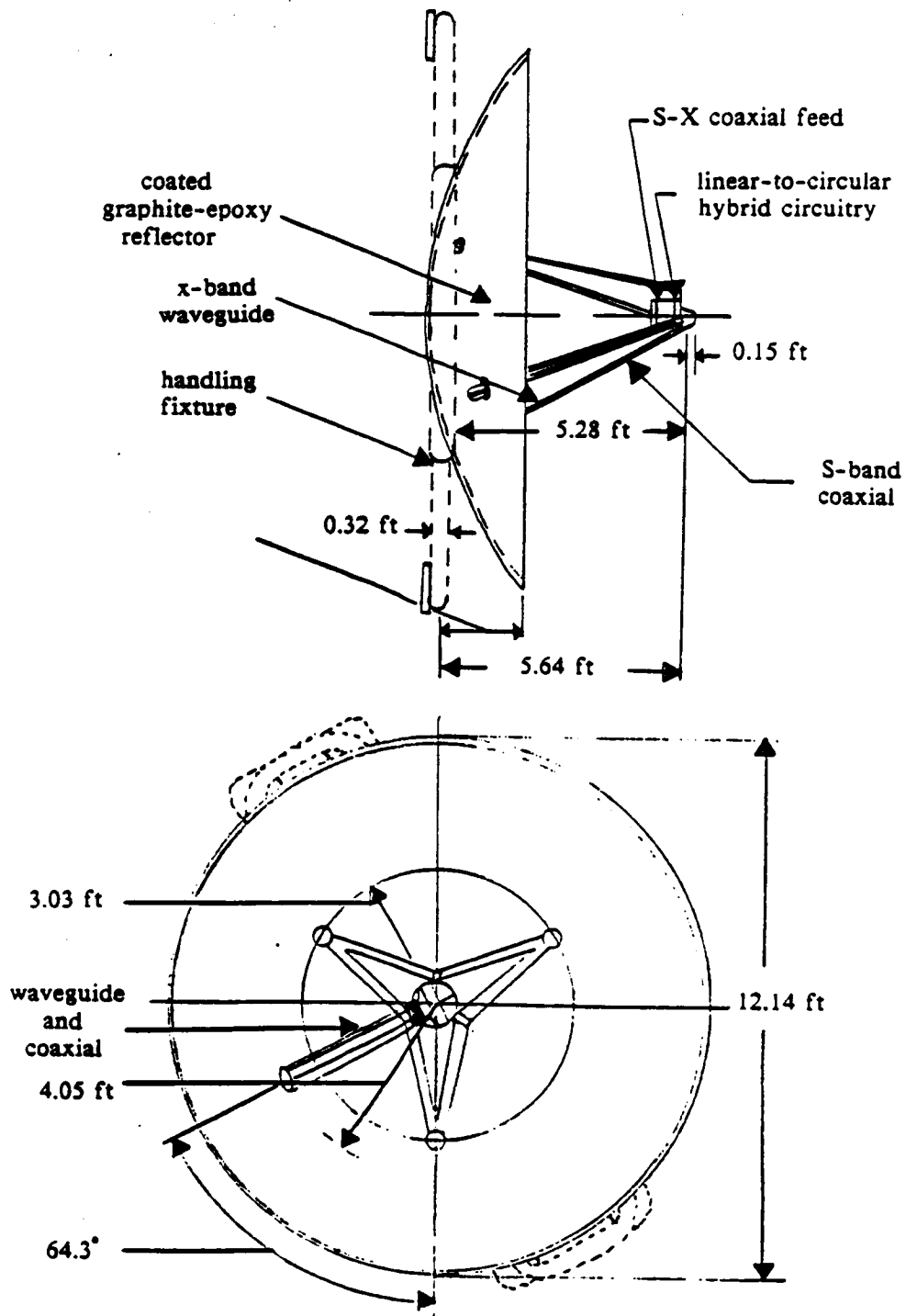
Figure 7.2.6

Satellite Link and Relay Systems

During the period in which the TAXI vehicle is orbiting the planet Mars, and is not in direct line-of-sight transmission presentation with the Earth, the use of orbiting communication satellites will allow greater coverage. Since data compression is available, continual links between Earth and Mars are not necessary, but prove to be desirable. The options available to this mission configuration include a direct link system, or a system of coverage which involves both direct link and a relayed link system (McKinney,1981). The best choice is the combination coverage system. By the time of this mission, it is assumed that the communication link satellites will already be in orbit about Mars.

The satellites in question would be placed in orbit at angles of approximately 130 degrees from each other, and appropriately distanced from the orbiting station assumed present at Mars. Thus, regardless of the position of the TAXI vehicle, there will always be a link satellite within line-of-sight range to relay data to and from the Earth. The satellites will be placed in a minimum altitude orbit of 700 km, which will allow 96% coverage over the surface of Mars, and will thus allow for communication with any parties on the surface of the planet with the TAXI.

The satellites will be active type satellites, because of the marked decrease in output power with distance in the passive satellite. These will amplify the received signal and rebroadcast it towards its destination. The retransmission may be on a different frequency or band than the original transmission if the satellite is so equipped., the active satellite is the only feasible choice. The satellites will be equipped with a pair of rotatable, highly directional antennas in order to give the required beamwidths and allowable pointing errors.

Communication Module Design

The communication system has been designed in order that it may exist separately from the crew module, allowing for flexibility in the overall configuration. The communication module will store the communication system excluding one of the parabolic antennas, and the GNC computer. The module consists of a skin-structure of two layers of 0.6 inch thick aluminum. The two layers will be separated by four inches, where the graphite-polymide connection stringers will be housed. The stringers are approximately five inches high and are made of a graphite-polyimide composite. The stringers are spaced across the surface of the module at intervals of fourteen inches. The interval and height of the stringers was decided so that the system will be capable of withstanding up to 16 times the force of gravity. The strength of the system gives a large margin of safety to the components. The two 0.6 inch thick aluminum skins, separated by four inches of space, filled with insulation, give a radiation protection factor of 99% to the system, and also a 99% protection from micrometeoroids. The components of the system will be packed in soft-structure paddings and vibrational absorbers will be used to protect the system from vibrational load failure. The volume of the system will be approximately 33 cubic feet. The weight , including the computer system and structural weight (47.5 lb) will be about 385 lb (see table 7.2.7). The communications module will contain the spike antenna (retractable) and a compartment 6.8 ft long, 1.8 ft wide, and 1.8 ft high which will house the undeployed parabolic antenna. The module will be placed within the truss-structure of the crew module. Layouts of the communications module is shown in Figs. 7.2.7 and 7.2.8. A schematic of the Communication System Links is given in Fig. 7.2.9.

Table 7.2.7 Weights of Communication System Components

Structure and Covers	5.3 lb
Wiring, potting, and connectors	7.7 lb
Instrumentation	61.2 lb
Temperature-control materials	12.0 lb
Timer	0.7 lb
Radiation Package	7.9 lb
Optical Package	4.0 lb
Spike Antenna (and fairing)	2.9 lb
Parabolic Dish Antenna	92.0 lb
Module structure	47.5 lb
Total Communications Package	385 lb

parabolic
antenna support

retracted cone antenna

antenna bay

1.8 ft

4.6 ft

Figure 7.2.7

1.1 ft   6.8 ft   1.1 ft

1.6 ft

retraction
control

back-up
computer

data
storage

safety
control
systems

PLL receiver
system

modu-
lator
system

150 watt
transmitter

DC-DC

converter

guidance and
communications
computer

4.6 ft

4 in   15 watt transmitter

Figure 7.2.8

190
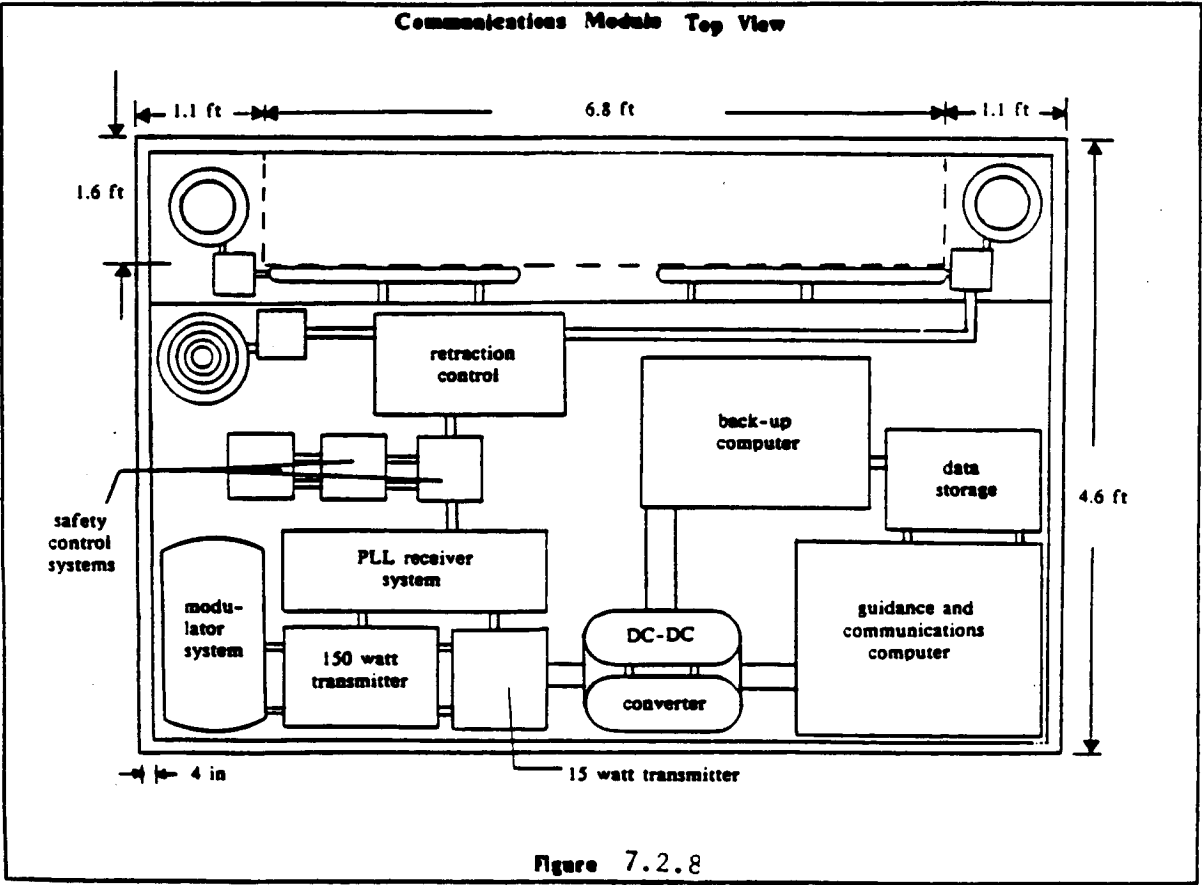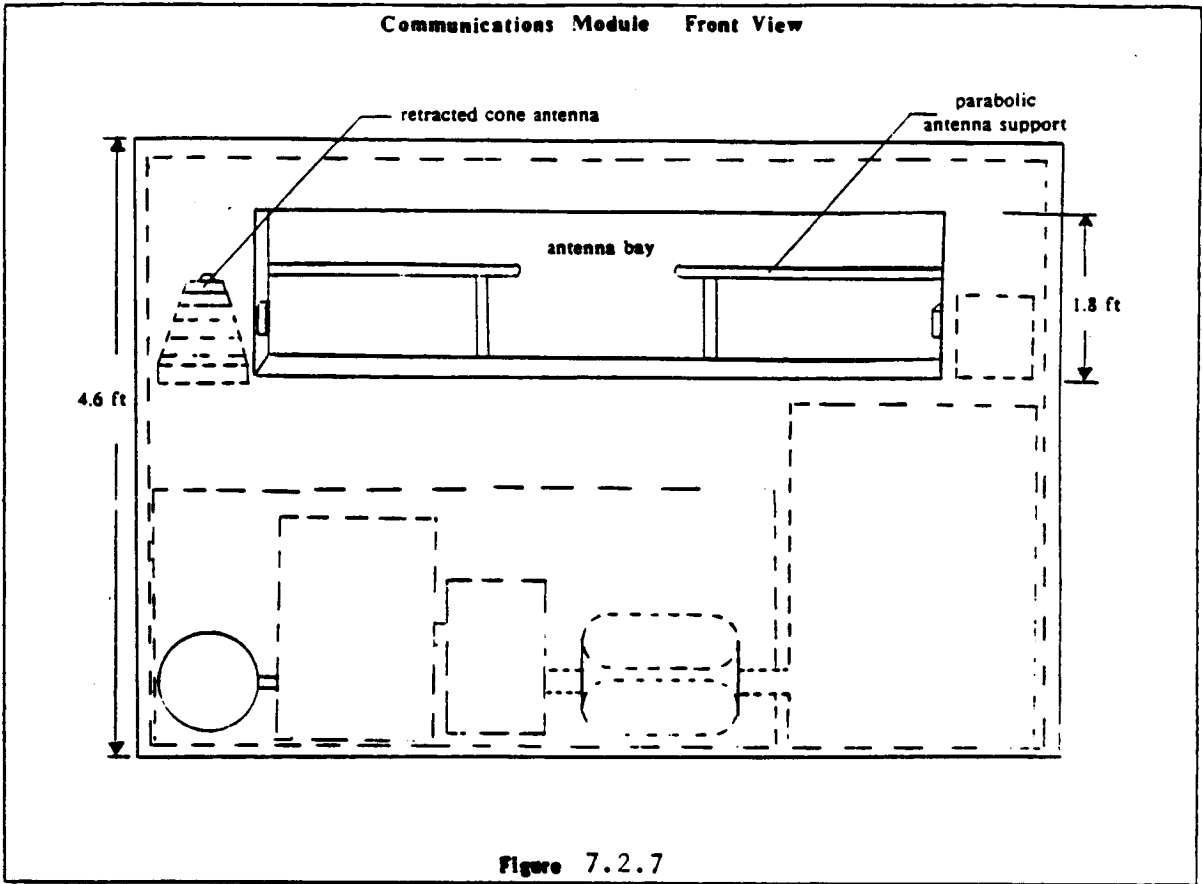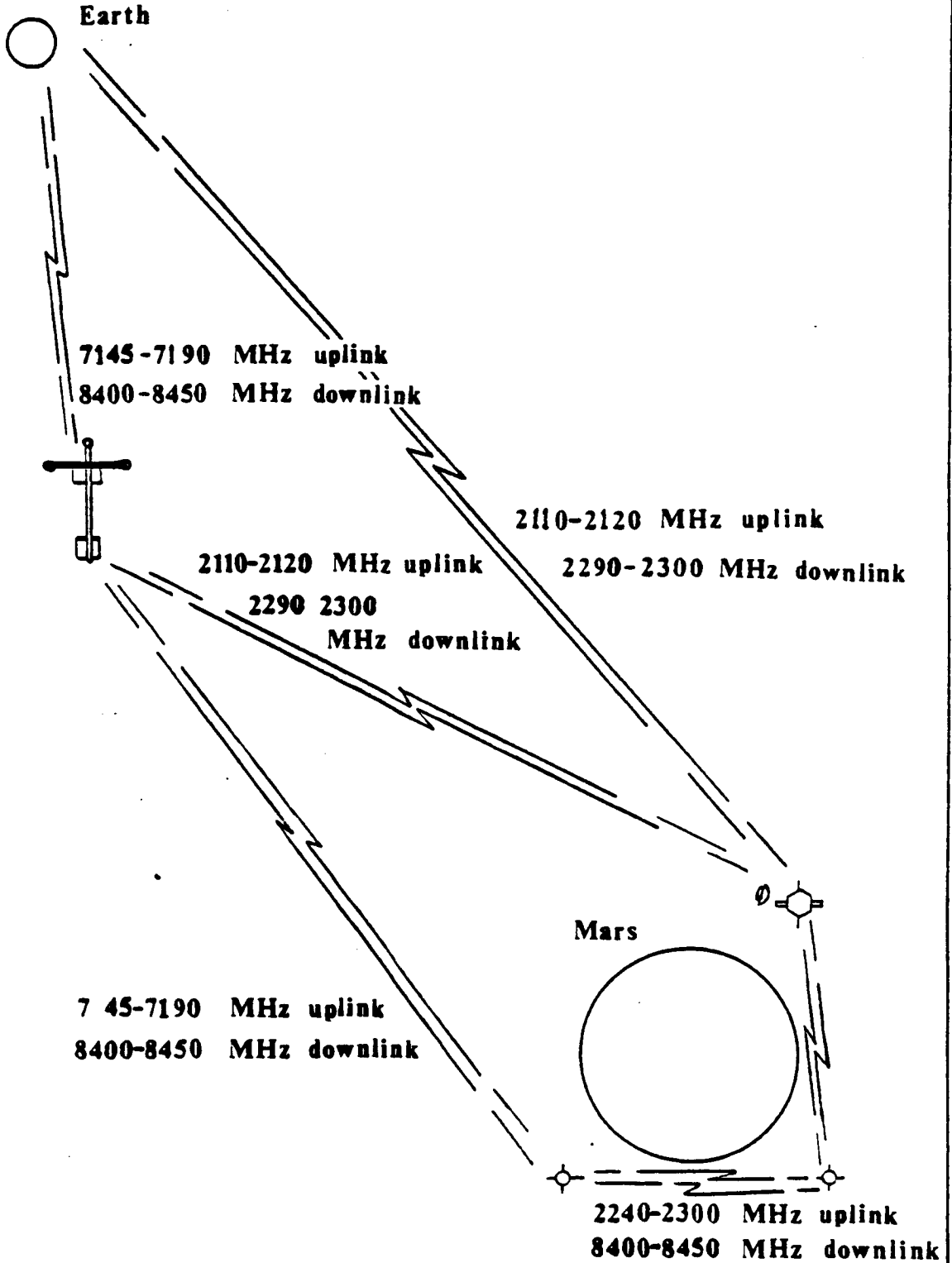
Figure 7.2.9

REFERENCES

1.Document STDN No. 108, <u>PN Codes For Use With</u> the Tracking and Data Relay Satellite System, Goddard SFC, USA, 1976

2.Faget,M., Manned Space Flight, Holt,Rhinehart
Winston Inc., New York, 1965

3.Heitchu, Space Systems Technology, Rheinhold Book Corporation, USA, 1968

4.IEEE Transactions on Communications, "Special Issue on Space Shuttle Communications and Tracking", Vol. Com-26, No.11, Nov. 1978

5.May, G.L., Space Exploitation and Utilization, "Advances in astronautical Sciences", AAS,Univelt, Inc., San Diego, 1986

6.McKinney, L., Satellite System Design, McGraw Hill, New York, 1981

7.NASA Report, N65-30482, Power Conditioning and Control System, NASA, 1969

8.NASA Report,, N65-32171, Voyager Design Study,NASA, 1974

9.NASA Report,, NASA-CP-244 N85-20751, Space System Radios, NASA, 1979

10.NASA Report, NASA-CP-2342 N85-16937, Space Shuttle, NASA, 1980

11.Springett, J.C., Space Shuttle Telecommunication Interfaces, Document 890- 123, JPL, USA, 1981

12.Univ. of California, Engineering and Science
Extension Series, McGraw Hill, New York, 1973

13.Wolfe, Space Technology, Spartan Books, Washington, D.C., 1972

14.Yuen, J., Deep Space Telecommunications Systems Engineering, JPL Publication, July 1982

8. Power Generation and Distribution .

The heart of a spacecraft is its power generation system. Electrical power is required for environmental control, waste processing, guidance and navigation, active cryogenic fuel regeneration, lighting, and communications. The procedure of this section is to first summarize the mission requirements, examine the possible options for the TAXI 's energy source, choose primary and back-up systems, and lastly provide critical design data on the selected systems.

8.1 Outline of Requirements

There are three phases of the TAXI mission requiring different power levels:

1. Transfer orbits to and from the cycling ship
2. Docking on cycling ship
3. Parking orbits about Earth and Mars

The transfer orbits require the highest power levels of the entire mission. The estimated average power consumption is 10 kW over each of the transfers. Assuming that the maximum duration of the four transfers will be 16 days, the energy production from the primary power generator is estimated at approximately 3850 kWh. To provide a margin of safety an additional ten percent (or 385 kWh) is included in the production requirement for the primary power system. Peak power levels of 20 kW are anticipated during periods of high crew activity.

When docked at the cycling ship or parked in orbit about a planet, the power consumption is expected to be quite low. For the conditioning of the secondary batteries and electronics systems only a few tens of watts should be required. Temperature control might require several hundreds of watts, however. As a rough estimate the power consumption is expected to be 350 W. This power will be provided by the secondary or back-up power system.

The minimum power required for the safe operation of the TAXI vehicle is estimated to be 4 kW. Thus the back-up power system must be able to supply 4 kW continuously over an entire transfer orbit.

8.2 Power Generator Options

Three sources of energy were considered for the TAXI vehicle power system:

1. Nuclear - fission reactors and radioisotopic generators
2. Electromagnetic - solar collectors
3. Chemical - fuel cells and secondary batteries

8.2.1 Nuclear

Nuclear fission reactors are primarily suited for high power missions such as electric propulsion spacecraft. Dynamic conversion processes are generally employed involving turbines, pumps, and condensers. Because of the massive radiation shielding requirements the low power reactors tend to be large and heavy for their output. The power density for outputs under 50 kW is usually much less than 2.3 W/lb (5W/kg). Active cooling systems add to the complexity of a fission reactor, making it even less attractive.

Radioisotopic generators have been extensively developed for low power space missions. A radioisotopic generator utilizing thermionic or thermoelectric elements for the direct conversion of thermal energy to electrical energy is known as an RTG. Due to the low efficiency of direct conversion processes (6-7%), an RTG typically has a power density in the range of 2.3 W/lb. A radioisotopic power generator using dynamic conversion (DIPS - dynamic isotopic power system) can achieve energy densities of 4.54 W/lb due to the higher efficiency of the dynamic conversion processes at the present time.

8.2.2 Electromagnetic

Solar arrays, particularly photovoltaic arrays, were extensively researched for a primary power supply. Solar power systems have been widely used on spacecraft, satellites, and interplanetary probes. The high power density of solar arrays (due to the fact that no onboard fuel is required) makes them very attractive for long-duration missions. A solar array was designed that would provide from 12.9 to 30.0 kW continuous power over a lifetime of ten years at a mass of only 1457.5 lb (662.2 kg). But to produce the power two deployable gallium arsenide concentrator arrays of 64.3ft by 22.0ft (19.6m by 6.7m) were required (Fig. 8.2.1). The unwieldiness of the design and susceptibility of the system to damage from heating and shocks during aerobraking maneuvers (even when folded) eliminated the solar array from consideration.

8.2.3 Chemical

Chemical power systems have been used on many manned space missions including Apollo and the Space Shuttle. The preferred chemical-to-electrical conversion device is the fuel cell. A fuel cell is a device that directly converts chemical energy to electrical energy via an oxidation/reduction reaction. The main components of a fuel cell power generation system are the fuel supply system, the temperature regulation system (preheater and radiator), the reaction cells, and the water bleed-off system (Fig. 8.2.2).

Each fuel cell supplies electrical energy at approximately .8 to .9 volts. A "stack" is a number of cells connected in series to produce a higher output voltage. The maximum current output of each stack depends on the individual cell membrane area and the maximum allowable current density of the membrane (amps/ft^2). A number of stacks are connected in parallel to achieve the desired current output. The total power output is the product of the stack voltage and the total current. Critical H_2/O_2 fuel cell performance data was obtained from the most recent operational data.

8.3 Selection of Power Generators

A decision for the TAXI power system selection was based on the mission duration, mission requirements, and the properties of the systems. Because the transfer missions are of relatively short duration, reliability and proven technology were emphasized over efficiency and power density. The low total energy requirements for the mission do not greatly favor high efficiency systems, particularly when reliability and cost of development are considered. In addition, other factors such as the availability of power reactants and the utility of the power supply option for the entire Mars mission were included. Because the manned development of space in the near future is expected to occur with hydrogen/oxygen based propulsion, the latter factors greatly favored the use of a fuel cell primary power system. Fuel cells are considered to be the best option for the TAXI primary power system for several additional reasons:

Design of a Deployable Concentrator Array

tension control and electrical pathway

guide wires

edge stiffener

solar cells (GaAs)

edge stiffener

corrugation

padding
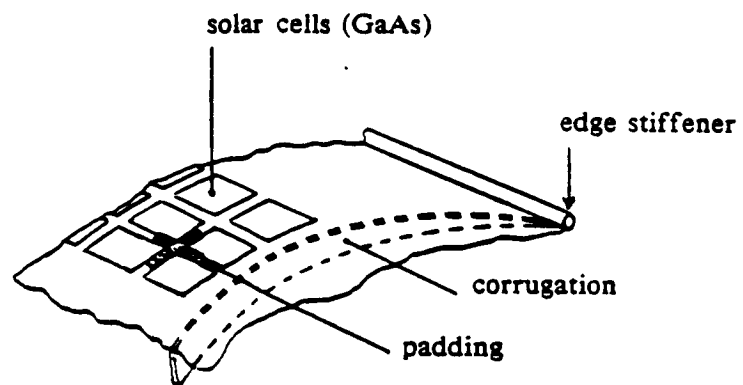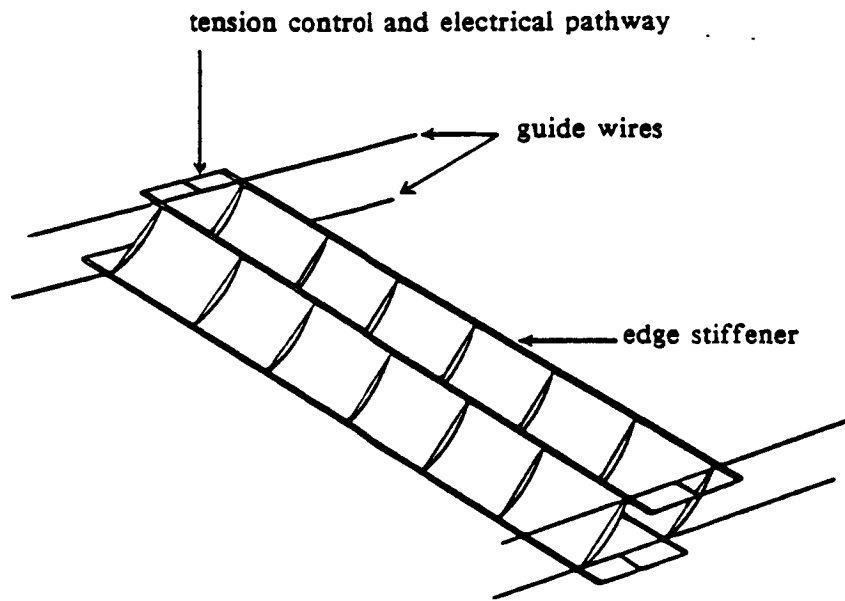
Figure 8.2.1

Basic Components of a Fuel Cell Power Generator

radiator

bypass valve

power output

liquid hydrogen pump

fuel cell stacks

preheater

liquid oxygen pump

coolant circulation tubing

H_2O vapor
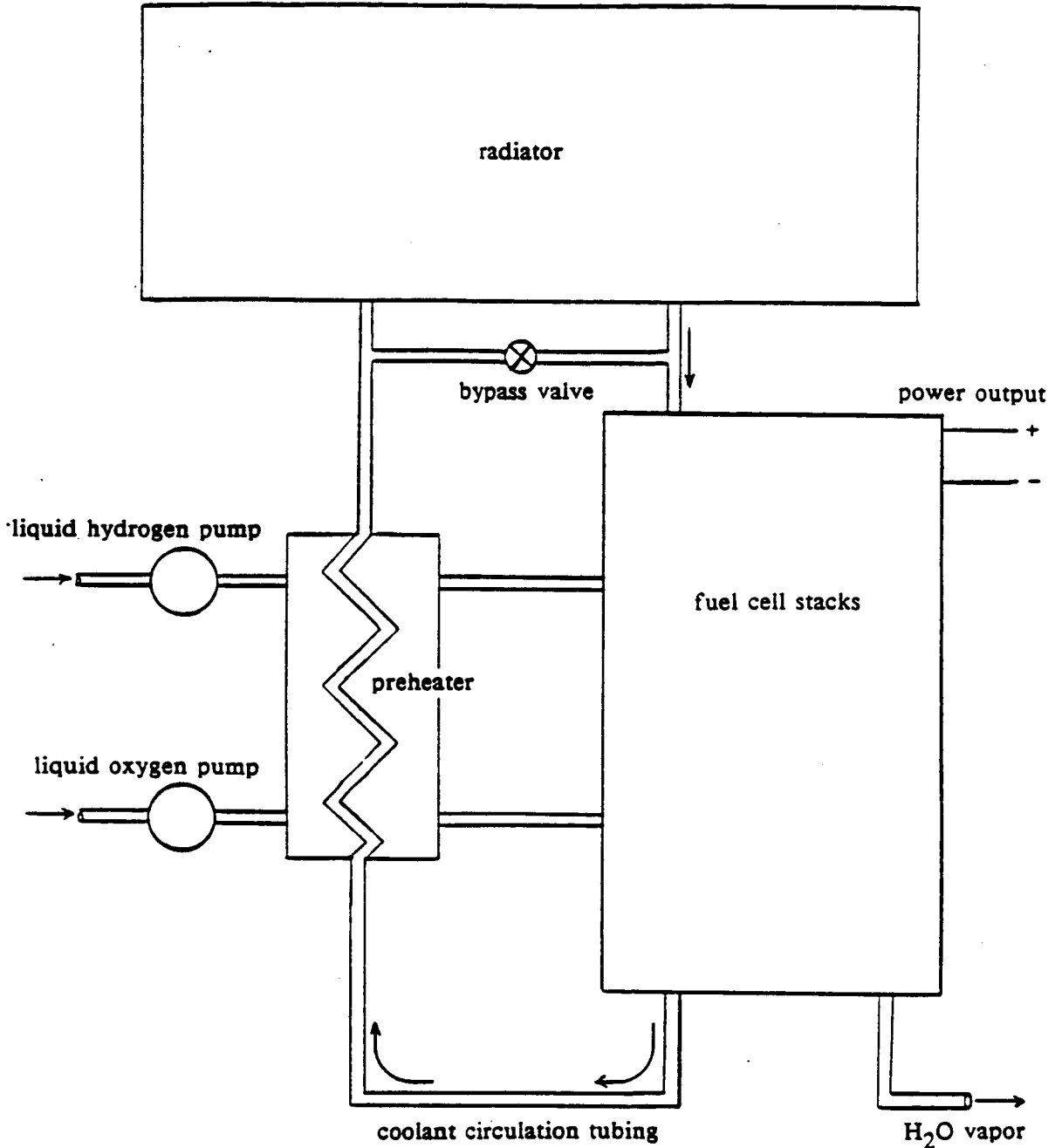
Figure 8.2.2

1. Compactness and reliability of the fuel cell
2. High conversion efficiency over a wide output range
3. Ability to tailor the system to mission requirements by altering the reactant payload mass
4. Zero fuel consumption during dormant periods

A nuclear back-up system was selected because of its long, reliable operation, compact size, portability, and ease of replacement. In addition, a passive conversion process was selected because of its inherent reliability and potential for future development. It is believed that research will yield thermionic conversion efficiencies in the range of twelve to fifteen percent, thus doubling the power density of the radioisotopic thermionic generator. A comparison of RTGs and DIPS will determine the optimum conversion process at the final design stage of the TAXI based on the actual progress of research.

8.4 Selected Design for the TAXI

8.4.1 Fuel Cells

The fuel supply is obtained from the main TAXI H_2/O_2 cryogenic tanks through the collector module. Fuel cells have been proven to provide long, reliable service using propulsion grade fuels with no significant impact on performance. Purge orifices on the reactant vent lines prevent the accumulation of contaminants within the reaction cells (with a slight loss of efficiency). Electric pumps raise the pressure of the fuels from 5 psia (34.5 kPa) for the main tanks to operational cell levels. The maximum reactant pressure is presently about 60 psia (413.6 kPa).

Temperature regulation is achieved by a combination of preheating and active cooling. A significant percentage of the waste heat can be employed in the preheater system which raises the temperature of the cryogenic fuels to operational cell temperatures of approximately 250°F (120°C). Any excess heat must be discarded through a radiator panel. Either an active coolant flow or a heat pipe system ca be used to transport the thermal energy to the panel. A future design possibility is the elimination of the need for active cooling by increasing the conversion efficiency and raising the operating temperature.

A reaction cell consists of an anode and a cathode region, each filled with electrolyte, at which the ion exchange occurs. Three main dividing plates are required for each cell: a hydrogen metering plate, an oxygen metering plate, and a sealed separation plate. The series of plates required for an operational fuel cell is shown in Fig. 8.4.1. The most modern designs employ a gold-platinum catalyst cathode and a platinum-on-carbon catalyst anode for high efficiency and endurance. Potassium titanate (PKT) is used as a matrix material because of its high resistance to corrosion at elevated temperatures. The use of PKT rather than asbestos was proven to reduce contamination of the reaction cell by forty percent, thus greatly improving the endurance qualities of the fuel cell. The reaction cell is the most critical section of the fuel cell system because of the possibility of coolant and reactant leaks between cells and the performance sensitivity to anode/cathode degradation.

Plate Assembly for a Fuel Cell

coolant outflow

coolant inflow

O_2 inflow

H_2 inflow

coolant flow field

coolant/O_2 barrier

O_2 flow field

cell membrane

electrolyte reservoir plate

H_2 flow field

gas barrier

electrolyte reservoir plate

teflon plate

H_2O flow field

H_2O vapor outflow
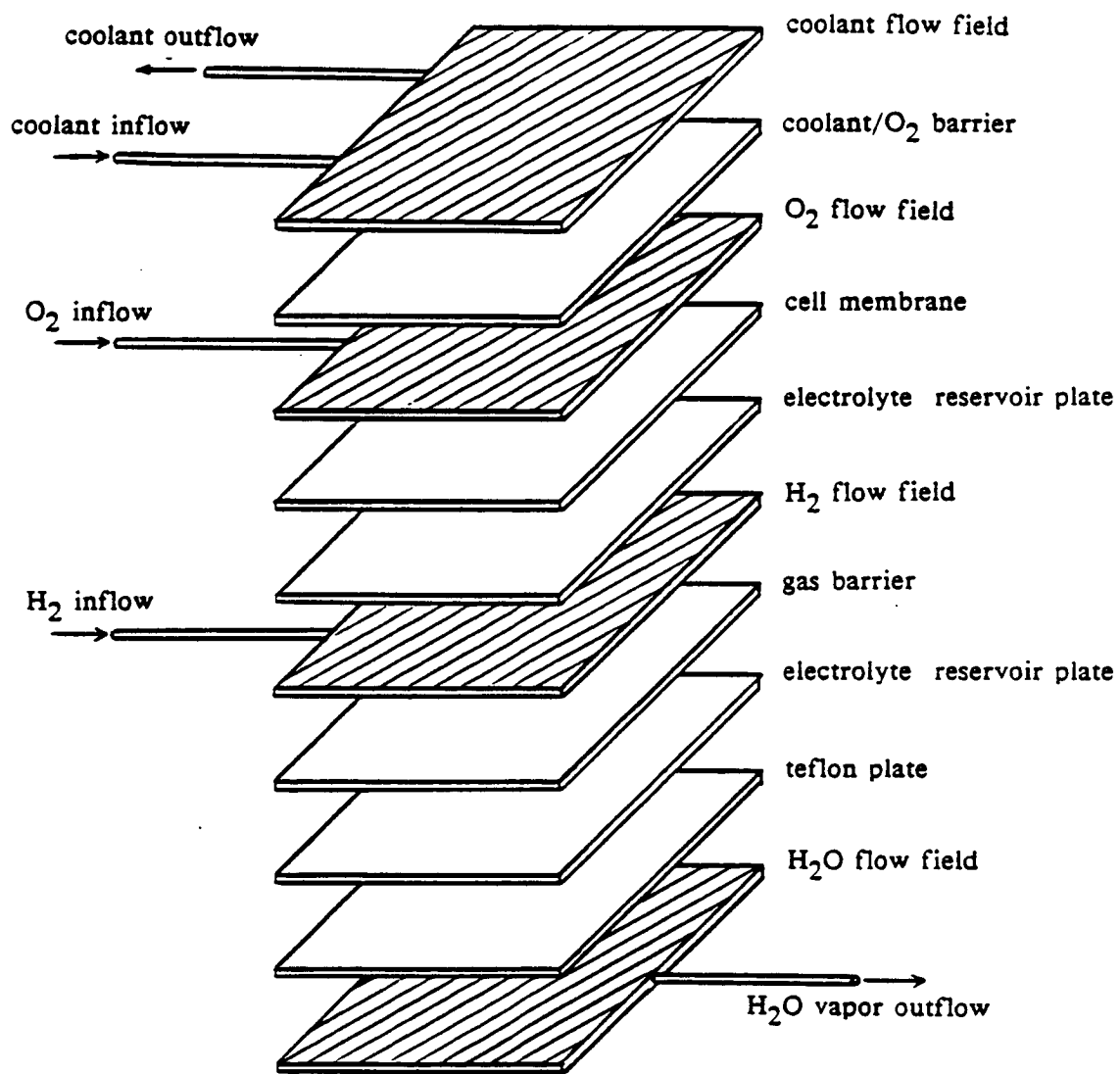
Figure 8.4.1

The removal of the product water from the electrolyte is necessary in order to prevent performance loss through dilution and to provide an outlet for the fuel mass flow. Active water removal systems employ hydrogen to "blow out" the water from the cell. A loss in efficiency occurs with the loss of the hydrogen fuel. Passive water removal systems consist of an asbestos gas barrier and a porous Teflon electrolyte barrier. The asbestos sheet provides a gas seal and a low resistance pathway for the diffusion of the water. The Teflon screen is a hydrophobic membrane that maintains the separation between the electrolyte and water despite the great difference in absolute pressure. A vacuum is required in order to draw the water through the membrane. The collected water vapor is condensed and pumped to the crew compartment for use. Passive water removal requires the use of electrically non-conducting plastic cell components and edge current transfer pathways.

Based on a cell voltage of .9V, a stack of thirty cells would provide approximately 27V of electromotive force. A voltage in the range of 20 to 30 volts allows conducting wires to be reasonably small while still minimizing the possibility of arcing in the spacecraft environment. Because the partial pressure of oxygen is generally quite high in spacecraft, the danger of arcing is an important design consideration.

A 20kW output at 27V requires a total current of nearly 750A. Using four stacks, the current output would be 187.5A per stack. Based on a current density of 200 A/ft^2 (2150 A/m^2) the corresponding membrane area (per stack) is .94 ft^2 (.0872 m^2). The volume of the total cell structure would be approximately 9.89 ft^3 (.28 m^3) using a specific volume of .50 ft^3/kW (.014 m^3/kW). Each stack would be approximately 1.0 by 1.0 feet (.30 x .30 meters) square and 2.6 feet (.80 meters) high. The resulting package would be approximately 2.0 x 2.0 x 2.6 feet (.60 x .60 x .80 meters) for a side-by-side arrangement including fuel connections and coolant circulation piping.

The radiator panel design shown in Fig. 8.4.2 provides multiple-redundant pathways for the coolant flow. Cut-off valves on each of the parallel circuits prevent the occurrence of a catastrophic loss of fluid by allowing the flow to be re-routed. The panel area of 107.6 ft^2 (10 m^2) is designed to provide a maximum of 6 kW heat rejection at a 170°F (77°C) coolant inlet temperature. The additional heat dissipation capacity built into the system allows full power operation of the fuel cells up to a damage level of 30% of full capacity. The coolant tubes chosen for this panel provide 99% protection from particle damage over a five year mission. The total mass of the radiator is approximately 110 lb (50 kg).

8.4.2 Radioisotopic Thermionic Generators

An RTG consists of a fuel core, an energy conversion section, a radiation shield, and an outer protective shell (Fig. 8.4.3). Based on the projected improvement in power density to 4.54 W/lb, a 4 kW system will have a mass of 880 lb and will occupy a volume of 32.1 ft^3 (.91 m^3). The four RTGs can be placed in a stack 1.8 feet in diameter and 13.1 feet high (.54 meters by 4 meters high). Each of the four units will supply 1000 kW over a design lifetime of five years. Replacement of the RTGs will thus be required every two round-trip missions. All of the waste heat is rejected by radiation fins fixed to the protective shell.

8.4.3 Batteries

A total of 1.35 kWh of Ni-H$_2$ battery storage is included in the total power system to provide emergency power. The battery array has a mass of 50 kg and is attached near the fuel cell pod.

Fuel Cell Radiator

cut-off valves

parallel coolant passages

coolant inflow

bypass valve

coolant outflow

8.8 ft

5.5 ft
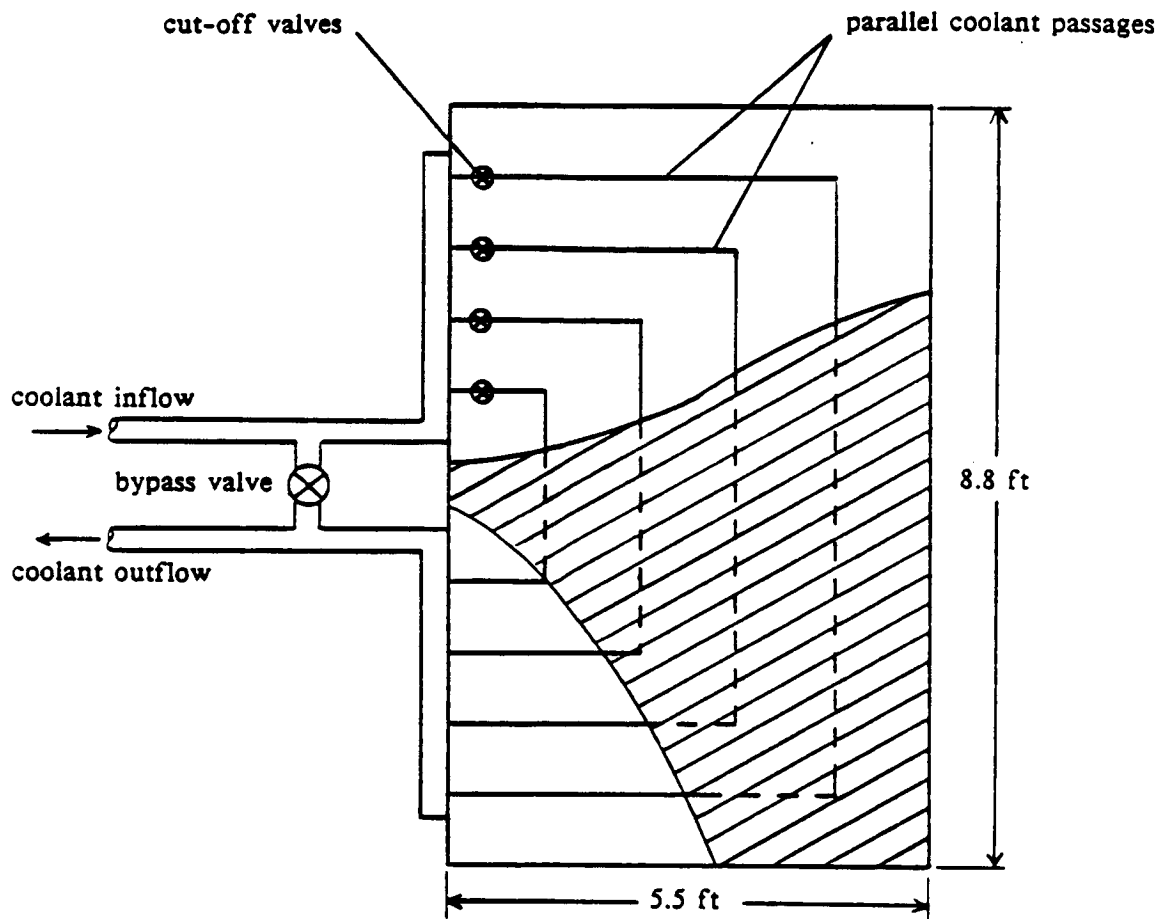
Figure 8.4.2

Radioisotopic Thermionic Generator (RTG)

3.3 ft

1.8 ft

thermionic conversion units

insulation

radioisotope fuel capsules

protective shell

fuel containment shell

radiator fin
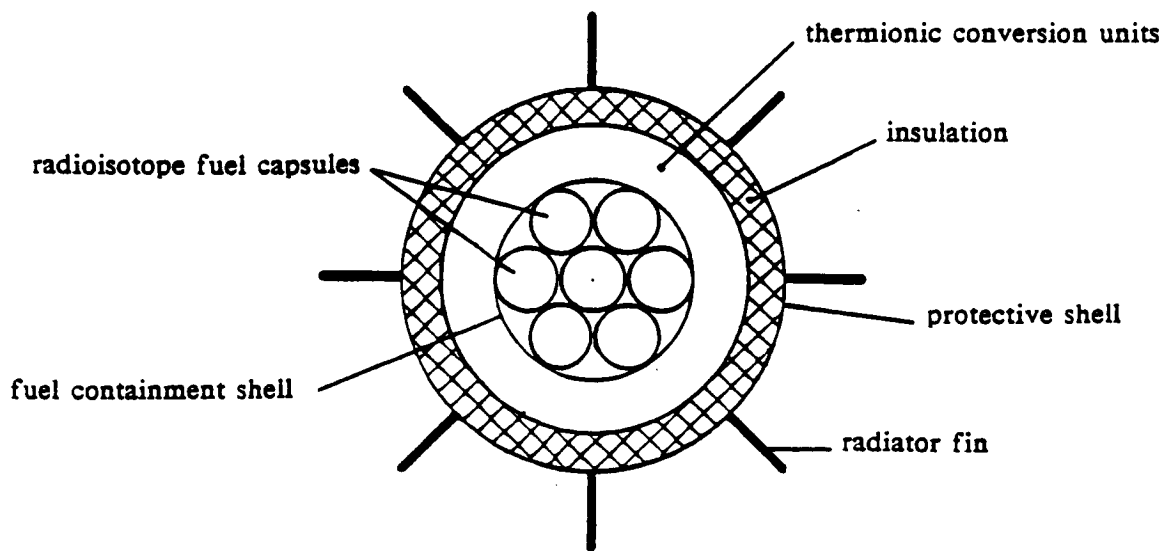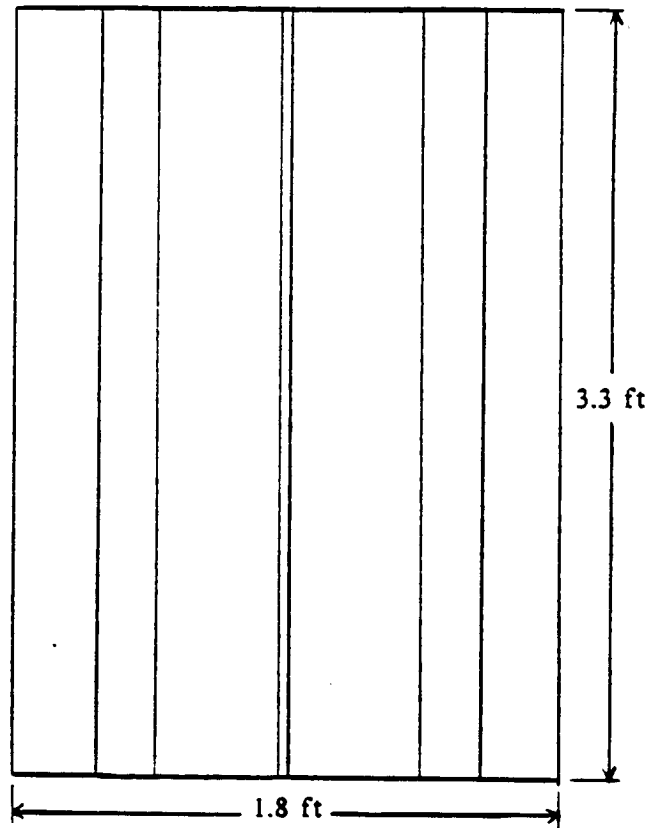
Figure 8.4.3

8.5 Packaging

The fuel cell is housed in a double-walled aluminum shell to provide protection from meteoroid strikes and radiation (Fig. 8.5.1) Each of the walls is .06 inches (.15 cm) thick. With a separation distance of 4.0 inches (10 cm) the shell should provide 99% particle protection and reject or dissipate over 97% of the incident radiation. The fuel cell system is hard mounted to the vehicle truss structure. The inner shell is 3.3 feet in diameter and 3.3 feet tall and has a mass of 259.6 lb (118.0 kg). The outer shell is 3.94 feet in diameter and 3.94 feet tall and has a mass of 328.5 lb (149.3 kg). The mounting apparatus is estimated to have a mass of 44 lb (10 kg). As previously mentioned, the RTG stack is self-contained.

8.6 Power Distribution System

The schematic of the power distribution network given in Fig. 8.6.1 shows the parallel input from the fuel cell and RTG units into the system. The RTGs operate continuously at 4 kW. The primary power management module adjusts the fuel cell output to load requirements to minimize fuel consumption. The auxiliary power management module can assume all control functions in the event of a primary system failure. At all levels of control provisions are included to allow a manual override of autonomous functions in case of software or hardware malfunctions. It is important to note that the fuel cell system is designed to be self-starting. If an RTG failure occurs during a dormant fuel cell period, the batteries can assist in re-start by powering the fuel preheaters if necessary.

Discussion for a new U.S. space station has involved the use of a 24-volt rather than a 12-volt power supply. This allows the use of more compact motors and equipment and reduces the size of the conductors by reducing the current. It is expected that use of a 24V power supply for the U.S. space program will be standard in the twenty-first century. Therefore, the power conditioners and voltage regulators for the TAXI are designated to supply power at 24V. It is expected that ordinary metallic conductors will be used for power transmission.

Fuel Cell Containment Package
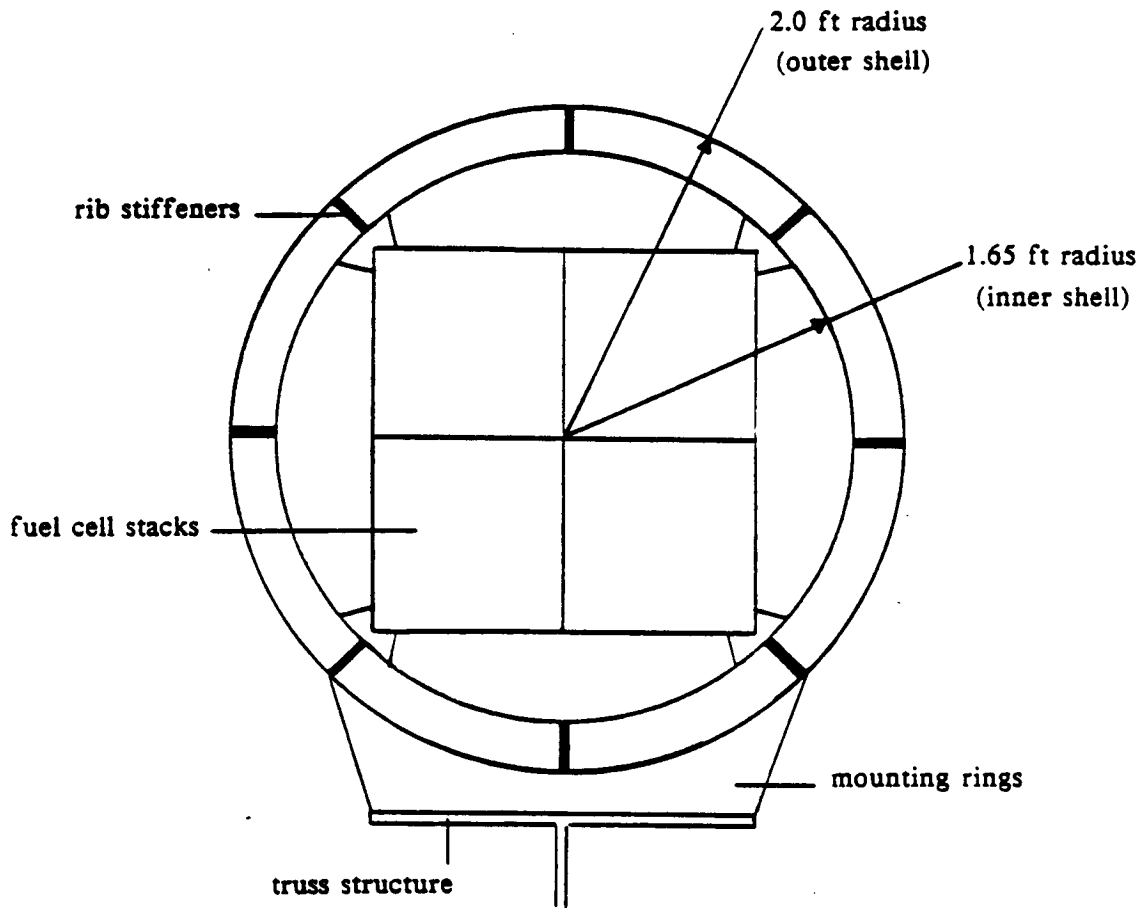
Figure 8.5.1

Schematic of Power Distribution System
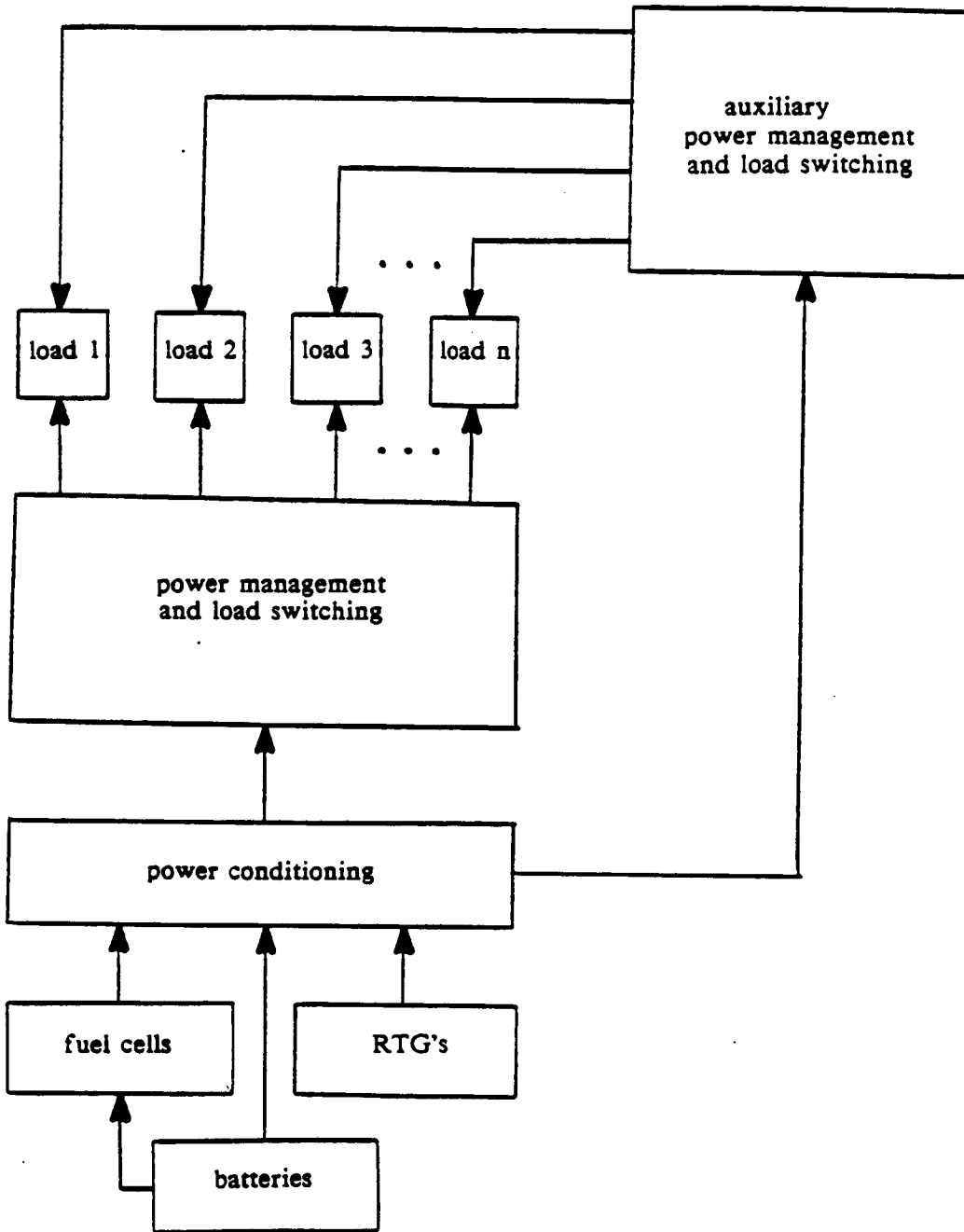
Figure 8.5.1

Table 8.1 Power System Specifications

Power output (max):

fuel cell generator (four stacks)	20.0 kW
radioisotopic thermionic generators	4.0 kW
Total:	24.0 kW

Mass:

fuel cell generator	400.0 lbm (181.8 kg)
fuel cell reactants*	3391.3 lbm (1541.5 kg)
shells and connectors	632.1 lbm (287.3 kg)
fuel cell radiator panel	110.0 lbm (50.0 kg)
radioisotopic generators	880.0 lbm (400.0 kg)
emergency batteries (Ni-H$_2$)	110.0 lbm (50.0 kg)
Total	5523.3 lbm (2510.6 kg)

*This mass of fuel will supply the estimated requirement of 4235 kWh of energy at a consumption rate of .80 lb/kWh.

8.7 References

POWER TECHNOLOGY. George E. Stephenson, Delmar Publishing Inc., 1973.

SPACE SYSTEMS TECHNOLOGY SP-593. Society of Automotive Engineers, Warrendale, Pa., 1984.

TECHNOLOGY FOR LARGE SPACE SYSTEMS. NASA, Washington, D.C.,1979.

RADIOISOTOPIC POWER GENERATION. William R. Corliss and Douglas G.Harvey, Prentice-Hall Inc., 1964.

THE CURRENT STATUS OF ION-EXCHANGE MEMBRANE FUEL CELLS. L.W. Niedrach & W.T. Grubb, 1971.

14th INTERSOCIETY ENERGY CONVERSION CONFERENCE. American Chemical Society, Vol. I & II, 1979.

"MANNED-UNMANNED LUNAR EXPLORER." University of Houston, September, 1970.

"HIGH-POWER SOLAR ARRAY (HPSA) STUDY." G.J. Hegemans, Royal Netherlands Aircraft Factories, 1985.

"SPACE SHUTTLE ELECTRICAL POWER GENERATION AND REACTANT SUPPLY SYSTEM." W.E. Simon, NASA Johnson Space Center, 1985.

"ADVANCED TECHNOLOGY LIGHTWEIGHT FUEL CELL PROGRAM: FINAL REPORT" R.E. Martin, United Technologies Corporation NASA CR-165417, 1980.

9. TAXI Assembly/Missions Schedule/Cost Analysis/Social, Political and Economic Considerations

9.1 TAXI Assembly

To outline a plan for the assembly and preparation of the TAXI, we use one major assumption: the various components (crew module, propellant tanks, structural members, engines, and aeroshield thermal protection system) will be manufactured on Earth and transported to LEO and then assembled into the final TAXI vehicle at the Space Station.

The time-frame for operation of the TAXI (2025-2040) has been placed beyond the operating lifetime of the current generation of Earth launch vehicles such as the Space Shuttle. Thus, for purposes of this discussion we shall base our estimates on two types of potential future launch vehicles: SDV-3R (Shuttle Derived Vehicle) and a HLLV (Heavy Lift Launch Vehicle) concept (NASA M001, 1985). The payload parameters for these two vehicles are as follows (for placement into a 270 n.mi 28.5° orbit):

SDV-3R: 183,000 lb, 25 ft dia x 90 ft

HLLV: 400,000 lb, 50 ft dia x 200 ft

For each of the TAXI versions, two plans will be outlined. The first involving the more near-term SDV-3R, and the other based on the farther future HLLV.

TAXI B

In the first launch plan scenario, one SDV would carry into orbit one fully loaded LOX tank, four fully loaded LH2 tanks, 2 engines, a few sections of the aeroshield TPS[*] and most if not all the structural members of the framework. Another SDV would carry the second fully fueled LOX tank and all the remaining components of the TAXI B including the crew module, third engine, RCS, GNC, communications and power system modules, remaining TPS sections and payload modules. Thus each TAXI B vehicle will require a maximum of two SDV-3R launches to place all its components in orbit for assembly.

In a launch scenario utilizing the HLLV concept, the entire set of TAXI B components can be fitted into one single HLLV. As a matter of fact, in this scenario, most of the components can be fitted to their support frames and combined into just a few assemblies prior to launching them into orbit. This would sharply reduce the assembly operations to be done in LEO.

---

[*] A brief discussion of launch packing considerations for the aeroshield TPS and structural components is given in subsection 4.5.8 and 4.6.2.

TAXI C

In the first launch scenario, one SDV would carry into orbit three fully loaded hydrogen tanks, one partially fueled (up to about 123,000 lbs) LOX tank, one engine and about one half of the aeroshield TPS. Another SDV would carry the second LOX tank, partially fueled up to about 103,000 lbs, and all the remaining TAXI C components including the fourth fully fueled LH2 tank, crew module, etc. If additional liquid oxygen is needed[*], it must either be shipped to orbit on a third SDV or be brought to LEO from a possible production facility on the Moon. Thus each TAXI C vehicle will nominally require two SDV-3R launches to place all its components in orbit for assembly, with possibly a third one to lift the additional liquid oxygen.

In a launch scenario utilizing HLLV vehicle, the entire set of TAXI C components can be fitted into one single HLLV provided that the LOX tanks will be fueled partially up to about 320,000 lbs. If additional liquid oxygen is required, it must be shipped to orbit in one SDV-3R (with plenty of spare space which can be utilized for lifting various equipment or material to LEO) or else be brought to Earth from the Moon. Thus the nominal number of HLLV launches per TAXI C is only one with a maximum of one HLLV and one SDV-3R ever needed for placement of components into LEO.

Once in orbit the structural members of the aerobrake frame, already partially assembled, will be fully assembled and the ribbing and thermal protection system will be attached as mentioned in chapter 4 to complete the first phase of construction. Once the aerobrake portion of the vehicle has been assembled and fully examined to assure soundness of all joints, fittings and members, the partially pre-assembled engine support frames will be connected to the aerobrake frame. Then the LOX and LH2 tanks can be fitted to their support frames and placed into their positions in the aerobrake frame. Following this the engines and propellant feed systems will be connected to the tanks and the engine support frames. After this second phase of assembly the vehicle is again examined for integrity of construction. The third and final phase will involve attaching the crew module and its support structure to the aerobrake structure and attaching all the other external systems (communications, RCS, power, GNC and payload modules). Again the vehicle must be inspected prior to approval for mission use and time allowed for final adjustments or repairs.

Estimates of actual assembly time are difficult to make at this time. Advances in space construction techniques, be they manned or robotic, currently await the deployment of the NASA Space Station. However,

---

[*] For a mission based on the nominal trajectory of the cycling ship (University of Michigan, 1987), about 148,000 lbs of additional LOX would be needed.

given substantial prefabrication on Earth, the in-orbit assembly time for each TAXI probably should not exceed 3 months. The major portion of any assembly time will most certainly be taken up by preparation of the aeroshield, its TPS and support structure followed by connection of the engine and propellant feed systems.

Reference:

NASA M001, Duke et al, "Manned Mars Missions: Working Group Summary Report", NASA Los Alamos, May 1986.

9.2 Missions Schedule

Since the University of Michigan is designing a single cycling spacecraft to be placed in orbit around the sun, the schedule of missions to the Mars system is relatively simple to compute. The arrangement of the Earth with respect to Mars repeats itself every 5472 days or about 15 years so that the mission scheduling also follows this cycle. Table 9.2.1 shows the encounter times of the cycling spacecraft at Mars and Earth and also includes the maneuvering dates for reference. The TAXI should launch from planetary orbit in a time frame 3 or 4 days long centered around the encounter line. Of course, the TAXI should launch from orbit as close to the optimum date as possible since any deviation from this results in a greater required delta-V to rendezvous with the cycling spacecraft.

Table 9.2.1 shows encounter times (optimum launch dates) for the era 2024 to 2040 since this is expected to be the operational phase of the Mars missions. There is a maximum of 7 possible missions during this time with an average mission length of around 4 years. The missions would overlap with one another; that is, one mission would leave Earth while the other was still at Mars. Using a single-cycling-ship scenario necessitates a minimum stay time at Mars of two years and a very long trip back to Earth. By deploying a second cycling ship in a mirrored, Down-Escalator orbit (Friedlander et al, AIAA 86-2009), the return trip duration can be brought down to the same duration as the trip to Mars. Additional missions would be possible by using two cycling ships in conjunction with one another. One of the cycling ships would be slightly precessed behind the other in their orbits around the sun. The TAXI would dock with the leading cycling spacecraft for a trip to Mars and then rendezvous with the trailing spacecraft for a trip back to Earth. Such missions scenario would allow the reduction of the stay time at Mars to a short (4 to 5 weeks) duration.

TABLE 9.2.1: MISSION SCHEDULING DATES

Earth	24 January	2024	begin mission #1
Mars	20 May	2024	
CS maneuver*	25 January	2025	
Earth	12 March	2026	begin mission #2
Mars	20 August	2026	
CS maneuver	31 March	2027	
Earth	13 May	2028	end mission #1 begin mission #3
Mars	23 November	2028	
Earth	18 June	2030	end mission #2 begin mission #4
Mars	05 December	2030	
Earth	21 July	2032	end mission #3 begin mission #5
Mars	04 January	2033	
Earth	03 September	2034	end mission #4 begin mission #6
Mars	31 January	2035	
Earth	11 October	2036	end mission #5 begin mission #7
Mars	09 March	2037	
CS maneuver	15 November	2037	
Earth	19 January	2039	end mission #6
Mars	14 May	2039	
CS maneuver	19 January	2040	
Earth	06 March	2041	end mission #7

* CS stands for cycling spacecraft

9.3 Cost Analysis

As a general rule, the more complex and technically involved a particular engineering project is, the more difficult it is to put a price tag on it. When dealing with hundreds or thousands of separate contractors for various systems of a project such as a spacecraft to be built at several different locations over perhaps a ten year period, the problem seems almost insurmountable. Various cost-analysis models have been developed, even some for interplanetary manned missions; however, most of these models were much too in-depth for our purposes as we only wanted a rough estimate of the mission cost.

The model we chose to base our cost estimate on uses a recurring/non-recurring labor hours algorithm to figure the direct labor hours involved in three major categories: flight hardware, development & support systems and flight project. This model was developed by taking existing data from thirteen unmanned lunar and planetary probes from the 60's and 70's and fitting various data to general formulas. The missions used as the basis for this model are listed below.

Mariner Mars 1964
Surveyor
Lunar Orbiter
Mariner Mars 1969
Mariner Mars 1971
Pioneer Jupiter/Saturn
Mariner Venus/Mercury 1973
Viking Lander capsule
Viking Orbiter
Voyager
Pioneer Venus:
   a)large probe
   b)small probe
   c)bus/orbiter

Since this model was developed by correlating data from a series of unmanned probes, various aspects of the model had to be altered for our specific mission. For example, since the model only considers unmanned spacecraft, a factor had to be introduced to consider the manned portion of our mission. Also, the materials for our craft will be launched to a space station in low Earth orbit where they will be constructed. This obviously will be considerably more expensive than construction on Earth, although major systems will be modularized for efficiency and economy.

The model considers 23 different components, some too detailed or unneccesary for our purpose but included anyway.

TABLE 9.4.1 COST ANALYSIS MODEL (ALTERED VERSION)

I)   flight hardware

II) development/support systems

III) flight project

IV) material launch & space construction

V)   crew considerations

Several of the formulas had to be altered from those given in the referenced report because they were exponential in form and tended to become extremely large when N, the number of spacecraft being constructed, was other than unity. They were changed from being exponential with respect to N to being linear. Since the maximum number of craft being considered for construction is five, a marginally small number, it is assumed that the deviation will not be disastrous.

The algorithms listed below output the direct labor hours (DLH) involved with that particular system in thousands of hours. To obtain the labor cost the DLH must be multiplied by the cost-to-labor ratio (CLR). To obtain the total cost of each system from the labor cost, the CLR is multiplied by the total-to-labor cost ratio (TLC).

Thus, TOTAL COST = DLH*CLR*TLC for each subsystem.

By using the above data in conjunction with the masses, mission and encounter duration times and the number of craft being constructed, a final cost can be calculated. As stated before, this model did not originally consider manned missions, so in order to accomodate this we are assuming that the life support systems, crew module and other necessities will have a linear relationship with the total cost of the flight hardware. We assume that the manned craft hardware will cost 40% more than the unmanned craft would, not only in additional hardware but in increased factors of safety.

The cost of launching the vehicle materials to the space station in LEO was assumed to be 500 1987 dollars per pound or adjusted to 1977 (base year for this cost estimate) dollars, 309 dollars per pound.

The cost of construction of the TAXI at the space station is difficult to estimate. Initially it will be very high, but as the program progresses and extra-vehicular activities become more commonplace the cost will drop drastically. For the purposes of a rough estimate we have assumed that the cost of constructing the major modularized components in LEO is 10% of the total cost of the flight hardware.

TABLE 9.4.2: SUMMARY OF COST MODEL ALGORITHMS

I) FLIGHT HARDWARE

structures & devices	$DLH=1.626(NM)^{.9046}$
thermal control, cabling	$DLH=Ne^{(4.2702+.00608M)}$
propulsion	$DLH=56.1878(NM)^{.4166}$
attitude control	$DLH=4.68(NM)^{.723}$
telecommunications	$DLH=4.471(NM)^{1.1306}$
antennas	$DLH=6.093(NM)^{1.1348}$
command & data handling	$DLH=Ne^{(4.2605+.02414M)}$
main power	$DLH=65.3(NM)^{.3554}$
battery power	$DLH=Ne^{(3.9633+.00911M)}$
aerobraking shield	$DLH=3.481(NM)^{.8416}$
landing radar/altimeter	$DLH=11.409(NM)^{.9579}$
line-scan imaging	$DLH=10.069(NM)^{1.257}$
vidicon imaging	$DLH=4.463(NM)^{1.0369}$
particle & field instr.	$DLH=25.948(NM)^{.7215}$
remote sensing instr.	$DLH=25.948(NM)^{.599}$
direct sensing/sampling	$DLH=6.173(NM)^{1.2737}$

II) DEVELOPMENT/SUPPORT SYSTEMS

system support/ground equ.	DLH=.36172(sum of DLH hardware)
launch + 30 days oper.	DLH=.09808(sum of DLH hardware)
imaging data development	$DLH=.00124(PPL)^{1.629}$
science data development	DLH=27.836(scientific DLH)
program management	DLH=.10097(sum of previous DLH)

III) FLIGHT PROJECT

flight operations	$DLH=(\text{sum DLH hardware}/3600)^{.06}*$ (10.7MD + 27ED)
data analysis	DLH=.425(DLH flight operations)

IV) MATERIAL LAUNCH AND SPACE CONSTRUCTION

flight harware to LEO	TOTAL COST= 309 dollars/pound
fuel to LEO	TOTAL COST= 309 dollars/pound

V) CREW CONSIDERATIONS

crew consideration factor TOTAL COST=1.4(sum of hardware)

M = mass of sub-system
N = number of spacecraft to be built
PPL = pixals per line of imaging system
MD = mission duration
ED = encounter duration

TABLE 9.4.3: LABOR/COST CONVERSION FACTORS

COST CATEGORY	CLR	TLC
structures/devices	10.45	3.303
thermal control/cabling	10.26	3.317
propulsion	10.54	3.616
attitude control	10.63	3.347
telecommunications	9.99	3.352
antennas	9.96	3.466
command & data handling	9.68	3.163
main power	9.51	3.177
battery power	10.41	3.148
aerobraking shield	10.73	3.296
landing radar/altimeter	10.08	3.158
line-scan imaging	10.57	3.604
vidicon imaging	9.52	3.586
particle & field instr.	10.62	3.395
remote sensing instr.	10.65	3.286
direct sensing/sampler	9.55	3.454
system support/ground equip.	10.55	3.076
launch + 30 days	10.71	3.214
image data development	11.46	3.130
science data development	12.76	3.987
program mangement	11.57	2.685
flight operations	10.44	3.247
data analysis	10.44	3.425

TABLE 9.4.4: SUBSYSTEM COST BREAKDOWN FOR TAXI A

Sub system	DLH (k-hrs)	DLC FY'77$/man hr)	TOTAL $1000's
engine support	91.8	959.1	3,167.7
payload	3,309.5	34,584.5	114,232.5
CM support	486.2	5,080.5	16,781.0
tank support	701.6	7,331.6	24,216.4
rod shielding	3,521.3	36,797.1	121,541.0
skin	445.1	4,651.8	15,364.8
bumper	326.4	3,410.6	11,265.3
rings/stringers	999.6	10,445.4	35,501.1
airlock	174.7	1,826.1	6,031.7
misc	577.7	6,036.7	19,939.1
thermal control	1.6	16.6	55.3
engines/piping	2,222.0	23,420.1	84,687.1
tanks	1,520.4	16,025.1	57,946.6
RCS	1,481.4	15,747.1	52,705.6
GNC/comm	1,830.5	18,286.7	61,297.0
onboard comp	212.3	2,054.6	6,498.7
power cells	749.3	7,125.8	22,638.8
fuel cells	325.5	3,388.5	10,666.9
aerobrake	3,454.3	37,064.8	122,165.5
thermal system	4,619.5	49,566.9	163,372.5
	27,050.7	283,819.7	949,044.6

·TABLE 9.4.5 COST SUMMARY (TAXI A)

I) FLIGHT HARDWARE

Subsystem	DLH (k-hrs)	DLC FY'77$ (man hr)	TOTAL $1000's
total	27,050.7	283,819.7	949,044.6

II) DEVELOPMENT/SUPPORT SYSTEMS

	DLH (k-hrs)	DLC FY'77$ (man hr)	TOTAL $1000's
system support and ground equip.	8,103.3	85,468.9	262,902.4
launch + days oper.	302,653.1	28,415.1	91,326.0
program mmgt	2,695.8	31,190.1	83,745.5

III) FLIGHT PROJECT

	DLH (k-hrs)	DLC FY'77$ (man hr)	TOTAL $1000's
flight operations	2,601.7	27,161.8	88,194.5
data analysis	1,105.7	11,543.7	39,537.3

IV) MATERIAL LAUNCH AND SPACE CONSTRUCTION

	TOTAL $1000's
flight hardware	45,000.0
fuel	92,700.0

V) CREW CONSIDERATION

	TOTAL $1000's
flight hardware for crew systems	379,617.8

TOTAL COST: (1977 DOLLARS)   2,032,168.1

To account for inflation between 1977 and 1987 we apply a factor of 1.62. This gives total cost of one single TAXI A = 3,292 million 1987 dollars. The base price of 3,292 million 1987 dollars for the design, development and deployment of one TAXI A vehicle must be accepted as an approximate cost estimate since the cost analysis was done roughly and with little guidelines. The fuel weight is different for every mission so an average fuel cost and delivery to LEO was used based on 300,000 lbs of fuel. A good range of numbers for the cost estimate is anywhere between 3.3 and 4.5 billion 1987 dollars.

Rough cost projections for the design, development and deployment of TAXI B and C are listed below

    TAXI B: 2.5 - 3.3 billion 1987 dollars
    TAXI C: 3.1 - 4.3 billion 1987 dollars.

Note that these cost estimates are for deployment of one craft only; for the development and deployment of several such TAXIs the cost per craft can be expected to drop anywhere from 30 to 60 percent.

9.4 Social, Political and Economic Considerations

There are many who question the expenditure of vast amounts of public money on space research and operations, reasoning that we should turn our attention to solving social and economic problems on Earth before tackling new ones in space. What is not realized, however, is that indirectly, further space development may solve major problems on Earth in ways that we cannot even imagine now. There are millions living on the brink of starvation and disease; perhaps the scientific advancements surely gained through space exploration will find new ways to grow food, to cure sickness. The Earth is currently comprised of some 360 different nations each with different political idealisms and cultures; in the past such differences have led to aggravated relations between peoples and even war. Perhaps cooperation in the conquering of space will indirectly bring nations towards peaceful solution to problems at home.

These are only possible results; there is no way to predict that these will actually be realized. However, there are some aspects of space developments whose benefits can be directly and accurately forecasted. In terms of material wealth and scientific knowledge, there stands to be gained an enormous profit in the development of space. Those who aggressively pursue space research will later reap the rewards that it has to offer, and the rewards could be staggering. The economic benefits will affect Earth politics and economics in such a way that the very survival of certain political structures could be determined in space.

The conclusion to be reached about whether space travel is worth the enormous amount of money and effort it requires is that it is indeed of significant worth. At the present time, space research is justified by the need to maintain a competitive edge in a new frontier. History has shown that those societies who failed to aggressively exploit new horizons underwent total decline, both politically and economically. In the future, space operations will justify themselves by being tangibly profitable; until then, we must accept the challenge as simply being the grandest aspiration that mankind has yet had. As Sir Edmund Hillary once said, we must go forth in space "because it's there".

10. Design Summary

This report presents a conceptual design study of an aeroassisted orbital transfer vehicle, nicknamed TAXI, for ferrying personnel and cargo between: (a) low Earth orbit and a spacecraft circling around the sun in permanent orbits intersecting gravitational fields of Earth and Mars and (b) Mars orbiting station (co-orbiting with Phobos) and the cycling spacecraft.

The starting date for the operation of such an advanced Mars transportation system is assumed to be around 2025. Throughout the design process, considerations of crew safety and mission flexibility (in terms of ability to provide a wide range of ΔV) were generally given higher priority than any other considerations. Three versions of the TAXI are considered. They use the same overall configuration based on a low L/D aerobrake and three gimbaled LOX/LH2 engines firing away from the aerobrake. The versions differ mainly in the size of aeroshields and propellant tanks. TAXI A version resulted from an initial effort to design a single transfer vehicle able to meet all possible ΔV requirements during a 15-year period of Mars mission operations. TAXI B version represents a transfer vehicle designed to function with the cycling spacecraft moving in a simplified, "nominal" trajectory, proposed by the University of Michigan design team, which designed the cycling spacecraft. In real-world, actual Mars missions, the TAXI B would be able to meet the requirements of all the missions, for which the relative approach velocity near Mars is less than 9.3 km/sec. Finally, TAXI C is a revised version of the TAXI A and defines a transfer vehicle capable to serve in those missions for which the relative approach velocity near Mars is larger than 9.3 km/sec. All versions are designed to carry a crew of 9 (or possibly 11 with some modifications) and a cargo of 10,000 lbm. Trip duration varies from about 1 day for transfer from LEO to the cycling ship to nearly 5 days for transfer from the cycling ship to the Phobos orbit.

The mass breakdown of the TAXIs A, B, and C is given in Table 10.1 and the characteristics of the TAXIs are summarized in Table 10.2.

Table 10.1 Vehicle Mass Breakdown

Component	Mass, lbm		
	TAXI A	TAXI B	TAXI C
Aeroshield TPS	11,300	5,420	7,860
Aeroshield support structure	8,600	4,370	6,260
Crew module	20,000	20,000	20,000
Crew module support structure	1,200	600	650
Main engines (3) + Ancillary systems + engine supports	15,200	11,800	16,500
Propellant feed systems		1,200	1,600
Propellant tanks	6,035	3,800	5,500
Tank support structures	1,800	1,100	1,300
RCS	6,000	3,600	4,700
GNC and communications modules	1,100	1,100	1,100
Power system	2,130	2,130	2,130
Cargo	10,000	10,000	10,000
Vehicle mass without LOX/LH2 propellant ("dry" mass including RCS propellant) .	83,365	65,120	77,600
Reserve and residual LOX/LH2 propellant, propellant for consumption in fuel cells	19,784	11,000	15,000
Max total LOX/LH2 propellant	677,000	285,702	605,000
Max initial vehicle mass	760,365	350,822	682,600

Table 10.2 Vehicle Specifications

Item	Vehicle		
	TAXI A	TAXI B	TAXI C
Crew size		9 (max 11)	
Cargo capacity		10,000 lbm	
Transfer duration		typically 1-5 days (max 7 days)	
ΔV Range			
Propulsive	4.9-9.5 km/s	4.9-7.3 km/s	4.9-9.5 km/s
Aeroassisted	1.8-5.5 km/s	1.8-5.5 km/s	1.8-5.5 km/s
Main propulsion:			
#/engine type	3/LOX-LH2	3/LOX-LH2	3/LOX-LH2
Isp	485 sec	485 sec	485 sec
Design Thrust	315,000 lbf	220,000 lbf	315,000 lbf
Mixture ratio, LOX/LH2	6	6	6
Throttling range	40% - 120%	40% - 100%	40% - 110%
Aerobrake:			
Geometry		Ellipsoidally-blunted raked-off cone with a toroidal skirt	
Diameter	120 ft	80 ft	100 ft
L/D	0.153	0.153	0.153
$M_{BAM}/C_D A$	6.26 lbm/ft^2	9.15 lbm/ft^2	8.05 lbm/ft^2
Thermal protection system		Flexible ceramic TPS on shape defining truss	
TPS materials		Colloidal particulate coating, Nicolon, Q-felt	
Structural materials		Graphite polymide, titanium joints	
Reaction control system		24 main and 12 vernier thrusters	
Power system:			
Primary		20 kW H_2/O_2 fuel cells	
Backup		4 kW radioisotopic thermionic generators	
Masses:			
Total dry mass (with RCS propellant)	83,365 lbm	65,120 lbm	77,600 lbm
Max total LOX/LH2 propellant	677,000 lbm	285,702 lbm	605,000 lbm
Max initial vehicle mass	760,365 lbm	350,822 lbm	682,600 lbm

11. Appendices

The appendices are numbered according to corresponding chapter numbers. The number following 11 indicates the chapter number.

11.3.1 Thermochemical Calculations

The thermochemical calculations used to justify the combustion chamber and nozzle performance parameters are derived from a thermochemical program produced by the Naval Ordinance Test Station (NOTS). The calculations justify attaining the Isp of 485 seconds at a combustion temperature of 6700 R, a combustion pressure of 2600 psi, an expansion ratio of 176 and a mixture ratio of 6:1 by weight (oxidizer:fuel). Sample results are shown below.

LH2/LO2,Pc=2600psi,MR=6,To1=6700R,Ae/At=176
AIR TOTAL TEMP = 6700   Po = 2600
INPUT MIXTURE   WT. % HF(C/MOLE)M.W.MOLECULAR FORMULA
1.000000   0.0   2.016 2.0000   H
1.000000   4600.0 32.000 2.0000   O
RESULTING GRAM ATOMS, 2 ELEMENTS ELEMENTAT. NO.AT. WT.VALGRAM ATOMS
        H   1   1.008   1.0   14.172337
        O   8   16.000   -2.0   5.357143
EQUIVALENCE RATIO   =   1.3228
STOIC FUEL/OX RATIO   =   0.1260
FUEL/OX RATIO(WF/WO)   =   0.1667
OX/FUEL RATIO(WO/WF)   =   6.0000
MIXTURE WT (GRAMS)   =   100.0000
MIXTURE ENTH (BTU/LB)   =   221.6407
ROC. EQ. FRAC.   =   0.5695
  ASSUMED PRODUCTS OF COMBUSTION

H2O(G)   H(G)   HO(G)   H2O(G)   O(G)   O2(R)
H2(R)

              REACTION/COMBUSTION AT   2600.00 PSIA

LH2/LO2,Pc=2600psi,MR=6,To1=6700R,Ae/At=176
AIR TOTAL TEMP = 6700   Po = 2600
PRESS (ATM)   176.919   SA(SEC)   0.00
TEMP (DEG.K)   3722.222   VELOCITY (FPS)   0.0
TEMP (DEG.F)   6240.600   MACH NO.   0.000
TEMP (DEG.R)   6700.000   SAR(SEC),ISPV   0.000
SENS. H (CAL/G)   2622.631   GAMMA   1.193
CHEM. H (CAL/G)   -2803.913   SOUND SPEED (FPS)   5399.4
ENTHALPY H (CAL/G)   -181.282   A/ASTAR   1000000.000
ENTROPY(CAL(G-K))   4.2062   WO/WF   6.0000
MOL. WT.(LB/LB-MOL)   13.632   A/W FT**2/(LB/SEC   0.0000E+00
DENSITY(LB/FT**3) 0.493081152   PERCENT CONDENSED   0.00
CSTAR (FPS)   0.0   ISP(PO=PE),SEC   0.000
    GAS COMPOSITION
    TOTAL GAS MOLES=   7.335450   P/FN   =   0.068046
        PRODUCTS   MOLE-PCT   PARTIAL   WEIGHT   MOLE   MOLECULAR
          GAS   OF GAS   PRESSURE   PCT   /100-GM   WEIGHT
    1 H2O(G)   34.9551   0.17448E+00 46.1951 2.564113   18.016   1
    2 H(G)   3.4514   0.17227E-01   0.2552 0.253174   1.008   2
    3 HO(G)   2.6393   0.13174E-01   3.2928 0.193602   17.008   3
    4 H2O(G)   34.9543   0.17447E+00 46.1940 2.564055   18.016   4
    5 O(G)   0.2238   0.11170E-02   0.2627 0.016416   16.000   5
    6 O2(R)   0.1292   0.64496E-03   0.3033 0.009478   32.000   6
    7 H2(R)   23.6470   0.11803E+00   3.4970 1.734612   2.016   7

SONIC/THROATH   (EQUILIBRIUM)

LH2/LO2,Pc=2600psi,MR=6,To1=6700R,Ae/At=176
  AIR TOTAL TEMP = 6700   Po = 2600
PRESS (ATM)   96.421   SA(SEC)   346.64
TEMP (DEG.K)   3466.469   VELOCITY (FPS)   5339.1
TEMP (DEG.F)   5780.245   MACH NO.   1.030
TEMP (DEG.R)   6239.645   SAR(SEC),ISPV   297.120
SENS. H (CAL/G)   2390.050   GAMMA   1.193
CHEM. H (CAL/G)   -2887.720   SOUND SPEED (FPS)   5185.6
ENTHALPY H (CAL/G)   -497.670   A/ASTAR   1.000
ENTROPY(CAL(G-K))   4.2062   WO/WF   6.0000
MOL. WT.(LB/LB-MOL)   13.764   A/W FT**2/(LB/SEC   0.6429E-03
DENSITY(LB/FT**3)   0.291346848   PERCENT CONDENSED   0.00
CSTAR (FPS)   7744.0   ISP(PO=PE),SEC   165.943
        GAS COMPOSITION
        TOTAL GAS MOLES=   7.265179   P/FN   =   0.068046
        PRODUCTS   MOLE-PCT   PARTIAL   WEIGHT   MOLE   MOLECULAR
          GAS   OF GAS   PRESSURE   PCT   /100-GM   WEIGHT
    1 H2O(G)   35.8147   0.17706E+00   46.8777   2.602002   18.016   1
    2 H(G)   2.6956   0.13326E-01   0.1974   0.195839   1.008   2
    3 HO(G)   1.8364   0.90785E-02   2.2692   0.133418   17.008   3
    4 H2O(G)   35.8143   0.17705E+00   46.8771   2.601973   18.016   4
    5 O(G)   0.1241   0.61360E-03   0.1443   0.009017   16.000   5
    6 O2(R)   0.0739   0.36512E-03   0.1717   0.005366   32.000   6
    7 H2(R)   23.6410   0.11687E+00   3.4626   1.717564   2.016   7

        EXPANSION (EQUILIBRIUM)

LH2/LO2,Pc=2600psi,MR=6,To1=6700R,Ae/At=176
  AIR TOTAL TEMP = 6700   Po = 2600
PRESS (ATM)   0.055   SA(SEC)   563.60
TEMP (DEG.K)   1006.946   VELOCITY (FPS)   15120.6
TEMP (DEG.F)   1353.103   MACH NO.   5.353
TEMP (DEG.R)   1812.503   SAR(SEC),ISPV   483.086
SENS. H (CAL/G)   377.408   GAMMA   1.250
CHEM. H (CAL/G)   -3096.320   SOUND SPEED (FPS)   2824.6
ENTHALPY H (CAL/G)   -2718.911   A/ASTAR   176.118
ENTROPY(CAL(G-K))   4.2062   WO/WF   6.0000
MOL. WT.(LB/LB-MOL)   14.112   A/W FT**2/(LB/SEC   0.1132E+00
DENSITY(LB/FT**3)   0.000584119   PERCENT CONDENSED   0.00
CSTAR (FPS)   1363863.6   ISP(PO=PE),SEC   469.963
        GAS COMPOSITION
        TOTAL GAS MOLES=   7.086168   P/FN   =   0.068046
        PRODUCTS   MOLE-PCT   PARTIAL   WEIGHT   MOLE   MOLECULAR
          GAS   OF GAS   PRESSURE   PCT   /100-GM   WEIGHT
    1 H2O(G)   37.8001   0.18227E+00   48.2573   2.678581   18.016   1
    2 H(G)   0.0000   0.27621E-08   0.0000   0.000000   1.008   2
    3 HO(G)   0.0000   0.79874E-11   0.0000   0.000000   17.008   3
    4 H2O(G)   37.7999   0.18226E+00   48.2570   2.678562   18.016   4
    5 O(G)   0.0000   0.23337E-18   0.0000   0.000000   16.000   5
    6 O2(R)   0.0000   0.17343E-18   0.0000   0.000000   32.000   6
    7 H2(R)   24.4000   0.11765E+00   3.4857   1.729026   2.016   7

223

11.3.2 Nozzle Contour

Table 11.3.1 lists the nozzle radius as a function of axial distance along the nozzle (TAXI A and C).

Table 11.3.1 Radius as a Function of Axial Distance (TAXI A and C)

Axial distance, x (in)	Radius r (in)
0	4.356
6	9.502
12	13.500
18	16.887
24	19.879
30	22.589
36	25.085
42	27.409
48	29.594
54	31.661
60	33.629
66	35.509
72	37.313
78	39.050
84	40.725
90	42.346
96	43.918
102	45.444
108	46.928
114	48.374
120	49.785
126	51.162
132	52.509
138	53.827
144	55.117
150	56.382
156	57.623
158.1	58.267

A parabolic equation approximating the nozzle contour is
$$(r + 8.9855)^2 = 27.3(x + 6.5199)$$

11.3.3 Tank Masses and Volumes

A program was written to estimate the fuel and oxidizer tank masses and volumes required for the TAXI vehicle. The major assumptions made about the tanks and their criteria were:

Shape: Spherical tanks were chosen for stress handling reasons (a sphere will handle the anticipated stresses more easily than a cylinder) and simplification of pumping procedures.

Materials: It was assumed that homogeneous materials (metal alloys) would be used, i.e., not composites.

Stresses: The program treats the tank as a pressure vessel, with a term added into the equation to estimate the load induced by the mass of the fluid on the tank walls during periods of acceleration.

Internal Baffling: The mass of slosh baffling has not been taken into account in this program. Before final decisions can be reached concerning tank masses, this must be accounted for.

For a single tank we have

$$\sigma_{max} = (\sigma_{pressure} + \sigma_{fluid})FS = \sigma_{allowable}$$

where

$\sigma_{pressure}$ = stress due to internal pressure
σ_{fluid} = approx. of stress due to acceleration of fluid mass
FS = factor of safety

The pressure stress term can be written as

$$\sigma_{pressure} = \frac{Pr}{2t}$$

where P = max internal pressure
r = mean radius of tank
t = thickness of tank wall

The difference between the mean radius and internal radius was considered insignificant because the radius is so large compared to the thickness.

The acceleration stress was approximated by

$$\sigma_{fluid} = \frac{fluid\ mass\ *\ max\ acceleration}{area\ on\ which\ force\ acts} = \frac{m*a}{area}$$

The thickness t becomes

$$t = \frac{0.5 \; Pr}{\dfrac{\sigma_{max}}{FS} - \dfrac{ma}{area}}$$

The maximum acceleration is a parameter whose constraints are determined by overall structural and human limitations, therefore it does not change from mission to mission. The area used was simply half of the surface area of the inside of the sphere. This is by no means an exact solution, simply a rough approximation. To find both the radius and the fluid mass the general rocket performance equation was used.

$$\Delta V = U_{eq} \; \ell n(m_{initial}/m_{final})$$

The useable propellant mass is

$$m_{propellant} = m_{final}[\exp(\Delta V/U_{eq}) - 1]$$

The total propellant mass includes reserve and residual propellant plus the propellant to be used by fuel cells.

The fuel and oxidizer masses are

$$M_{final} = m_{propellant}[1/(MR + 1)]$$

$$M_{oxidizer} = m_{propellant}[MR/(MR + 1)]$$

where

MR = mixture ratio = oxidizer to fuel ratio

The mass of fluid per tank and the tank radius can then be easily found.

The main inputs are:

Fuel (LH2) and oxidizer (LOX) tank material	TA-6AL-4V
Max tensile (yield) stress of tank material	1.2×10^5 psi
Factor of safety, FS	2.0
Max internal fuel and oxidizer tank pressure	5 psia
Insulation thickness	2 in
Insulation mass per unit area	0.463 lbm/ft^2

The main outputs are:

	TAXI A	TAXI B	TAXI C
Diameter of LH2 tank	21.9 ft	16.43 ft	21.1 ft
Calculated thickness of LH2 tank pressure vessel	0.0041 in	0.0030 in	0.0039 in
Diameter of LOX tank	19.88 ft	14.9 ft	19.14 ft
Calculated thickness of LOX tank pressure vessel	0.0038 in	0.0028 in	0.0037 in
Total tankage mass (pressure vessel + insulation)	4763.8 lbm	2651.2 lbm	4412.4 lbm

11.5.1 Crew Medical Training

Table 11.5.1, taken from Nicogossian and Parker ("Space Physiology and Medicine", NASA SP-447, 1982), lists the basic medical training each crew member should receive.

Table 11.5.1 STS-1 Crew Medical Training

VITAL SIGNS	Pulse, Blood Pressure, Temperature Respiratory Rate, Pupil Size and Reaction
PHYSICAL EXAMINATION AND TREATMENT:	
EYE	Opthalmoscopy, Lid Eversion, Foreign Body Reaction and Treatment, Fluorescein Staining
EAR	Otoscopy
NOSE	Control of Nose Bleeds
THROAT	Examination, Oral Airway Insertion
AUSCULATION	Heart, Lung and Bowel Sounds
EMERGENCY PROCEDURES	One-man CPR, Heimlich Maneuver, Cricothyrotomy
HEMORRHAGE CONTROL	Direct Pressure, Pressure Points, Tourniquets, Pressure Bandaging
BANDAGING	Extremities, Chest Abdomen
SPLINTING	Neck, Fingers, Upper and Lower Extremities
LACERATION TREATMENT	Bleeding Control, Steristrip Application
DENTAL PROCEDURES	Temporary Fillings, Gingival Injections
EKG	Use of OBS
MOTION SICKNESS	Prophylactic Medications, Treatment, Head Positioning and Movement
SOMS-A	Organization, Drug Usage, Medical Checklist Organization and Use

11.6.1 Propellant Tank and Engine Support Structures (TAXI A)

For the purpose of initial, rough estimates, it is assumed that the basic support structure for all propellant tanks and engines will be made of tubular truss members, fabricated of graphite polymide. The latter has the following properties:

Density	100 lbm/ft(1600 kg/m^3)	
Modulus of Elasticity	2.64 x 10^9 psf	(12.62 TPa)
Ultimate Tensile Strength	2.92 x 10^7 psf	(1.4 GPa)
Ultimate Compressive Strength	2.92 x 10^7 psf	(1.4 GPa)

In determining the cross-sectional area of the truss members, an initial guess was made and each structure was tested using "Structural Analysis Software for Microcomputers" by B.J. Korits. According to the results of each analysis and the requirements for preventing buckling and axial failures, a second guess was made. The program was run again with this new area and the results were analyzed. This process was repeated until an area was found that satisfied both failure criteria using a 1.5 factor of safety.

Based on the above procedure, two different cross-sectional areas were chosen. The larger members will be used to attach the hydrogen and oxygen tank structures to the aerobrake truss structure. These particular members will have to support the greatest load. The other smaller members surround the fuel tanks and provide support for the engines. The dimensions for both are given below.

Area	1.55 in^2	(10 cm^2)
Outer radius	3.0 in	(7.62 cm)
Inner radius	2.92 in	(7.41 cm)
I	6.73 in^4	(280 m^4)

Area	0.775 in^2	(5 cm^2)
Outer radius	3.0 in	(7.62 cm)
Inner radius	2.96 in	(7.51 cm)
I	3.6 in^4	(150 cm^4)

The cage supporting the fuel tanks and the structure supporting the engines can be seen in Figures 11.6.1, 11.6.2 and 11.6.3. The tank structure is square on top and bottom. Around the outside of the tank, an octagon shaped truss is used. Each member of the octagon is attached at a tangent to the surface of the tank. Cross members were added to each side of the squares. Other members lead from the corners of the square to one of the points of the octagon. The overall height of the oxygen tank cage is 19.2 ft (5.85 m) and the height of the hydrogen tank cage is 21.75 ft (6.63 m).

The fuel tanks and cages are placed in the aerobrake shield and connected to the aerobrake truss. The oxygen tank is set 9.6 ft (2.9 m) deep into the shield. It connects to the aerobrake truss at node points 17, 18, 19, and 20 (see Figure 11.6.1). The hydrogen tank is placed 3.9 ft (1.2 m) into the shield. The cage connects to the shield truss at node points 17, 18, 19, and 20 (see Figure 11.6.2).

The engine support structure consists of an equilateral triangular truss, with each of the three engines at one corner of the triangle (nodes 5, 6, 7 in Figure 11.6.3). This triangular plane is 12.0 ft (3.66 m) above the center of the aerobrake truss structure. The base of the structure is a square frame attached to the aerobrake structure at points 1, 2, 3, and 4.

Truss Analysis of Each Structure (TAXI A)

Case 1:

Thrusting (4 g)

Structure	Applied Load (N)	Maximum Overall Deflection
Oxygen tank	1,066,670.	0.228 in (0.58 cm)
Hydrogen tank	88,890.	0.150 in (0.38 cm)
Engine	270,000.	0.665 in (1.69 cm)

Case 2:

Aerobraking (3 g)

Structure	Applied Load (N)	Maximum Overall Deflection
Oxygen tank	143,333.	0.031 in (0.08 cm)
Hydrogen tank	11,666.	0.023 in (0.058 cm)
Engine	133,400.	0.307 in (0.78 cm)

Maximum Stress Condition

At Aerobraking

Mass:			
	LOX tank	21,500.0 lb (9,772.7 kg)	10,750.0 lb/tank (4,886.4 kg/tank)
	LH2 tank	3,500.0 lb (1,590.9 kg)	875.0 lb/tank (397.7 kg/tank)
	Engine	5,000.0 lb/engine (2,272 kg/engine)	

At Thrusting

Mass:			
	LOX tank	120,000.0 lb (54,545.5 lb)	60,000.0 lb/tank (27,272.7 kg/tank)
	LH2	20,000.0 lb (9,090.9 kg)	5,000.0 lb/tank (2,272.7 kg/tank)
	Engine	5,000.0 lb/engine (2,272 kg/engine)	

Structure Weight Analysis

Oxygen Tank Support Structure (Figure 11.6.1)

16 members @	11.5 ft	(3.5 m)
8 members @	13.0 ft	(3.96 m)
8 members @	9.7 ft	(2.95 m)
8 members @	7.7 ft	(2.36 m)
4 members @	6.6 ft	(2.0 m)
4 members @	12.5 ft	(3.8 m)
Total length =	503.1 ft	(153.4 m)

Mass = 280 lbm (127 kg)

Hydrogen Tank Support Structure (Figure 11.6.2)

|		
16 members @	13.8 ft	(4.2 m)
8 members @	15.4 ft	(4.7 m)
8 members @	11.5 ft	(3.5 m)
8 members @	9.2 ft	(2.8 m)
4 members @	8.0 ft	(2.45 m)
4 members @	9.3 ft	(2.84 m)
Total length =	578.0 ft	(176.36 m)

Mass = 310 lbm (140.6 kg)

Total structural mass of tank supports 1800 lbm (816.3 kg)

Engine Support Structure (Figure 11.6.3)

Member	Length (ft)	(m)
1,5 and 2,6	13.5 ft	(4.1 m)
1,7 and 2,7	24.6 ft	(7.5 m)
3,7 and 4,7	18.0 ft	(5.5 m)
5,6; 5,7 and 6,7	13.6 ft	(4.14 m)
5,8 and 6,8	15.1 ft	(4.6 m)
5,9 and 5,10	22.6 ft	(6.9 m)
6,9	13.7 ft	(4.18 m)
7,9 and 7,10	18.6 ft	(5.68 m)
7,11 and 7,12	14.1 ft	(4.3 m)
Total Length	298.7 ft	(91.04 m)
Total Mass	171.6 lbm	(72.8 kg)

Oxygen Tank Structure
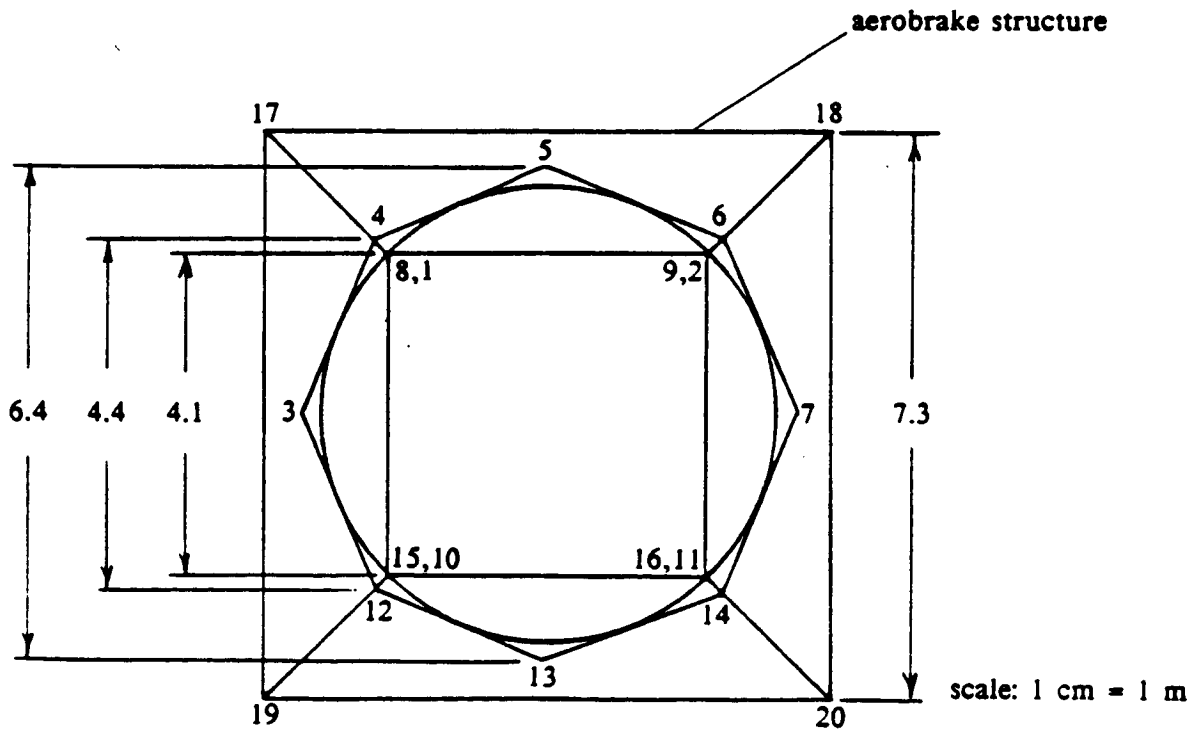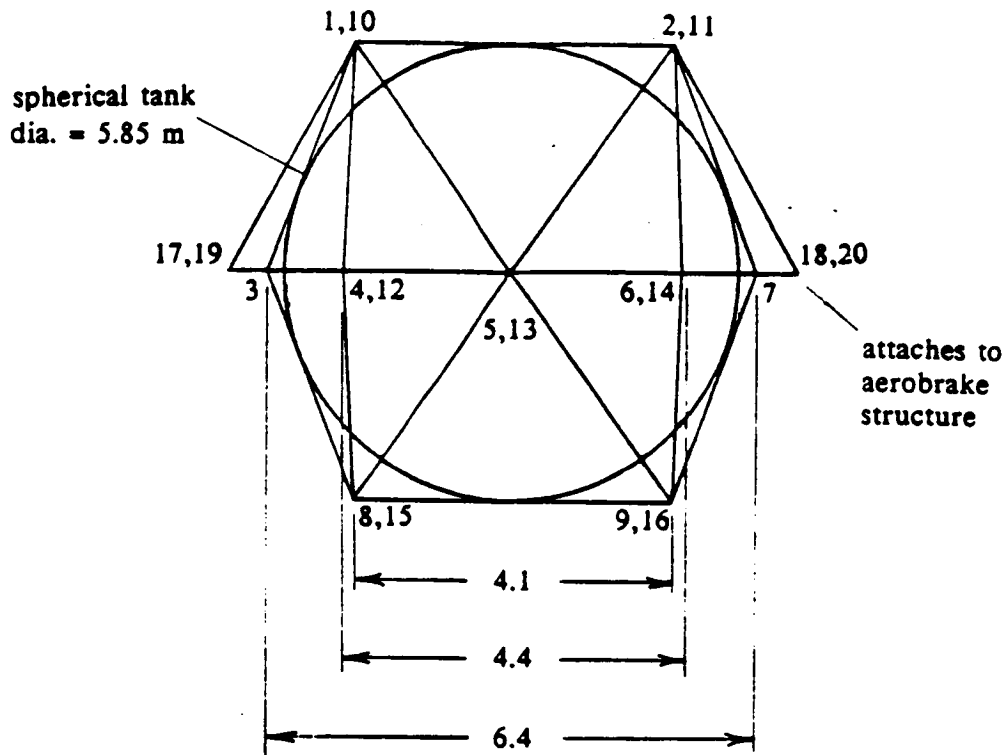
FIGURE 11.6.1

Hydrogen Tank Structure

spherical tank
dia. = 6.63 m

18,20
attaches to
aerobrake
structure

aerobrake structure

scale: 1 cm = 1 m
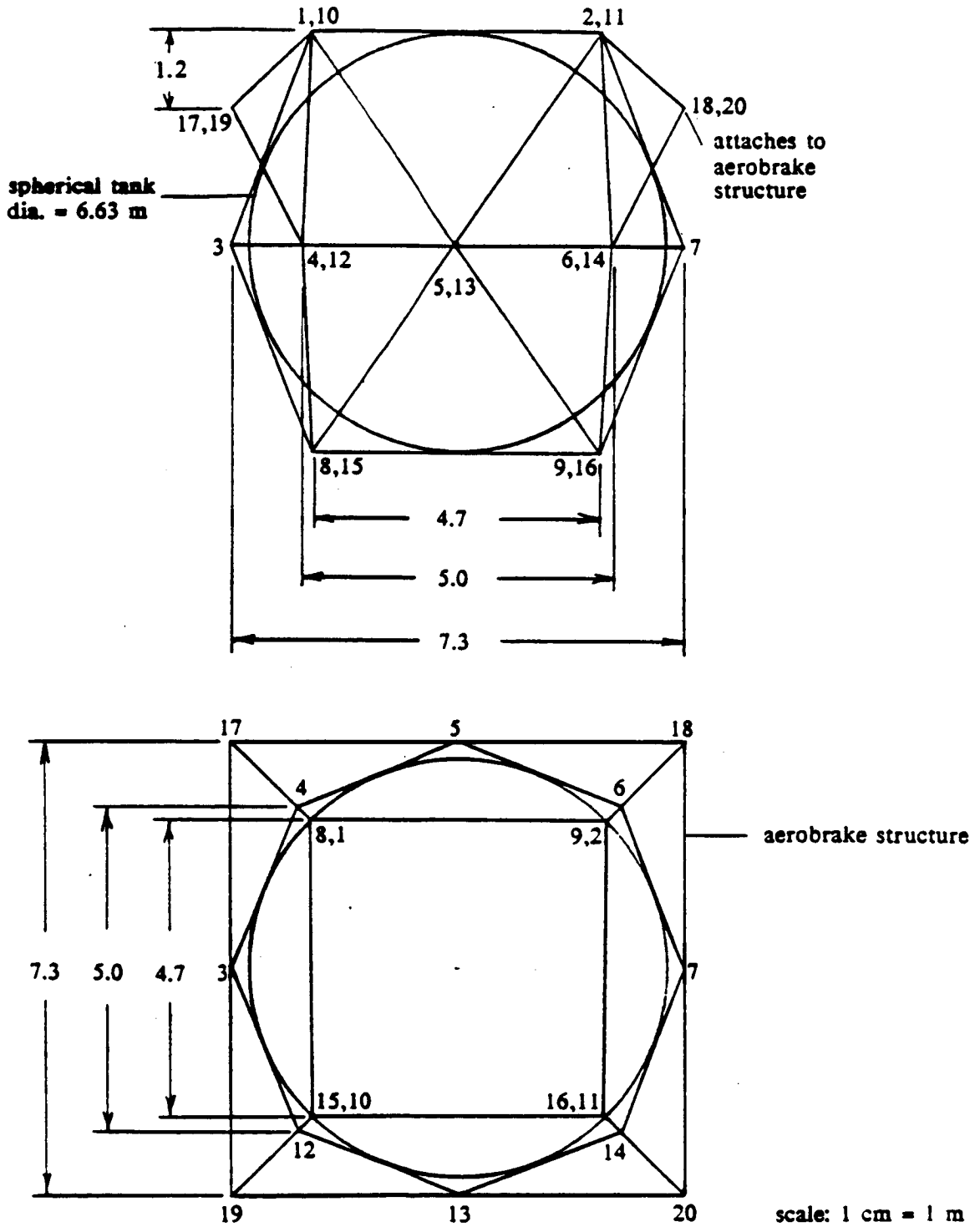
FIGURE 11.6.2

Engine Support Structure
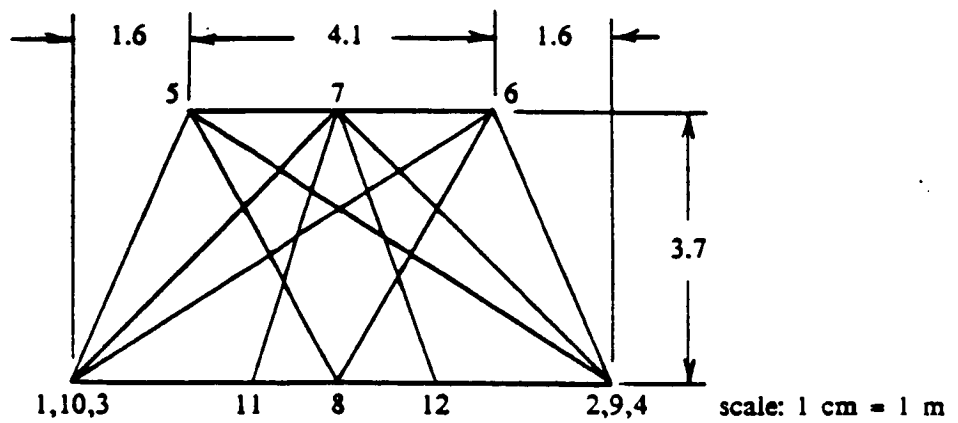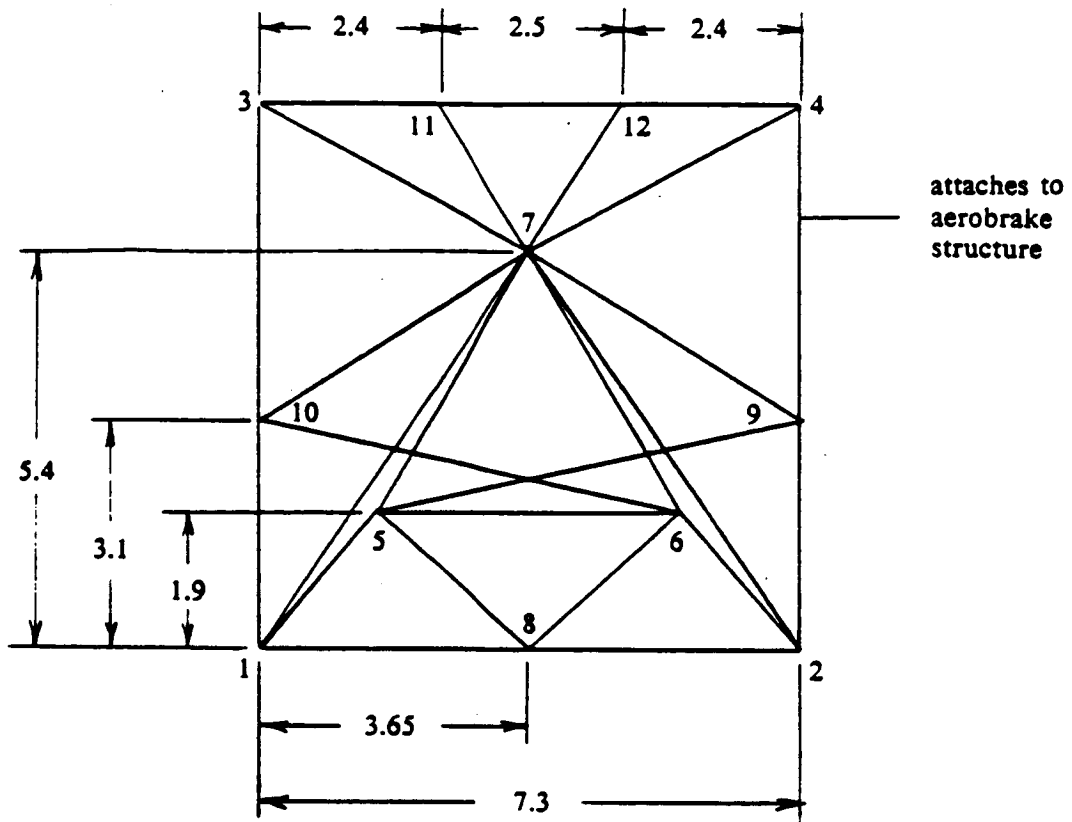
FIGURE 11.6.3

Calculations for the RCS System of the TAXI A:

- Fundamental equation:

    d/dt(Iw) = N - ml^2w

    I = moment of inertia tensor
    N = applied torque
    w = angular velocity
    m = rate of propellant consumption
    l = distance from spin axis to the thruster

The ml^2w term is disregarded because it represents the change in moment of inertia due to the mass of expelled propellant. This amount of change is very small compared to the magnitude of I.

This gives:

    d/dt(Iw) = N

For constant moments of inertia,

    Idw/dt = N or I = N

- The calculated moments of inertia are:

    Ixx = 4.928E+07 lbm ft^2 = 1.530E+06 slugs ft^2 (dry)
          7.251E+07 lbm ft^2 = 2.252E+06 slugs ft^2 (burnout)

    Iyy = 5.647E+07 lbm ft^2 = 1.754E+06 slugs ft^2 (dry)
          5.939E+07 lbm ft^2 = 1.844E+06 slugs ft^2 (burnout)

    Izz = 4.862E+07 lbm ft^2 = 1.510E+06 slugs ft^2 (dry)
          6.806E+07 lbm ft^2 = 2.114E+06 slugs ft^2 (burnout)

The burnout moments of inertia are used in the calculations since the attitude maneuvers are performed after the main burn.

- For the roll maneuver:

A requirement for the aerobraking maneuver is   = 5 deg/sec^2
about the roll axis

    N = I = 2.252E+06 slug ft^2 * .0873 rad/sec^2
      = 1.966E+05 lbs ft

where N = Thrust * moment arm = Thrust * 50.9 ft

note - the moment arm of 50.9 is the maximum distance from the spin axis that the thrusters can be placed so that they are still on a node of the truss.

The required thrust is determined from:

    Thrust = 1.966E+05 lbs ft / 50.9 ft
           = 3861.5 lbs

Four 1,000 lb RCS engines are required at a distance 50.9 ft
from the spin axis for both positive and negative roll.

- For pitch maneuvers: (= 4 deg/sec^2, max moment arm = 36 ft.)

note -   = 4 deg/sec^2 is used for pitch and yaw maneuvers
because the performance requirements about these axes come
from orbital mechanics and are not as strict as they are for
aerobraking. Additionally, the thrust levels required for
this   will allow the RCS system to make small velocity changes.

    Thrust = 1.844E+06 * .0698 rad/sec^2 / 36 ft
           = 3575.3 lbs

Four 1,000 lb RCS engines are required at a distance 36 ft
from the spin axis for both positive and negative pitch.

- For yaw maneuvers: (= 4 deg/sec^2, max moment arm = 36 ft.)

    Thrust = 2.114E+06 * .0698 rad/sec^2 / 36 ft
           = 4098.8 lbs

Four 1,000 lb RCS engines are required at a distance 36 ft
from the spin axis for both positive and negative yaw.

- Turning times are determined from the following equation:

    T = t +   / (* t)

    T = time to turn through an angle
    t = RCS burn time
      = angle of rotation
      = rate of angular acceleration

note - this formula was calculated for turns starting from
and ending at rest. This means that two RCS burns of time
t are required for a rotation through , one for acceleration
and one for deceleration. This also requires that the RCS
engines burn for less than half of the total turn time
(i.e. t < .5 * T).

- Redundancy:

The RCS system is designed for the four parallel half system
redundancy approach as follows:

Roll:

    Positive - system 1: 2 main RCS engines, 1 vernier

              system 2: 2 main, 1 vernier

    Negative - system 1: 2 main, 1 vernier

              system 2: 2 main, 1 vernier

The pitch and yaw axes are set up in the same way.

- Fuel:

  The fuel consumption rate for an engine is determined from:

  m = thrust / (Isp * g)

  m = fuel consumption rate
  Isp = specific impulse
      = 300 sec for hydrazine and nitrogen tetroxide

main engine:

  m = 1000 / (300 * 32.2) = .1035 slugs/sec

vernier engine:

  m = 25 / (300 *32.2) = .0026 slugs/sec

The amount of fuel required for the RCS system is difficult to
determine due to the possible need for perturbation corrections,
attitude thruster failure, etc. The amount of fuel allowed for
the RCS system is approxiamtely 4500 lbs. This amount allows
the RCS system to make small velocity changes for the transfer
vehicle and the necessary attitude adjustments. This gives each
of the 12 half systems 375 lbs of fuel. The engines use roughly
equal amounts of the oxidizer and fuel, so each half system will
have 187.5 lbs of nitrogen tetroxide and hydrazine. The density of
nitrogen tetroxide is approxiamtely 89.9 lbm/ft^3, so a tank of
radius .8 ft will be required for each half system. The density
of hydrazine is 63.1 lbm/ft^3, so a tank of radius .9 ft will be
required for each half system.

- Weights:

  The approximate weight of a 1,000 lb thrust RCS engine is
  50 lbs. The approximate weight of a 25 lb thrust vernier
  engine is 10 lbs.

  Total number of engines:

          positive roll - 4 main   2 vernier
          negative roll - 4   2
          positive yaw   - 4   2
          negative yaw   - 4   2
          positive pitch - 4   2
          negative pitch - 4   2

                 total - 24   12

Total engine weight - 24 * 50 lbs + 12 * 10 lbs = 1320 lbs

          fuel weight   - 4500 lbs
          engine weight - 1320 lbs

          total RCS system - 5820 lbs

- Locations of the attitude thrusters are shown in figure 11.7.1
  A specific diagram of the half system approach is shown
  in figure 11.7.2.

RCS THRUSTER LOCATIONS

FIGURE   11.7.1

237
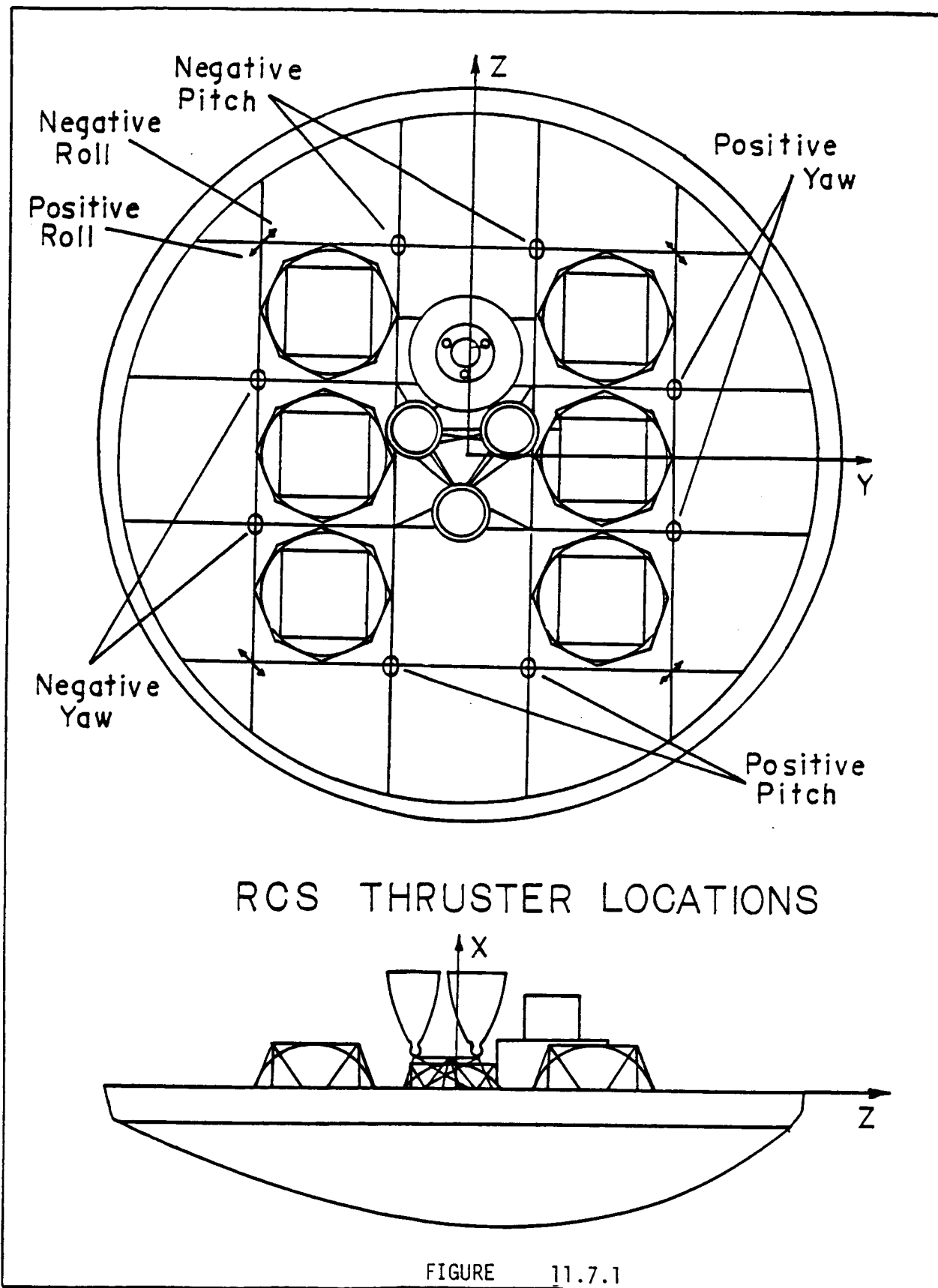
TYPICAL RCS SYSTEM
FOUR PARALLEL HALF SYSTEMS

System 1   Positive

Negative

Sensors — Computer

System 2   Positive

Negative

N_2H_4

N_2O_4

N_2H_4

N_2O_2

N_2H_4

N_2O_2

N_2H_4

N_2O_2
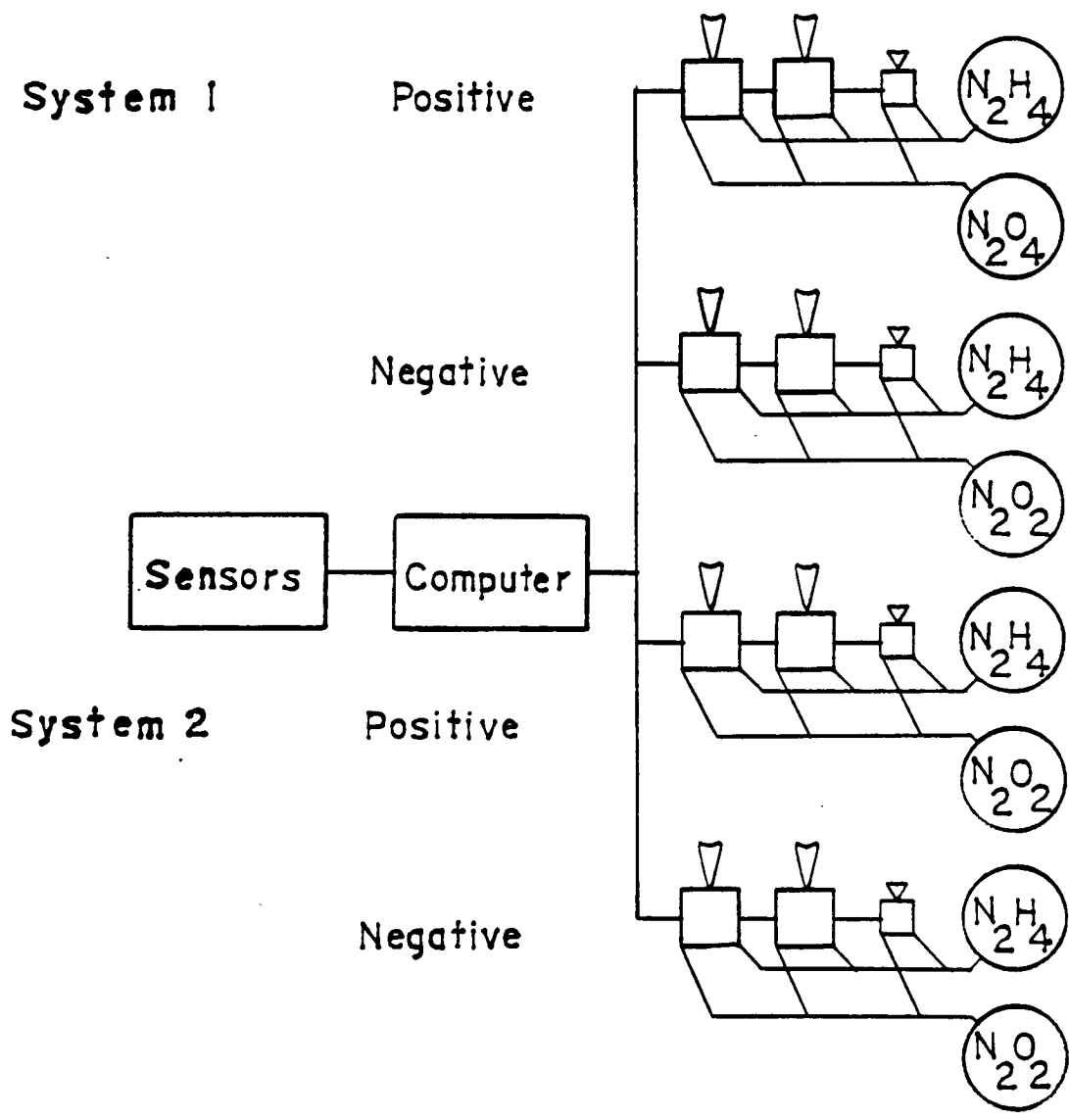
FIGURE 11.7.2

CG AND MOMENT OF INERTIA CALCULATIONS

| STRUCTURE	DRY MASS	B.O. MASS	FUELED MASS	XBAR	YBAR	ZBAR	M*XBAR (D)	M*YBAR (D)	M*ZBAR (D)	M*ZBAR (BO)	M*ZBAR (F)
TRUSS	6.011E+03	6.011E+03	6.011E+03	3.700E-01	0.000E+00	4.560E+00	2.224E+03	0.000E+00	2.741E+04	2.741E+04	2.741E+04
RIBBING	2.600E+03	2.600E+03	2.600E+03	0.000E+00	0.000E+00	0.009E+00	0.000E+00	0.000E+00	0.000E+00	0.000E+00	0.000E+00
SHIELD	1.130E+04	1.130E+04	1.130E+04	6.300E-01	0.000E+00	6.030E+00	7.684E+03	0.000E+00	6.814E+04	6.814E+04	6.814E+04
ENGINES	1.500E+04	1.500E+04	1.500E+04	0.000E+00	0.000E+00	-1.500E+01	0.000E+00	0.000E+00	-2.250E+05	-2.250E+05	-2.250E+05
CREW MODULE	2.000E+04	2.000E+04	2.000E+04	1.825E+01	-5.000E-01	-5.700E+00	3.650E+05	-1.000E+04	-1.140E+05	-1.140E+05	-1.140E+05
PAYLOAD	1.000E+04	1.000E+04	1.000E+04	-1.800E+01	0.000E+00	-1.000E+01	-1.800E+05	0.000E+00	-1.000E+05	-1.000E+05	-1.000E+05
O2 #1	9.080E+02	7.237E+03	2.568E+05	0.000E+00	3.600E+01	0.000E+00	0.000E+00	2.909E+04	0.000E+00	0.000E+00	0.000E+00
O2 #2	8.080E+02	7.237E+03	2.568E+05	0.000E+00	-3.600E+01	0.000E+00	0.000E+00	-2.909E+04	0.000E+00	0.000E+00	0.000E+00
H2 #1	9.880E+02	1.526E+03	2.530E+04	3.600E+01	3.600E+01	-3.900E+00	3.557E+04	3.557E+04	-3.853E+03	-5.950E+03	-9.867E+04
H2 #2	9.880E+02	1.526E+03	2.530E+04	-3.600E+01	3.600E+01	-3.900E+00	-3.557E+04	3.557E+04	-3.853E+03	-5.950E+03	-9.867E+04
H2 #3	9.880E+02	1.526E+03	2.530E+04	3.600E+01	-3.600E+01	-3.900E+00	3.557E+04	-3.557E+04	-3.853E+03	-5.950E+03	-9.867E+04
H2 #4	9.880E+02	1.526E+03	2.530E+04	-3.600E+01	-3.600E+01	-3.900E+00	-3.557E+04	-3.557E+04	-3.853E+03	-5.950E+03	-9.867E+04
C.M.SUPPORT	1.200E+03	1.200E+03	1.200E+03	1.800E+01	0.000E+00	1.000E+00	2.160E+04	0.000E+00	1.200E+03	1.200E+03	1.200E+03
POWER SYS.	2.100E+03	2.100E+03	2.100E+03	1.800E+01	3.000E+00	2.000E+00	3.780E+04	6.300E+03	4.200E+03	4.200E+03	4.200E+03
GNC & COMM.	1.100E+03	1.100E+03	1.100E+03	1.800E+01	1.000E+01	-1.300E+01	1.980E+04	1.100E+04	-1.430E+04	-1.430E+04	-1.430E+04
RCS	6.000E+03	6.000E+03	6.000E+03	0.000E+00	0.000E+00	0.000E+00	0.000E+00	0.000E+00	0.000E+00	0.000E+00	0.000E+00

	DRY MASS	B.O. MASS	FUELED MASS								
TOTALS	8.088E+04	9.589E+04	6.901E+05				2.741E+05	7.300E+03	-3.678E+05	-3.762E+05	-7.470E+05

		XBAR	YBAR	ZBAR
CG LOCATION	DRY	3.389E+00	9.026E-02	-4.547E+00
(FT)	BURNOUT	2.859E+00	7.613E-02	-3.923E+00
	FUELED	3.972E-01	1.059E-02	-1.082E+00

STRUCTURE	DRY MASS	Ixx (D)	Iyy (D)	Izz (D)	Dx (D)	Dy (D)	Dz (D)	IxxBAR	IyyBAR	IzzBAR
TRUSS	6.011E+03	4.022E+06	4.004E+06	8.026E+06	3.019E+00	9.026E-02	9.107E+00	4.040E+06	4.004E+06	8.080E+06
RIBBING	2.600E+03	6.820E+06	6.800E+06	4.200E+06	3.389E+00	9.026E-02	4.547E+00	6.929E+06	6.800E+06	4.212E+06
SHIELD	1.130E+04	3.489E+07	3.891E+07	2.983E+07	2.709E+00	9.026E-02	1.058E+01	3.492E+07	3.891E+07	2.995E+07
ENGINES	1.500E+04	4.658E+05	5.239E+05	9.897E+05	3.389E+00	9.026E-02	1.045E+01	5.168E+05	5.253E+05	1.147E+06
CREW MODULE	2.000E+04	1.175E+06	1.063E+06	6.941E+05	1.486E+01	5.903E-01	1.153E+00	1.473E+06	1.075E+06	7.172E+05
PAYLOAD	1.000E+04	0.000E+00	3.240E+06	3.240E+06	2.139E+01	9.026E-02	5.453E+00	2.139E+05	3.241E+06	3.295E+06
O2 #1	9.080E+02	3.826E+04	3.826E+04	3.826E+04	3.389E+00	3.591E+01	4.547E+00	4.100E+04	6.727E+04	4.193E+04
O2 #2	8.080E+02	3.826E+04	3.826E+04	3.826E+04	3.389E+00	3.609E+01	4.547E+00	4.100E+04	6.742E+04	4.193E+04
H2 #1	9.880E+02	4.678E+04	4.678E+04	4.678E+04	3.261E+01	3.591E+01	6.471E-01	7.900E+04	8.226E+04	4.742E+04
H2 #2	9.880E+02	4.678E+04	4.678E+04	4.678E+04	3.939E+01	3.591E+01	6.471E-01	8.570E+04	8.226E+04	4.742E+04
H2 #3	9.880E+02	4.678E+04	4.678E+04	4.678E+04	3.261E+01	3.609E+01	6.471E-01	7.900E+04	8.244E+04	4.742E+04
H2 #4	9.880E+02	4.678E+04	4.678E+04	4.678E+04	3.939E+01	3.609E+01	6.471E-01	8.570E+04	8.244E+04	4.742E+04
C.M.SUPPORT	1.200E+03	0.000E+00	3.888E+05	3.888E+05	1.461E+01	9.026E-02	5.547E+00	1.753E+04	3.389E+05	3.955E+05
POWER SYS.	2.100E+03	1.890E+04	6.804E+05	6.993E+05	1.461E+01	2.910E+00	6.547E+00	4.958E+04	6.865E+05	7.130E+05
GNC & COMM.	1.100E+03	1.100E+05	3.564E+05	4.664E+05	1.461E+01	9.910E+00	8.453E+00	1.261E+05	3.673E+05	4.757E+05
RCS	6.000E+03	0.000E+00	0.000E+00	0.000E+00	3.389E+00	9.026E-02	4.547E+00	2.033E+04	5.416E+02	2.728E+04

	Ixx	Iyy	Izz	
TOTALS(DRY)	4.862E+07	5.647E+07	4.928E+07	LBS*FT^2
TOTALS (BO)	6.306E+07	5.939E+07	7.251E+07	LBS*FT^2

		Ixx	Iyy	Izz	
Ship's axes	Dry	4.928E+07	5.647E+07	4.862E+07	LB*FT^2
	Burnout	7.251E+07	5.939E+07	6.306E+07	LB*FT^2